

Science

17 January 2014 | \$10

HOW **ROUND** IS THE **ELECTRON**?

EDITORIAL

- 229 Reproducibility
Marcia McNutt

NEWS OF THE WEEK

- 234 A roundup of the week's top stories

NEWS & ANALYSIS

- 236 Guinea Worm Eradication at Risk in South Sudanese War
- 237 Final 2014 Budget Helps Science Agencies Rebound
- 238 Ammonia Pollution From Farming May Exact Hefty Health Costs
- 239 Parasitic Puppeteers Begin to Yield Their Secrets
- 240 Star-Crossing Planets Literally Strut Their Stuff

NEWS FOCUS

- 241 Gut Instinct
>> Science Podcast; Slideshow
- 244 The Second Act

LETTERS

- 248 Biodiversity: Broaden the Search
A. Hochkirch
- Biodiversity: Ecuador Deters Protection Efforts
K. Vega-Villa
- Targeting Deforestation
B. Dias
- Urban Forests on the Front Line
C. A. Nock et al.
- Response
I. L. Boyd et al.

BOOKS ET AL.

- 250 Does Science Need a Global Language?
S. L. Montgomery, reviewed by Y. Peled
- 251 Authors' Words

POLICY FORUM

- 252 Straining Emergency Rooms by Expanding Health Insurance
R. Fisman

PERSPECTIVES

- 254 Smells Like Queen Since the Cretaceous
M. Chapuisat
>> Report p. 287
- 255 Probing the Electron
K. R. Brown
>> Report p. 269
- 256 How Thalidomide Works Against Cancer
A. K. Stewart
>> Reports pp. 301 and 305
- 258 A Clear Path for Polymer Crystallization
N. S. Goroff
>> Report p. 272
- 259 Many Paths to the Origin of Life
J. Gollihar et al.
- 260 Ribose—An Internal Threat to DNA
K. W. Caldecott
- 262 Retrospective: Frederick Sanger (1918–2013)
S. Brenner

CONTENTS continued >>



page 241



pages 254 & 287

ON THE WEB THIS WEEK

>> Science Podcast

Listen to stories on what we can learn from the gut bacteria of modern hunter-gatherers, testing the weathering speed limit, and more.

>> Find More Online

Check out *Science Express*, our podcast, videos, daily news, our research journals, and *Science Careers* at www.sciencemag.org.



COVER

Artist's conception of the charge distribution associated with virtual particles surrounding an electron. Spin precession measurements in molecular thorium oxide show that any deviation from perfect roundness (as depicted here, greatly exaggerated) must be smaller than one part in a quadrillion. This finding strongly constrains proposed extensions to the Standard Model of particle physics. See pages 255 and 269.

Image: Gary Pikovsky

DEPARTMENTS

- 228 This Week in *Science*
- 230 Editors' Choice
- 232 *Science* Staff
- 331 New Products
- 332 *Science* Careers

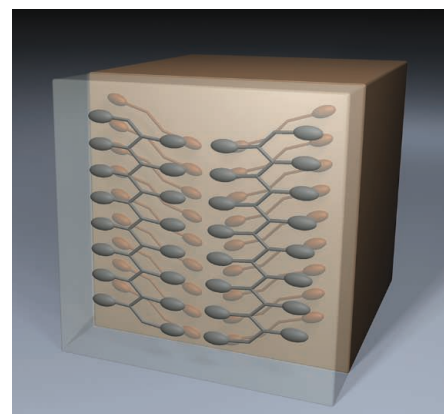
RESEARCH ARTICLE

- 263** Medicaid Increases Emergency-Department Use: Evidence from Oregon's Health Insurance Experiment
S. L. Taubman et al.
Expanding health coverage of low-income adults can result in increased usage of hospital emergency departments.

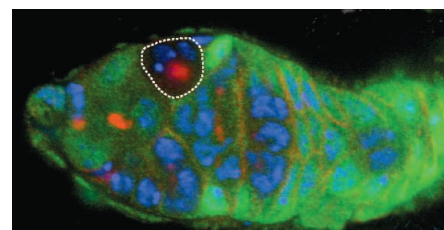
REPORTS

- 269** Order of Magnitude Smaller Limit on the Electric Dipole Moment of the Electron
The ACME Collaboration et al.
Spin precession measurements in the polar molecule thorium monoxide indicate a nearly spherical charge distribution of an electron.
>> *Perspective p. 255*
- 272** Single-Crystal Linear Polymers Through Visible Light-Triggered Topochemical Quantitative Polymerization
L. Dou et al.
Conjugated dye molecules can be polymerized through a topochemical reaction to produce exceptionally long, ordered chains.
>> *Perspective p. 258*
- 277** Nonenzymatic Sugar Production from Biomass Using Biomass-Derived γ -Valerolactone
J. S. Luterbacher et al.
A solvent sourced from biomass may offer a cost-effective means of breaking down cellulose for biofuels production.
- 281** Atomic-Scale Variability and Control of III-V Nanowire Growth Kinetics
Y.-C. Chou et al.
Fluctuations and defects in III-V nanowire growth can be avoided by growing at a low V/III ratio.
- 284** Temporal Constraints on Hydrate-Controlled Methane Seepage off Svalbard
C. Berndt et al.
Seasonal gas hydrate destabilization has been releasing methane from marine sediments near Svalbard for at least 3000 years.
- 287** Conserved Class of Queen Pheromones Stops Social Insect Workers from Reproducing
A. Van Oystaeyen et al.
Social insect queens use an ancient, evolutionarily conserved class of pheromones to prevent worker reproduction.
>> *Perspective p. 254*

- 290** Identification of a Plant Receptor for Extracellular ATP
J. Choi et al.
An *Arabidopsis* lectin receptor kinase, DORN1, is the plant receptor for extracellular adenosine triphosphate.
- 294** Btk29A Promotes Wnt4 Signaling in the Niche to Terminate Germ Cell Proliferation in *Drosophila*
N. Hamada-Kawaguchi et al.
Phosphorylation of β -catenin in somatic niche cells of the fly ovary stops germ cell division and prevents tumorigenesis.
- 298** Changes in rRNA Transcription Influence Proliferation and Cell Fate Within a Stem Cell Lineage
Q. Zhang et al.
The RNA polymerase I regulatory complex promotes dynamic regulation of ribosomal RNA synthesis within the *Drosophila* germline.
- 301** Lenalidomide Causes Selective Degradation of IKZF1 and IKZF3 in Multiple Myeloma Cells
J. Krönke et al.
- 305** The Myeloma Drug Lenalidomide Promotes the Cereblon-Dependent Destruction of Ikaros Proteins
G. Lu et al.
A drug with potent activity in multiple myeloma patients acts by inducing degradation of two specific transcription factors.
>> *Perspective p. 256*
- 309** Direct in Vivo RNAi Screen Unveils Myosin IIa as a Tumor Suppressor of Squamous Cell Carcinomas
D. Schramek et al.
Myh9 regulates p53 activation and is reduced in certain carcinomas associated with poor survival.
- 313** Vaccine Activation of the Nutrient Sensor GCN2 in Dendritic Cells Enhances Antigen Presentation
R. Ravindran et al.
The success of the yellow fever vaccine is linked to the amino acid starvation pathway, which promotes adaptive immunity.



pages 258 & 272



page 298

SCIENCE (ISSN 0036-8075) is published weekly on Friday, except the last week in December, by the American Association for the Advancement of Science, 1200 New York Avenue, NW, Washington, DC 20005. Periodicals Mail postage (publication No. 484460) paid at Washington, DC, and additional mailing offices. Copyright © 2014 by the American Association for the Advancement of Science. The title SCIENCE is a registered trademark of the AAAS. Domestic individual membership and subscription (51 issues): \$149 (\$74 allocated to subscription). Domestic institutional subscription (51 issues): \$990; Foreign postage extra: Mexico, Caribbean (surface mail) \$55; other countries (air assist delivery) \$85. First class, airmail, student, and emeritus rates on request. Canadian rates with GST available upon request, GST #1254 88122. Publications Mail Agreement Number 1069624. Printed in the U.S.A.

Change of address: Allow 4 weeks, giving old and new addresses and 8-digit account number. Postmaster: Send change of address to AAAS, P.O. Box 96178, Washington, DC 20090-6178. Single-copy sales: \$10.00 current issue, \$15.00 back issue prepaid includes surface postage; bulk rates on request. Authorization to photocopy material for internal or personal use under circumstances not falling within the fair use provisions of the Copyright Act is granted by AAAS to libraries and other users registered with the Copyright Clearance Center (CCC) Transactional Reporting Service, provided that \$30.00 per article is paid directly to CCC, 222 Rosewood Drive, Danvers, MA 01923. The identification code for Science is 0036-8075. Science is indexed in the Reader's Guide to Periodical Literature and in several specialized indexes.

Health Economy?

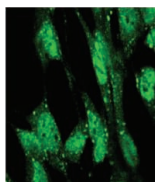
The intensity of arguments over social science issues often seems inversely correlated with the quantity of experimental evidence. **Taubman *et al.*** (p. 263, published online 2 January; see the Policy Forum by **Fisman**) report on the latest analysis of an ongoing controlled experiment—the Oregon Health Insurance Experiment—that seeks to identify and quantify the effects of extending health insurance coverage to a low-income adult population. A substantial increase was observed in visits to the emergency departments of hospitals, corresponding to approximately 120 U.S. dollars per year more in hospital costs.

Topochemical Polymerization

In a topochemical reaction, chemical changes start at active sites in the solid and then proceed autocatalytically to neighboring regions. If one starts with a monomer that can form ordered structures similar to the final polymer, it is possible to polymerize chains in a fully ordered state and thus make very long single chains. **Dou *et al.*** (p. 272; see the Perspective by **Goroff**) describe an unexpected visible-light–induced polymerization of derivatives of a dye. Two of the derivatives underwent photoinduced single-crystal-to-single-crystal topochemical polymerization.

The Secret Life of a Vaccine

Antigen-specific CD8⁺ T cells play a central role in the adaptive immune response to viral infections and to cancer. **Ravindran *et al.*** (p. 313, published online 5 December) studied the successful yellow fever virus vaccine YF-17D to gain insight into its mechanism of action. The vaccine activated the nutrient deprivation sensor, GCN2 kinase, in dendritic cells. In transgenic mouse models, GCN2 activation promoted autophagy and antigen cross-presentation, enhancing the virus-specific CD8⁺ T cell response. The findings suggest an important role for nutrient availability and autophagy in vaccine efficacy, which could aid more successful vaccine development.



Regular Nanowires

For a range of nanotechnology applications, semiconductor nanowires will need to be grown with high precision and control. **Chou *et al.*** (p. 281) studied the growth of gallium phosphide

What Does It All Mean?

Strong emissions of methane have recently been observed from shallow sediments in Arctic seas. **Berndt *et al.*** (p. 284, published online 2 January) present a record of methane seepage from marine sediments off the coast of Svalbard showing that such emissions have been present for at least 3000 years, the result of normal seasonal fluctuations of bottom waters. Thus, contemporary observations of strong methane venting do not necessarily mean that the clathrates that are the source of the methane are decomposing at a faster rate than in the past.



(GaP) nanowires using chemical vapor deposition within a transmission electron microscope and worked out conditions that could generate regular and predictable wire growth.

Renewable Breakdown Routine

In order to transform cellulose-containing biomass into liquid fuels such as ethanol, it is first necessary to break down the cellulose into its constituent sugars. Efforts toward this end have focused on chemical protocols using concentrated acid or ionic liquid solvents, and on biochemical protocols using cellulase enzymes. **Luterbacher *et al.*** (p. 277) now show that γ -valerolactone, a small molecule solvent that can itself be sourced renewably from biomass, promotes efficient and selective thermal breakdown of cellulose in the presence of dilute aqueous acid.

Drug With a (Re)Purpose

Thalidomide, once infamous for its deleterious effects on fetal development, has re-emerged as a drug of great interest because of its beneficial immunomodulatory effects. A derivative drug called lenalidomide significantly extends the survival of patients with multiple myeloma, but the molecular mechanisms underlying its efficacy remain unclear (see the Perspective by **Stewart**). Building on a previous observation that thalidomide binds to cereblon, a ubiquitin ligase, **Lu *et al.*** (p. 305, published online 28 November) and **Krönke *et al.*** (p. 301, published online 28 November) show that in the presence of lenalidomide, cereblon selectively targets two B cell transcription factors (Ikaros family members, IKZF1 and IKZF3) for degradation.

In myeloma cell lines and patient cells, down-regulation of IKZF1 and IKZF3 was necessary and sufficient for the drug's anticancer activity. Thus, lenalidomide may act, at least in part, by "repurposing" a ubiquitin ligase.

Identifying Drivers and Passengers

Modern genomics is unearthing hundreds of genetic and epigenetic alterations associated with human cancers. It is important to delineate which of these alterations participate actively in tumor progression and/or metastases (driver mutations) and which are inconsequential (passenger mutations). To this end, **Schramek *et al.*** (p. 309) conducted an in vivo RNA interference screen in mice to test simultaneously the functionality of putative cancer genes and down-regulated messenger RNAs associated with tumor-initiating cells of squamous cell carcinomas (SCCs). Several candidates, including nonmuscle myosin-IIa, not previously viewed as tumor suppressors were uncovered.

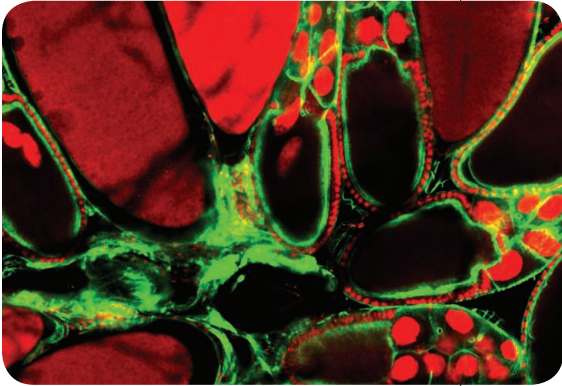
Long Live the Queen

Eusociality is often considered to have arisen, at least in part, due to the inclusive fitness that workers gain through helping their queen sister to raise her offspring. **Van Oystaeyen *et al.*** (p. 287; see the Perspective by **Chapuisat**) characterized the sterility-inducing queen pheromone across three distantly related eusocial hymenopterans (a wasp, a bumblebee, and a desert ant) and synthesized data across 69 other species. Queen pheromones appear to be remarkably conserved, which suggests that reproductive manipulation has ancient roots.

Additional summaries

Wnt- β -Catenin in Germ Cells

The Wnt- β -catenin pathway contributes to many signaling mechanisms during organismal development and carcinogenesis by regulating both transcription and cell adhesion. **Hamada-**



Kawaguchi *et al.* (p. 294) demonstrate that this pathway must be activated in ovarian somatic cells to stop proliferation of germ cells in *Drosophila*. Phosphorylation of a tyrosine residue on β -catenin by the tyrosine kinase

Btk turns on signaling in the niche cells by promoting transcriptional activity of β -catenin. Failure in this process resulted in ovarian tumors in the flies.

Stubbornly Spherical

The shape of the electron's charge distribution reflects the degree to which switching the direction of time impacts the basic ingredients of the universe. The Standard Model (SM) of particle physics predicts a very slight asphericity of the charge distribution, whereas SM extensions such as supersymmetry posit bigger and potentially measurable, but still tiny, deviations from a perfect sphere. Polar molecules have been identified as ideal settings for measuring this asymmetry, which should be reflected in a finite electric dipole moment (EDM)

because of the extremely large effective electric fields that act on an electron inside such molecules. Using electron spin precession in the molecule ThO, **Baron *et al.*** (p. 269, published online 19 December; see the cover; see the

Perspective by **Brown**) measured the EDM of the electron as consistent with zero. This excludes some of the extensions to the SM and sets a bound to the search for a nonzero EDM in other facilities, such as the Large Hadron Collider.

ATP Receptor in *Arabidopsis*

As well as its role as an intracellular energy source, extracellular adenosine triphosphate (ATP) has diverse functions as a signaling molecule. ATP receptors have been identified in animal cells, but searches based on structural homology have not identified ATP receptors in plants. **Choi *et al.*** (p. 290) have now identified an ATP receptor in the model plant *Arabidopsis thaliana* by tracking down the cause of mutations that leave mutant plants unresponsive to ATP signals. The receptor identified carries an intracellular kinase domain and an extracellular lectin domain.

Germline Pol I

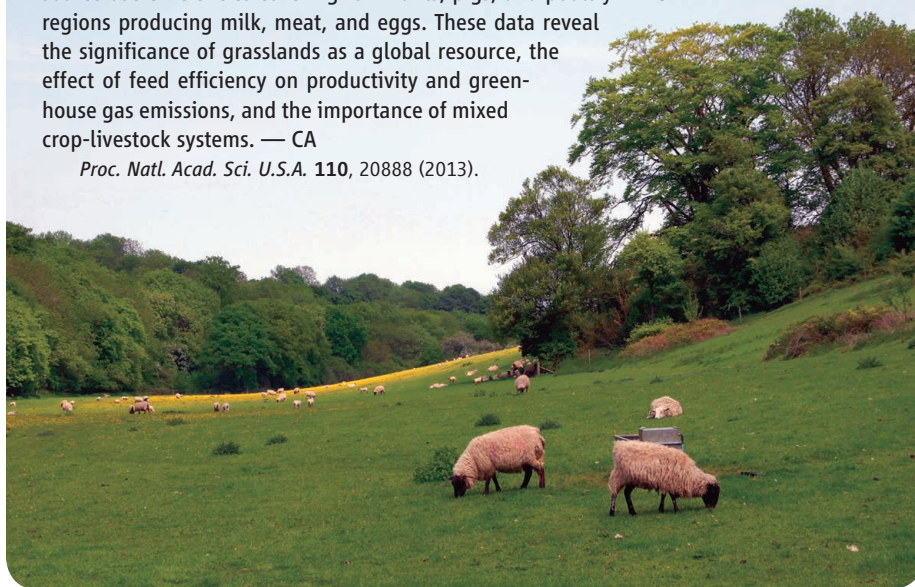
RNA polymerase I (Pol I)-directed ribosomal RNA (rRNA) transcription has been extensively studied in mammalian cell lines and yeast. However, the functional significance of cell-specific regulation of Pol I transcription within developmental contexts *in vivo* remains unclear. **Zhang *et al.*** (p. 298) characterized a *Drosophila* Pol I regulatory complex and found that germline stem cells (GSCs) of the ovary exhibited increased levels of rRNA transcription relative to their immediate daughter cells. High levels of rRNA expression promoted GSC proliferation, with attenuation of Pol I activity showing effects during early germ cell differentiation.

ECOLOGY

Domestication Duality

Livestock occupy a third of Earth's ice-free surface, use a third of its freshwater supplies, and contribute to pollution, climate warming, and obesity. Yet they also feed and provide income for billions of people, supplying critical micronutrients and 40% of global agricultural gross domestic product. But Herrero *et al.* contend that we lack microdata that would allow us to assess and mitigate these challenges at meaningful scales, and they have produced a spatially disaggregated data set on biomass use, productivity, emissions, and resource-use efficiencies covering ruminants, pigs, and poultry in 28 regions producing milk, meat, and eggs. These data reveal the significance of grasslands as a global resource, the effect of feed efficiency on productivity and greenhouse gas emissions, and the importance of mixed crop-livestock systems. — CA

Proc. Natl. Acad. Sci. U.S.A. **110**, 20888 (2013).



develop a three-dimensional picture of what happens as the stroma develops, Young *et al.* collected a series of scanning electron microscope images, where either a focused ion beam or an ultramicrotome was used to scrape away the surface. Corneas were harvested from 10- to 18-day-old chick embryos, and over that time period, the collagenous matrix increased from 20 to 70% of the cornea volume. But the authors were surprised to find that 20% of the cornea was occupied by keratocytes. These cells adopt a flattened morphology featuring extended cell membranes that align with the collagen fibrils. They observed an orthogonal network of actin filaments that resembled filopodia, with tubular membrane projections sometimes traveling more than 30 μm . Some clusters of cells attached to one set of collagen bundles, whereas others would bridge between two or more. The authors believe that this extensive network of cells and collagen bundles is key for the construction of the lamellar structure of the stroma. — MSL

Proc. Natl. Acad. Sci. U.S.A. **10**, 1073/ pnas.1313561110 (2014).

PSYCHOLOGY

Simulating Metaphors

Embodied cognition refers to the association of abstract concepts, such as interpersonal warmth, with concrete sensations, such as physical warmth; psychologists have begun to explore how the abstract and the concrete are linked. A bidirectional conduit would imply that individuals who feel warmer would offer more positive judgments of others and those who are lonely would feel colder. Another view is that sensory processes can influence cognitive ones, but not the other way around. Slepian and Ambady taught people contrasting embodied metaphors: For the first group, past history was described as being weightier than present experience, whereas for the second group, the decisions of the present were described as carrying more weight than those of the past. They found that the first group rated old books as heavier than the same books camouflaged with a new dust jacket, whereas the pattern reversed for the other group. Furthermore, these differences were only observed when the books were actually touched, leading the authors to propose that

PSYCHOLOGY

Self-Esteem

Being identified as a member of a group associated with unfavorable stereotypes can evoke behavior that conforms to those stereotypes. One remedy for which there is empirical support from field experiments is to elicit a brief episode of autobiographical self-affirmation. Hall *et al.* have adapted this methodology to enhance the performance of soup kitchen habitués on two standard cognitive function tests: fluid intelligence and executive control. In the treatment group, some of these impoverished individuals were asked to describe verbally an event that had made them feel successful or proud; people in the two control groups were asked either to describe their daily diet, which might have served to make the poverty stereotype more salient, or to watch a funny video, which did in fact serve to elevate their mood. The self-affirming group performed significantly better than the control groups on both tests. Furthermore, as one would predict, the performance-enhancing effect of self-affirmation was not observed when wealthy people (whose average annual income was 10

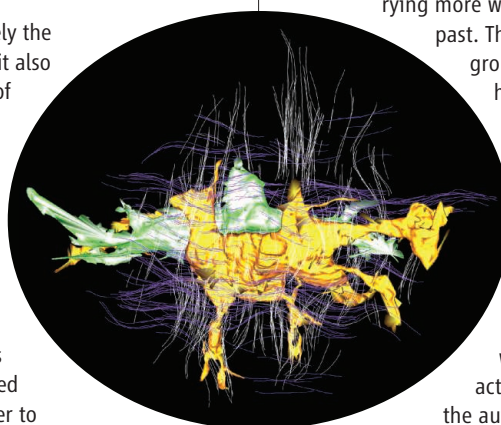
times that of the poor participants) were tested. Finally, the upside potential for this kind of intervention was revealed when three times as many treated (versus control) individuals stopped on their way out of the soup kitchen to collect fliers containing information about benefit programs aimed at the working poor. — GJC

Psychol. Sci. **10**, 1177/0956797613510949 (2013).

BIOPHYSICS

Collagen Clarity

The cornea is not merely the front layer of the eye; it also provides the majority of the focusing power. It is an unusual kind of tissue because it is transparent to light; hence, it does not contain blood vessels. The bulk of the cornea consists of the stroma, which contains stacked layers of aligned collagen fibrils. In order to



times that of the poor participants) were tested. Finally, the upside potential for this kind of intervention was revealed when three times as many treated (versus control) individuals stopped on their way out of the soup kitchen to collect fliers containing information about benefit programs aimed at the working poor. — GJC

sensorimotor simulation of a learned metaphor creates the potential for concepts to influence sensations. — GJC

Cognition **130**, 309 (2014).

ENVIRONMENTAL SCIENCE

Lead in the Blood

Exposure to lead can lead to numerous adverse health effects in humans, with particular concern over neurotoxic effects. Between the mid-1970s and the early 2000s, the use of lead compounds in gasoline was phased out in most industrialized countries, and since then, the lead content of ambient air has fallen markedly. In the United States, the national ambient air quality standard is set for the lead content of ambient air (PbA), but humans can be exposed to lead via sources other than air, leading to the total lead measured in blood (PbB). Using PbB data from the National Health and Nutrition Examination survey and PbA data from the U.S. Environmental Protection Agency Air Quality System for 1999–2008, Meng *et al.* investigated the relationship between PbA and PbB since the phase-out of leaded gasoline. They found that the emission sources for lead have changed,



leading to a shift from a fine to a coarse PbA particle size distribution, and show that PbA in coarse airborne particles is a statistically significant predictor of PbB. The PbB levels of children are more sensitive to changes in PbA concentrations than are those of adults. — JFU

Environ. Sci. Technol. **10.1021/es4039825** (2013).

APPLIED PHYSICS

Reading Speckle Patterns

Intensity and pinpoint focus over long distances are probably the most familiar features of laser light. It is the spatial and temporal coherence of the light, with the photons in the laser beam marching in lockstep, that lends itself to the above features but also provides the most valu-

able properties for the vast applications in communication and imaging. When a laser beam hits a random medium, such as a wall or sheet of paper, the coherence of the photons results in the formation of a speckle pattern. This pattern is determined by the properties of the propagating light and the diffusing medium. Using a thin layer of alumina particles as a highly scattering medium, Mazilu *et al.* show that they can “read” the generated speckle pattern, and by modeling it with a number of principal components describing the propagating light beam can determine the wavelength of the light with high resolution. Because the speckle pattern is dependent on a number of parameters that can be encoded onto the propagating laser light, the relative simplicity of the technique may find application in areas such as lab-on-chip spectroscopy or security features in bank notes or sensitive documents. — ISO

Opt. Lett. **39**, 96 (2014).

PHYSICS

A Very Thin Superconductor

Manipulating the dimensionality of materials can lead to profound changes in their electronic properties. The iron-based superconductor FeSe has a relatively low superconducting transition temperature T_c of about 8 K in the bulk; however, spectroscopic measurements have suggested that a single-unit-cell layer of this material has a much higher T_c . Transport measurements needed to confirm this finding proved challenging; now, Zhang *et al.* overcome these difficulties by growing the FeSe layer on a SrTiO_3 substrate and capping it with FeTe, with an additional layer of Si deposited on top of the FeTe to prevent its exposure to air. By measuring the electrical resistance as a function of temperature, they detected the onset of superconductivity at a temperature higher than 40 K; the critical current density, important for practical applications, was much higher than in the bulk. Because neither the substrate nor the capping layer exhibited superconductivity, and the transport characteristics power laws were consistent with the Berezinskii-Kosterlitz-Thouless transition, the superconductivity appears to be a genuine property of the FeSe layer and has a two-dimensional nature. Because of its relative simplicity, the system presents a good testing ground for unconventional superconductivity. — JS

Chin. Phys. Lett. **31**, 017401 (2014).

1200 New York Avenue, NW
Washington, DC 20005

Editorial: 202-326-6550, FAX 202-289-7562
News: 202-326-6591, FAX 202-371-9227

Bateman House, 82-88 Hills Road

Cambridge, UK CB2 1LQ
+44 (0) 1223 326500, FAX +44 (0) 1223 326501

SUBSCRIPTION SERVICES For change of address, missing issues, new orders and renewals, and payment questions: 866-434-AAAS (2227) or 202-326-6417, FAX 202-842-1065. Mailing addresses: AAAS, P.O. Box 96178, Washington, DC 20090-6178 or AAAS Member Services, 1200 New York Avenue, NW, Washington, DC 20005

INSTITUTIONAL SITE LICENSES please call 202-326-6755 for any questions or information

REPRINTS: Author Inquiries 800-635-7181

Commercial Inquiries 803-359-4578

PERMISSIONS 202-326-6765, permissions@aaas.org

MEMBER BENEFITS AAAS Travels: Bethchart Expeditions 800-252-4910; Apple Store www.store.apple.com/us/go/epstore/aaas; NASA Federal, 1-888-NASA-FCU (1-888-627-2328) or www.nasafcu.com; Cold Spring Harbor Laboratory Press Publications www.cshlpress.com/affiliates/aaas.htm; Hertz 800-654-2200 CDP#343457; Seabury & Smith Life Insurance 800-424-9883; Subaru VIP Program 202-326-6417; Nationwide Insurance http://nationwide.com/aaas; Other Benefits: AAAS Member Services 202-326-6417 or http://membercentral.aaas.org/discounts.

science_editors@aaas.org (for general editorial queries)
science_letters@aaas.org (for queries about letters)
science_reviews@aaas.org (for returning manuscript reviews)
science_bookrevs@aaas.org (for book review queries)

Published by the American Association for the Advancement of Science (AAAS), *Science* serves its readers as a forum for the presentation and discussion of important issues related to the advancement of science, including the presentation of minority or conflicting points of view, rather than by publishing only material on which a consensus has been reached. Accordingly, all articles published in *Science*—including editorials, news and comment, and book reviews—are signed and reflect the individual views of the authors and not official points of view adopted by AAAS or the institutions with which the authors are affiliated.

AAAS was founded in 1848 and incorporated in 1874. Its mission is to advance science, engineering, and innovation throughout the world for the benefit of all people. The goals of the association are to: enhance communication among scientists, engineers, and the public; promote and defend the integrity of science and its use; strengthen support for the science and technology enterprise; provide a voice for science on societal issues; promote the responsible use of science in public policy; strengthen and diversify the science and technology workforce; foster education in science and technology for everyone; increase public engagement with science and technology; and advance international cooperation in science.

INFORMATION FOR AUTHORS

See pages 716 and 717 of the 8 February 2013 issue or access www.sciencemag.org/about/authors

SENIOR EDITORIAL BOARD

A. Paul Alivisatos, Lawrence Berkeley Nat'l. Laboratory
Ernst Fehr, Univ. of Zurich
Susan M. Rosenberg, Baylor College of Medicine
Michael S. Turner, University of Chicago

BOARD OF REVIEWING EDITORS

Adriano Aguzzi, Univ. Hospital Zürich
Takuzo Aizawa, Univ. of Tokyo
Leslie Aiello, Wenner-Gren Foundation
Sonia Altizer, Univ. of Georgia
Virginia Armbrust, Univ. of Washington
Sebastian Amigorena, Institut Curie
Kathryn Anderson, Memorial Sloan-Kettering Cancer Center
Peter Andolfatto, Princeton Univ.
Meinrat O. Andreae, Max Planck Inst., Mainz
Paola Ariotti, Harvard Univ.
Johan Auwerx, EPFL
David Auschallom, Univ. of Chicago
Jordi Bascompte, Estación Biológica de Doñana, CSIC
Facundo Batista, London Research Inst.
Ray H. Baughman, Univ. of Texas, Dallas
David Baum, Univ. of Wisconsin
Mark Bear, Massachusetts Inst. of Technology
Kamran Behnia, Paris-Sud Univ.
Yasmine Belkaid, NIAID, NIH
Philip Benfey, Duke Univ.
Stephen J. Benkovic, Penn State Univ.
Gabriele Berg, Univ. of California, San Francisco
Christophe Bernard, Aix-Marseille Univ.
Gregory C. Berzosa, Stanford Univ.
Peer Bork, EMBL
Bernard Bourdon, Ecole Normale Supérieure de Lyon
Chris Bowler, Ecole Normale Supérieure
Ian Boyd, Univ. of St. Andrews
Christian Büchel, Universitätsklinikum Hamburg-Eppendorf
Joseph A. Burns, Cornell Univ.
William P. Butz, Population Reference Bureau
György Buzsáki, New York Univ., School of Medicine
Blanche Capel, Duke Univ.
Mats Carlsson, Univ. of Oslo
David Clapham, Children's Hospital, Boston
David Clary, Univ. of Oxford
Joel Cohen, Rockefeller Univ., Columbia Univ.
Jonathan D. Cohen, Princeton Univ.
Robert Cook-Deegan, Duke Univ.
James Collins, Boston Univ.
Alan Cowman, Walter & Eliza Hall Inst.
Robert H. Crabtree, Yale Univ.
Janet Currier, Princeton Univ.
Jeff L. Dangl, Univ. of North Carolina

Tom Daniel, Univ. of Washington
Frans de Waal, Emory Univ., Univ. of Tokyo
Stanislav Dehaene, Collège de France
Robert Desimone, MIT
Claude Desplan, New York Univ.
Ap Dijksterhuis, Radboud Univ. of Nijmegen
Dennis Discher, Univ. of Pennsylvania
Gerald W. Dorn II, Washington Univ. School of Medicine
Jennifer A. Doudna, Univ. of California, Berkeley
Bruce Dunn, Univ. of California, Los Angeles
Christopher Dye, WHO
Todd Ehlers, University of Tuebingen
David Ehrhardt, Carnegie Inst. of Washington
Tim Elston, Univ. of North Carolina at Chapel Hill
Gerhard Ertl, Fritz-Haber-Institut, Berlin
Barry Everitt, Univ. of Cambridge
Ernst Fehr, Univ. of Zurich
Michael Feuer, The George Washington Univ.
Alain Fischer, INSERM
Anne C. Ferguson-Smith, Univ. of Cambridge
Peter Fratzl, Max Planck Inst.
Elaine Fuchs, Rockefeller Univ.
Wulfraam Gerstner, EPFL Lausanne
Daniel Geschwind, UCLA
Andrew Gewirth, Univ. of Illinois
Karl-Heinz Glassner, TU Braunschweig
Julia R. Greer, Caltech
Elizabeth Grove, Univ. of Chicago
Kip Guy, St. Jude's Children's Research Hospital
Taekjip Ha, Univ. of Illinois at Urbana-Champaign
Christian Hassel, Ludwig Maximilians Univ.
Steven Hahn, Fred Hutchinson Cancer Research Center
Gregory J. Hannon, Cold Spring Harbor Lab.
Michael Hasselmo, Boston Univ.
Martin Heimann, Max Planck Inst., Jena
Yka Helariutta, Univ. of Finland
James A. Hendler, Rensselaer Polytechnic Inst.
Janet G. Hering, Swiss Fed. Inst. of Aquatic Science & Technology
Michael E. Himmel, National Renewable Energy Lab.
Kai-Uwe Hinrichs, Univ. of Bremen
Kei Hirose, Tokyo Inst. of Technology
David Holdell, Univ. of Cambridge
Lora Hooper, UT Southwestern Medical Ctr at Dallas
Thomas Hudson, Ontario Inst. for Cancer Research
Raymond Huey, Univ. of Washington
Steven Jacobsen, Univ. of California, Los Angeles
Kai Johnson, EPFL Lausanne
Peter Jonas, Inst. of Technology (IST) Austria
Matthäus Kaeberlein, Univ. of Washington
William Kaelin Jr., Dana-Farber Cancer Inst.
Daniel Kahne, Harvard Univ.

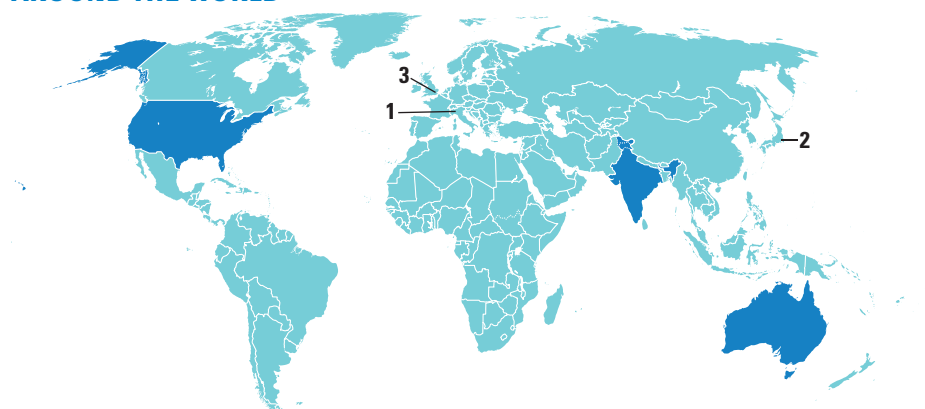
Daniel Kammen, Univ. of California, Berkeley
Masashi Katsuki, Univ. of Tokyo
Joel Kingsolver, Univ. of North Carolina at Chapel Hill
Robert Kingston, Harvard Medical School
Alexander Kolodkin, Johns Hopkins Univ.
Robert Kolter, Harvard Medical School
Alberto R. Kornblith, Univ. of Buenos Aires
Leonid Kruglyak, Princeton Univ.
Thomas Langer, Univ. of Cologne
Mitchell A. Lazar, Univ. of Pennsylvania
David Lazer, Harvard Univ.
Virginia Lee, Univ. of Pennsylvania
Thomas Lecuit, IBC
Stanley Lemon, Univ. of North Carolina at Chapel Hill
Ottoline Leyser, Cambridge Univ.
Marcia C. Litt, Univ. of California, Berkeley
Jianguo Liu, Michigan State Univ.
Liz Liz-Marzan, CIC bioGUNE
Jonathan Losos, Harvard Univ.
Ke Lu, Chinese Acad. of Sciences
Christian Lüscher, Univ. of Geneva
Laura Machesky, CRUK Beatson Inst. for Cancer Research
Anne Magurran, Univ. of St. Andrews
Oscar Marin, CSIC & Univ. Miguel Hernández
Charles Marshall, Univ. of California, Berkeley
Chris Marshall, Inst. of Cancer Research
C. Robertson McClung, Dartmouth College
Graham Medley, Univ. of Warwick
Yasushi Miyashita, Univ. of Tokyo
Richard Morris, Univ. of Edinburgh
Sean Munro, MRC Lab. of Molecular Biology
Thomas Murray, The Hastings Center
Naoto Nagaosa, Univ. of Tokyo
James Nelson, Stanford Univ. School of Med.
Daniel Neufeld, Univ. of California, Berkeley
Timothy W. Nilsen, Case Western Reserve Univ.
Pär Nordlund, Karolinska Inst.
Helga Nowotny, European Research Advisory Board
Luke O'Neill, Trinity College, Dublin
Ben Olsen, MIT
N. Phuan Ong, Princeton Univ.
Joe Oreinstein, Univ. of California, Berkeley & Lawrence Berkeley National Lab
Harry Orr, Univ. of Minnesota
Andrew Osa Oweid, Univ. of Warwick
Steve Palumbi, Stanford Univ.
Jane Parker, Max-Planck Inst. of Plant Breeding Research
Donald R. Paul, Univ. of Texas at Austin
John H. J. Petrij, Memorial Sloan-Kettering Cancer Center
Joshua Plotkin, Univ. of Pennsylvania
Philippe Poulin, CNRS
Colin Renfrew, Univ. of Cambridge
Trevor Robbins, Univ. of Cambridge

Jim Roberts, Fred Hutchinson Cancer Research Ctr.
Barbara A. Romanowicz, Univ. of California, Berkeley
Jens Rostrup-Nielsen, Haldor Topsøe
Mike Ryan, Univ. of Texas, Austin
Mitsunori Saitou, Kyoto Univ.
Shimon Sakaguchi, Kyoto Univ.
Miguel Salmeron, Lawrence Berkeley National Lab
Jürgen Sandkühler, Medical Univ. of Vienna
Alexander Schier, Harvard Univ.
Randy Seeley, Univ. of Cincinnati
Vladimir Shalaya, Purdue Univ.
Joseph Silk, Institut d'Astronomie de Paris
Denis Simon, Arizona State Univ.
Alison Smith, John Innes Centre
John Speakman, Univ. of Aberdeen
Allan C. Spradling, Carnegie Institution of Washington
Jonathan Sprent, Garvan Inst. of Medical Research
Eric Steig, Univ. of Washington
Molly Stevens, Imperial College London
Paula Stephan, Georgia State Univ. and National Bureau of Economic Research
V. S. Subramanian, Univ. of Maryland
Ira Tabas, Columbia Univ.
Sarah Teichmann, Cambridge Univ.
John Thomas, North Carolina State Univ.
Christopher T. Taylor, The Wellcome Trust Sanger Inst.
Herbert Virgin, Washington Univ.
Bert Vogelstein, Johns Hopkins Univ.
Cynthia Volkert, Univ. of Göttingen
Bruce D. Walker, Harvard Medical School
Douglas Wallace, Dalhousie Univ.
David Wallach, Weizmann Inst. of Science
Ian Walmaley, Univ. of Oxford
David A. Wardle, Swedish Inst. of Agric Sciences
David Waxman, Fudan Univ.
Jonathan Weissman, Univ. of California, San Francisco
John Willis, Oxford Univ.
Ian A. Wilson, The Scripps Res. Inst.
Timothy D. Wilson, Univ. of Virginia
Rosemary Wyse, Johns Hopkins Univ.
Jan Zaenen, Leiden Univ.
Kenneth Zaret, Univ. of Penn. School of Medicine
Jonathan Zehr, Univ. of California, Santa Cruz
Len Zon, Children's Hospital Boston
Mila Zubek, MIT

BOOK REVIEW BOARD

David Bloom, Harvard Univ.
Samuel Bowring, MIT
Angela Creager, Princeton Univ.
Richard Swedell, Univ. of Chicago
Ed Wasserman, DuPont

AROUND THE WORLD



Milan, Italy 1

Italian Animal Rights Fliers Get Personal

An anonymous group against animal experimentation shocked the Italian research community last week by posting leaflets that show photos, home addresses, and telephone numbers of scientists involved in animal research at the Univer-



Attacked. One animal rights flier reads, “call this executioner and tell him what you think of him.”

sity of Milan and labeling them “murderers.” The posters targeted physiologist Edgardo D’Angelo, parasitologist Claudio Genchi, pharmacologist Alberto Corsini, and biologist Maura Francolini.

Although the fliers didn’t contain a specific call to violence, Italian scientists say the implicit threat is unmistakable. “It’s unacceptable that those who work for

the good of science and public health are called murderers by someone who publicly incites violence against them,” says Dario Padovan, president of Pro-Test Italia, an organization that seeks to defend and explain animal research. Many politicians, including Maria Chiara Carrozza, Italy’s minister of education, universities and research, also condemned the tactic. The University of Milan has filed a complaint and the city’s police department has started an investigation.

Animal research has recently generated intense debate in Italy; a bill to drastically limit animal testing is expected to be approved soon, over scientists’ protests. http://scim.ag/_fliers

Tokyo 2

Allegations Mar Alzheimer’s Study

A \$31 million Japanese study looking for early signs of Alzheimer’s disease is plagued by falsified data and other problems, according to an article published last week by one of the country’s most respected newspapers. Based on an interview with one of the researchers and a review of project documents, the *Asahi Shimbun* alleges that scientists behind the ongoing Japanese Alzheimer’s Disease Neuroimaging Initiative manipulated details of some memory tests after they were completed and included patients that were probably too ill for meaningful study.

Japan’s Ministry of Health plans to investigate the allegations; an official says the scope and timing of the investigation are still being determined. The study involves 38 medical institutions and has received funding from the health ministry, the education ministry, and a consortium of 11 pharmaceutical firms.

THEY SAID IT

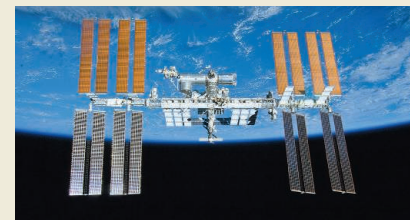
“[T]he chances of being successful just by sprinkling something on your food, rubbing cream on your thighs, or using a supplement are slim to none. The science just isn’t there.”

—Jessica Rich, director of the Federal Trade Commission’s Bureau of Consumer Protection, in a statement last week after charging four companies with deceptively marketing weight-loss products.

London 3

Public Encouraged to Share Medical Data

U.K. medical research charities last week launched a colorful advertisement campaign in the national press, urging residents to allow scientists to access patient data from the country’s National Health Service (NHS). The records in NHS—which is free for all and paid for through taxation—are now held by a patient’s general practitioner. But in a few months, doctors will begin sending that data to a central NHS database known as *care.data*, where it will be made available, anonymously, to researchers and possibly also to drug companies. Some physicians have criticized the database for intruding on the trust between doctor and patient, while



NOTED

>NASA’s request to **keep the International Space Station alive** for an additional 4 years beyond 2020 was approved last week by the White House. The 15-year-old station, operated by a partnership of 14 nations including Canada, Russia, and Japan, was originally set to be decommissioned in 2016. It’s unclear whether the partner countries will join the United States in funding it through 2024.

Science LIVE

Join us on Thursday, 23 January, at 3 p.m. EST for a live chat with experts on a hot topic in science. <http://scim.ag/science-live>

Random Sample

The Unlikely Link Between Federer and Marsupials

Robbie Wilson, a performance biologist at the University of Queensland in Australia, thinks we're too obsessed with record-setting feats. Although it is tempting to focus on just how fast an animal can run, or how high it can jump, such "peak" performances can obscure a more important ecological issue: the trade-offs that shape an organism's *optimal* performance. Gathering the data needed to quantify optimal performance in nature is difficult, however, so Wilson's team turned to a more easily observed ecosystem: the 2013 Australian Open Tennis Championship. (This year's tourney began on 13 January.) They analyzed some 13,000 serves to find the optimal strategy for winning a point. For most players, accuracy dropped off sharply as speed increased, so players who delivered first serves at about 90% of their peak speed, and second serves at 75%, tended to maximize points, he reported last week at the annual meeting of the Society for Integrative and Comparative Biology in Austin.

Now, Wilson and his colleagues are trying to apply such concepts to performance trade-offs among quolls, endangered carnivorous marsupials. By analyzing how the creatures run and turn, for instance, they're hoping to tease out how certain human activities, such as mining, might be influencing their fitness. But Frank Fish, a biomechanicist at West Chester University in Pennsylvania, says there are limits to what tennis can teach us about wild creatures. Tennis players get a second serve should they miss the first one, Fish notes, but "there's no do-over" in nature.



civil liberties groups worry that the anonymity of the data cannot be guaranteed.

This month, the government will send a leaflet to all 22 million U.K. households explaining the data-sharing and telling people how to opt out. But the charities behind the new ads, including Arthritis Research UK, Cancer Research UK, Diabetes UK, the British Heart Foundation, and the Wellcome Trust, are hoping that not too many will take that option. http://scim.ag/_share

NEWSMAKERS

Agency Veteran Tapped To Head USGS



President Barack Obama has nominated coastal geologist **Suzette Kimball**, the acting head of the U.S. Geological Survey (USGS), to become the \$1 billion agency's permanent director. If

confirmed by the Senate, Kimball would be "the first director in 20 years to come from within" the agency, notes Charles "Chip" Groat, who led USGS from 1998 to 2005. She's an "excellent choice," adds Mark Myers, USGS director from 2006 to 2009. "She is a skilled scientist, very good communicator and talented manager."

Kimball joined the agency in 1998 after stints with the National Park Service, the College of William & Mary in Virginia, and the U.S. Army Corps of Engineers. She earned a Ph.D. in the environmental sciences from the University of Virginia in Charlottesville, specializing in the processes that shape coastal zones. Kimball would succeed Marcia McNutt, who resigned in February 2013 and is now editor of *Science*. http://scim.ag/_Kimball

FINDINGS

Parasite Quells Locusts' Urge to Swarm

What turns a single, harmless locust into an apocalyptic, crop-destroying swarm? Scientists know that pheromones in a locust's feces signal neighbors to assemble by the billions. But new research shows how a gut parasite can disrupt this signal, potentially sparing crops.

In 2004, entomologist Wangpeng Shi of China Agricultural University in Beijing noticed that migratory locusts infected by the sporing microbe *Paranosema locustae* were less likely to swarm than their healthy counterparts.

To explore this effect, Shi and colleagues placed healthy locusts in chambers containing infected locust droppings. Sure enough, the exposed locusts were significantly less likely to swarm than those exposed to scat from uninfected locusts, the researchers report this week in the *Proceedings of the National Academy of Sciences*.

The infected feces contained fewer swarm-inducing pheromones, and a look into the locusts' guts revealed why: The parasite acidifies its host's intestines, subduing the bacteria responsible for creating the pheromones. Countries fighting locust infestations could one day replicate *P. locustae*'s swarm-stopping tricks, the researchers say. http://scim.ag/_swarms





Countdown to zero. Children in South Sudan, one of the last strongholds of the guinea worm, use pipe filters to protect themselves from larvae in drinking water.

INFECTIOUS DISEASES

Guinea Worm Eradication at Risk in South Sudanese War

It was supposed to be a day of hope for the world's youngest country—and for global health. Next week, former U.S. President Jimmy Carter was scheduled to travel to the South Sudanese capital Juba and announce that the world is now closer than ever to eradicating guinea worm disease. In all of 2013, only 149 people, in just four African countries, suffered from the painful, debilitating infection, according to the provisional figures that Carter was due to announce. South Sudan, an impoverished country that split off from Sudan in 2011 after decades of civil war, is the main remaining stronghold, with 114 cases; but even that number is down 78% compared with 2012.

But now that progress is in peril. In December, violence erupted between rebels and the South Sudanese government, leading the Carter Center in Atlanta, in charge of the 3-decade fight against the guinea worm, to evacuate its expat staff of more than 30 people and cancel the Juba meeting. If the violence continues and spreads, it could wipe out recent progress in South Sudan and the region. “The potential for a serious setback is there,” says Donald Hopkins, the center’s vice

president for health programs.

Guinea worm disease, also known as dracunculiasis, is caused by a roundworm called *Dracunculus medinensis*. People become infected by drinking water containing copepods—tiny crustaceans—carrying the worm’s larvae; after developing inside the human body for a year, the mature worm emerges from the skin, usually at the foot, causing an intense burning sensation that sufferers often relieve by plunging the foot into a pond or pool—which can start the cycle anew.

The campaign to eradicate the guinea worm relies solely on simple measures such as providing clean drinking water through wells and filtration and preventing

people with known or suspected infections from setting foot in reservoirs. Yet it has been tremendously successful; the current case numbers are down from an estimated 3.5 million in 20 countries, including India, Pakistan, and Yemen, in the mid-1980s.

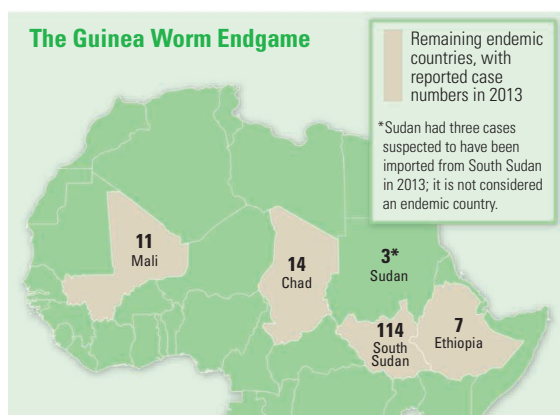
But recent fighting between forces loyal to South Sudan’s president, Salva Kiir, and rebels headed by former Vice President Riek Machar has created tens of thousands of refugees and disrupted public health efforts. Fortunately, the war broke out during the annual lull in cases, reducing the risk of spread, says Gautam Biswas, team leader for guinea worm eradication at the World Health Organization in Geneva. Most cases are also in the far southeast of the country, which has been spared from violence. Even if fighting continues, containment operations already done in 2013 should pay off in another sharp drop in cases in 2014, Hopkins says.

The big question is whether the campaign can find the 2014 cases and contain them before they trigger a new wave; a single uncontrolled guinea worm case can give rise to dozens of new infections. “We need a cease-fire and peace quickly,” Hopkins says.

South Sudan isn’t the only worry. The campaign hasn’t had access to rebel-controlled areas in northern Mali for some time, and surveillance there is inadequate; the country may have had more than the 11 cases reported in 2013. In Chad, meanwhile, the disease now follows a “very peculiar epidemiological pattern” that defies existing control methods, says Mark Eberhard, a senior microbiologist at the Centers for Disease Control and Prevention in Atlanta. Instead of clusters around a contaminated water source, epidemiologists found 14 scattered cases in villages along the Chari River in 2013; in another unusual twist, dogs have become infected, too.

Both humans and dogs may contract the disease from fish that have eaten infected copepods, Eberhard says. Why this is happening only now, and apparently only in Chad, “we have absolutely no idea,” he adds. Genomic studies have not shown any evidence of changes in the worm. But it may mean that people in Chad need to take extra control measures, such as thoroughly cooking fish, Eberhard says, to stamp out this latest turn of the worm.

—MARTIN ENSERINK



U.S. SPENDING

Final 2014 Budget Helps Science Agencies Rebound

The ghost of former President George W. Bush permeates the 2014 budget that Congress was expected to approve this week. His presence is good news for physical scientists, but less cheery for biomedical researchers.

On 10 December, legislators had struck a spending deal that eased the pain of the across-the-board cuts known as sequestration. It called for \$1.012 trillion in 2014 discretionary spending, some \$44 billion more than would have been available under a 2011 agreement that called for reducing the federal deficit by a trillion dollars over the next decade. But it took until 13 January for lawmakers to decide how to divvy up the money.

For agencies that provide major support for the physical sciences, the new budget represents a healthy boost over 2013 spending levels, which were depressed by the sequester's 5% bite. The National Science Foundation (NSF) will receive \$7.17 billion, an increase of 4.2%, for example, and NASA's science programs will get \$5.15 billion, a 7.7% jump. The Department of Energy's (DOE's) Office of Science enjoys a 9.7% increase, to \$5.07 billion, and DOE's Advanced Research Projects Agency-Energy gets an 11.2% boost to \$280 million. The National Institutes of Standards and Technology will see its budget grow 10.4%, to \$850 million.

Except for NASA, those agencies were all part of a 2006 initiative launched by the Bush administration to increase funding for the physical sciences. Congress formalized the idea in a 2007 law, the America COMPETES Act. Although agencies never received the generous funding called for by COMPETES, its message appears to have survived: The physical sciences need to be boosted to help the U.S. economy remain strong. President Barack Obama has continued that theme in his budget requests,

including last spring's bid for big boosts at several agencies (see table).

COMPETES did not cover the National Institutes of Health (NIH), whose budget had doubled between 1998 and 2004, to \$27.2 billion. Since then, it has received much smaller boosts—with the huge exception of the 2009 stimulus, a one-time boost of \$10.4 billion. Congress maintained that pattern

budget sequester and ensure the nation's biomedical research enterprise makes continued progress," says Carrie Wolinetz of United for Medical Research, a coalition of academic and industry groups.

The final spending plan wraps up 12 individual appropriation bills into a 1582-page package that, despite the absence of actual earmarks, is stuffed with provisions

addressing the concerns of individual legislators. For example, NASA is asked to carve out \$80 million from its science budget to develop plans for a mission to Jupiter's moon Europa. NSF is told that several major new facilities already under construction should get priority, leaving its only requested new start, the Large Synoptic Survey Telescope, with only about half of what NSF requested. In a rare display of support in these tight fiscal times, lawmakers also fully funded the president's request for two NSF activities—the international ocean drilling program and the Noyce scholars program to train science teachers.

Lawmakers also showed their support for the domestic fusion science program at DOE. They rejected proposed cuts to several domestic facilities, and told DOE it could spend only \$22 million of its planned \$200 million contribution to ITER, an international fusion test reactor under construction in France, until ITER puts its financial house in order.

Another portion of the massive bill orders NIH to reopen a tiny science education office it had shuttered last fall and resume generating lesson

plans for teachers and museums based on new medical research. Those activities were shut down last spring at the same time Obama proposed a major reorganization of federal science education programs. But Congress has rejected the plan and now told NIH to resume its precollege education activities.

—JEFFREY MERVIS

How the Science Agencies Will Fare in 2014 (\$ Billions)

Agency or program	2013	2014 request	2014 actual
National Institutes of Health	28.92	31.10	29.93
National Science Foundation	6.884	7.626	7.172
Research	5.543	6.213	5.809
Education	0.833	0.880	0.846
DOE Office of Science	4.621	5.153	5.071
Advanced Research Projects Agency-Energy	0.252	0.379	0.280
National Institute of Standards and Technology	0.769	0.928	0.850
Science and technology labs	0.580	0.694	0.651
Census Bureau	0.905	0.982	0.945
U.S. Geological Survey	1.012	1.167	1.032
NASA	16.9	17.7	17.6
Science office	4.78	5.02	5.15
Agricultural Research Service	1.019	1.303	1.123
National Institute of Food and Agriculture	0.656	0.801	0.772
Agriculture and Food Research Initiative	0.276	0.383	0.316
NOAA Office of Oceanic and Atmospheric Research	0.336	0.472	0.416

of smaller increases this year: NIH's 2014 budget will rise by 3.5%, to \$29.9 billion.

"It's hard not to be pleased with a billion-dollar increase," says David Moore of the Association of American Medical Colleges. But some biomedical lobbyists remain disappointed. It "won't adequately reverse the damage done by last year's

AIR POLLUTION

Ammonia Pollution From Farming May Exact Hefty Health Costs

If the U.S. trade balance has a bright spot, it's farming. The value of agricultural exports has doubled over the past decade, driven largely by demand from China and other developing countries. But when ships packed with corn, wheat, and pork depart for foreign ports, many kinds of pollution are left behind. One is ammonia, which wafts into the atmosphere from fertilizer used on fields and from urine and manure produced by livestock. Ammonia reacts with other air pollutants to create tiny particles that can lodge deep in the lungs, causing asthma attacks, bronchitis, and heart attacks.

A new analysis suggests that ammonia does even more health damage in the United States than was thought. The annual cost—associated with thousands of premature deaths—may even exceed the profit reaped by farmers. Some analysts say the startling numbers highlight the need for greater U.S. regulation of agricultural emissions and a review of farm subsidies. If the pollution caused by farming “makes us worse off,

An extensive study of the burgeoning hog farm industry in North Carolina, completed in 2003, found that ammonia-related $PM_{2.5}$ exacted higher health costs than other farm pollutants. “It was striking,” says C. M. Williams of North Carolina State University in Raleigh, who led the study. Other researchers have calculated that the average U.S. health cost of ammonia ranges from \$10 to \$73 per kilogram.

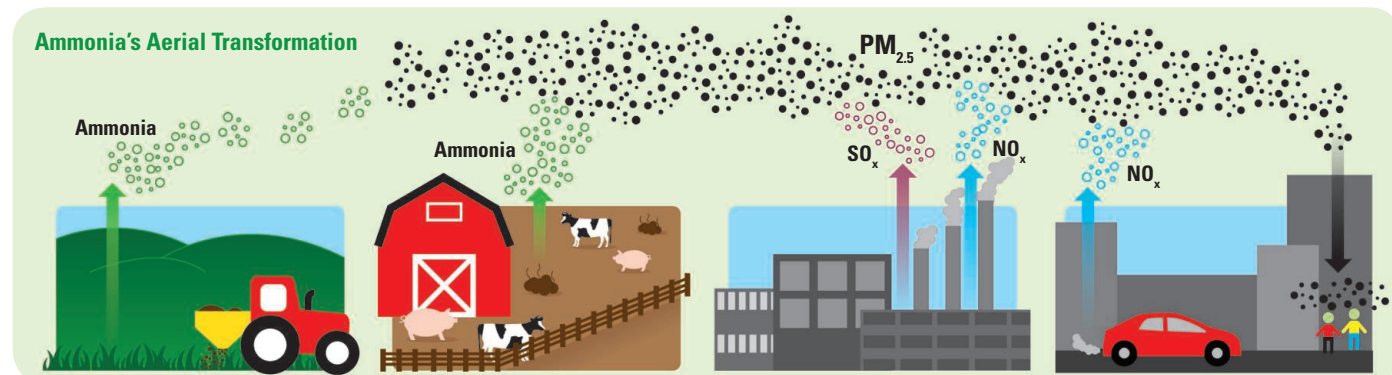
To fine-tune such estimates, Fabien Paulot and Daniel Jacob, atmospheric chemists at Harvard University, developed a new model of where and when ammonia is emitted from farming activities. This model is coupled to another, which accounts for temperature, humidity, and abundance of NO_x and SO_x . “It is a step forward over much of the modeling that’s been done before,” says air quality modeler Daven Henze of the University of Colorado, Boulder.

Paulot and Jacob used their model to calculate how much ammonia and $PM_{2.5}$ is a result of the food that the United States

Some experts are skeptical of those numbers, pointing out that the new air pollution model has not yet been peer-reviewed and that the health effects of various $PM_{2.5}$ chemistries are still uncertain. “Ammonia emissions do not appear to be a driver of toxicity,” says Kathy Mathers of the Fertilizer Institute in Washington, D.C. But Nicholas Muller, an economist at Middlebury College in Vermont, fears that farm-related health costs may in fact be even higher if other farm-related air pollutants are included, such as $PM_{2.5}$ from diesel engines. “This study provides more evidence that, in certain cases, more stringent controls are likely justified,” Muller says.

So far, U.S. regulators have neglected ammonia emissions because it has been cheaper and easier to choke off sources of SO_x and NO_x , such as power plants. As a result, states in the heavily populated northeastern United States are already in compliance with EPA limits for $PM_{2.5}$, even though they are downwind of many power plants. But these states are also downwind of major farming areas. If the $PM_{2.5}$ standards are tightened, which is under discussion, ammonia may be regulators’ next target.

The biggest gains could be made by keeping livestock and dairy operations



it doesn't make any sense,” says Robert Mendelsohn, an economist at Yale University. “Ammonia may be the next big frontier in public health protection,” says Paul Miller, chief scientist of Northeast States for Coordinated Air Use Management, an association of air quality agencies, in Boston.

Ammonia enters the air mostly from agriculture, although it can also come from vehicles and wildfires. Emissions are growing worldwide and are largely unregulated. When molecules of ammonia react with oxides of nitrogen or sulfur (NO_x or SO_x) created by burning fossil fuels, they turn into particulate matter less than 2.5 microns wide ($PM_{2.5}$)—the most dangerous kind, for which there is no known safe level.

exports. Next, they used equations developed by the U.S. Environmental Protection Agency (EPA) to calculate the health impact and associated economic costs (calculated by asking people how much they would pay to reduce the risk of premature death). About 5100 people die prematurely each year from $PM_{2.5}$ exposure associated with the emissions, they reported online on 25 December in *Environmental Science & Technology*. Although the health toll varies greatly by location, the burden is heaviest in cities, because of the concentration of NO_x and people. And the total impact is eye-opening: about \$100 per kilogram of ammonia, or \$36 billion annually. In contrast, the net value of the exported food is \$23.5 billion.

Dangerous reaction. Ammonia (green) reacts with sulfur (red) and nitrogen (blue) oxides to produce tiny, dangerous particles.

away from cities. Best management practices can also reduce losses from fertilizer and livestock. In North Carolina, Williams says he's encouraged that many hog farmers are thinking about generating power from manure, which could reduce ammonia emissions. Other research is investigating how to capture ammonia for use as fertilizer. But with U.S. exports of pork to Asia continuing to rise, it may be a while before emissions in North Carolina and elsewhere start to head down.

—ERIK STOKSTAD



Zombie ant. A fungus infecting this ant caused it to bite down on the underside of a leaf and die while the fungus grows and shed spores.

ECOLOGY

Parasitic Puppeteers Begin To Yield Their Secrets

AUSTIN—Shelley Adamo just wanted to scare a few crickets. But when she caged them with cricket-eating lizards to see how stress would affect the insects' immune systems, something unexpected happened. The crickets caught a virus from the lizards, and it made them curiously frisky. Males mated with females more eagerly than before—a behavior that benefits the virus by enabling it to spread. Adamo proposed here last week at the annual meeting of the Society for Integrative and Comparative Biology (SICB).

With her results, Adamo, an eco-immunologist at Dalhousie University in Halifax, Canada, has added to a growing catalog of parasites—in this case, a virus—that manipulate the behavior of their hosts to improve their chances for survival and spread. Killifish infected with a certain flatworm flash their sides in the sun, attracting fish-eating herons and enabling the parasite to enter the avian stage of its life. Cockroaches stung by a parasitic wasp become enslaved, with the wasp guiding them to a burrow to be eaten alive by its young. And rats infected by the protozoan *Toxoplasma gondii* become less afraid of cats, the mammal in which the parasite actually reproduces. “We keep seeing new ways by which manipulation takes place,” says Brian Fredensborg, a parasitologist at the University of Copenhagen who studies the behavior-bending abilities of parasitic worms called helminths.

Now, Adamo, Fredensborg, and others are trying to understand just how these parasites seize control of their hosts' brains. “We’ve gone from a stage of ‘now we’ve found [manipulation] in this host system’ to [having] a lot more focus on

the mechanisms,” Fredensborg says. “But there’s a lot we don’t know.”

Adamo found that in infected crickets, the virus overruns the fat body, the organ that makes most of the insect's proteins, stores other nutrients, and mounts immune responses. She and her colleagues found a sheen of viral particles covering the fat body, indicating that it had become a viral production center. As a result, it could no longer make the proteins and other molecules needed for healthy reproductive organs, cutting off egg production in infected females and damaging sperm in males. “They are reproductively dead,” she reported. Yet both sexes are sexually active, with males initiating courtship twice as fast as normal males do.

Adamo is now hoping to identify the parasite's molecular signals responsible for the revved-up sexual behavior—and for countering the appetite-killing, lethargy-inducing inflammatory molecules typically produced by infected creatures. Suppressing the effects of those latter signals, she suggests, may be a universal trait of sexually transmitted parasites.

Charissa de Bekker, a postdoc at Pennsylvania State University (Penn State), University Park, has begun to pinpoint the molecules behind another manipulative parasite—*Ophiocordyceps unilateralis*, a fungus that infects carpenter ants. It eventually causes an ant to leave its colony, climb a tree, chomp down on a twig or the underside of a leaf and die, freeing fungal spores to fall onto the ground, where they can reinfect new ants. Darwin's contemporary, Alfred Russel Wallace, described this fungus growing out of ants' heads in the mid-1800s,

but not until 2009 did David Hughes, a Penn State behavioral ecologist, document the suicidal behavior it caused.

Learning how the fungus takes control has not been easy. De Bekker reported at the meeting. First, she had to figure out how to grow the fungus and its relatives in the lab. She also had to culture two ant tissues affected by the fungus—brain and muscle—expose each to fungus, and analyze what compounds the parasite subsequently secretes.

To figure out which of those compounds manipulate the ants' behavior, she and Hughes compared the array of molecules secreted by the fungus in ant species that are resistant to the parasite's manipulations with those secreted in susceptible ant species. About 70% of the fungal proteins and other metabolites can be found only in the suicidal ants, she reported, suggesting they are key to turning the ants into zombies.

Using mass spectrometry, she identified several possible mind-controlling molecules. One, sphingosine, is a component of neuronal signaling molecules and thus may influence the ant's nervous system, De Bekker suggests. Another fungal product, γ -guanidinobutyric acid, was linked to lethal mushroom poisonings in China.

De Bekker, Hughes, and their colleagues are also beginning to examine how fungal gene activity changes throughout the course of infection. When the fungus first infects the ant, the ant lives normally. Gradually, the fungus grows, displacing ever more of the brain, perhaps with the help of sphingosine—a similar fungal toxin degrades brain tissue in horses—and finally causing the suicidal behavior.

Some researchers are skeptical that such behavioral changes actually benefit the parasites that cause them, saying the evidence isn't definitive and the mechanisms are unclear. That will change, though it will take time, says Kelly Weinersmith, a parasitologist at the University of California, Davis. “You find a lot of things . . . and it's probably a lot of mechanisms [operating] at once.”

And those attending the SICB session say there are now too many examples to dismiss the role of parasites in animal behavior. “What's become apparent is that parasites change how animals interact and how they are distributed,” says Janice Moore, a behavioral biologist at Colorado State University, Fort Collins. “This is too big to scoop under the rug.”

—ELIZABETH PENNISI

CREDIT: DAVID HUGHES

ASTRONOMY

Star-Crossing Planets Literally Strut Their Stuff

WASHINGTON, D.C.—When exoplanet hunters announced last week that they had found a tribe of “mini-Neptunes” and the lightest planet ever detected outside our solar system, they highlighted more than just the diversity of exoplanets. The results, announced here at a meeting of the American Astronomical Society, also show the power of an up-and-coming method of calculating the masses of alien worlds from the way they eclipse their stars.

The new technique, called transit timing variation (TTV), is enabling astronomers to fill out their picture of dozens of exoplanets detected by NASA’s Kepler spacecraft. The eclipses, or “transits,” that Kepler detected reveal only a planet’s size and orbital period. To know whether it is rocky, gaseous, or some mixture of the two, astronomers also need its mass. Traditionally, they have resorted to ground-based telescopes to determine it, by measuring the wobble of the star as the planet tugs on it. But TTV can determine masses from transit data alone.

“We’ve entered the age of TTVs,” says David Kipping, an astronomer at the Harvard-Smithsonian Center for Astrophysics in Cambridge, Massachusetts, who announced the lightweight planet, known as KOI-314c. “When we find Earth 2.0, our best bet for getting the mass—which is crucial to understand if the planet is truly Earth 2.0—is through transit timing variation.”

The technique was the brainchild of Matthew Holman, an astrophysicist at Harvard University, and others. If two or more planets happened to be orbiting a star in close proximity, they reasoned, their gravitational tugs on each other would alter their orbital periods. If one of them was a transiting planet—dimming the light of its parent star as it passed between the star and Earth—astronomers would see its transit timing vary over multiple orbits, betraying the presence of a companion planet. If *both* planets were transiting, astronomers could measure the perturbations in both their orbits and work out the planets’ masses.

Holman and a colleague published the idea in 2005, and Eric Agol of the

University of Washington, Seattle, and colleagues put forward a similar scheme almost simultaneously. For years afterward, however, astronomers failed to detect transit timing variations because almost all known exoplanets were gas giants spinning around their stars in tight orbits. Theorists think such planets formed farther from the star and later barreled inward, clearing away any potential wobble-inducing companions.

The technique became practical thanks to the Kepler spacecraft, which until 2013 was monitoring the brightness of 160,000 nearby stars for the telltale dimming due to transiting planets (*Science*, 3 May 2013,

each other,” Kipping says. “It was obvious that these two planets must be interacting.”

By simulating the dance on a computer, the researchers worked out the masses of the two planets. They found that the outer planet, KOI-314c, which orbits the star every 23 days, has the same mass as Earth, although it is about 60% larger than Earth in radius. Kipping and his colleagues infer that the planet—the lightest exoplanet so far discovered—has a rocky core and a thick, gaseous atmosphere. The inner planet, KOI-314b, is similar in size but about four times as massive.

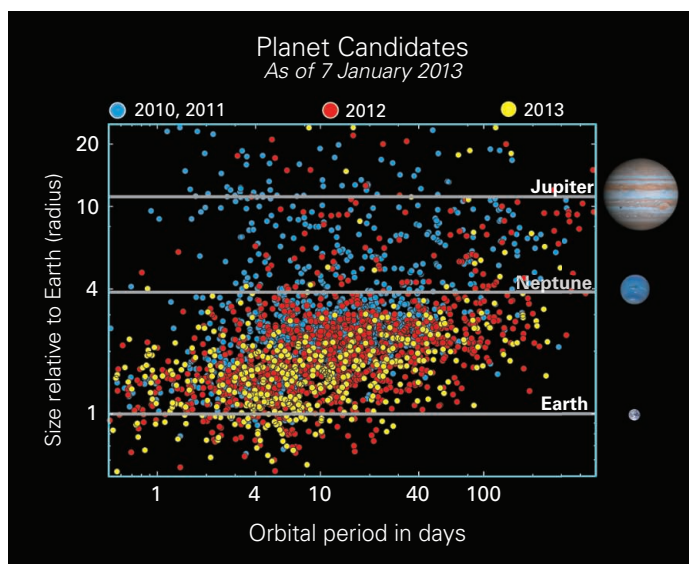
Meanwhile, researchers led by Yoram Lithwick, an astronomer at Northwestern University in Evanston, Illinois, were looking at the TTV signatures of 163 exoplanets found by Kepler. The team determined that about 60 of them occupy a mass range between Earth and Neptune and are larger than expected for a rocky planet of that mass, suggesting they are blanketed by thick, extended atmospheres. They also found a pattern: As the planets grew bigger in radius, their density declined. “If you make something twice as big, it becomes four times less dense,” Lithwick says. “So from going from a less than two Earth radii to four Earth radii, the density goes from rock-like all the way to gas.” Lithwick predicts the surprising finding “will

have big implications for understanding planet formation.”

The best thing about TTV, Kipping notes, is that it can be teased out from the Kepler data itself. It can also find masses of planets too far from the star to make it wobble detectably—as an Earth-like planet in the habitable zone of a sunlike star would be. “The beauty of the transit timing variation technique is that it doesn’t really matter how far away from the star it is,” Kipping says.

“I wouldn’t have expected that TTVs could yield the kind of precision that we are seeing,” says Harvard’s Holman. The surprisingly high quality of Kepler’s data, as well as nature’s generosity in packing the universe with multiplanet systems, made all the difference.

—YUDHIJIT BHATTACHARJEE



Worlds galore. Kepler’s later discoveries included many small, close-in exoplanet candidates—a rich hunting ground for transit studies.

pp. 542 and 566). Kepler began delivering data on dozens of planetary systems, many of them consisting of multiple planets. In 2010, astronomers began making TTV detections. Their expertise has been growing ever since.

Kipping and his colleagues came across KOI-314c while combing Kepler data for TTV signatures due to exomoons, which should cause transiting exoplanets to wobble and change their transit timing. But the transits seen around the star KOI-314, a red dwarf some 200 light-years from Earth, pointed instead to the presence of two planets. Their transit times were varying in lockstep: When one planet slowed down in its orbit around the star, the other would speed up, and vice versa. “We saw the same TTV signature, just in opposite phase to



Gut Instinct

Do bacteria in the guts of African hunter-gatherers hold the key to a healthier life? An American anthropologist plans to find out

MANG'OLA, TANZANIA—Jeff Leach hasn't showered in a month. Living in a small dome tent close to Lake Eyasi in northern Tanzania, he stopped washing one day because he wants to know how that will change the microbial populations in and on his body. Leach is taking daily samples of his own stool and skin, which he carefully stores in a liquid nitrogen tank until they can be shipped to the United States.

Later this month, the 46-year-old graduate student at the London School of Hygiene & Tropical Medicine (LSHTM) will also adopt the lifestyle of the local people here. He will

sleep in their open grass huts, eat their food, and share their tools, to see if his gut flora become more like theirs.

Leach, who obtained a Ph.D. in anthropology in 2005, is studying the Hadza, one of the last true African hunter-gatherer communities, because he thinks their gut microbes may hold clues to improving human health worldwide. The Hadza's lifestyle is thought to resemble that of early humans; they also seem to suffer far less from "modern" diseases, such as diabetes, cancer, and cardiovascular problems.

Leach believes there is a connection. An

increasing body of evidence has shown that gut microbes regulate their hosts' immune systems and assist them by eliminating dangerous bacteria, and several studies have linked changes in microbial populations to specific illnesses. The Hadza's close contact with the vast diversity of microbes in soil, water, and wild food may somehow help protect them, he says—and he plans to spend two full years living here to sample microbial diversity in the people and their environment. His own experiment in Hadza living, which will last a month, will test whether the microbial ecology of a Texan apartment dweller can shift to that of an African hunter-gatherer.

Some scientists are skeptical of the premise. They don't believe our ancestors had such healthy lifestyles or that modern-day Hadza are models of health—and even if they are, their gut microbes may have little to do with it. But many agree that the Hadza project will offer new insights into the complex relationship between humans and their microbiota and that Leach's roots in anthropology make him the right man for this study. "With his unique background and perspective, Jeff sheds light on questions that I have been thinking of, but haven't had an avenue to pursue," says Justin Sonnenburg of Stanford University in Palo Alto, California, one of many microbiologists who will study his samples.

Sterile environment

Leach's motivation is highly personal. Eleven years ago, at age 2, his daughter was diagnosed with type 1 diabetes. After digging through the literature and contacting leading scientists, Leach came to the conclusion that, in addition to a genetic predisposition, a lack of contact with bacteria caused her disease. Leach's daughter was delivered through a cesarean section, which prevented her from being exposed to the maternal bacteria that most babies encounter in the birth canal. She was breast-fed for a few months instead of the 2 years or more seen in traditional societies, and grew up in a rather sterile suburban U.S. home dominated by antimicrobial soaps and chlorine-wiped tables.

This led to an imbalance in her gut microbiota, Leach says, which caused the gut to become inflamed and leaky; that allowed bacterial products to enter the bloodstream and inflame insulin-producing cells in the pancreas, which were then attacked and

Online

sciencemag.org

Podcast with author Jop de Vrieze and slideshow (http://scim.ag/med_6168).

destroyed by immune cells. (Several recent studies support this hypothesis.) “Realizing there was a causal relationship between my daughter’s health and the environment my ex-wife and I had created made me feel guilty and angry,” he says.

It motivated him to drop his studies of ancient cooking techniques and focus on a crucial question: How can we rebalance our microbiota to improve health? In 2011, Leach enrolled at LSHTM to obtain a master’s and a Ph.D. in microbiology; a year later, he co-founded the American Gut project, which maps the gut microbiota of thousands of people in the United States.

His Tanzania study is the first to compare lifestyle and microbiota in pure hunter-gatherers with those of Westerners. Previous studies have looked at rural and traditional people in Burkina Faso and Malawi and at several Amerindian communities, but the subjects all practiced agriculture or ate farm products. The Hadza don’t have cattle and don’t grow crops; their diet varies seasonally and consists of fresh game, baobab fruits, berries, tubers, and honey.

On a sweltering day in late October, Leach drives his Land Cruiser through arid terrain dominated by baobab, acacia trees, and small bushes, on his way to a settlement called Kipamba. The day before, he had provided about 40 villagers with plastic tubes and, with the help of his local translator, instructed them how to collect about a tablespoon of their stool in the morning. At our arrival, a young English-speaking boy leads us to a place close to the village where the subjects have gathered.



Ready to ship. Leach collects fecal samples from the Hadza and has them studied at U.S. labs.

Leach sets up a table and three chairs, a scale, and a measuring stick. One by one, the men, women, and children hand in their tubes. Leach swabs their right hand for a skin sample, and two local assistants fill out a short diet questionnaire for each subject and measure basic body characteristics such as height and weight. Then Leach takes a series of samples from the environment: drinking water, tubers, animal stool, honeycombs, and fresh meat.

On our arrival, the boy had warned us not

to go into the village. “A group of men has been drinking since dawn,” he said. The warning reflects a reality in the 21st century Hadza community: Not all its members are exclusive hunter-gatherers anymore. Some 200 Hadza—mostly those living higher up in the hills—practice the “pure” lifestyle most consistently, Leach says. The 900 or so people living closer to the nearest town, Mang’ola, are leading more Western lives; many have cell phones and regularly consume maize and alcohol. Sodas and snacks are for sale in town.

Leach sees this as an opportunity rather than a problem. By sampling subgroups, he hopes to see reflections of the transitions our ancestors went through, from hunter-gatherer communities to basic agriculture and small-scale farming, and eventually to high-sugar, high-fat Western diets and life in a built environment. The Hadza, who have been studied extensively by Western scientists for more than a century, are happy to help Leach, whom they call Dr. Mavi, which is Swahili for Dr. Shit.

Like other scientists before him, Leach is aware that he’s bringing change to the very lifestyle he’s studying. The Hadza seek benefits from their participation, such as knives, clothes, and, increasingly, money. Leach refuses to pay them directly but makes contributions to community funds for emergency care and education.

That night, as he sits by a fire at his camp and sips cheap scotch from a coffee mug, Leach talks incessantly about the Hadza’s eating habits. Their average daily fiber intake is 75 to 100 grams, seven times the U.S. average, mostly from pulp and seeds of baobab fruits. Gut microbes turn these fibers into short-chain fatty acids that nurture intestinal cells and increase the acidity of the colon, he says, which has been shown to thwart opportunistic pathogens. He describes how the Hadza occasionally gorge on meat from a fresh kill, and the huge amounts of honey they eat when it’s plentiful during the wet months of February, March, and April. “From a registered nutritionist perspective, the diet makes no sense,” Leach says. “Yet it does not seem to harm them at all.”

Dying from other causes

Underlying Leach’s research is the assumption that, in their lifestyle and diet, these modern-day hunter-gatherers are as close to humani-



Sweet tooth. The Hadza, a hunter-gatherer community in northern Tanzania, often gorge on honey in the wet season.

ty’s ancestors as we can hope to get and that they may be healthier because of the way they live. Modern-day humans, in this view, have strayed far from these ancient eating habits and microbes, and our bodies haven’t had the time to adapt.

Not everyone accepts this picture. Humans haven’t stopped evolving since they took up agriculture and settled down some 9000 years ago, says evolutionary biologist Marlene Zuk, the author of the 2013 book *Paleofantasy*, a sharp attack on the idea that we should emulate our forefathers. European farmers, for instance, evolved lactose tolerance, enabling them to digest cow milk.

Yale University anthropologist Brian Wood, who has studied Hadza health and demography, is also skeptical that the Hadza enjoy rude health. “It seems like they have less cancer and cardiovascular disease than we do, but we do not have good data to evaluate the actual incidence,” he says. In any case, he notes, accidents, malaria, tuberculosis, and other diseases limit the Hadza’s life expectancy at birth to only 34 years, too short for cancer and heart disease to be significant killers. If the Hadza really are healthier than, say, the

CREDITS: JEFF LEACH



Meat and microbes. After killing a kudu, Hadza hunters eat raw meat and rub the content of the animal's stomach—including billions of bacteria—on their arms.



average German or American, Wood says there's an explanation that has little to do with microbes: His own research has shown that they eat far fewer calories and are much leaner than Westerners.

As a result, says anthropologist Herman Pontzer of the City University of New York's Hunter College, the Hadza lifestyle can't be translated into health recommendations. Leach agrees, but says the research can still tell us a lot about the interaction between humans and microbes before the modern era. "We do not regard the Hadza as a disease-free society," he says. What he's most interested in, he says, is "their microbes, their origin, and their interaction with the body. How do these people assemble their microbiota?"

The real payoff of Leach's research, Pontzer says, could be to show how ancient habits affected the microbiome. "Seasonality in diet and lifestyle is a universal thing that modern societies dropped," Pontzer says. "The high fiber consumption is likely to have been universal, too. The same for the intimate relationship with environmental microbes."

Dream team

The next day, during a visit to another Hadza community, Leach points to a man who is sharpening his arrows for a hunt. "He's the perfect guy for our study," he says. "Born vaginally, breast-fed for 2.5 years, has not had malaria or any Western medication, has never

been to town. His shit will probably end up in a germ-free mouse."

Leach is referring to the fate of his samples: Sonnenburg and his colleagues will infuse stool from Hadza people into the guts of mice that have been born in a sterile environment, allowing the researchers to test the effects of specific microbial communities. They will compare the animals' physiology and metabolism with those of mice colonized by the microbes in Western poop.

Leach says he's "not a lab rat"; he relies on what Sonnenburg calls a "dream team" of collaborators to carry out most of the analyses. Labs in Colorado and Chicago will do basic taxonomical and functional analyses. Rob Knight at the University of Colorado, Boulder, and Jose Clemente of Mount Sinai Hospital in New York City will compare the Hadza data with American groups, including people following paleo diets, also known as "caveman diets." Other researchers will use germ-free mice to test the hypothesis that gut microbes help Hadza women, normally quite skinny, put on fat during pregnancy.

The comparison between pure hunter-gatherers and more westernized Hadza will be done by Maria Dominguez-Bello of New York University in New York City, who also wants to compare the Hadza with Amerindians in

South America, who have a far more diverse gut flora than U.S. residents. Traditional Africans should have the highest microbial diversity of all, she says, because other populations probably lost species as they went through evolutionary bottlenecks. "I am interested in the disappearance of these microbes," she says. "Have we lost functions?"

Scientists think that people in modern societies have so little exposure to microbes in the environment that their diets largely determine the composition of their gut microbiota. But in the Hadza, exposure to a daily microbial bombardment from the environment may override any impact of the food, Leach hypothesizes—and he hopes to test that. "Hadza men eat more meat and less plant foods than women," he says. "If their microbiota turn out to be similar, the environment is the great equalizer."

Just how intense that exposure can be becomes clear the next day, when Leach receives news that Hadza hunters have killed

a huge female kudu, a great antelope, with their poison arrows. One of the men slits the animal's throat. Then they cut open its belly, blood spilling everywhere. The men take out the stomach and intestines and hang them in a nearby tree. They cut out the ribs and chew on the raw flesh. Leach starts taking swabs of the men's hands and their prey.

Next, the men take the stomach, cut it open, and start rubbing its content all over their arms to wash off the sticky blood. As they do so, Leach explains, the hunters are transferring billions of bacteria to their skin. They cut the stomach in pieces and eat it; then they squeeze the green, fibrous content from the intestines, another rich source of microbes, and eat them, too, still screaming with excitement. The rest of the meat is stripped from the carcass and given to men arriving from other villages.

Tonight, men and women in several Hadza camps will be eating meat. As they hand each other the pieces, they will be passing on many strains of microbes as well—just as they swap bacteria from honeycombs, tubers, berries, and drinking water. This "social network of humans and their microbes," as he calls it, may be the most important thing missing from Westerners' disinfected lives, Leach says—and it's the one thing he failed to provide for his daughter.

—JOP DE VRIEZE



The Second Act

After his first turn on the world stage ended in scandal, Woo Suk Hwang has quietly rebuilt his scientific career

SEOUL—Watching a pair of German shepherd puppies frolic on the lawn of a research institute, Chang Hyun Choi likes what he sees. Few puppies from breeders have the temperament and trainability required in a police dog, says Choi, an officer with the police canine unit in the city of Busan. The look-alike pups scampering about may well have the right stuff to sniff for bombs and track down missing people: They are clones of one of the country's top police dogs. With clones, Choi says, "there is less chance of rejection" during training. Before driving off, Choi and a couple of colleagues pose for

a photo with the puppies, and with the man who oversaw the cloning: Woo Suk Hwang.

Eight years after Seoul National University (SNU) dismissed him for his central role in one of history's most notorious scientific frauds, Hwang, 61, is in a position many researchers would envy. He heads Soom Biotech Research Foundation, a nonprofit institute with a staff of 40, a \$4 million annual budget, and a new, well-equipped six-story building. His team publishes a steady stream of papers. Devoted dog owners from around the world, as well as the Korean police, seek their services. The institute is applying its

cloning know-how to rescuing endangered species and improving livestock breeds, as well as to fundamental research in developmental biology. And Hwang reportedly hopes to someday resume work with human embryonic stem cells.

Some say that the disgraced icon of science in South Korea has come far on the road to rehabilitation. "For animal cloning, his team is one of the best in the world," says Yang Huanming, chair of the Chinese sequencing powerhouse BGI-Shenzhen. Eventually, Yang predicts, Hwang "will regain respect from the scientific community."

CREDIT: DENNIS NORMILE

Downloaded from www.sciencemag.org on January 17, 2014

Back to work. Barred from handling human tissue, Woo Suk Hwang concentrates on animal cloning.

Others are not so sure. “I highly doubt that Hwang will gain respect in the scientific community at large, even with his ongoing successes in animal cloning,” says Insoo Hyun, a bioethicist at Case Western Reserve University in Cleveland, Ohio, who once advised Hwang. “[Hwang’s] scientific fraud was simply too great.”

Meteoric rise and fall

At the start of 2004, Hwang was toiling in obscurity in South Korea, engaged in routine livestock cloning. Then on 12 February, in a paper published online in *Science*, Hwang’s team claimed it had created stem cells from a cloned human blastocyst (*Science*, 13 February 2004, p. 937). From out of nowhere, the group had leapt ahead of dozens of labs worldwide seeking to generate stem cells genetically matched to individual patients; such cells, researchers hoped, would evade immune rejection and be used someday to treat or cure diseases like diabetes and Parkinson’s. Hwang’s team took another apparent step toward this goal with a second *Science* paper, published online on 19 May 2005, describing the creation of 11 embryonic stem cell lines using genetic material from patients suffering spinal cord injuries, a genetic immune deficiency, and diabetes. And in August, the team unveiled in *Nature* the first cloned dog, an Afghan hound named Snuppy.

In 18 months, the once-anonymous veterinarian had become a superstar. Colleagues described his findings as “a breakthrough” and “spectacular.” *Time* magazine named Snuppy 2005’s “Most Amazing Invention.” In South Korea, Hwang became a national hero. The government proclaimed him the country’s top scientist and launched a generously funded World Stem Cell Hub just for him. It issued a postage stamp featuring the expected fruits of Hwang’s research: a silhouetted figure rising from a wheelchair and leaping, with the caption referring to embryonic stem cells. Hundreds of women volunteered to donate eggs for his use.

As fast as he shot to fame, Hwang’s career began to unravel. A May 2004 news report in *Nature* claimed that one of Hwang’s Ph.D. students had said she and another member of the group donated their own eggs for

Hwang’s research, a dubious practice that ethicists feel could reflect lab heads pressuring junior researchers. For more than a year, Hwang denied he’d used their eggs, until a Korean TV broadcast in November 2005 showcased hard evidence from a whistleblower on Hwang’s team. In the days that followed, Korean bloggers started pointing to duplicated images and questionable data in Hwang’s papers. That drew an SNU investigation; on 29 December, the university’s panel reported that none of the 11 embryonic stem cell lines described in the second *Science* paper ever existed.

In their final report on 10 January 2006, the investigators cast doubt on the first



Better days. Hwang and Snuppy in 2005. The world’s first dog clone was his only achievement of that era to withstand scrutiny.

Science paper as well, stating that the human stem cell line was probably not derived from a cloned blastocyst but rather from an unfertilized oocyte that started developing into an embryo, a phenomenon known as parthenogenesis. The panel concluded that virtually all the images and data in the two papers had been fabricated. Hwang’s sole legitimate achievement was Snuppy: The panel confirmed that the dog really was a clone.

Hwang did not challenge the SNU panel’s findings. During a 12 January news conference broadcast on national TV, he tearfully admitted that both *Science* papers were bogus and pointed the finger at junior researchers, who he claimed had deceived him. *Science* retracted both papers in a notice posted online on 12 January.

SNU dismissed Hwang in March 2006. In October 2009, a South Korean court found him guilty of embezzling research funds and of illegally buying human eggs. Completing his downfall, an appeals court upheld the conviction in December 2010 and sentenced him to 18 months in prison. The sentence was suspended for 2 years, and he did not serve any jail time.

Starting over

As the disgraced researcher faded from view, a small band of supporters rallied to his cause. “I thought there was going to be no chance of helping disabled people and many other patients if we lost him from the scientific community,” says Byung Soo Park, a Korean electronics industry businessman and philanthropist who chairs the Sooram Foundation, which is separate from the research foundation and provides scholarships for Korean students. Park had known Hwang before he became famous. In 2000, on a mission to war-ravaged East Timor that Park organized, Hwang offered advice on improving cattle breeds and later hosted East Timorese scholars for training at SNU. “I was deeply touched and inspired by his effort and commitment,” Park says.

With the ax about to fall on Hwang at SNU, Park raised \$3.5 million and in July 2006 helped launch the Sooram Biotech Research Foundation to allow Hwang to continue his research activities. Many members of his group remained loyal to Hwang, a charismatic figure who inspired staff members through his long hours in the lab and dedication. “I believed that the team could prove it had the cloning technology” described in the *Science* papers, says Yeon Woo Jeong, a veterinarian who was among a couple dozen members of Hwang’s SNU lab to decamp to the fledgling institute.

At Sooram, barred by the government from working with human eggs and stem cells, Hwang returned to his roots in cloning livestock. But he soon had a chance to build on his one real accomplishment. After the birth in 1996 of the first cloned mammal, Dolly the sheep, U.S. billionaire John Sperling had bankrolled a venture to clone dogs—specifically Missy, a collie-husky mix owned by his friend Joan Hawthorne and her son Lou (*Science*, 4 September 1998, p. 1443). The Missyplicity Project and related pet cloning efforts ended up producing several cat clones, but no dogs.

In cloning Snuppy, Hwang's SNU group showed that it had mastered the complexities of dog cloning. Doing so requires synchronizing the reproductive cycles of egg donors and surrogate mothers, harvesting eggs at the right moment, and figuring out where in the reproductive tract to insert cloned oocytes—riddles that had all proved trickier to crack in dogs than in other cloned species. In early 2007, the Missyplicity Project sent Sooam tissue from Missy, who had died in 2002. Sooam promptly succeeded in cloning her. “The first surrogate got pregnant” and produced a pup that December, says In Sung Hwang, a Sooam researcher not related to Woo Suk Hwang.

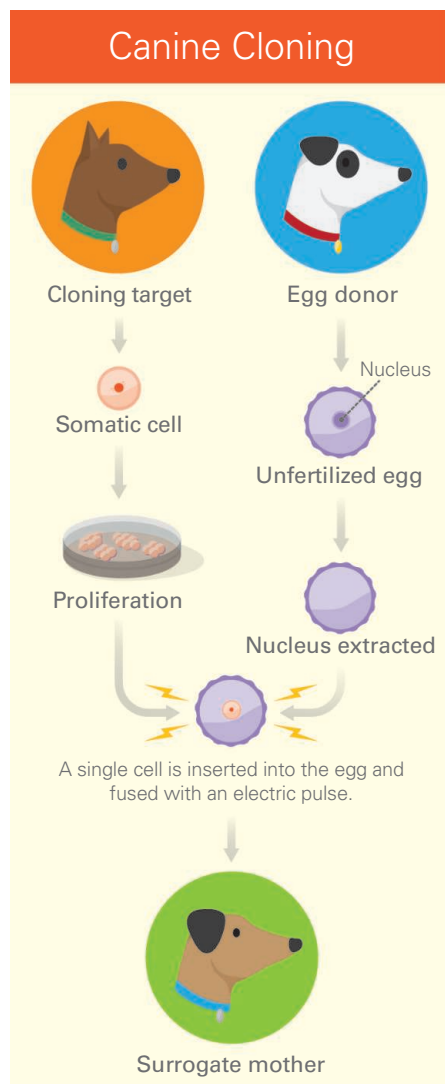
Fresh off that success, Lou Hawthorne started marketing dog cloning services through BioArts International, a business venture he set up to invest in biotechnology, with Sooam doing the cloning. BioArts gave up on dog cloning in 2009, citing the tiny market, the unpredictable results of cloning, and other issues. But determined pet lovers continued to find their way to Sooam.

In 5 years, the institute has cloned about 200 pet dogs, charging \$100,000 each time they are successful. (To prove that the puppies are genetic copies, the institute says it has an outside lab perform a genetic analysis on the original dog and the clone.) Sooam has also cloned another 200 or so dogs for the police, to preserve rare or valuable breeds, and for research purposes. While producing Snuppy required more than a thousand embryos and 123 surrogates, Sooam now typically needs only three surrogates, each of which gets three embryos, according to In Sung Hwang.

Mass production

In a clean room at Sooam, Kyung Hee Ko, a technician from Hwang's SNU days, peers through a microscope, wielding manipulators that control needles and probes. With metronomic constancy, she positions a bovine oocyte, sucks out the nucleus, replaces it with a somatic—or mature—cell from the target cow, and then positions the next oocyte. It's essentially the same somatic cell nuclear transfer technique used to create Dolly.

Woo Suk Hwang declined to be interviewed for this article. But in the surgery down the hall, there he is in blue scrubs and a white mask, slicing into the belly of an anesthetized dog and inserting a clutch of cloned oocytes into her oviduct. The dog is sewn up and wheeled out; in all, the procedure takes less than 10 minutes. Then, in quick succession, two pregnant dogs are wheeled in and Hwang performs cesarean deliveries of cloned puppies.



Recipe for a clone. Dog eggs must be harvested after they enter the oviduct, rather than taken from ovaries, as is done with livestock. Cloned oocytes must be implanted quickly into surrogates, rather than allowed to mature into blastocysts in culture before implantation.

Sooam had never advertised its dog cloning service. But as a first foray into marketing, last year it launched a contest in which pet owners described on the United Kingdom's Channel 4 why they believe their dogs deserve to be cloned. The winner of a cloned pet will be announced on TV later this year.

One objective of the contest is to “figure out what the public thinks about cloning,” In Sung Hwang says. Some researchers are critical. Robin Lovell-Badge, a developmental geneticist at the MRC National Institute for Medical Research in London, points out that the cloning process in general is inefficient, that clones may not be identical physically to the original because of developmental factors, and that many cloned pups die as

embryos or soon after birth. Surrogates, meanwhile, bear the hardships of pregnancy and losing embryos and newborns. “Is the outcome worth it?” Lovell-Badge asks.

In Sung Hwang responds that Lovell-Badge's impressions of dog cloning are out of date. Experience acquired through cloning hundreds of animals and continual tweaking of the process has dramatically improved efficiency and reduced the number of clones with birth defects, he says. But he agrees that the issue of whether it is right to impregnate surrogates for the benefit of human pet owners “is a moral question that should be answered through discussion.”

The Korean police need no more convincing. They point to a case that began in March 2007, when a 9-year-old girl went missing on Jeju Island. After a futile monthlong search, the Jeju police put their best bomb-sniffing dog, Quinn, through a crash course on searching for human remains. Less than an hour after being put on the job, Quinn found the girl's body in a barn near her home, leading to the arrest of her murderer. The Korean police do not allow working dogs to mate. Hoping nevertheless to propagate Quinn's talents, Jeju's police chief in 2009 asked Sooam to clone the champ. All five clones completed training and were put into service. Three were sent to Incheon, where they work in security at the airport, and two went to Jeju, where one died of a congenital heart defect. The other is healthy and “doing pretty well” working alongside Quinn, says Yong Shik Choi, a Jeju police department dog trainer.

While about one in three puppies from breeders complete police training and enter service, 90% or more of cloned puppies make the grade, claims Yongsuk Cho, Sooam's chief administrator, pointing to data released last May by the Rural Development Administration. Sooam provided more than 30 cloned dogs to police departments last year.

Working on dogs is allowing Sooam researchers to tackle fundamental questions in developmental biology. For example, apparently female puppies born occasionally when cloning a male dog could yield clues to why sexual development sometimes goes awry in human embryos. Sooam molecular biologist Kyu-Chan Hwang (unrelated to the other Hwangs in this story) says the team has determined that the gene on the Y chromosome that controls testes development is sometimes blocked by methylation in cloned canine embryos. He hopes further work in dogs might lead to a better understanding of Swyer syndrome, a rare condition in which a person with a Y chromosome has female genitalia—though no ovaries.

Hwang's team also clones prize livestock and uses the technique to generate transgenic cows that produce human drugs in their milk and transgenic pigs for xenotransplantation of organs into humans. Such work accounts for most of the 45 or so papers Hwang's team has published since 2006, including in respected journals such as *PLOS ONE*. These applied efforts also attract government grants—from Gyeonggi province, the city of Seoul, and the Rural Development Administration of Korea—which cover about 80% of the institute's annual budget.

To the rescue

Hwang's team is trying to extend their cloning know-how to endangered and extinct species. The scheme for both involves obtaining DNA for the species to be cloned and inserting it into the egg of a closely related living species to create an embryo that can be implanted into a surrogate. Interspecies somatic cell nuclear transfer has worked in seven species to date, including the Boer goat, a wild sheep known as a mouflon, two species of wild cats, and a gaur, an endangered wild ox native to Southeast Asia, according to a paper that appeared online on 13 September in *Cellular Reprogramming*. Hwang had a hand in creating the remaining two beasts in this menagerie—a gray wolf, reported in *Cloning and Stem Cells* in 2007, and coyotes, described online in *Reproduction, Fertility and Development* in December 2012. (Coyotes are not endangered, but Sooam wanted to develop expertise in interspecies cloning.) The team is now working on the endangered *Lycaon pictus*, or African wild dog. In a near miss, a *Lycaon* fetus in a surrogate dog mother died 2 weeks shy of expected delivery.

A more quixotic quest may be Sooam's project to revive the woolly mammoth. The team hopes to produce a clone using DNA from frozen mammoth remains and the eggs and womb of an elephant. Working with North-Eastern Federal University in Yakutsk in Russia, Sooam has sponsored two expeditions to hunt for mammoth remains preserved for thousands of years in Siberian permafrost.

"Cloning the woolly mammoth using the approach envisaged by the Sooam team is with all certainty never going to work," says Love Dalén, a paleogeneticist at the Swedish Museum of Natural History in Stockholm. Even in the best preserved mammoth samples, he says, "the nuclear genome is fragmented into some 50 million pieces. There is simply no way such a fragmented genome would be viable if transferred into an elephant cell." Sooam's In Sung Hwang acknowledges that the project is "a long shot."



Reporting for duty. Korean police officer Chang Hyun Choi says clones like this one make good police dogs.

The chance to work on everything from dog cloning to mammoth resurrection has attracted a cadre of young researchers willing to ignore Hwang's past. "Of course, there was a little bit of hesitation" about joining Sooam, says In Sung Hwang, who started at the institute in February 2010 after earning a master's in biomedicine at Duke University. However, he says, "I could see potential in what

Hwang's fraudulent papers, he says, "were a setback to the field at a time when human embryonic stem cell research was vulnerable and under attack from political opponents here in the U.S." Nonetheless, Daley is sympathetic. "We are all flawed and imperfect, and I believe everyone deserves a chance at redemption," he says.

Jeong-Sun Seo, a geneticist at SNU's College of Medicine, sees little chance that Hwang can achieve his ultimate goal: working on human cloning again. Many in the Korean scientific community oppose allowing Hwang to resume work with human material because of his past ethical lapses and his use of massive numbers of eggs to get a few viable embryos, Seo says. This approach may be acceptable in animals, he adds, but it would be problematic if applied to humans.

The Korean health ministry has turned down two applications from Sooam to work on human stem cells. And Sooam's Jeong notes that any in-depth stem cell research would require collaborations with hospitals, physicians, and biomedical researchers that will be difficult to forge. "There are a lot of



Resurrection team. Hoping to clone a woolly mammoth, Hwang (second from left) and colleagues have ventured twice to northern Siberia in search of well-preserved remains of the extinct beast.

was being done here." Hanna Heejin Song, who studied veterinary science in Hungary and joined Sooam in 2012, had no qualms. "In Korea [animal cloning] really happens, and it's really good, so why not be in my own country?" she asks.

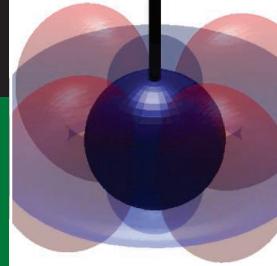
Established scientists are more skeptical. "Hwang's rehabilitation faces an uphill climb," says George Daley, a stem cell researcher at Harvard Medical School in Boston and Boston Children's Hospital.

limitations on what we can do," says Jeong, who blames "prejudice" against Sooam because of Hwang's past.

According to In Sung Hwang, Woo Suk Hwang "still has dreams about [human embryonic] stem cell research." Woo Suk Hwang has risen further from his disgrace than many predicted, but those dreams are unlikely to come true.

—DENNIS NORMILE

With reporting by Mi-Young Ahn.



LETTERS

edited by Jennifer Sills

Biodiversity: Broaden the Search

IN THEIR POLICY FORUM "PROTECTED AREAS AND EFFECTIVE BIODIVERSITY CONSERVATION" (15 November 2013, p. 803), S. Le Saout *et al.* have provided a useful analysis to identify protected areas of global importance for the conservation of amphibians, nonmarine mammals, and birds. Indeed, reserve-specific identification of priority species is crucial to reach global

biodiversity targets, such as Aichi Biodiversity Target 12 (to prevent the extinction of threatened species by 2020 and improve their status). However, as the current analysis only includes a small fraction of biodiversity (1.2% of the described species), it is obvious that this approach needs to be broadened.

Single protected areas may easily hold 100% of the global populations of plant or invertebrate species. It is likely that these isolated populations will turn out to be the real priority species, using the distribution overlap criterion. However, as a complete assessment of all invertebrate species is not feasible, they will remain ignored in such global prioritization approaches. It thus remains the responsibility of protected area authorities to (i) com-

mence species inventories for a broad set of taxa; (ii) identify priority species based on the percentage overlap of their distribution with the reserve (population size overlap would be even better, but it is unfortunately not attainable); and (iii) implement monitoring and management strategies for these species.

The implementation of such prioritizations could be encouraged by making them mandatory for categorization as a World Heritage Site under the World Heritage Centre's "criterion (x)" (which declares that "Outstanding Universal Value" is met if a site contains the most important habitats for biodiversity conservation) or by providing incentives (such as green-listing reserves). If the global identification of potential World Heritage Sites remains purely based on vertebrates, we may lose a major part of our natural heritage.

AXEL HOCHKIRCH

Department of Biogeography, Trier University, D-54286 Trier, Germany. E-mail: hochkirch@uni-trier.de

Biodiversity: Ecuador Deters Protection Efforts

IN THEIR POLICY FORUMS, BOTH S. LE SAOUT *et al.* ("Protected areas and effective biodiversity conservation," 15 November 2013, p. 803) and N. Butt *et al.* ("Biodiversity risks from fossil fuel extraction," 25 October 2013, p. 425) identified protected areas in the Ecuadorian Amazon that need further pro-

tections and management. Because Ecuador has irreplaceable areas that overlap with fossil fuel reserves, an initiative launched by the Ecuadorian government in 2007 to keep its oil underground was considered historic and attracted worldwide support (1). Its recent cancellation by the Ecuadorian government on 16 August 2013 was followed by unexpectedly few bids from international corporations to extract oil (2). Amid great public opposition, government officials are moving

forward with the selection of the best offer.

Unfortunately, in the process, the Ecuadorian government is disregarding, and even dismantling, environmental organizations that have voiced their opposition (3). The environmental and indigenous rights group Fundación Pachamama was shut down on 4 December 2013 after their alleged involvement in the physical harassment of oil executives during protests against the government-sponsored XI Oil Round. President Rafael Correa's administration characterized the protests as "threatening the security of the state" (4). The group rejected violent demonstrations and vowed to dispute the government's decision and to continue their efforts to defend the collective rights of indigenous people and the rights of nature as enacted in the Ecuadorian Constitution (5).

The history of environmental damage and displacement of indigenous groups associated with oil extraction in Ecuador demands that the international community keep a watchful eye on these events as they continue to unfold.

KARINA VEGA-VILLA

Wenatchee, WA 98801, USA. E-mail: vegavilla1@gmail.com

References

1. United Nations Development Group, Multi-Partner Trust Fund Office (<http://mptf.undp.org/yasuni>).
2. Iniciativa Yasuni-ITT (<http://yasuni-itt.gob.ec/inicio.aspx>).
3. "Presidenta de ONG disuelta apelara acción del Ministerio del Ambiente," *El Comercio* (2013) [in Spanish].
4. "ONG disuelta tras 16 años de activismos," *El Universo* (2013); www.eluniverso.com/noticias/2013/12/22/nota/1945116/ong-disuelta-tras-16-anos-activismo [in Spanish].
5. "Fundación Pachamama releases statement on shutdown of their offices" (www.pachamama.org/news/fundacion-pachamama-on-international-and-public-opinion).

Targeting Deforestation

IN THEIR POLICY FORUM "WHAT DOES ZERO deforestation mean?" (15 November 2013, p. 805), S. Brown and D. Zarin emphasize the need for clarity in setting targets for reduced deforestation. They argue that separate



How thalidomide
beats cancer

256



Many paths
to life

259

targets for gross deforestation and reforestation are preferable to targets for net deforestation. We agree.

In addition to the national, corporate, and nongovernmental targets tabulated by Brown and Zarin, the international community has agreed on a set of 20 time-bound Aichi Biodiversity Targets as part of the Strategic Plan for Biodiversity 2011–2020 (1). Target 5 calls for the rate of loss of all natural habitats, including forests, to be at least halved by 2020, and Target 15 calls for the restoration of at least 15% of degraded ecosystems by 2020, which will contribute to climate change mitigation and adaptation and to combating desertification. The Targets were adopted by the Convention on Biological Diversity at its 10th meeting in Nagoya Japan in October 2010 (1). They have subsequently been supported by other biodiversity conventions and the United Nations (2–7). Also in line with the approach recommended by Brown and Zarin, these global targets provide a framework for the establishment of national targets, taking into account national priorities and capacities with a view also of contributing to the global Aichi Biodiversity Targets.

BRAULIO DIAS

Convention on Biological Diversity, Montreal, QC H2Y 1N9, Canada. E-mail: braulio.dias@cbd.int

References

1. Convention on Biological Diversity, "Decision X/2: The strategic plan for biodiversity 2011–2020 and the Aichi Biodiversity Targets" (www.cbd.int).
2. Resolution 10.18 of the Convention on the Conservation of Migratory Species of Wild Animals (www.cms.int).
3. Resolution 16.4 of the Convention on International Trade in Endangered Species of Wild Fauna and Flora (www.cites.org).
4. Resolution XI.6 of the Convention on Wetlands of International Importance (The Ramsar Convention) (www.ramsar.org).
5. Resolution 8/2011 of the International Treaty on

Plant Genetic Resources for Food and Agriculture (www.planttreaty.org).

6. Decision 37 COM 5A of the World Heritage Convention (who.unesco.org).
7. General Assembly Resolution 65/161 (11 March 2011); www.cbd.int/undb/goals/undb-unresolution.pdf.

Urban Forests on the Front Line

IN THEIR REVIEW "THE CONSEQUENCE OF TREE pests and diseases for ecosystem services" (15 November 2013, p. 823), I. L. Boyd *et al.* discuss the effects of pests on forest ecosystem services. However, urban forests garnered little attention.

With increasing global trade, urban trees are among the first affected by newly introduced pests. Low tree diversity combined with low tree density in cities limits the potential for compensatory responses of ecosystems, unlike the model presented by Boyd *et al.* Decades ago, diseased elms were felled en masse in cities in eastern North America; many of the same cities are bracing yet again for extensive canopy loss, this time due to emerald ash borer (1). Boyd *et al.* suggest that cultural services are affected, but a more complete portfolio includes services important to city dwellers, such as air pollution removal and climate regulation (2, 3).

As Boyd *et al.* suggest, planting more species and species selection will reduce losses to new tree pests. However, few species tolerate urban conditions, leading to overuse of those that do. Greater genetic diversity within species is particularly important to address enhanced pest risks in urban areas (4). Chemical treatments of urban trees can prolong their service life while also controlling pest spread (1). Outbreak-related tree removals cost millions. A greater investment in better infrastructure and soil [e.g., (5)] would be a cost-effective way to reduce stress and permit more species to be planted.

C. A. NOCK,^{1*} O. TAUGOURDEAU,¹ T. WORK,¹ C. MESSIER,² D. KNEESHAW¹

¹Center for Forest Research, Département des Sciences Biologiques, Université du Québec à Montréal, Montréal, QC H3C 3P8, Canada. ²Institut des Sciences de la Forêt Tempérée, Département des Sciences Naturelles, Université du Québec en Outaouais, Ripon, QC J0V 1V0, Canada.

*Corresponding author. E-mail: charles.nock@gmail.com

References

1. K. F. Kovacs *et al.*, *Ecol. Econ.* **69**, 569 (2010).
2. D. J. Nowak, D. E. Crane, J. C. Stevens, *Urban For. Urban Green.* **4**, 115 (2006).
3. D. E. Pataki *et al.*, *Front. Ecol. Environ.* **9**, 27 (2011).
4. D. W. MacFarlane, S. P. Meyer, *For. Ecol. Manage.* **213**, 15 (2005).
5. N. Bassuk, J. Grabosky, P. Trowbridge, J. Urban, "Structural soil: An innovative medium under pavement that improves street tree vigor" (1998); www.hort.cornell.edu/uhi/outreach/csc/article.html.

Response

URBAN TREES MUST SUPPLY ECOSYSTEM SERVICES that are out of proportion to their numbers, meaning that the initial impact of pests and diseases can be higher in urban environments, including gardens, parks, and street trees, than in areas with higher concentrations of trees (1). There are also fewer options to compensate for the loss of trees in urban environments (2, 3). Consequently, Nock *et al.* argue that our model of the adaptive response of ecosystem services to the effects of infestation by tree pests and diseases does not adequately represent the limited capacity for response in urban environments.

We agree that over recent decades, a growing proportion of the commonly used tree species has exhibited increasing difficulties in coping with the conditions of urban sites. This negative trend and the challenges of climate change and pest and disease attacks have led to a search for a greater diversity of species and particularly for the selection of stress-tolerant species and genotypes (2, 4). With appropriately focused research in tree genetics, silviculture, and future urban cultivation, we also see considerable capacity for adaptation in urban environments.

Focusing on urban trees is also important because they have the capacity to act as receptors and sentinels for newly introduced pests and diseases. They are often in closest contact with recent introductions, and they are easy to monitor. Experience has shown that early detection in urban environments can lead to effective management (5).

I. L. BOYD,^{1*} P. H. FREER-SMITH,² C. A. GILLIGAN,³ H. C. J. GODFRAY⁴

¹College Gate, University of St. Andrews, St. Andrews, KY18 9LB, UK. ²Forest Research, Alice Holt Lodge, Farnham, Surrey, GU10 4LH, UK. ³Department of Plant Science, University of Cambridge, Cambridge, CB2 3EA, UK. ⁴Department of Zoology, University of Oxford, Oxford, OX1 3PS, UK.

*Corresponding author. E-mail: ilb@st-andrews.ac.uk

References

1. P. Bolund, S. Hunhammar, *Ecol. Econ.* **29**, 293 (1999).
2. A. Roloff *et al.*, *Urban For. Urban Green.* **8**, 295 (2009).
3. H. Sjöman, J. Ostberg, O. Buhler, *Urban For. Urban Green.* **11**, 31 (2012).
4. S. Pauleit, *Proc. Instit. Civil Engineers Municipal Engineer.* **156**, 43 (2003).
5. T. J. Centner, S. Ferreira, *Plant Pathol.* **61**, 821 (2012).

Letters to the Editor

Letters (~300 words) discuss material published in *Science* in the past 3 months or matters of general interest. Letters are not acknowledged upon receipt. Whether published in full or in part, Letters are subject to editing for clarity and space. Letters submitted, published, or posted elsewhere, in print or online, will be disqualified. To submit a Letter, go to www.submit2science.org.

SCIENCE COMMUNITY

One Tongue to Rule Them All?

Yael Peled

Scott Montgomery's *Does Science Need a Global Language?* examines the changing linguistic landscape of science and the contemporary undisputed and unrivaled status of English as the common language of international communication. The book makes a timely contribution to the emerging literature on English as a (global) lingua franca (ELF), a debate that has been taking place mostly in the humanities and the social sciences rather than in the STEM (science, technology, engineering, and mathematics) subjects. In the latter, competence in English is more often a professional prerequisite than the topic of dedicated investigations.

In contrast, Montgomery (who teaches at the University of Washington) undertakes the task of unpacking the evidently complex issue of ELF in science, particularly international science. He explores fine-grained questions such as how "scientific English" fits into the model of "world Englishes" (distinct nativized varieties that "vary from one another in pronunciation, vocabulary, and, at times, grammar"). He presents nuanced, historical discussions on topics including whether the fate of previous scientific lingua francas such as Greek, Latin, or Arabic can tell us something about the fate of English and the important and often overlooked contributions of the scientific and industrial revolutions to the contemporary status of English as a global scientific language. Commandably, Montgomery builds his account on a comprehensive body of research not only in the history of science but also in linguistics (his reference to which as "profession" further reflects the divide in the philosophy of science between the concepts of "science" and "Wissenschaft").

The book makes it clear from the outset that the answer to the question in its own title is emphatically positive. An international scientific language, Montgomery argues, enables easier and more effective knowledge production and sharing, by eliminating the

need to rely on linguistic mediators in the processes of scientific research (particularly international collaborative work), evaluation (e.g., peer review), and dissemination (publication and conference presentation).

It is likewise advantageous for individual scientists, as it makes them more mobile in the current era of more rapid, more global, and more collaborative scientific work. At the same time, Montgomery is careful to raise important concerns, such as the clear advantages of native speakers (and, more important, writers) of the scientific lingua franca and the increasing use of English in non-Anglophone scientific institutions and communities. In another insightful discussion, he examines the bias toward English in the growing bibliometrics industry of evaluating scientific output, visibility, and impact.

Although some of the advantages of a global language for science that Montgomery identifies are clear (e.g., the possibility of direct interactions among researchers and with scientific work), others are less so. For example, while it is true that competence in English makes non-Anglophone researchers more spatially mobile, that does

(1). So, while the emergence of a highly skilled and highly mobile workforce is certainly useful in various ways to academia and the corporate world, it is not always clear whether their interests are sufficiently aligned with those of individual scientists. Similarly not always apparent is whether the undisputed benefits of professional mobility in its current form definitely outweigh its less desirable repercussions on individuals' social and personal life.

The tension between incentives presented to individuals and their problematic larger-scale effects in the linguistic internationalization of science could thus be said to resemble a collective-action problem (2). One can extend the same logic to the discussion on the desired equilibrium between English and local national languages in non-Anglophone scientific institutions and communities. It certainly seems suggestive that the countries that seem to fare best in this context are welfare states (particularly the Netherlands and Scandinavian nations). Of course, the issue of collective action in language is by no means unique to the scientific community and is shared by any group of human associations faced with the inescapable tension between linguistic difference and societal (social, political, and economic) interdependence. Such interdependence, however, is certainly crucial for the scientific community at a time when, as Montgomery notes, both science and the issues it addresses are increasingly transnational.

Opting for a global language of science (English or otherwise) seemingly offers scientists a solution to the problem of linguistic



not necessarily guarantee increased social, economic, or professional mobility. The image most often conjured by mobility—an individual from a disadvantaged background achieving great professional and socioeconomic success due to their English competence, as in the case of the Ugandan chemist with which Montgomery begins his first chapter—is certainly appealing. Nevertheless, that image captures only a certain part of the broader picture of international mobility, which is very rarely purely voluntary or meritocratic and includes less positive elements such as low pay, contractual insecurity, and a challenging work-life balance

difference. The removal of linguistic barriers thus should facilitate scientific interdependence and lead to a greater democratization of knowledge. Such a view, however, is fraught with problems, some practical and some more substantial. Keeping in mind the existence of deaf scientists, the vision of a global scientific tongue may refer at best to a written variant (to date, sign languages lack a codified corpus of scientific terminology). The democratization of knowledge, likewise, crucially relies not only on the feasibility of quality universal English teaching but also on prevailing business models of the corporate publishing industry. Similarly,

The reviewer is at the Centre de recherche en éthique de l'Université de Montréal and the Faculty of Law, McGill University, Chancellor Day Hall, 3644 Peel Street, 28, Downtown Station, Montréal, QC H3A 1W9, Canada. www.peledy.com

“global” does not necessarily imply “equal opportunities”: describing Saudi Arabia’s King Abdullah University of Science and Technology as a global university seems to disregard the evident difficulties facing, for example, Israeli-born students and researchers interested in developing ties with the university. This certainly illustrates the point that the human element, so to speak, of scientific inquiry is never entirely divorced from the messiness—and difference—of human affairs, even when the language is shared.

More important, however, the question “does science need a global language?” does not address the issue of what ought to be the linguistic repertoire of scientists—apart from making a clear (and convincing) case that English ought to form a part of that. Plurilingualism (individual multilingualism) seems certainly more pronounced in the social sciences and humanities, where competence in additional language(s) is in many cases a prerequisite. But it is also pertinent in neighboring STEM domains such as social epidemiology and cultural psychiatry.

For non-Anglophone scientists, of course, the question of linguistic repertoire will always be pertinent. Anglophone researchers may find themselves in the same boat, given the possibility of a future break between scientific English and its various localized variants—especially because, as David Crystal notes in his short Foreword, “for every native speaker of English there are now four or five nonnative English speakers.” Such a preponderance of nonnative speakers could shift the linguistic-power relations between those who set linguistic norms and those who adhere to them. In a future in which “scinglish” (scientific English) is as mutually intelligible with British or American English as Singlish (Singaporean Creole) is today, Anglophone scientists may well find linguistic repertoire to be a must have rather than an optional endeavor.

A final point concerning linguistic repertoire in science is the potential risk of ontological reductionism. Commenting on the largely unknown repository of knowledge being lost to humanity as a result of today’s rapid extinction of languages, linguist K. David Harrison coined the term “science bias” to refer to the popular conviction that everything worth knowing is already more or less known to, or at least handled by, science. In a similar vein, the appeal of a common scientific language runs the risk of “English bias,” namely, the conviction that everything worth knowing is written in English. As an example of the invisibility of work published

in languages other than English and the dangers of being unaware of such findings, Montgomery points out that important research on avian influenza went unnoticed as it was published in Mandarin. These concerns are echoed in current working documents such as the Cochrane Collaboration *Handbook* (3). Being conscious of the risks of English bias may ultimately determine whether international science can efficiently capitalize on the clear benefits of a global scientific tongue while successfully avoiding its potential drawbacks. *Does Science Need a Global Language?* certainly makes a very convincing

case for the advantages of a scientific lingua franca. One hopes that the important questions Montgomery raises and the nuanced discussion he presents will be followed by further work on the complex interplay among science, power, and language.

References and Notes

1. L. Ackers, *Minterva* 46, 411 (2008).
2. I thank D. Weinstock for this point.
3. “Language Bias,” in *Cochrane Handbook for Systematic Reviews of Interventions* 5.1.0, P. T. Higgins, S. Green, Eds. (Cochrane Collaboration, 2011); http://handbook.cochrane.org/chapter_10/10_2_2_4_language_bias.htm.

10.1126/science.1247871

Authors’ Words

“I’ve coined the word *stressism* to describe the current belief that the tensions of contemporary life are primarily individual lifestyle problems to be solved through managing stress, as opposed to the belief that these tensions are linked to social forces and need to be resolved primarily through social and political means. Analysis of stressism brings into sharp focus significant polarities in Western thought, principally the sharp divisions between mind and body, health and illness, public and private, social responsibility and individual self-actualization. Examining stress brings to light many of our cherished cultural preoccupations and predispositions, exposing existing tensions and inequities related to class and gender; and our increasing dependence on stress to explain our lives has consequences for the way we see ourselves and the world, the way we act, and the world we create as a consequence of that vision and those actions.”

One Nation Under Stress: The Trouble with Stress as an Idea.

Dana Becker. Oxford University Press, 2013 (ISBN 9780199742912).

...

“If we do make a serious effort to corral the national and world economies within ecologically supportable boundaries, the method we choose for divvying up the resources that humanity can afford to consume must be a method we can all live with. In fact—considering the many tragic consequences of rationing by ability to pay in a world with such enormous imbalances of economic power—we might even find that we can devise ways of sharing scarce resources that produce a happier, better-fed, healthier, more comfortable, and more secure world than the one we inhabit today. But such methods cannot be expected to pop up spontaneously. That is why it is important to examine how nonprice rationing works, on paper and in the real world, and to find out if it will be possible to paint our society out of its corner.”

Any Way You Slice It: The Past, Present, and Future of Rationing.

Stan Cox. New Press, 2013 (ISBN 9781595588098).

...

“Just as beliefs fuel a ‘this dance can go on forever’ mentality of investors and speculators, the beliefs and ideologies of politicians and voters sustain political bubbles. First, the fact that politicians and voters may share in the investor’s ‘irrational exuberance’ makes them loath to support corrective policies. If a savings glut reduces the natural level of interest rates, it would be folly to use monetary policies to keep them artificially high. If the information economy is the wave of the future, it would be Luddism to tighten standards for either the public offerings that would capitalize the firms of the future or the pricing of stock options in accounting statements.

But beyond the beliefs that underpin a particular bubble, basic ideological beliefs about the nature of markets and the role of government also fuel bubbles.”

Political Bubbles: Financial Crises and the Failure of American Democracy.

Nolan McCarty, Keith T. Poole, and Howard Rosenthal. Princeton University Press, 2013 (ISBN 9780691145013).

Straining Emergency Rooms by Expanding Health Insurance

Raymond Fisman

The crowded, chaotic emergency room (ER) is often invoked as a symbol of all that's wrong with the American health care system. The uninsured, the story goes, cram into ERs—legally prohibited from turning away patients—for routine medical attention that could be provided more cost-effectively through primary care providers (also known as general practitioners in many countries). It's an image of America's dysfunctional approach to providing “free” health care for those who cannot afford it. In policy circles, this take on ER medicine has been cited by, among others, Health and Human Services Secretary Kathleen Sebelius, as justification for universal health coverage, because the current system “has forced too many uninsured Americans to depend on the emergency room for the care they need.”

Many in the medical profession dispute this picture of the ER overrun with uninsured patients. A 2008 literature survey (1), for example, found that most uninsured prefer self-treatment or just hope their maladies will disappear, rather than deal with the financial catastrophe that can follow a visit to the ER (2, 3). If the uninsured are not coming to the ER in great numbers in the first place, then there is little basis for the claim that universal coverage will reduce the current strain on emergency care.

The new study by Taubman *et al.* [(4), page 263] provides compelling evidence to adjudicate on this question of whether health insurance increases or decreases ER usage. This work, which builds on earlier analyses of the Oregon Health Insurance Experiment (OHIE), finds that low-income, uninsured adults randomly selected to get Medicaid health insurance coverage go to the ER more, not less. And the impact is enormous—in the 18 months after the program's start, ER visits increased by about 40% relative to those

not offered coverage through the Medicaid expansion (see the graph).

These findings explode the myth that health insurance access will reduce the strain on emergency services and thus undermine the hope that expanded coverage will put an end to this particular inefficiency in America's bloated health care market.

That the insurance expansion in the study involved random assignment is particularly important, given the difficulties in interpreting the results of observational studies: Insured and uninsured populations are simply too different from one another to allow for a straightforward apples-to-apples comparison of ER usage. That is why a randomized controlled study is so valuable; by construction, an individual who signed up for and was selected by the Oregon Medicaid lottery for coverage is identical, on average, to someone who signed up for the lottery but was not selected (5, 6).

Nor does economic theory provide any guidance on whether insurance should increase or decrease ER use. From the patient's perspective, insurance is essentially an across-the-board price cut that makes all health services a lot cheaper. The direct effect is, naturally, more consumption of health care of all sorts—primary care, ER, and everything else. But different forms of health services—particularly primary and emergency care—could substitute for one another, an effect that insurance coverage proponents clearly have in mind. In an earlier study based on the OHIE, researchers found an increased use of primary care after Medicaid enrollment, and if these primary care visits substitute for what would otherwise have been trips to the ER, insurance could cause overall ER use to decline (7). (Primary care use could, in theory, act to increase ER use instead if primary care providers refer patients on to the ER for treatment, a point I return to below.)

The fact that primary care access does not crowd out ER usage says a great deal about the nature of health care delivery in America

A randomized trial shows that patients newly covered by Medicaid increased their emergency room visits by 40%.

today: A remarkable fraction of care [as well as admissions (8)], takes place at the ER. Further, ERs manage cases that span a range of circumstance, some of it emergent but much that, according to Taubman *et al.* and others, could have been managed through lower-cost primary care.

To appreciate why there is this apparent mismatch of patient needs and type of service—and whether the increase in emergency care constitutes unnecessarily expensive treatment or the provision of important care—it is critical first to understand why people choose to go to the ER. It certainly is not because it presents a more pleasant option.

A recent RAND Corporation survey of ER usage (9) argues that, in many cases, patients go to the ER simply because they are told to do so by their primary care physician or some other health care professional they contact. This is the case even for nonemergency injuries like sprains or cuts that nonetheless require immediate attention. That is, primary-care practices fill their schedules with appointments for regular, predictable treatment and are de facto using ERs as a referral for urgent or time-consuming cases. (This finding highlights the difficulty in predicting, before this study, whether expanding primary care would substitute for ERs or increase traffic to them.) Additionally, patients quite reasonably show up at the ER in situations that may, ex post, turn out to be harmless but present reasonable cause for concern. A 70-year-old with chest pain would be wise to go straight to the ER without seeking further advice and would have been instructed to do so by any professional he or she consulted (10, 11).

The diversity of reasons that lead patients to go to the ER highlights the impossibility of adjudicating, solely on the basis of data and analyses in this paper, whether insurance leads to overuse of emergency services. As the authors note in their conclusion, the retroactive classification of visit types based on eventual diagnosis separates heartburn from cardiac arrest, although both just seemed like chest pain to the patient. More important, given the nature of health care delivery in America today, it would be dangerous to label an ER patient with non-emergent needs

These findings explode the myth that health insurance access will reduce the strain on emergency services ...

Columbia University, New York, NY 10027, USA. E-mail: rf250@columbia.edu

as seeking “unnecessary ER care.” As noted earlier, in a great many cases, the patient has gone to the ER at the instruction of a health professional who was consulted with the hope of finding other, possibly lower-cost, more convenient care (12).

This lack of resolution matters a great deal for the policy implications that will no doubt be sought from the study on both sides of the Affordable Care Act debate. This study runs the risk of suffering the same fate as the two previously published articles based on the OHIE, which served as health insurance policy Rorschach ink blots for many readers: People saw in the results whatever they wished to see in order to validate preexisting positions on Obamacare and health insurance more generally.

The first study, published in the *Quarterly Journal of Economics*, found that Medicaid coverage increased the use of health services (including preventive care) and led to higher self-reported physical well-being and happiness (13). Supporters of universal care pointed to it as evidence of both the

suppressed demand for health care among the poor and nascent evidence of its benefits. Critics emphasized that health care costs went up (because of increased use of care) without any impact on medical outcomes.

The second study, published in the *New England Journal of Medicine* (7), showed modest improvements in biomarkers like cholesterol and blood pressure, although none were statistically significant (5, 6). At the same time, Medicaid enrollees showed significant improvements in financial well-being and declines in depression. Again, both sides claimed victory—universal care naysayers had a field day with the lack of significant physical health results, which was interpreted as showing that more spending had no impact on actual health. Their adversaries took the results as proving nothing, owing to lack of statistical precision, and further pointed to mental-health improvements and financial benefits as showing that Medicaid—fundamentally an insurance product designed to offer protection against health-induced financial catastrophe—was doing exactly what it was supposed to do. (As some commentators put it at the time, fire insurance does not prevent fires, but many people still think it is a good investment.)

For the current study, it is possible to argue that the observed increase in ER use likely represents greater access to necessary care, or that it shows that insurance serves as further encouragement to seek unnecessarily expensive treatment. But both sides would do well to focus on what this latest study does tell us—that Medicaid access increases ER use—rather than emphasizing the very different spins that can potentially be put on the findings (i.e., whether the observed increase in ER use represents greater access to necessary care or further encouragement to seek unnecessarily expensive treatment).

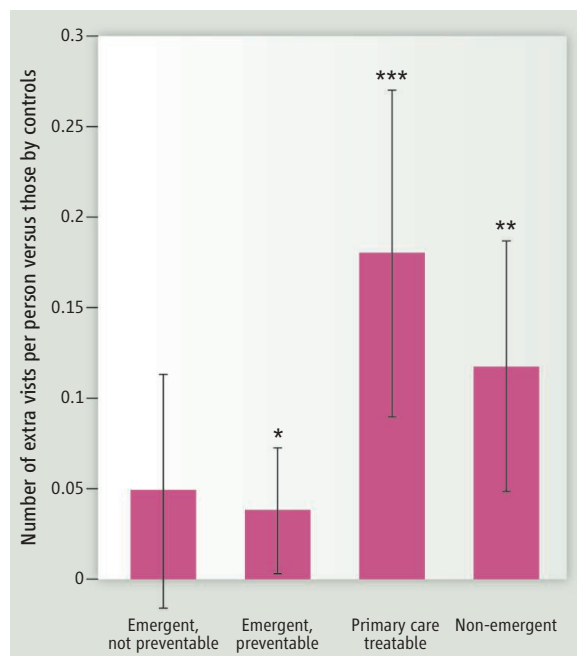
If all goes as planned, many more Americans will soon be covered by some type of health insurance. Although much of the United States looks very different from white, liberal, urban Portland, and the OHIE involved a small, rather than universal, expansion in coverage, there is no obvious reason

to expect that insurance will have drastically different effects elsewhere. That is, based on this paper's findings, we have good reason to anticipate a large increase—and almost surely not a decrease—in traffic to already overburdened emergency departments across the country. Whether or not you think universal coverage is a good idea, we had better start planning for it.

Clearly, the answer is unlikely to be just increasing ER budgets to accommodate more patients: There are surely better ways to manage health delivery to low-income populations, particularly with an eye to long-term preventive care rather than short-term treatment. This study gives that discussion that much more of a sense of urgency and, one hopes, will further spur new innovations aimed at solving America's health care problems.

References and Notes

1. M. F. Newton, C. C. Keirns, R. Cunningham, R. A. Hayward, R. Stanley, *JAMA* **300**, 1914 (2008).
2. A separate study debunks the urban legend of the supposed preponderance of drug addicts and indigents populating the ER. See (3).
3. J. Billings, M. Raven, *Health Aff.* **32**, 2099 (2013).
4. S. L. Taubman, H. L. Allen, B. J. Wright, K. Baicker, A. N. Finkelstein, *Science* **10.1126/science.1246183** (2014).
5. Although Taubman *et al.*'s research design provides the cleanest evidence on the link between insurance coverage and ER use, it is worth noting that earlier research—reviewed in Taubman *et al.*—finds mixed results. In particular, an analysis of the impact of the Massachusetts health care reform (6), which caused a large expansion in insurance coverage, found no effect on ER use. This still indicates that the best-case scenario is likely no increase in ER traffic as a result of increased insurance coverage.
6. C. Chen, G. Scheffler, A. Chandra, *N. Engl. J. Med.* **365**, e25 (2011).
7. K. Baicker *et al.*, Oregon Health Study Group, *N. Engl. J. Med.* **368**, 1713 (2013).
8. J. D. Schuur, A. K. Venkatesh, *N. Engl. J. Med.* **367**, 391 (2012).
9. K. Morganti *et al.*, “The evolving role of emergency departments in the United States” (RAND Corporation, Santa Monica, CA, 2013); www.rand.org/pubs/research_reports/RR280.
10. Also, although most Medicaid recipients in the OHIE sample reported having a usual source of care, prior research has found that many physicians are averse to taking Medicaid patients, given their lower reimbursement rates. A 2011 study, for example, found that physicians were less likely to accept new patients on Medicaid than new patients with Medicare or with private, noncapitated insurance (11). Thus, some Medicaid patients in other parts of the country may also end up in the ER because they have not found a primary care provider, which could further increase the effect size documented by Taubman *et al.*
11. T. F. Bishop, A. D. Federman, S. Keyhani, *Arch. Intern. Med.* **171**, 1117 (2011).
12. Many hospitals are set up with the expectation that many of the cases that come through the door would have been better dealt with in other settings. For example, ER “fast tracks” that triage patients into urgent (but not emergency) care are common in U.S. hospitals.
13. A. Finkelstein *et al.*, Oregon Health Study Group, *Q. J. Econ.* **127**, 1057 (2012).



Medicaid insurance coverage increases the number of ER visits, compared to a non-Medicaid control baseline. Bar heights (and 95% confidence intervals) reflect the number of increased visits per person during the 18-month study period. Visits that require immediate ER care and could not have been prevented are “emergent, not preventable.” Visits that require immediate ER care and could have been prevented with ambulatory care are “emergent, preventable.” Visits that require immediate care but could be treated in an outpatient setting are “primary care treatable.” Visits that do not require immediate care are “non-emergent.” Control group baseline levels of ER use differed across categories. Overall, ER use increased by 0.41 visits relative to control baseline value of 1.02 visits, an increase of 41%. * $P < 0.05$, ** $P < 0.01$, *** $P < 0.001$. See (4), particularly table 4, for data and details.

EVOLUTION

Smells Like Queen Since the Cretaceous

Michel Chapuisat

The hallmark of insect societies is reproductive division of labor. In the presence of a fertile queen, workers do not reproduce. It has long been recognized that chemical substances emitted by queens induce infertility in workers (1). However, the few queen pheromones that have been characterized appeared to be chemically unrelated (1–3). On page 287 of this issue, Van Oystaeyen *et al.* (4) show that a class of structurally similar queen-specific hydrocarbons suppresses worker reproduction in ants, wasps, and bumblebees. A comparative analysis indicates that these long-chained saturated hydrocarbons were associated with fertility in solitary ancestors, providing fresh insights into the evolution of queen pheromones and eusociality.

In societies of Hymenoptera (ants, bees, and wasps), queens and workers are usually related. By helping the queens, workers therefore indirectly pass on copies of their own genes to future generations. However, because queens and workers are not clones, they still have potential conflicts over who will reproduce in the colony (5). In most hymenopteran lineages, workers retain some ability to lay eggs and often do so after the death of the queen.

The presence of potential conflicts raises interesting questions about the function and evolution of queen pheromones (1). A long-standing hypothesis is that queens use pheromones to control worker reproduction (6). Under this scenario, queen pheromones are expected to evolve quickly because workers are selected to resist manipulation, generating an evolutionary arms race (1). Alternatively, queen pheromones may be honest signals of her fertility, with workers reacting to the signal because helping fertile queens maximizes their genetic representation in the next generation through the rearing of kin (7). In that case, the pheromones are expected to have evolved from physiological by-products of reproduction that are cues of fertility and to be evolutionarily stable (3). Studying the nature and diversity of queen pheromones

Department of Ecology and Evolution, University of Lausanne, 1015 Lausanne, Switzerland. E-mail: michel.chapuisat@unil.ch

Chemically similar queen pheromones inhibit worker reproduction in ants, wasps, and some bees, suggesting that these pheromones have served to signal fertility for 150 million years.



Follow the queen. A bumblebee queen surrounded by her worker offspring. Van Oystaeyen *et al.* show that the queen overproduces pentacosane, a long-chained alkane that inhibits ovary development in the workers. Yet, toward the end of the egg-laying season, many workers start reproducing. The chemical communication that regulates reproductive competition may be bidirectional: Nonreproductive bumblebee workers produce specific esters that might protect them from being aggressed by the queen (12).

can thus help to determine whether the pheromone has a control or a signal function.

Van Oystaeyen *et al.* identified queen pheromones inhibiting worker reproduction in an ant, a wasp, and a bumblebee species. They compared the hydrocarbon profiles on the cuticles of queens and workers, selected several compounds that are overproduced in queens, and tested their effect on queenless groups of workers. Control groups of workers exposed to pentane quickly developed their ovaries. By contrast, workers exposed to several synthetic long-chained alkanes remained infertile and even exhibited ovarian regression. Thus, queen-produced, long-chained saturated hydrocarbons stop workers from reproducing in three divergent lineages of Hymenoptera.

Next, the authors reviewed existing data on putative queen pheromones across 64 species of social Hymenoptera, mapped them on the phylogeny, and reconstructed the ancestral state. They show that a class of saturated cuticular hydrocarbons is more abundant in queens than workers in the vast majority of species and in all major lineages.

Differences in cuticular hydrocarbons between reproductive and nonreproductive individuals are so widespread throughout the phylogeny that they were most likely already present in the basal solitary lineage at the origin of all hymenopteran lineages that later acquired eusociality independently. Before the emergence of communication, such differences constituted unselected cues. Because cuticular hydrocarbons are produced during egg formation, they convey inadvertent information on the fertility of their bearers (8). If some individuals react to these cues in ways that benefit them and the producer, selection can enhance the emission and reception until an efficient communication system based on evolved signals is established. In line with this reasoning, cuticular hydrocarbons appear to have become fertility signals in ants, bees, and wasps (4, 8).

Given the diversity of cuticular hydrocarbons, it is remarkable that a few structurally similar compounds suppress worker reproduction in lineages as divergent as ants, wasps, and bees. Based on this similarity, Van Oystaeyen *et al.* suggest that cuticular hydro-

PHOTO: RICARDO CALLARI OLIVEIRA

carbons were already used as signals of fertility in solitary ancestors of social Hymenoptera before the major lineages diverged in the early Cretaceous (~145 million years ago). One might wonder why such a communication system would evolve in solitary ancestors. Van Oystaeyen *et al.* propose that the ancestral fertility signal was directed to males. In support of this hypothesis, cuticular hydrocarbons are used as contact sex pheromones in solitary wasps (9). Communication among solitary females is a possible alternative. Indeed, parasitoid wasps use cuticular hydrocarbons to inform other females that an egg has already been deposited in a host (10).

The hypothesis that queen pheromones evolved from a preexisting communication system in solitary ancestors has interesting implications for the evolution of eusociality. In the early stage of sociality, daughters may respond to maternal fertility signals by helping the mother if she is highly fertile, and reproducing if she is not (3). By allowing this conditional response, a preexisting pheromonal communication of fertility may have facilitated the transition to eusociality.

Alternatively, queen pheromones may have evolved independently in several

hymenopteran lineages from a small number of major fertility cues that were already present in solitary ancestors. Similar selection pressures can lead to convergent adaptations across distant species. To rule out the possibility of convergence in the queen-worker communication system, the precise degree of conservation of each compound should be further investigated. This could be done by testing a representative array of queen-specific compounds across divergent species and by investigating the genetic basis of pheromone biosynthesis (11). Studies of cuticular hydrocarbon presence and perception in solitary species and in highly social species with permanently sterile workers will also shed light on the origin and maintenance of queen pheromones.

Van Oystaeyen *et al.*'s finding that queen pheromones are stable in multiple lineages of Hymenoptera is consistent with the hypothesis that queen pheromones are honest fertility signals that benefit both queens and workers (7). There was no sign of rapid evolutionary changes and shifts in classes of chemicals, as expected in conflict situations. This is not to say that conflicts are absent. For example, cases where workers escaped pheromonal

inhibition have been documented in the honeybee (5). But the persistence of the queen's perfume over 150 million years of evolution suggests that workers generally benefit when they refrain from reproducing in the presence of a fertile queen. It is striking that, in the absence of the queen perfume, some ant, bee, and wasp workers still start laying eggs today, as they probably did in the Cretaceous.

References

1. Y. Le Conte, A. Hefetz, *Annu. Rev. Entomol.* **53**, 523 (2008).
2. K. Matsuura *et al.*, *Proc. Natl. Acad. Sci. U.S.A.* **107**, 12963 (2010).
3. L. Holman, R. Lanfear, P. d'Ettorre, *J. Evol. Biol.* **26**, 1549 (2013).
4. A. Van Oystaeyen *et al.*, *Science* **343**, 287 (2014).
5. F. L. W. Ratnieks *et al.*, *Annu. Rev. Entomol.* **51**, 581 (2006).
6. B. Hölldobler, E. O. Wilson, *Ann. Entomol. Soc. Am.* **76**, 235 (1983).
7. L. Keller, P. Nonacs, *Anim. Behav.* **45**, 787 (1993).
8. J. Liebig, in *Insect Hydrocarbons: Biology, Biochemistry, and Chemical Ecology*, G. J. Blomquist, A. G. Bagnères, Eds. (Cambridge Univ. Press, Cambridge, 2010), pp. 254–281.
9. K. Böröczky *et al.*, *J. Chem. Ecol.* **35**, 1202 (2009).
10. E. Darrouzet *et al.*, *J. Chem. Ecol.* **36**, 1092 (2010).
11. O. Niehuis *et al.*, *Nature* **494**, 345 (2013).
12. E. Amsalem *et al.*, *Proc. Biol. Sci.* **276**, 1295 (2009).

10.1126/science.1249285

PHYSICS

Probing the Electron

Kenneth R. Brown

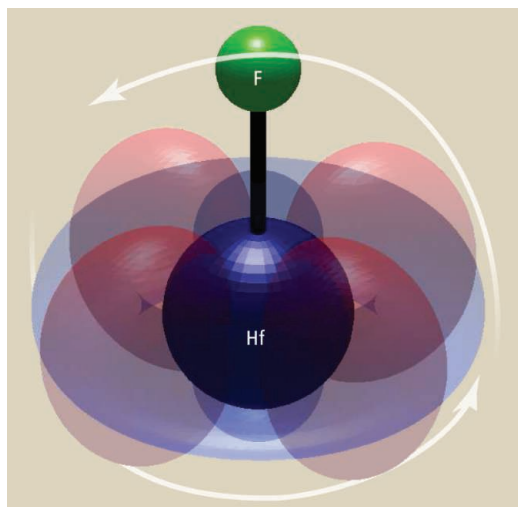
Ordinary matter is made of fast-moving electrons and slow-moving nuclei. The dynamics of electrons accounts for most material properties from color to reactivity. Our success in predicting the physics of semiconductors and the chemistry of molecules depends on our ability to characterize the electron. The electron is vanishingly small, and its properties can be well described by three parameters: mass, charge, and magnetic dipole. All of these parameters have been measured to extreme precision. Theoretical models of physics predict that the electron will also have a very small electric dipole moment. A strong electric field is required to detect a small electric dipole, and one proposed method is to observe the properties of the electron in the internal electric field of a polar molecule. Loh *et al.* (1) recently demonstrated that molecular ions can

also be used for this task. On page 269 of this issue, Baron *et al.* (2) report on measurements that lower the bound for the electron's electric dipole moment.

To observe the strong internal fields, the molecule or molecular ion must be aligned.

Can tabletop experiments using polar molecules to reveal the internal structure of the electron point to physics beyond the Standard Model?

Otherwise, the rotation of the molecule will wash out any possible signal. For a polar molecule, this alignment can be performed by applying an external electric field (2, 3). Baron *et al.* use a cryogenic buffer gas beam of thorium monoxide (ThO) molecules between two electric plates. An electric field of approximately 100 V/cm orients the molecular dipole, and lasers then interrogate the molecule for a possible signature of the electron electric dipole moment. The measurements of Baron *et al.* place a bound on the electron electric dipole moment to be below 8.7×10^{-29} e-cm, an



Spin it up and peek inside. Schematic of the experiment of Loh *et al.* from the perspective of the molecular ion HfF^+ . The red and blue shapes approximate the orbitals of the two highest energy electrons. The white arrow represents the motion of the molecule as it follows the field.

Schools of Chemistry and Biochemistry; Computational Science and Engineering; and Physics, Georgia Institute of Technology, Atlanta, GA 30332–0400, USA. E-mail: ken.brown@chemistry.gatech.edu

order of magnitude improvement over the previous bound measured in YbF (3).

An alternative approach to neutral beams is to use trapped molecular ions. For an ion held in a radio-frequency trap, a static electric field of sufficient strength to polarize the molecule will also push it out of the trap. The proposed solution to the problem was applying a strong rotating field (4). In the frame of that field, one gains the benefits of both holding trapped ions for a long time and polarization of the molecule (see the figure).

Loh *et al.* use the rotating field method to limit the electron electric dipole moment to be less than 1.5×10^{-25} e-cm. This initial experiment is three orders of magnitude above the ThO result of Baron *et al.* The experiment of Loh *et al.* shows that precision measurements can be performed with molecular ions, and future experiments will be competitive with the neutral molecule and atom measurements.

Of course, more exciting than limiting the electron electric dipole moment would be to measure it. Why does theoretical physics tell us to expect it, and what do we expect

the magnitude to be? These are both challenging questions to explain simply. An electric dipole moment requires an interaction that violates both parity and time symmetry. Everyday laws of physics are invariant if we relabel forward and backward in space and time. However, the laws that govern subatomic particles are not. They satisfy a combined symmetry of charge conjugation, parity, and time.

The Standard Model of particle physics allows for a violation of time and parity symmetry, and from the known interactions we can estimate that the electron electric dipole moment will be smaller than 10^{-38} e-cm (5). Extensions to the Standard Model, for example, supersymmetric or left-right symmetric models, can produce electron electric dipole moments near the current limits of detection. As a result, tabletop experiments are beginning to limit which theoretical models are compatible with the observed world.

Normally, when considering questions about particle physics, one thinks of large particle accelerator experiments. The excitement of the discovery of the Higgs boson at

the Large Hadron Collider (LHC) (6, 7) and the award of this year's Nobel prize for its prediction are testaments to this method of inquiry. A challenge for the tabletop experiments is that at present the results at the LHC are consistent with the Standard Model. The lack of detection of other new particles also limits possible theoretical models of our world and, as a result, the value of the electron electric dipole moment. It is unclear at the moment whether investigation at high precision or investigation at high energy will be first to reveal additional physics beyond the Standard Model.

References

1. H. Loh *et al.*, *Science* **342**, 1220 (2013).
2. J. Baron *et al.*, *Science* **343**, 269 (2014); 10.1126/science.1248213.
3. J. J. Hudson *et al.*, *Nature* **473**, 493 (2011).
4. A. E. Leanhardt *et al.*, *J. Mol. Spectrosc.* **270**, 1 (2011).
5. E. D. Commins, in *Advances in Atomic, Molecular, and Optical Physics*, B. Bederson, H. Walther, Eds. (Academic Press, 1999), vol. 40, pp. 1–55.
6. ATLAS Collaboration, *Phys. Lett. B* **716**, 1 (2012).
7. C. M. S. Collaboration, *Phys. Lett. B* **716**, 30 (2012).

Published online 19 December 2013

10.1126/science.1246820

MEDICINE

How Thalidomide Works Against Cancer

A. Keith Stewart

The 55-year history of the drug thalidomide is Shakespearean in scope, awash in unintended consequences, tragedy, resilience, driven characters, and redemption. Indeed, the most notorious pharmaceutical of modern times comes replete with images of devastating birth defects still firmly embedded in the public consciousness. Less well known has been the resurgence in its use as a therapy to treat hematologic malignancy. On pages 305 and 301 of this issue, Lu *et al.* (1) and Krönke *et al.* (2), respectively, report that thalidomide and derivative compounds have a toxic effect on multiple myeloma by causing the degradation of two transcription factors, Ikaros and Aiolos. This loss halts myeloma growth while simultaneously altering immune cell function.

In an archetypal example of drug repositioning, reports emerged 15 years ago that

thalidomide could be profoundly effective in patients with multiple myeloma (3), a tumor of antibody-producing plasma cells in the bone marrow. The malignancy is characterized by anemia, bone fractures, kidney failure, and recurrent infection. Subsequently, the thalidomide analogs lenalidomide and pomalidomide (collectively called immune modulating drugs or IMiDs) were shown to be even more potent in treating multiple myeloma, and today these small molecules form a highly effective backbone of therapy for this increasingly treatable cancer and for other hematologic malignancies (4).

Many studies over the years have sought to explain the mechanism of teratogenicity of thalidomide. Thalidomide, lenalidomide, and pomalidomide were found to have wide-ranging and seemingly disparate cellular actions, including induction of oxidative stress and inhibition of angiogenesis, as well as multiple effects on the immune system—enhanced production of the cyto-

The surprising ability of thalidomide and its analogs to treat various hematologic malignancies is through the loss of two transcription factors.

kine interleukin-2 (IL-2) (which spurs T cell production), inhibition of the cytokine tumor necrosis factor (TNF), and the stimulation of natural killer cells (5). The property of antiangiogenesis inspired the suggestion that thalidomide might be useful as a last-gasp attempt to control drug-resistant multiple myeloma. A remarkable success story in controlling this cancer with thalidomide soon followed (3). Unfortunately, it did not take long to show that although antiangiogenesis may be a consequence of thalidomide therapy, it was not the mechanism of action that explained its clinical effect.

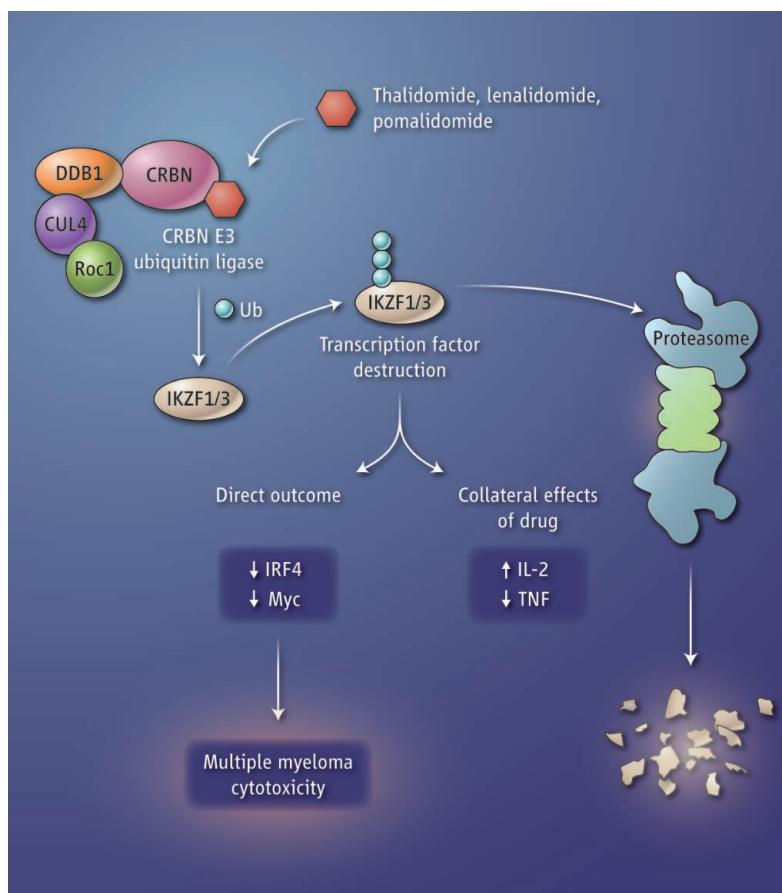
The seminal breakthrough emerged in 2010 when thalidomide was found to bind to the protein cereblon (6). Cereblon forms an E3 ubiquitin ligase complex with the proteins damaged DNA binding protein 1 (DDB1), Cullin-4A (CUL4A), and regulator of cullins 1 (Roc1). This complex tags specific proteins with ubiquitin, thereby targeting them for proteolysis. The drug-protein interaction

Mayo Clinic, 13400 East Shea Boulevard, Scottsdale, AZ 85259, USA. E-mail: stewart.Keith@mayo.edu

disrupts the activity of the E3 ubiquitin ligase complex, which underpins the cytotoxic and immune-modulating effects of IMiDs. Some of these effects were reversible by overexpressing the downstream proteins whose expression was reduced following IMiD treatment, such as the transcription factors interferon regulatory factor 4 (IRF4) and Myc (7–9). Although research into the clinical importance of this observation is still fresh, it seems clear that low amounts of cereblon in multiple myeloma cells correlate with clinical drug resistance and poor survival outcomes (10).

Lu *et al.* and Krönke *et al.* demonstrate that the zinc finger-containing transcription factors Ikaros (IKZF1) and Aiolos (IKZF3) are selectively bound by cereblon. After direct binding, IMiDs activate cereblon's E3 ligase activity, resulting in the rapid ubiquitination and degradation of Ikaros and Aiolos. Ikaros and Aiolos are transcriptional regulators of B and T cell development (11, 12). Aiolos is required for normal plasma cell development in mice (13). The toxic effects on multiple myeloma cells resulting from the loss of these two transcription factors are reversed by deletion of critical cereblon-binding regions of Ikaros prior to drug treatment. Under normal conditions, Ikaros suppresses expression of the gene encoding IL-2 in T cells but conversely stimulates expression of IRF4 (a transcription factor that responds to infection). Thus, a decrease in Ikaros explains the perplexing question of how one drug can both activate the immune system (a boost in IL-2 production by T cells stimulates immune responses) and degrade B cell function (as the result of reduced IRF4 expression) simultaneously.

Analysis of the cereblon–Ikaros/Aiolos–IRF4/Myc signaling pathway now opens doors to developing of more precise and effective therapeutics and biomarkers for drug response while raising some more issues for biologists and clinicians. For example, how can Ikaros depletion simultaneously be



Immune modulators and myeloma. The small-molecule drugs thalidomide, lenalidomide, and pomalidomide bind to the protein cereblon (CRBN), which activates the enzymatic activity of the CRBN E3 ubiquitin ligase complex. The transcription factors Ikaros (IKZF1) and Aiolos (IKZF3) are modified with ubiquitin (Ub) molecules, targeting them for proteolysis. This alters the function of T cells and B cells, with a toxic outcome for multiple myeloma cells.

an effective anticancer target but also act as a tumor suppressor underpinning the development of acute lymphoblastic leukemia, an early B cell malignancy (14)? Presumably, different Ikaros isoforms function as regulators of gene expression in different cellular contexts. A logical progression might be that deletion of Ikaros by the IMiDs, under the wrong circumstances, could simultaneously kill multiple myeloma cells but promote pre-B cell leukemogenesis. Indeed, clinical experience demonstrates a slightly higher risk of leukemias and B cell malignancies in patients treated with immune modulatory drugs, albeit only after exposure to a second genotoxic DNA-damaging agent, such as Melphalan, a commonly used multiple myeloma treatment (15). There are other clinical dilemmas that remain unexplained, such as why only one-third of relapsed patients respond to a single-agent immune modulatory drug and why patients lose cereblon or find alternative pathways to become resistant to these drugs.

Another perplexing clinical dilemma is that the action of IMiD drugs seems to absolutely require effective proteasomal degradation of Ikaros and Aiolos—a finding that flies in the face of clinical experience, which seems to support that combining an immune modulator with a proteasome inhibitor as a highly effective strategy for treating multiple myeloma (4). Evidently, the scientific saga of thalidomide and its analogs is a story still not fully told.

It is tempting to update the mythic tale of the Greek god Ikaros flying too close to the Sun, only to have his waxed wings melt, to the genomic-era equivalent as the namesake Ikaros transcription factor comes too close to its molecular sun—namely, cereblon that is bound to an immune modulatory drug, with its inevitable degradation (see the figure). A final but speculative conclusion of the studies by Lu *et al.* and Krönke *et al.* is that small molecules that enhance the ubiquitination and degradation of specific target proteins may represent a new class of therapeutics for manipulating proteins that were previously viewed as undruggable.

References

1. G. Lu *et al.*, *Science* **343**, 305 (2014); 10.1126/science.1244917.
2. J. Krönke *et al.*, *Science* **343**, 301 (2014); 10.1126/science.1244851.
3. S. Singhal *et al.*, *N. Engl. J. Med.* **341**, 1565 (1999).
4. A. K. Stewart, P. G. Richardson, J. F. San-Miguel, *Blood* **114**, 5436 (2009).
5. Y. X. Zhu, K. M. Kortuem, A. K. Stewart, *Leuk. Lymphoma* **54**, 683 (2013).
6. T. Ito *et al.*, *Science* **327**, 1345 (2010).
7. Y. X. Zhu *et al.*, *Blood* **118**, 4771 (2011).
8. A. L. Shaffer *et al.*, *Nature* **454**, 226 (2008).
9. L. H. Zhang *et al.*, *Br. J. Haematol.* **160**, 487 (2013).
10. S. R. Schuster *et al.*, *Leuk. Res.* **38**, 23 (2014).
11. B. Morgan *et al.*, *EMBO J.* **16**, 2004 (1997).
12. K. Georgopoulos *et al.*, *Cell* **79**, 143 (1994).
13. M. Cortés, K. Georgopoulos, *J. Exp. Med.* **199**, 209 (2004).
14. C. G. Mullighan *et al.*, *Nature* **453**, 110 (2008).
15. H. Ludwig *et al.*, *Blood* **119**, 3003 (2012).

10.1126/science.1249543

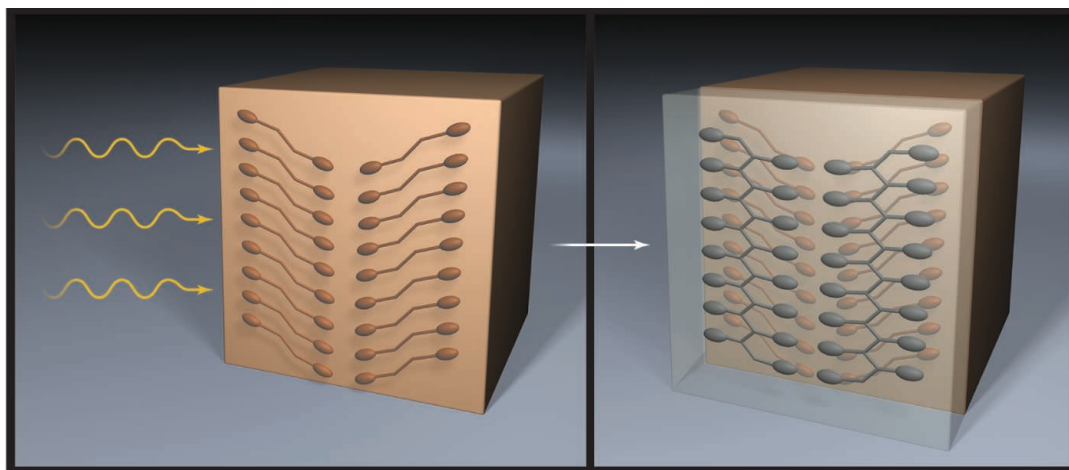
CHEMISTRY

A Clear Path for Polymer Crystallization

Nancy S. Goroff

The interior of a molecular crystal may not seem like the ideal environment for setting up a chemical reaction. The molecules in the crystal are held rigid, and there is no way to introduce new reagents or catalysts. However, for some reactions, a crystalline environment brings molecules together in a preferred orientation that leads to products that could not be formed in solution (1). The periodicity and high degree of order that characterize crystalline materials are particularly well suited to polymerization reactions, which can stitch monomers together into a highly ordered, nearly defect-free chain. The most commonly studied class of polymers made in this way are polydiacetylenes, prepared from crystals of molecular diyne monomers (2, 3). On page 272 of this issue, Dou *et al.* (4) report that a new class of polymers can be prepared by solid-state polymerization of organic dye molecules. Both the crystallization and the polymerization in this system are so favorable that the reaction can be carried out in highly concentrated solutions, where micro- or nano-crystalline aggregates control the chemistry.

Solid-state polymerization requires that the reactive parts of the monomers be near one another in the crystal structure. To initiate a reaction, energy must be added to the system in some way. Most solid-state polymerization reactions get started by subjecting the crystals to heat, ultraviolet light, or even pressure. The polymerization reported by Dou *et al.* is one of few known where visible light induces the reaction between monomers. The bis(indenone) monomers are highly colored conjugated organic dyes, but polymerization breaks the conjugation, so the resulting polymer strands are colorless. Thus, as layers in



Clearly connected. Dou *et al.* start with crystals of an organic dye molecule (shown in orange). Shining light on these crystals causes a solid-state reaction that produces a highly ordered, crystalline, and colorless polymer. Once one layer in the crystal has reacted, it becomes transparent, allowing the light to penetrate farther and induce further reaction in deeper layers.

the crystal undergo reaction, they become more transparent, making it easier for light to penetrate deeper in the crystal. When the reaction is done, the entire crystal is colorless (see the figure).

Dou *et al.* report that the polymerization reaction is reversible and that the polymer strands break back into monomers when heated. This reversibility may play a role in the polymerization from solution. They found that the solution-phase reaction produces a microcrystalline polymer rather than an amorphous material, which suggests that ordered growth of the crystals occurs simultaneously with polymerization. The reaction occurs only in highly concentrated solutions, where aggregates are presumably forming in dynamic equilibrium. A high-intensity visible light source provides the necessary energy to promote reaction in the aggregate. Once such a reaction occurs between monomers, the aggregate becomes fixed; the addition of new monomers lengthens the chain further.

The ability to obtain ordered crystalline materials from such conditions is very unusual. In solution, “mismatched” reaction of poorly aligned monomers often competes with the desired reaction, leading to disordered materials. However, if the mismatched connections between monomers are more likely to break apart, then over time an

Visible light polymerizes aggregates of colored organic molecules to create transparent polymer microcrystals.

ordered material can result. More important, the ability to prepare the polymer via solution processing or in thin films means that such materials can be used practically for a much broader set of applications.

One advantage of a high-yielding solid-state reaction is that the length of the resulting polymer depends entirely on the size of the crystal. Control over crystal growth then allows control over the growth of the polymer chain, resulting in very uniform polymer lengths. The flexibility of the polymerization process in this system means that Dou *et al.* have the opportunity to prepare different polymer samples in a wide range of lengths, but with relatively narrow size distribution (polydispersity) within each sample.

Dou *et al.* have also found a way to isolate individual polymer strands or small bundles of strands from within the crystal. Borrowing from the world of graphene research, they used the well-known “scotch tape” method for mechanical exfoliation (5)—in this case, separating individual polymer chains from the solid samples. This method should be applicable to other polymers formed in the solid state, including polydiacetylenes, thereby opening up new routes to characterize the properties of single polymer chains.

It remains to be seen whether the bis(indenone) polymers will be useful materi-

Department of Chemistry, Stony Brook University, Stony Brook, NY 11794, USA. E-mail: nancy.goroff@stonybrook.edu

als. One possible application is as a strengthening component in composite materials. Dou *et al.* report that these polymers are very strong along the polymer axis, whereas the strands are only very weakly held together. When a polymer strand does break, the color of the monomer returns, providing an internal diagnostic for detecting such damage. In such cases, irradiation with visible light may be able to repair the system.

Thus far, Dou *et al.* report only two examples of bis(indenones) that crystallize appropriately to form polymer. As is often the case,

relatively small changes in molecular structure lead to substantial changes in the crystal packing. Thus, it can be difficult to predict which molecular derivatives will successfully crystallize and lead to new polymers, or to design such derivatives with particular materials applications in mind. In the realm of polydiacetylene synthesis, a clear description of the structural crystal parameters necessary for polymerization, provided by Baughman in the 1970s (6), established an important framework for further design of new materials. If a similar structural understanding can be estab-

lished for the bis(indenone) polymers, new derivatives may broaden the available properties for this new class of materials.

References

1. K. Biradha, R. Santra, *Chem. Soc. Rev.* **42**, 950 (2013).
2. D. Bloor, R. R. Chance, Eds., *Polydiacetylenes: Synthesis, Structure and Electronic Properties* (Nijhoff, Dordrecht, Netherlands, 1985).
3. V. Enkelmann, *Adv. Polym. Sci.* **63**, 91 (1984).
4. L. Dou *et al.*, *Science* **343**, 272 (2014).
5. K. S. Novoselov *et al.*, *Science* **306**, 666 (2004).
6. R. H. Baughman, *J. Polym. Sci. Polym. Phys. Ed.* **12**, 1511 (1974).

10.1126/science.1249064

BIOCHEMISTRY

Many Paths to the Origin of Life

Jimmy Gollihar,¹ Matthew Levy,² Andrew D. Ellington¹

The origin of life remains a daunting mystery in part because rather than knowing too little, we increasingly know about too many possible mechanisms that might have led to the self-sustaining replication of nucleic acids and the cellularization of genetic material that is the basis of life on Earth.

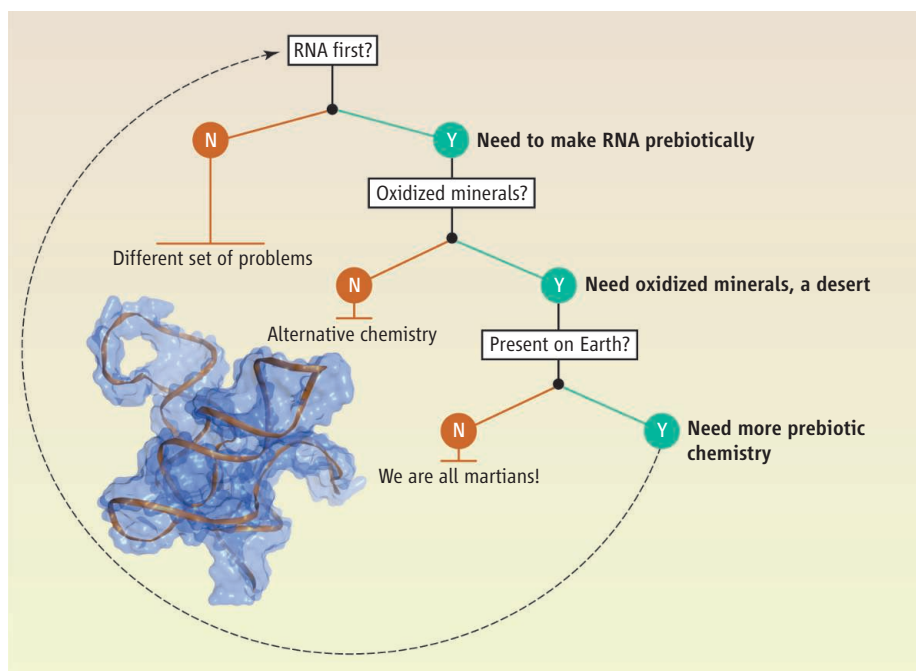
Initial insights that biological compounds could be generated by prebiotic means quickly ran up against a gap in our understanding of how unguided syntheses could result in defined templates for replication. For example, the proposed prebiotic formose reaction for the synthesis of the ribose sugar in nucleic acids from formaldehyde produces little more than intractable tars (1). How ribose might be produced in higher yields turned out to involve both clever synthetic transformations and synthetic adjuncts, in the form of minerals such as boron and molybdenum (2). Nonetheless, speculation that a boron-rich environment, such as Mars, may have initially resulted in life arising and then being seeded to Earth (see the figure) (3) merely moved prebiotic chemistry off-planet without dispelling our ignorance regarding which of the many possible pathways actually led to life.

It is possible that it is not a knowledge of prebiotic synthesis that is wanting, but knowledge of prebiotic replication. Simple organic replicators can be generated with varying degrees of efficiency and fidelity (4), and it is easy to imagine how such simple

replicators might have evolved in complexity. However, what remains unknown is the degree to which the replication cycle would have led to the purification of materials (such as ribose) from otherwise complex mixtures of prebiotic chemicals. For example, it has been argued that enantiomerically pure nucleic acids would have served as better substrates for short replicators than impure ones, in part because the ability to form tight bonds with a nascent template would have been improved. In contrast, the argument can also be made that some mismatches in

template-substrate pairings would have led to more robust replicators.

Once an early replicator established itself, and assuming that it selfishly favored chemically pure oligonucleotides or other substrates, the feedback cycle leading to the evolution of additional catalysts would have been difficult to derail. Ribozymes have been crafted that make carbon-carbon bonds, glycosidic bonds, phosphodiester bonds, and others (5), and it is possible that prebiotic analogs of these enzymes might have assisted in chemical syntheses in such an “RNA



A logic tree for the origin of life. A series of questions surrounding the chemistry and precursors required for life's origin on Earth or Mars. The inset is a modification of PDB 3R1L, a ligase ribozyme that has been further developed into a polymerase.

¹Center for Systems and Synthetic Biology, University of Texas, Austin, TX 78712, USA. ²Department of Biochemistry, Albert Einstein College of Medicine, Bronx, NY 10461, USA. E-mail: ellingtonlab@gmail.com

world” [a term originally credited to Gilbert (6)]. Biochemistry occurred on geochemical time scales, in which millions of years of a poor replicator (a blink on the geological time scale) might well have been necessary to craft a feedback cycle that led to a slightly better replicator, or to a replicator that could better feed itself by directing the chemistry around it. Of course, none of these speculations even touches on key issues relative to surface chemistry and nascent cellularizations (7).

We don’t need to displace prebiotic chemistry to Mars in order to have a well-defined path to life. Although there are many ill-defined paths (in some ways all equally plausible and all equally implausible) to life on Earth, recent research has begun to expand the likelihood of several of these paths. Primordial carbon fixation pathways, reminiscent of reactions found in extant methanotrophs, have been proposed in “metabolism-first” models of chemical evolution. By concentrating the necessary ingredients of life in compartments near hydrothermal vents, it may not be necessary to hypothesize reactions specific to martian deserts and the scarce methane atmosphere of a Hadean planet (8).

Once at least some metabolites become available and templates of whatever sort arise, the chance of “kick-starting” self-polymerizing ribozymes is an increasingly realistic option. A complex ribozyme ligase has been engineered to serve as a limited ribozyme polymerase capable of generating RNA transcripts long enough to have their own catalytic activity (9). This is not quite a demonstration of a self-replicase, but it nonetheless provides a means for understanding how the raw material of ribose-based life could have begun to accumulate. Similarly, oligonucleotides not much longer than those transcribed by the polymerase ribozyme can self-ligate in an exponential amplification cycle (10). When coupled with the demonstration that RNA oligonucleotides can self-assemble into autocatalytic networks (11), an origin can be imagined that involves the accumulation of short oligonucleotides by polymerization and ligation, and the parallel self-assembly of autocatalytic networks of longer enzymes that assisted with polymerization and ligation. Ultimately, a fully functional RNA polymerase should evolve from the heady broth of reactions in the primordial soup.

We on Earth are still left with a distinct lack of prebiotically synthesized, ribose-based oligonucleotides to feed the RNA world. But, as previously noted (12), we don’t necessarily have to start with ribose (see the figure, left). Several lines of evidence suggest that backbone and linkage heterogene-

ities, once considered problematic in early synthesis strategies, are permissible in functional RNAs. Ribozymes and aptamers have both been shown to tolerate such heterogeneity. Indeed, such a mixed pool may have afforded a selective advantage by lowering the melting temperatures needed to separate polymer strands (13). Such mixed pools may also be more accessible via other prebiotic synthesis pathways (14).

As RNA or an alternative precursor nucleic acid begins to self-replicate, protection from molecular parasites and the low concentrations of needed substrates become paramount in propagating chemical information content. Compartmentalization of the genetic/catalytic machinery would have necessarily been an early invention or co-option of a self-replicase. The demonstration of protocell division based on simple physical and chemical mechanisms (15) lends credence to the idea that nucleic acid and vesicle replicators got together for mutual benefit.

The great benefit of the demonstration of prebiotic amino acid synthesis from a simple gas mix and an electrical spark was not that it was a cookbook for how things occurred, but rather that it was the identification of a

plausible path to an origin of life that would continue to bear experimental fruit. So it is with the chemistry, catalysts, and self-reproducing networks of today. The demonstration of ribose formation under some prebiotic conditions does not necessarily mean that we have to punt to Mars, but rather that a problem once thought intractable is now yielding to broader scientific inquiry (13, 14).

References

1. R. Shapiro, *Origins: A Skeptic's Guide to the Creation of Life on Earth* (Summit, New York, 1986).
2. S. A. Benner, H.-J. Kim, M. A. Carrigan, *Acc. Chem. Res.* **45**, 2025 (2012).
3. S. A. Benner, *Mineral. Mag.* **77**, 686 (2013).
4. A. J. Meyer et al., *Chem. Res.* **45**, 2097 (2012).
5. G. F. Joyce, *Angew. Chem. Int. Ed.* **46**, 6420 (2007).
6. W. Gilbert, *Nature* **319**, 618 (1986).
7. T. Matsuura et al., *Proc. Natl. Acad. Sci. U.S.A.* **99**, 7514 (2002).
8. W. Nitschke, M. J. Russell, *Philos. Trans. R. Soc. London Ser. B* **368**, 20120258 (2013).
9. A. Wochner et al., *Science* **332**, 209 (2011).
10. A. C. Ferretti, G. F. Joyce, *Biochemistry* **52**, 1227 (2013).
11. N. Vaidya et al., *Nature* **491**, 72 (2012).
12. A. Eschenmoser, *Science* **284**, 2118 (1999).
13. A. E. Engelhart et al., *Nat. Chem.* **5**, 390 (2013).
14. M. W. Powner, S.-L. Zheng, J. W. Szostak, *J. Am. Chem. Soc.* **134**, 13889 (2012).
15. T. F. Zhu, K. Adamala, N. Zhang, J. W. Szostak, *Proc. Natl. Acad. Sci. U.S.A.* **109**, 9828 (2012).

10.1126/science.1246704

MOLECULAR BIOLOGY

Ribose—An Internal Threat to DNA

Keith W. Caldecott

The removal of RNA inadvertently incorporated into our DNA is critical for maintaining genome integrity.

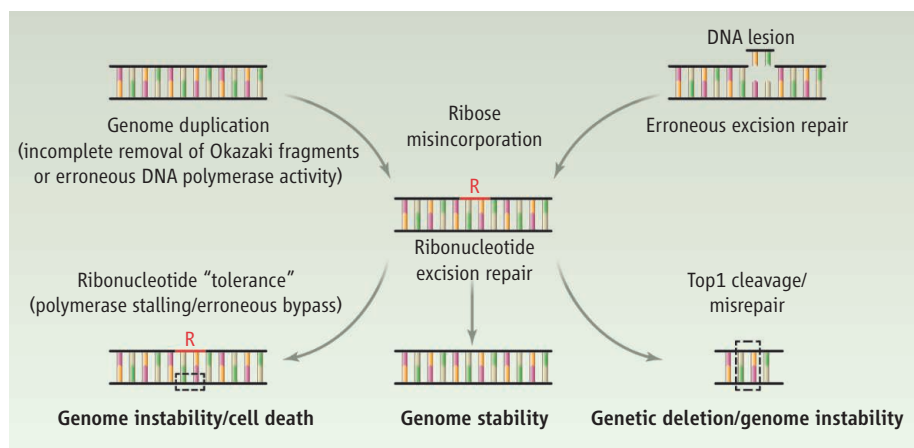
Our genomes possess an intrinsic level of instability, resulting both from an inherent lability of the chemical bonds of the deoxyribonucleotides that make up DNA and from their vulnerability to endogenous reactive molecules within the cell. Yet, there is an additional, more insidious, source of attack on our genetic material: the misincorporation of RNA, the chemical sister of DNA.

The contamination of DNA with ribonucleotides, the normal constituents of RNA, can arise in several ways (see the figure). Because DNA polymerases synthesize DNA in only one direction, copying of one of the two strands of DNA during genome duplication is discontinuous, employing short hybrid molecules—Okazaki frag-

ments—that consist of a stretch of RNA (~10 nucleotides) followed by a stretch of DNA (200 to 300 nucleotides). The ribonucleotides in Okazaki fragments are normally removed and replaced with deoxyribonucleotides during DNA replication by the concerted action of DNA polymerases, endonucleases, and DNA ligases. However, failure to completely remove the ribonucleotides can result in the retention of short stretches of ribose, the backbone sugar of RNA, in DNA.

Ribonucleotides can also be misincorporated by the erroneous activity of DNA polymerases, either during the process of genome replication or during the “cut-and-patch” processes by which damaged genomes are repaired (1, 2). Although DNA polymerases exhibit a marked preference for incorporation of deoxyribonucleotides, the greater cellular abundance of ribonucleo-

Genome Damage and Stability Centre, University of Sussex, Falmer, UK. E-mail: k.w.caldecott@sussex.ac.uk



RNA contamination in DNA. Routes of ribonucleotide (R) misincorporation into DNA are shown in the upper part of the figure. Mechanisms of ribonucleotide removal or tolerance are shown in the lower part of the figure.

tides enables sporadic incorporation of the latter in DNA at an appreciable frequency. While some DNA polymerases possess an intrinsic exonuclease “proofreading” function, to remove incorrectly incorporated nucleotides, this activity is limited on ribonucleotides (3, 4). It has been estimated that >10,000 or >1,000,000 ribonucleotides are incorporated, respectively, into yeast and mouse genomes during each cell division, making ribose contamination likely the most frequent source of cellular DNA damage in eukaryotic cells (5, 6).

Although there are specific circumstances in which ribonucleotide incorporation in DNA may be useful (1, 7, 8), overall the presence of ribose in DNA is detrimental. Ribose and deoxyribose differ only in the additional presence of an oxygen atom at the C2' position of the sugar in the former, yet the nucleophilicity of this oxygen renders the sugar-phosphate backbone in RNA several orders of magnitude more susceptible to strand breakage than in DNA. The ribonucleotides themselves and/or the DNA single-strand breaks (SSBs) that arise from them directly or indirectly can result in blockages to DNA or RNA polymerases and/or nucleotide deletions during DNA replication, threatening genetic stability and cell viability (4–6) (see the figure).

The threat posed by ribose contamination in the genome is countered by a number of DNA repair processes that remove this sugar (see the figure). The primary such pathway, ribonucleotide excision repair (RER), uses endoribonucleases [principally ribonuclease (RNase) H2] to cut the DNA backbone immediately 5' to a ribonucleotide, creating a SSB intermediate in which the ribonucleotide is attached to the 5' terminus (9). This pathway then uses DNA polymerase, flap endonuclease,

and DNA ligase to remove and replace the section of nucleic acid containing ribose in a manner reminiscent of the process that removes ribonucleotides from Okazaki fragments during genome duplication. Another possible route for ribose removal from DNA, particularly in the absence of RER, uses the nicking activity of topoisomerase I (Top1) (10). In contrast to RNase H2, Top1 cuts the DNA backbone on the 3' side of ribonucleotides, creating a SSB in which the ribonucleotide is attached to the 3' terminus. The latter pathway is unlikely to be favored, however, because it appears to promote deletions in DNA. Should DNA repair mechanisms fail to remove genomic ribonucleotides quickly enough, “tolerance” pathways are available that enable cells to replicate, and possibly transcribe, DNA containing ribose, albeit at reduced efficiency and with an increased chance of inducing mutations and/or cell death (4, 11) (see the figure).

Many of these studies were conducted in lower eukaryotes. However, it is likely that ribose is also a threat to mammalian genomes. Whereas in wild-type mouse cells genomic ribonucleotides are below current detection limits, it has been estimated that they are present at a steady-state level of ~1,000,000 per genome (~1 per 8000 base pairs) in cells lacking RNase H2 (and thus lacking RER) (5). Such cells exhibit p53-dependent cell cycle arrest, genome instability, and embryonic lethality. Although this could reflect the role for RNase H2 in removing aberrant RNA-DNA hybrids (“R loops”) generated during transcription, it could also reflect the replication stress arising from increased ribose and/or ribose-induced SSBs encountered during the rapid cycles of genome duplication during embryo development. Intriguingly, hypomorphic mutations in

RNase H2 result in Aicardi-Goutieres syndrome—a neuroinflammatory disorder that may result from a pathological inflammatory response to increased amounts of a nucleic acid species in blood and tissues arising from ribose-contaminated DNA (12).

While it is obvious why dividing cells suffer from ribose contamination in DNA, such contamination may also threaten postmitotic cells. Although global duplication of the nuclear genome does not occur in such cells, duplication of the mitochondrial genome continues. In addition, as mentioned above, short patches of 1 to 30 nucleotides of DNA are excised and replaced continuously in nuclear genomes during the “cut-and-patch” repair of other types of DNA lesion, such as those induced by oxidative stress. Given that the amount of ribonucleotides (relative to deoxyribonucleotides) is particularly high in postmitotic cells, it is possible that these DNA repair reactions are an important source of ribose contamination in postmitotic genomes. This may be especially true in long-lived postmitotic tissues such as the brain, in which the high level of oxidative stress (the brain consumes 20% of inhaled oxygen) and the longevity of postmitotic neurons (which must last a lifetime) may render this tissue particularly susceptible to ribose accumulation. Notably, defects in SSB repair have been linked to accelerated neurodegeneration (13), and genomic ribose may thus be one source of these SSBs. Consistent with this idea, the SSB intermediates arising during RER appear to be a preferred substrate for aprataxin (14), one of the SSB repair proteins that, if mutated, leads to progressive neurodegeneration.

The studies described above challenge the notion that the purity of DNA is an intrinsic property of its synthesis, and illustrate the effort required by cells to ensure that our genetic material retains its DNA identity.

References

1. J. Z. Dalgaard, *Trends Genet.* **28**, 592 (2012).
2. R. A. Gosavi, A. F. Moon, T. A. Kunkel, L. C. Pedersen, K. Bebenek, *Nucleic Acids Res.* **40**, 7518 (2012).
3. A. Y. Göksenin et al., *J. Biol. Chem.* **287**, 42675 (2012).
4. A. R. Clausen et al., *DNA Repair* **12**, 121 (2013).
5. M. A. M. Reijns et al., *Cell* **149**, 1008 (2012).
6. S. A. N. McElhinny et al., *Nat. Chem. Biol.* **6**, 774 (2010).
7. M. M. Ghodgaonkar et al., *Mol. Cell* **50**, 323 (2013).
8. S. A. Lujan et al., *Mol. Cell* **50**, 437 (2013).
9. J. L. Sparks et al., *Mol. Cell* **47**, 980 (2012).
10. J. S. Williams et al., *Mol. Cell* **49**, 1010 (2013).
11. F. Lazzaro et al., *Mol. Cell* **45**, 99 (2012).
12. Y. J. Crow et al., *Nat. Genet.* **38**, 910 (2006).
13. K. W. Caldecott, *Nat. Rev. Genet.* **9**, 619 (2008).
14. P. Tumbale et al., *Nature*, 10.1038/nature12824 (2013).

10.1126/science.1248234

RETROSPECTIVE

Frederick Sanger (1918–2013)

Sydney Brenner

Fred Sanger was a remarkable and unique scientist, and with his passing on 19 November 2013 we have lost one of the founders of molecular biology. He won two Nobel Prizes for chemistry, but we claim him for molecular biology because the methods he developed for sequencing proteins and nucleic acids provide the basis for much of what we do today.

Fred was born in Gloucestershire, UK, in 1918. He was educated at the University of Cambridge where he received his bachelor's degree in 1939 and his doctorate in 1943. In 1953, I attended the lecture he gave to the Alembic Club in Oxford on insulin. The meeting has remained in my mind for two reasons. One was the way he explained his work. He had a set of triangular blocks with the blank face turned to the audience, and as he went through the characterization of the peptide fragments, he turned the blocks around to display the amino acid, until he had assembled the sequences of the A and B chains of insulin. He would receive the Nobel Prize in Chemistry 5 years later for deciphering insulin's sequence. The other reason was a comment made by Nobel laureate Sir Robert Robinson in which he pointed out that chemists had viewed proteins as amorphous polymers, but Sanger had now proved that they had a definite chemical structure in the form of their amino acid sequences. This was an essential requirement for what the Nobel laureate Francis Crick later called the sequence hypothesis—that proteins were specified by the conversion of the one-dimensional sequence of nucleotides in DNA into the one-dimensional sequence of amino acids in the polypeptide chain; the conversion table was the genetic code. Proving this became the central problem of the early phase of molecular biology.

The geneticist Seymour Benzer had shown that recombination between mutations could be measured at single-nucleotide resolution, and combining this with chemical mutagenesis might allow us to compare a gene with its protein product—"sequencing" the gene by genetics and the protein product by Fred Sanger's techniques. When I came to the University of Cambridge in 1956, I went to see Fred in the Biochemistry Depart-



ment. I found him developing methods for sequencing small amounts of proteins using radioactive techniques. He was synthesizing ovalbumin, labeling it with radioactive amino acids, digesting the protein, and separating peptides by a "fingerprinting" method that combined high-voltage electrophoresis and chromatography (he had invented this procedure for his insulin work). We were later to use this method on bacteriophage T4 head protein, the first of the many examples of exploiting Fred's approaches to solve biological problems.

After Fred joined the Medical Research Council (MRC) Laboratory of Molecular Biology in 1962, he began to develop methods to sequence RNA because the small RNAs could be purified. Although the Nobel laureate Robert Holley was the first to sequence a transfer RNA (tRNA), Fred and his colleagues published the sequence of the 5S ribosomal RNA in 1967. Again, his methods were used to sequence and study suppressor tRNAs and their mutants.

Fred then turned his attention to DNA and developed the "plus-minus" method that produced fragments with defined ends. By 1975, he had sequenced most of the 5-kb genome of bacteriophage phiX178. He published the dideoxy method in 1977 and used it to sequence the 17-kb DNA of human mitochondria and the 46.5-kb genome of bacteriophage lambda. With the advent of cloning techniques in 1974, it had become clear to most molecular biologists that a new era of research was beginning. Fred would share the 1980 Nobel Prize for chemistry with Walter Gilbert and Paul Berg for leading the way. Certainly, genetics would be different; we

Twice awarded the Nobel Prize, a biochemist's work on protein and DNA structure opened the door to modern biomedical science.

were no longer tied to the reproductive cycles of organism and could study the DNA directly, even of organisms long extinct. And biochemistry would change as well, because the nucleic acid can be used to produce any amount of the protein we require. Being able to sequence DNA turned embryology into a science and provided insights into physiology that we could not have acquired so easily. It will continue to give us an understanding into the most interesting organism on

this planet—ourselves.

Fred has often been called a modest person, but his objectives were far from modest. He combined a singularity of purpose with a mastery of the laconic understatement. He often referred to his scientific work as "messing around in a lab," and Seymour Benzer told me that when he met Fred in 1954, he asked Fred whether he knew Francis Crick. "Yes," said Fred, "the fellow who is rather keen on genes." When we met in Cambridge in 1961 to discuss how we would organize the new lab, Nobel laureate Max Perutz was worried that Fred might be chosen to be chairman, but Fred said "I don't do that sort of thing."

A Fred Sanger would not survive today's world of science. With continuous reporting and appraisals, some committee would note that he published little of import between insulin in 1952 and his first paper on RNA sequencing in 1967 with another long gap until DNA sequencing in 1977. He would be labeled as unproductive, and his modest personal support would be denied. We no longer have a culture that allows individuals to embark on long-term—and what would be considered today extremely risky—projects.

Fred retired in 1983. Although the MRC wanted directors to move on after retirement, an exception was made for Max Perutz. I asked Fred whether he would like to keep his small office and laboratory and stay on. In a characteristic way he said: "No. I have had enough. I want to build a boat and spend some time messing about in my garden." On the afternoon of his retirement, he put down his pipette, went to a small farewell party, and walked out of the lab and science.

Institute of Molecular and Cell Biology, 61 Biopolis Drive, Singapore, 138673. E-mail: sydney.brenner@hotmail.com

Medicaid Increases Emergency-Department Use: Evidence from Oregon's Health Insurance Experiment

Sarah L. Taubman,^{1*} Heidi L. Allen,² Bill J. Wright,³ Katherine Baicker,^{1,4} Amy N. Finkelstein^{1,5}

In 2008, Oregon initiated a limited expansion of a Medicaid program for uninsured, low-income adults, drawing names from a waiting list by lottery. This lottery created a rare opportunity to study the effects of Medicaid coverage by using a randomized controlled design. By using the randomization provided by the lottery and emergency-department records from Portland-area hospitals, we studied the emergency department use of about 25,000 lottery participants over about 18 months after the lottery. We found that Medicaid coverage significantly increases overall emergency use by 0.41 visits per person, or 40% relative to an average of 1.02 visits per person in the control group. We found increases in emergency-department visits across a broad range of types of visits, conditions, and subgroups, including increases in visits for conditions that may be most readily treatable in primary care settings.

In describing the merits of expanding Medicaid to the uninsured, federal and state policymakers often argue that expanding Medicaid will reduce inefficient and expensive use of the emergency department (*1–4*). However, expanded Medicaid coverage could either increase or decrease emergency-department use. On the one hand, by reducing the cost to the patient of emergency-department care, expanding Medicaid could increase use and total health care costs. On the other hand, if Medicaid increases primary care access and use or improves health, expanding Medicaid could reduce emergency-department use and perhaps even total health care costs. Despite the many claims made in public discourse, existing evidence on this topic is relatively sparse, and the results are mixed. Analyses of the 2006 health insurance expansion in Massachusetts found either unchanged (*5*) or reduced (*6*) use of emergency departments. A quasi-experimental analysis of expanded Medicaid eligibility for children found no statistically significant change in emergency-department use (*7*). However, quasi-experimental evidence from young adults' changes in insurance coverage found that coverage increased emergency-department use (*8, 9*). Likewise, the RAND Health Insurance Experiment from the 1970s, which randomized the level of consumer cost-sharing among insured individuals,

found that more comprehensive coverage increased emergency-department use (*10*).

In 2008, Oregon initiated a limited expansion of its Medicaid program for low-income adults, drawing about 30,000 names by lottery from a waiting list of almost 90,000 individuals. Those selected were enrolled in Medicaid if they completed the application and met eligibility requirements. This lottery presents a rare opportunity to study the effects of Medicaid coverage for the uninsured on emergency-department use with a randomized controlled design. By using Oregon's Medicaid lottery and administrative data from the emergency departments of hospitals in the Portland area, we examined the impact of Medicaid coverage on emergency-department use overall and for specific types of visits, conditions, and groups. The lottery allowed us to isolate the causal effect of insurance on emergency-department visits and care; random assignment through the lottery can be used to study the impact of insurance without the problem of confounding factors that might otherwise differ between insured and uninsured populations.

The Oregon Health Insurance Experiment

The lottery studied was for Oregon Health Plan (OHP) Standard, a Medicaid expansion program that provides benefits to low-income adults who are not categorically eligible for Oregon's traditional Medicaid program. To be eligible, individuals must be aged 19 to 64, Oregon residents, U.S. citizens or legal immigrants, without health insurance for 6 months, and not otherwise eligible for Medicaid or other public insurance. They must have income below the federal poverty level (which was \$10,400 for an individual and \$21,200 for a family of four in 2008) and

have less than \$2000 in assets. OHP Standard provides relatively comprehensive medical benefits (including prescription drug coverage) with no consumer cost sharing and low monthly premiums (between \$0 and \$20, based on income), provided mostly through managed care organizations.

Oregon conducted eight lottery drawings from a waiting list for this Medicaid program between March and September 2008. Among the individuals randomly selected by lottery, those who completed the application process and met the eligibility criteria were enrolled (fig. S1). The lottery process and the insurance program are described in more detail elsewhere (*11*). Multiple institutional review boards have approved the Oregon Health Insurance Experiment research.

Our prior work on the Oregon Health Insurance Experiment used the random assignment of the lottery to study the impacts of the first 2 years of Medicaid coverage (*11–13*). We found that Medicaid improved self-reported general health and reduced depression; we did not find statistically significant effects on measured physical health, specifically blood pressure, cholesterol, or glycated hemoglobin levels. We also found that Medicaid decreased financial strain but did not have statistically significant effects on employment or earnings. Perhaps most directly relevant to the current analysis, we found that Medicaid increased health care use. In particular, we found that Medicaid coverage increased self-reported access to and use of primary care, as well as self-reported use of prescription drugs and preventive care. Additionally, we found no statistically significant effect of Medicaid on self-reported use of the hospital or the emergency department; however, we did find that Medicaid increased hospital use as measured in hospital administrative data. We returned to this disparity between estimates from self-reported and administrative data below.

Data

We obtained visit-level data for all emergency-department visits to 12 hospitals in the Portland area from 2007 through 2009. Individuals residing in Portland and neighboring suburbs almost exclusively use these 12 hospitals (fig. S2). These hospitals also are responsible for nearly half of all inpatient hospital admissions in Oregon (*14*). We briefly describe the data here; additional details are given in the supplementary materials (*15*). The data are similar to those included in the National Emergency Department Sample (*16*) and include a hospital identifier, date and time of visit, detail on diagnoses, and whether the visit resulted in the patient being admitted to the hospital. We probabilistically matched these data to the Oregon Health Insurance Experiment study population on the basis of name, date of birth, and gender. We used these data to count emergency-department visits and to characterize the nature of

¹National Bureau of Economic Research (NBER), Cambridge, MA 02138, USA. ²Columbia University School of Social Work, New York, NY 10027, USA. ³Center for Outcomes Research and Education, Providence Portland Medical Center, Portland, OR 97213, USA. ⁴Department of Health Policy and Management, Harvard School of Public Health, Boston, MA 02115, USA. ⁵Department of Economics, Massachusetts Institute of Technology, Cambridge, MA 02142, USA.

*Corresponding author. E-mail: staub@nber.org

each visit, including the reason for the visit and whether it was an outpatient visit or resulted in a hospital admission.

The state provided us with detailed data on Medicaid enrollment for everyone on the lottery list. We used this to construct our measures of Medicaid coverage. We also obtained pre-randomization demographic information that people provided when they signed up for the lottery. We used these data (17), together with prerandomization measures of our outcome variables, in our examination of treatment and control balance.

We collected survey data from individuals on the lottery list, including Oregon-wide mail surveys about 1 year after the lottery and Portland-area in-person interviews about 2 years after the lottery. We used these data, described in more detail elsewhere (11, 12), to compare previously reported findings on self-reports of overall emergency-department use to the results in the administrative data.

Our study period included 10 March 2008 (the first day that anyone was notified of being selected in the lottery) through 30 September 2009 [the end date used in our previous analysis of administrative and mail survey data (11)]. This 18-month observation period represented, on average, 15.6 months (standard deviation = 2.0 months) after individuals were notified of their selection in the lottery. Our pre-randomization period included 1 January 2007 (the earliest date in the data) through 9 March 2008 (just before the first notification of lottery selection).

Statistical Analysis

The analyses reported here were prespecified and publicly archived (18). Prespecification was done to minimize issues of data and specification mining and to provide a record of the full set of planned analyses.

We compared outcomes between the treatment group (those randomly selected in the lottery) and the control group (those not randomly selected). Those randomly selected could enroll in the lotteried Medicaid program (OHP Standard) if they completed the application and met eligibility requirements; those not selected could not enroll in OHP Standard. Our intent-to-treat analysis, comparing the outcomes in the treatment and control groups, provides an estimate of the causal effect of winning the lottery (and being permitted to apply for OHP Standard).

Of greater interest may be the effect of Medicaid coverage itself. Not everyone selected by the lottery enrolled in Medicaid; some did not apply, and some who applied were not eligible for coverage (19). To estimate the causal effect of Medicaid coverage, we used a standard instrumental-variable approach with lottery selection as an instrument for Medicaid coverage. This analysis used the lottery’s random assignment to isolate the causal effect of Medicaid coverage (20). Specifically, it estimated

a local average treatment effect capturing the causal effect of Medicaid for those who were covered because of the lottery, under the assumption that winning the lottery only affects the outcomes studied through Medicaid coverage. In earlier work, we explored potential threats to this assumption and, where we could investigate them, did not find cause for concern (11). Imperfect (and nonrandom) take-up of Medicaid among those selected in the lottery reduced statistical power but did not confound the causal interpretation of the effect of Medicaid.

In the main tables and text, we present local-average-treatment-effect estimates of the effect of Medicaid coverage. In tables S2 to S5, we also present intent-to-treat estimates of the effect of lottery selection (i.e., of winning permission to apply for OHP Standard). Both the intent-to-treat and local-average-treatment-effect estimates are driven by the variation created by the lottery, and the *P* values are the same for both sets of estimates. The intent-

to-treat estimate may be a relevant parameter for gauging the effect of the ability to apply for Medicaid; the local-average-treatment-effect estimate is the relevant parameter for evaluating the causal effect of Medicaid for those actually covered.

The supplementary materials provide more detail on our analytic specifications (15). We analyzed outcomes at the level of the individual. Because the state randomly selected individuals from the lottery list but then allowed all of the selected individuals’ household members to apply for insurance, an individual’s treatment probability (i.e., the probability of random selection in the lottery) varied by the number of the individual’s household members on the list. To account for this, all analyses controlled for indicators for the individual’s number of household members on the list (who were linked through a common identifier used by the state), and all standard errors were clustered according to household. Except where we stratified on pre-randomization use of the emergency department,

Table 1. Treatment-control balance. We report the control mean (with standard deviation for continuous variables in parentheses) and the estimated difference between treatments and controls (with standard errors in parentheses) for the outcome shown in the left-hand column. The final rows report the pooled *F* statistics and *P* values from testing treatment-control balance on sets of variables jointly. These sets include the lottery list variables in the bottom section, the prerandomization versions of our outcome variables (table S6), and the combination. The top sample consists of individuals in the full Oregon Health Insurance Experiment (OHIE) sample (*N* = 74,922); the bottom sample consists of individuals in Portland-area postal codes (*N* = 24,646), also referred to as the emergency-department (ED) analysis sample. For variables that are percentages, the treatment-control differences are shown as percentage points.

	Control mean	Treatment-control difference
<i>Percent of full OHIE sample included in ED analysis sample</i>		
Included in ED analysis sample (%)	33.3	−0.1 (0.4)
<i>Lottery list characteristics, conditional on being in ED analysis sample</i>		
Year of birth	1968.3 (12.1)	0.1 (0.2)
Female (%)	55.4	−1.0 (0.6)
English as preferred language (%)	87.5	0.9 (0.5)
Signed up self for lottery (%)	92.9	0.1 (0.0)
Signed up first day of lottery (%)	9.1	0.6 (0.4)
Gave phone number (%)	86.6	0.3 (0.5)
Address a post office box (%)	2.6	0.1 (0.2)
Postal code median household income (\$)	43,027 (9406)	182 (136)
<i>F</i> statistic for lottery list variables		1.498
<i>P</i> value		0.152
<i>F</i> statistic for prerandomization versions of the outcome variables		0.909
<i>P</i> value		0.622
<i>F</i> statistic for lottery list and prerandomization variables		1.013
<i>P</i> value		0.448

outcome analyses also controlled for the pre-randomization version of the outcome (such as the presence of an emergency-department visit in the pre-March 2008 period when examining the outcome of having an emergency-department visit in the post-March 2008 study period). This is not required to estimate the causal effect of Medicaid but, by explaining some of the variance in the outcome, may improve the precision of the estimates. Our results are not sensitive either to excluding these prerandomization versions of the outcomes or to additionally including demographic characteristics (measured before randomization) as covariates (table S15). We fit linear models for all outcomes; our results are not sensitive to instead estimating the average marginal effects from logistic regressions for binary outcomes or negative binomial regressions for continuous outcomes (table S16).

Emergency-Department Analysis Sample

We restricted our analysis to individuals who, at the time of the lottery, lived in a five-digit postal code where residents almost exclusively used 1 of the 12 hospitals in our data (15). Fig. S1 shows the evolution of the study population from submitting names for the lottery to inclusion in the emergency-department analysis sample. Because of the postal code restriction, our analysis sample included about one-third of the full Oregon Health Insurance Experiment study population. Table 1 shows the characteristics of the included

sample. As expected, there was no difference in probability of inclusion in our analytic subsample between those selected in the lottery (treatments) and those not selected (controls) (-0.1 percentage points; $SE = 0.4$). There were also no statistically significant differences between the groups in demographic characteristics measured at the time of lottery sign-up (F statistic 1.498; $P = 0.152$), in measures of emergency-department use in the prerandomization period (F statistic 0.909; $P = 0.622$), or the combination of both (F statistic 1.013; $P = 0.448$).

Insurance Coverage

In our analysis, we defined Medicaid coverage as being covered at any point during the study period (10 March 2008 to 30 September 2009) by any Medicaid program. This included both the lotteried Medicaid program (OHP Standard) and the other nonlotteried Medicaid programs. The nonlotteried Medicaid programs are available to any low-income individual falling into particular eligibility categories, such as being pregnant or disabled; some individuals in both our treatment and control groups became covered through one of these alternative channels.

Being selected in the lottery increased the probability of having Medicaid coverage at any point during our study period by 24.7 percentage points ($SE = 0.6$). The lottery affected coverage through increasing enrollment in the lotteried Medicaid program (table S7). Previous estimates from survey data suggested that there was no

“crowd-out” of private insurance; the lottery did not affect self-reports of private insurance coverage (11, 12). For those who obtained Medicaid coverage through the lottery, there was an increase of 13.2 months of Medicaid coverage ($SE = 0.2$). This is less than the 18 months of the study period for several reasons: Lottery selection occurred in eight draws between March and October 2008, initial enrollment in Medicaid took 1 to 2 months after lottery selection, and some of those enrolled in Medicaid through the lottery lost coverage by failing to recertify as required every 6 months.

Emergency-Department Use

As shown in Table 2, top, Medicaid increased emergency-department use. In the control group, 34.5% of individuals had an emergency-department visit during our 18-month study period. Medicaid increased the probability of having a visit by 7.0 percentage points ($SE = 2.4$; $P = 0.003$). Medicaid increased the number of emergency-department visits by 0.41 visits ($SE = 0.12$; $P < 0.001$), a 41% increase relative to the control mean of 1.02 visits.

Table 2, bottom, shows the effects of Medicaid on emergency-department use separately for those with no visits, one visit, two or more visits, and five or more visits in the period before randomization. We also looked at those with two or more outpatient visits (visits that did not result in a hospital admission) before randomization. In all groups, Medicaid increased use (although results are not statistically significant in most of the smaller subsamples).

We also examined how the effects of Medicaid on emergency-department use differ in various other subgroups (see table S14 for estimates). Across the numerous subpopulations we considered, we did not find any in which Medicaid caused a statistically significant decline in emergency-department use; indeed, with one exception, all of the point estimates are positive. The increase in emergency-department use is larger for men than for women; there is some evidence of larger increases for younger individuals than for older individuals and of larger increases for those in poorer health.

Types of Emergency-Department Visits

We separated visits by whether they resulted in a hospital admission and by what time of day they occurred (Table 3). About 90% of emergency-department visits in the control sample are outpatient visits. The increase in emergency-department use from Medicaid was solely in outpatient visits; we found no statistically significant effect of Medicaid on emergency-department visits that result in an inpatient admission to the hospital.

We next separated visits into those occurring during on hours (7 a.m. to 8 p.m. Monday through Friday) and those occurring during off hours (nights or weekends). Just over half of the visits in our control sample occurred during on hours.

Table 2. Emergency-department use. We report the estimated effect of Medicaid on emergency-department use over our study period (10 March 2008 to 30 September 2009) in the entire sample and in subpopulations based on prerandomization emergency-department use. For each subpopulation, we report the sample size, the control mean of the dependent variable (with standard deviation for continuous outcomes in parentheses), the estimated effect of Medicaid coverage (with standard error in parentheses), and the P value of the estimated effect. Sample consists of individuals in Portland-area postal codes ($N = 24,646$) or specified subpopulation (N in table). For the percent-with-any-visits measures, the estimated effects of Medicaid coverage are shown as percentage points. The number-of-visits measures are unconditional, including those with no visits.

	<i>N</i>	Percent with any visits			Number of visits		
		Mean value in control group	Effect of Medicaid coverage	<i>P</i> value	Mean value in control group	Effect of Medicaid coverage	<i>P</i> value
<i>Overall</i>							
All visits	24,646	34.5	7.0 (2.4)	0.003	1.022 (2.632)	0.408 (0.116)	<0.001
<i>By emergency-department use in the prerandomization period</i>							
No visits	16,930	22.5	6.7 (2.9)	0.019	0.418 (1.103)	0.261 (0.084)	0.002
One visit	3881	47.2	9.2 (6.0)	0.127	1.115 (1.898)	0.652 (0.254)	0.010
Two+ visits	3835	72.2	7.1 (5.6)	0.206	3.484 (5.171)	0.380 (0.648)	0.557
Five+ visits	957	89.4	0.7 (8.3)	0.932	6.948 (7.635)	2.486 (2.079)	0.232
Two+ outpatient visits	3402	73.2	9.6 (6.0)	0.111	3.658 (5.375)	0.560 (0.742)	0.450

Both on- and off-hours use increased with Medicaid coverage.

We also classified visits by using an algorithm developed by Billings *et al.* (21) that is based on the primary diagnosis code for the visit. fig. S3 provides more detail on this algorithm and the most common conditions contributing to each classification. Those visits that required immediate care in the emergency department and that could not have been prevented were referred to as emergent, not preventable (21% of control sample visits). Visits that required immediate care in the emergency department but could have been prevented through timely ambulatory care were referred to as emergent, preventable (7%). Those visits that required immediate care but that could have been treated in an outpatient setting are referred to as primary care treatable (34%). Visits that did not require immediate care were classified as nonemergent (19%) (22). Medicaid statistically significantly increased visits in all classifications except for the emergent, nonpreventable category (Table 4). The increases were most pronounced in those classified as primary care treatable (0.18 visits; SE = 0.05; $P < 0.001$) and nonemergent (0.12 visits; SE = 0.04; $P = 0.001$). We also examined the impact of Medicaid on visits for a variety of different conditions (table S11), although even the most prevalent individual conditions represented a relatively small share of emergency-department visits (table S10). We did not find that Medicaid caused a statistically significant decrease in emergency-department use for any of the conditions we considered; indeed, once again the vast majority of point estimates are positive. We found statistically significant increases in emergency-department use for several specific conditions, including injuries, headaches, and chronic conditions.

Comparison to Results from Self-Reports

Table 5 compares the results of this analysis of administrative records to previously reported results from our mail survey data (11) and our in-person interview data (12). The top section summarizes the previously reported effects of Medicaid on overall emergency-department use (the only outcome measured in the self-reported data) in each of the three data sources. In contrast to the results from administrative records, neither set of self-reports produced statistically significant changes in emergency-department use. In prior work, we similarly found statistically significant effects of Medicaid on hospital use as measured in administrative data but not as measured in self-reports (11). This suggests that there may be some systematic reasons that changes in use are detectable in administrative data but not in self-reported data.

The results from the administrative data may differ from results from the self-reported data for a variety of reasons. We briefly summarize them

here and provide more detail in the supplementary materials (15). First, the time frame of analysis is different; in particular, we were able to study outcomes over longer periods in the administrative data. Second, the study populations were different; in particular, the self-reported data were by necessity limited to individuals who respond to the surveys or complete the interviews. Third, self-reports may differ from the admin-

istrative record even for the same individual over the same time frame (because of incorrect recollections, for example, or mistakes about the site of care).

The rest of Table 5 attempts to disentangle these factors by limiting the analysis to the same set of individuals and capturing use over the same time frame. In the second section, for respondents to the mail survey who are also in

Table 3. Emergency-department use by hospital admission and timing. We report the control mean of the dependent variable (with standard deviation for continuous outcomes in parentheses), the estimated effect of Medicaid coverage (with standard error in parentheses), and the *P* value of the estimated effect. Visits were on hours if they occurred from 7 a.m. to 8 p.m. Monday through Friday and off hours otherwise. Sample consists of individuals in Portland-area postal codes (*N* = 24,646). For the percent-with-any-visits measures, the estimated effects of Medicaid coverage are shown as percentage points. The number-of-visits measures are unconditional, including those with no visits.

	Percent with any visits			Number of visits		
	Mean value in control group	Effect of Medicaid coverage	<i>P</i> value	Mean value in control group	Effect of Medicaid coverage	<i>P</i> value
<i>By hospital admission</i>						
Inpatient visits	7.5	−1.2 (1.3)	0.385	0.126 (0.602)	−0.023 (0.028)	0.396
Outpatient visits	32.0	8.2 (2.4)	<0.001	0.897 (2.362)	0.425 (0.107)	<0.001
<i>By timing of visit</i>						
On-hours visits	25.7	5.7 (2.2)	0.010	0.574 (1.555)	0.232 (0.072)	0.001
Off-hours visits	21.9	6.1 (2.2)	0.005	0.456 (1.394)	0.208 (0.068)	0.002

Table 4. Emergency-department use by type of visit. We report the control mean of the dependent variable (with standard deviation in parentheses), the estimated effect of Medicaid coverage (with standard error in parentheses), and the *P* value of the estimated effect. We used the Billings *et al.* (21) algorithm to assign probabilities of a visit being each type and therefore analyzed only the number of visits (not the percent with any visits) as obtained by summing the probabilities across all visits for an individual. Sample consists of individuals in Portland-area postal codes (*N* = 24,646). The number-of-visits measures are unconditional, including those with no visits.

	Number of visits		
	Mean value in control group	Effect of Medicaid coverage	<i>P</i> value
<i>Required immediate care</i>			
Emergent, not preventable (Required ED care, could not have been prevented)	0.213 (0.685)	0.049 (0.033)	0.138
Emergent, preventable (Required ED care, could have been prevented)	0.074 (0.342)	0.038 (0.018)	0.032
Primary care treatable (Did not require ED care)	0.343 (0.948)	0.180 (0.046)	<0.001
<i>Did not require immediate care</i>			
Nonemergent	0.201 (0.688)	0.118 (0.035)	0.001
<i>Unclassified</i>			
	0.196 (0.734)	0.059 (0.037)	0.107

the administrative data sample, we compared results from self-reported use in the surveys to results from the administrative data for the same 6-month period as the survey. We did the same in the third section for the in-person interviews: For respondents to the in-person interview who are also in the administrative data sample, we compared results from self-reported use to results from the administrative data for the same 12-month period as the interview. For the same individuals and time frames, our point estimates were larger and our standard errors were smaller in the administrative data compared with the self-reports.

These results highlight important advantages of administrative data. Even for outcomes that can be self-reported, the emergency-department administrative data are able to capture a longer period and may have less misclassification, allowing for more precise estimates. An additional advantage of administrative data, of course, is that all of the analyses performed elsewhere in the paper on timing of visits and the detailed classification of visit type are only realistically possible with administrative records.

Discussion

Neither theory nor existing evidence provides a definitive answer to the important policy ques-

tion of whether we should expect increases or decreases in emergency-department use when Medicaid expands. Uninsured patients may seek treatment in the emergency department because of the legal requirement that hospitals provide care for emergent conditions regardless of insurance status (23), but uninsured patients can be charged for this legally required care. All else equal, basic economic theory suggests that by reducing the out-of-pocket cost of a visit that an uninsured person would face, Medicaid coverage should increase use of the emergency department. It is also possible that Medicaid coverage may increase real or perceived access to emergency-department care. There are, however, several potential offsetting channels by which Medicaid coverage could decrease emergency-department use. By increasing access to primary care, Medicaid coverage might allow patients to receive some care in physician offices rather than in the emergency department. Additionally, Medicaid coverage might lead to improved health and thus reduced need for emergency-department care.

It is difficult to isolate the impact of Medicaid on emergency-department use in observational data, because the uninsured and Medicaid enrollees may differ on many characteristics

(including health and income) that are correlated with use of the emergency department. Indeed, we show (table S17) that observational estimates that did not account for such confounding factors suggested much larger increases in emergency-department use associated with Medicaid coverage than the results from our randomized controlled setting.

By using the random assignment of the Oregon lottery, we could isolate the causal effect of Medicaid coverage on emergency-department use among low-income, uninsured adults. We found that Medicaid increases emergency-department use and estimated an average increase of 0.41 visits per covered person over an 18-month period, or about a 40% increase relative to the control average of 1.02 visits. A back-of-the-envelope calculation, using \$435 as the average cost of an emergency-department visit (24), suggests that Medicaid increases annual spending in the emergency department by about \$120 per covered individual.

We also examined the impact of Medicaid on types of visits, conditions, and populations in which we might expect the offsetting effects to be the strongest. In none of these did we detect a decline in emergency-department use. Emergency-department use increased even in classes of visits that might be most

Table 5. Comparing results from administrative data and self-reports.

We report the control mean of the dependent variable (with standard deviation for continuous outcomes in parentheses), the estimated effect of Medicaid coverage (with standard error in parentheses), and the *P* value of the estimated effect. At top, we report the estimates from table V in Finkelstein *et al.* (11), from table 5 in Baicker *et al.* (12), and from Table 2. Table 5 in Baicker *et al.* (12) reports only the number-of-visits measure; here, we also present the percent-with-any-visits measure

analyzed by using the same methodology. In the next two sections, we limited the previously published analyses to individuals also in the emergency-department data and compared the self-reported answers to the survey questions to the answers to the same survey questions constructed from administrative data. For the percent-with-any-visits measures, the estimated effects of Medicaid coverage are shown as percentage points. The number-of-visits measures are unconditional, including those with no visits.

	<i>N</i>	Percent with any visits			Number of visits		
		Mean value in control group	Effect of Medicaid coverage	<i>P</i> value	Mean value in control group	Effect of Medicaid coverage	<i>P</i> value
<i>Estimates in mail-survey, in-person, and emergency-department data</i>							
Mail survey	23,741	26.1	2.2	0.335	0.470	0.026	0.645
6 months before response			(2.3)		(1.037)	(0.056)	
In-person interview	12,229	40.2	5.4	0.189	0.997	0.094	0.572
12 months before interview			(4.1)		(1.999)	(0.166)	
Emergency-department data	24,646	34.5	7.0	0.003	1.022	0.408	<0.001
18-month study period			(2.4)		(2.632)	(0.116)	
<i>Limited to overlap sample between mail-survey and emergency-department data</i>							
Self-report of use	7239	25.6	−0.01	0.997	0.482	−0.046	0.666
6 months before response			(4.2)		(1.090)	(0.107)	
Administrative record of use	7239	16.2	4.6	0.197	0.296	0.052	0.538
6 months before response			(3.6)		(0.933)	(0.085)	
<i>Limited to overlap sample between in-person and emergency-department data</i>							
Self-report of use	10,178	40.2	6.0	0.179	0.980	0.150	0.396
12 months before interview			(4.5)		(1.959)	(0.177)	
Administrative record of use	10,178	26.8	6.8	0.089	0.635	0.351	0.037
12 months before interview			(4.0)		(1.828)	(0.168)	

substitutable for other outpatient care, such as those during standard hours (on hours) and those for nonemergent and primary care-treatable conditions. This is in contrast to prior, quasi-experimental work finding that health insurance decreased this type of emergency-department visit (6). We also found that Medicaid increases emergent, preventable visits, or visits for conditions likely preventable by timely outpatient care. By contrast, there is no statistically significant change in emergent, nonpreventable visits. Relying on eventual diagnosis (as we do in our decomposition of visits types) can be problematic and may not accurately differentiate necessary and unnecessary emergency-department use (25, 26). However, the overall picture is similar with use of different classification systems (such as on-hour visits relative to off-hour visits, or outpatient emergency-department visits relative to inpatient emergency-department visits).

One interpretation of these findings is that Medicaid did not decrease emergency-department use because it did not improve health or increase access to and use of primary care. The prior findings of the Oregon Health Insurance Experiment address this conjecture. They indicate that the increase in emergency-department use occurred despite Medicaid increasing access to other types and sites of care, even within the first year. Medicaid increased self-reported primary care use, including outpatient physician visits, prescriptions, and recommended preventive care. Medicaid also improved self-reported access to and quality of care, such as getting all of the care needed, receiving high-quality care, and having a usual place of care that was not an emergency department. The evidence on health is more mixed; Medicaid improved self-reported health and decreased depression in this population, but it did not produce statistically significant improvements in several different measures of physical health (11, 12).

Our estimates of the impact of Medicaid on emergency-department use apply to able-bodied, uninsured adults with income below the federal poverty level who express interest in insurance coverage. This population is of considerable policy interest given states' opportunity to expand Medicaid to all adults up to 138% of the federal poverty level under the Affordable Care Act. However, there are important limits to the generalizability of our findings. Our sample population differs on several dimensions from those who will be covered by other Medicaid expansions (11, 19). For example, ours is disproportionately white and urban-dwelling. It is also a population who voluntarily signed up for coverage; effects may differ in a population covered by an insurance mandate. In addition, we examined changes in emergency-department use for people gaining an average of 13 months of coverage; longer-run effects may differ. Last, the newly insured in our study comprise a very small share of the uninsured or total population

in Oregon, limiting the system-level effects that insuring a larger share of the population might generate (27).

These limitations to generalizability notwithstanding, our study was able to make use of a randomized design that is rarely available in the evaluation of social insurance programs to estimate the causal effects of Medicaid on emergency-department care. We found that expanding Medicaid coverage increased emergency-department use across a broad range of visit types, including visits that may be most readily treatable in other outpatient settings. These findings speak to one cost of expanding Medicaid, as well as its net effect on the efficiency of care delivered, and may thus be a useful input for informed decision-making that balances the costs and benefits of expanding Medicaid.

References and Notes

- U.S. Department of Health and Human Services, "New data say uninsured account for nearly one-fifth of emergency room visits" (2009); www.hhs.gov/news/press/2009pres/07/20090715b.html.
- R. Snyder, "Facts about Medicaid expansion: Improving care, saving money" (2013); www.michigan.gov/documents/snyder/Medicaid_expansion_-_factsheet_final_2-6-13_410658_7.pdf.
- S. Palm-Houser, "Governor Kasich includes Medicaid expansion in proposed Ohio budget" (2013); www.examiner.com/article/governor-kasich-includes-medicaid-expansion-proposed-ohio-budget.
- Z. Dudiak, "Pittsburgh area legislators react to governor's budget proposals" (2013); <http://foresthills-regentsquare.patch.com/groups/politics-and-elections/p/pittsburgh-area-legislators-react-to-governor-s-budg5c772c0e4b>.
- C. Chen, G. Scheffler, A. Chandra, *N. Engl. J. Med.* **365**, e25 (2011).
- S. Miller, *J. Public Econ.* **96**, 893–908 (2012).
- J. Currie, J. Gruber, *Q. J. Econ.* **111**, 431–466 (1996).
- M. Anderson, C. Dobkin, T. Gross, *Am. Econ. J. Econ. Policy* **4**, 1–27 (2012).
- M. Anderson, C. Dobkin, T. Gross, *Rev. Econ. Stat.*, published online 2 April 2013 (10.1162/REST_a_00378); available online at www.mitpressjournals.org/doi/pdf/10.1162/REST_a_00378.
- J. P. Newhouse, the Insurance Experiment Group, *Free for All?: Lessons from the RAND Health Insurance Experiment* (Harvard Univ. Press, Cambridge, MA, 1993).
- A. Finkelstein *et al.*, *Q. J. Econ.* **127**, 1057–1106 (2012).
- K. Baicker *et al.*, *N. Engl. J. Med.* **368**, 1713–1722 (2013).
- K. Baicker, A. Finkelstein, J. Song, S. Taubman, "The Impact of Medicaid on Labor Force Activity and Program Participation: Evidence from the Oregon Health Insurance Experiment" (NBER Working Paper No. 19547, NBER, Cambridge, MA, 2013).
- We calculated this percent by using 2008 and 2009 hospital discharge data for all 58 hospitals in the entire state of Oregon.
- Materials and methods are available as supplementary materials on Science Online.
- Healthcare Cost and Utilization Project, Overview of the Nationwide Emergency Department Sample (NEDS), www.hcup-us.ahrq.gov/nedsoverview.jsp [accessed 2 May 2013].
- Specifically, we used year of birth, sex, whether English is the preferred language for receiving materials, whether the individuals signed themselves up for the lottery or were signed up by a household member, whether they provided a phone number on sign-up, whether the individuals gave their address as a post office box, whether they signed up the first day the lottery list was open, and the median household income in the 2000 Census from their postal code.
- S. Taubman *et al.*, The Oregon Health Insurance Experiment: Evidence from Emergency Department Data Analysis Plan (2013); archived on 6 March 2013 with hypotheses@povertyactionlab.org; www.nber.org/oregon.
- H. Allen *et al.*, *Health Aff.* **29**, 1498–1506 (2010).
- J. D. Angrist, G. W. Imbens, D. B. Rubin, *J. Am. Stat. Assoc.* **91**, 444–455 (1996).
- J. Billings, N. Parikh, T. Mijanovich, *Emergency Room Use: The New York Story* (Commonwealth Fund, New York, 2000).
- The remaining 19% of visits are not classified by the algorithm. Illustrative examples of each group are as follows: cardiac dysrhythmia for emergent, not preventable; asthma attack for emergent, preventable; ear infection for primary care treatable; and sore throat for nonemergent.
- "Examination and treatment for emergency medical conditions and women in labor," § 1395dd of U.S. Code 2006 Edition, Supplement 4, Title 42—The Public Health and Welfare.
- We calculated this cost of an emergency-department visit by using data from the 2002 to 2007 (pooled) Medical Expenditure Panel Survey on expenditures of all nonelderly (19 to 64) adults below 100% of poverty who are publicly insured.
- R. A. Lowe, R. Fu, *Acad. Emerg. Med.* **15**, 506–516 (2008).
- M. C. Raven, R. A. Lowe, J. Maselli, R. Y. Hsia, *JAMA* **309**, 1145–1153 (2013).
- A. Finkelstein, *Q. J. Econ.* **122**, 1–37 (2007).

Acknowledgments: We are grateful to A. Chandra, J. Levin, R. Levin, B. Olken, J. Shapiro, and H. Williams for helpful comments and advice; to Mira Bernstein for immeasurable contribution to the study; to I. Colaiacovo, N. Subramanian, A. Zhou, A. Barnett, and J. Dennett for expert research assistance; to M. Callan for invaluable expertise in collecting and processing the data; to the Oregon Association of Hospital and Health Systems and the hospitals who provided emergency-department data; to numerous Oregon state employees for help acquiring the necessary data and for answering our many questions about the administration of state programs; and to our generous funders. The Oregon Health Insurance Experiment study was funded by the Assistant Secretary for Planning and Evaluation in the U.S. Department of Health and Human Services, the California HealthCare Foundation, the John D. and Catherine T. MacArthur Foundation, the National Institute on Aging (grants P30AG012810, RC2AG036631, and R01AG0345151), the Robert Wood Johnson Foundation, the Alfred P. Sloan Foundation, the Smith Richardson Foundation, the U.S. Social Security Administration (through grant 5 RRC 08098400-03-00 to NBER as part of the SSA Retirement Research Consortium), and the Centers for Medicare and Medicaid Services. The findings and conclusions expressed are solely those of the authors and do not represent the views of the funders. Replication code and a modified version of the data are available on the Oregon Health Insurance Experiment Web site (www.nber.org/oregon/data.html).

Supplementary Materials

www.sciencemag.org/content/343/6168/263/suppl/DC1
Materials and Methods
Supplementary Text
Figs. S1 to S3
Tables S1 to S17
References (28–40)

18 September 2013; accepted 3 December 2013
Published online 2 January 2014;
10.1126/science.1246183

Order of Magnitude Smaller Limit on the Electric Dipole Moment of the Electron

The ACME Collaboration,* J. Baron,¹ W. C. Campbell,² D. DeMille,^{3†} J. M. Doyle,^{1†} G. Gabrielse,^{1‡} Y. V. Gurevich,^{1‡} P. W. Hess,¹ N. R. Hutzler,¹ E. Kirilov,^{3§} I. Kozyryev,^{3||} B. R. O'Leary,³ C. D. Panda,¹ M. F. Parsons,¹ E. S. Petrik,¹ B. Spaun,¹ A. C. Vutha,⁴ A. D. West³

The Standard Model of particle physics is known to be incomplete. Extensions to the Standard Model, such as weak-scale supersymmetry, posit the existence of new particles and interactions that are asymmetric under time reversal (T) and nearly always predict a small yet potentially measurable electron electric dipole moment (EDM), d_e , in the range of 10^{-27} to 10^{-30} $e \cdot \text{cm}$. The EDM is an asymmetric charge distribution along the electron spin (\vec{S}) that is also asymmetric under T. Using the polar molecule thorium monoxide, we measured $d_e = (-2.1 \pm 3.7_{\text{stat}} \pm 2.5_{\text{syst}}) \times 10^{-29}$ $e \cdot \text{cm}$. This corresponds to an upper limit of $|d_e| < 8.7 \times 10^{-29}$ $e \cdot \text{cm}$ with 90% confidence, an order of magnitude improvement in sensitivity relative to the previous best limit. Our result constrains T-violating physics at the TeV energy scale.

The exceptionally high internal effective electric field \mathcal{E}_{eff} of heavy neutral atoms and molecules can be used to precisely probe for the electron electric dipole moment (EDM), d_e , via the energy shift $U = -\vec{d}_e \cdot \vec{\mathcal{E}}_{\text{eff}}$, where $\vec{d}_e = d_e \vec{S} / (\hbar/2)$, \vec{S} is electron spin, and \hbar is the reduced Planck constant. Valence electrons travel relativistically near the heavy nucleus, making \mathcal{E}_{eff} up to a million times the size of any static laboratory field (1–3). The previous best limits on d_e came from experiments with thallium (Tl) atoms (4) ($|d_e| < 1.6 \times 10^{-27}$ $e \cdot \text{cm}$) and ytterbium fluoride (YbF) molecules (5, 6) ($|d_e| < 1.06 \times 10^{-27}$ $e \cdot \text{cm}$). The latter demonstrated that molecules can be used to suppress the motional electric fields and geometric phases that limited the Tl measurement (5) [this suppression is also present

in certain atoms (7)]. Insofar as polar molecules can be fully polarized in laboratory-scale electric fields, \mathcal{E}_{eff} can be much greater than in atoms. The $H^3\Delta_1$ electronic state in the thorium monoxide (ThO) molecule provides an $\mathcal{E}_{\text{eff}} \approx 84$ GV/cm, larger than those previously used in EDM measurements (8, 9). This state's unusually small magnetic moment reduces its sensitivity to spurious magnetic fields (10, 11). Improved systematic error rejection is possible because internal state selection allows the reversal of \mathcal{E}_{eff} with no change in the laboratory electric field (12, 13).

To measure d_e , we perform a spin precession measurement (10, 14, 15) on pulses of $^{232}\text{Th}^{16}\text{O}$ molecules from a cryogenic buffer gas beam source that generate a laboratory electric field $\mathcal{E}_z \hat{z}$ (Fig.

1A). A coherent superposition of two spin states, corresponding to a spin aligned in the xy plane, is prepared using optical pumping and state preparation lasers. Parallel electric ($\vec{\mathcal{E}}$) and magnetic (\vec{B}) fields exert torques on the electric and magnetic dipole moments, causing the spin vector to precess in the xy plane. The precession angle is measured with a readout laser and fluorescence detection. A change in this angle as $\vec{\mathcal{E}}_{\text{eff}}$ is reversed is proportional to d_e .

In more detail, a laser beam (wavelength 943 nm) optically pumps molecules from the ground electronic state into the lowest rotational level, $J = 1$, of the metastable (lifetime ~ 2 ms) electronic $H^3\Delta_1$ state manifold (Fig. 1B), in an incoherent mixture of the $\tilde{N} = \pm 1, M = \pm 1$ states. M is the angular momentum projection along the \hat{z} axis. \tilde{N} refers to the internuclear axis, \hat{n} , aligned ($+1$) or antialigned (-1) with respect to $\vec{\mathcal{E}}$, when $|\vec{\mathcal{E}}| \geq 1$ V/cm (11). The linearly polarized state preparation laser's frequency is resonant with the $H \rightarrow C$ transition at 1090 nm (Fig. 1B). Within the short-lived (500 ns) electronic C state, there are two opposite-parity $\tilde{P} = \pm 1$ states with $J = 1, M = 0$. For a given spin precession measurement, the laser frequency determines the \tilde{N} and \tilde{P} states that are addressed. This laser optically pumps the bright

¹Department of Physics, Harvard University, Cambridge, MA 02138, USA. ²Department of Physics and Astronomy, University of California, Los Angeles, CA 90095, USA. ³Department of Physics, Yale University, New Haven, CT 06511, USA. ⁴Department of Physics and Astronomy, York University, Toronto, Ontario M3J 1P3, Canada.

*The collaboration consists of all listed authors. There are no additional collaborators.

†Corresponding author. E-mail: acme@physics.harvard.edu (D.D., J.M.D., G.G.)

‡Present address: Department of Physics, Yale University, New Haven, CT 06511, USA.

§Present address: Institut für Experimentalphysik, Universität Innsbruck, A-6020 Innsbruck, Austria.

||Present address: Department of Physics, Harvard University, Cambridge, MA 02138, USA.

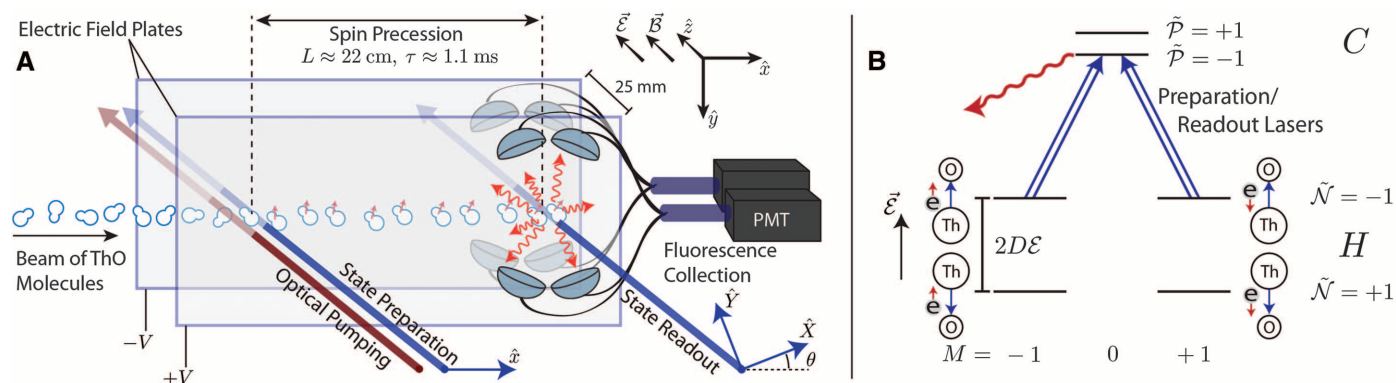


Fig. 1. Schematic of the apparatus and energy level diagram. (A) A collimated pulse of ThO molecules enters a magnetically shielded region (not to scale). An aligned spin state (smallest red arrows), prepared via optical pumping, precesses in parallel electric and magnetic fields. The final spin alignment is read out by a laser with rapidly alternating linear polarizations, \hat{X} and \hat{Y} , with the resulting fluorescence collected and detected with photomultiplier tubes (PMTs). (B) The state preparation and readout lasers (double-lined

blue arrows) drive one molecule orientation $\tilde{N} = \pm 1$ (split by $2D\mathcal{E} \sim 100$ MHz, where D is the electric dipole moment of the H state to C , with parity $\tilde{P} = \pm 1$ (split by 50 MHz). Population in the C state decays via spontaneous emission, and we detect the resulting fluorescence (red wiggly arrow). H state levels are accompanied by cartoons displaying the orientation of $\vec{\mathcal{E}}_{\text{eff}}$ (blue arrows) and the spin of the electron (red arrows) that dominantly contributes to the d_e shift.

superposition of the two resonant $M = \pm 1$ sub-levels out of the H state, leaving behind the orthogonal dark superposition that cannot absorb the laser light; we use this dark state as our initial state (19). If the state preparation laser is polarized along \hat{x} , then the prepared state, $|\psi(\tau = 0)\rangle$, has the electron spin aligned along the \hat{y} axis. The spin then precesses in the xy plane by angle ϕ to

$$|\psi(\tau)\rangle = \frac{\exp(-i\phi)|M = +1, \tilde{N}\rangle - \exp(+i\phi)|M = -1, \tilde{N}\rangle}{\sqrt{2}} \quad (1)$$

Because $\vec{\mathcal{E}}$ and $\vec{\mathcal{B}}$ are aligned along \hat{z} , the phase ϕ is determined by $|\mathcal{B}_z| = |\vec{\mathcal{B}} \cdot \hat{z}|$, its sign, $\tilde{\mathcal{B}} = \text{sgn}(\vec{\mathcal{B}} \cdot \hat{z})$, and the electron's EDM, d_e :

$$\phi \approx \frac{-(\mu_B g \tilde{\mathcal{B}} |\mathcal{B}_z| + \tilde{N} \tilde{\mathcal{E}} d_e \mathcal{E}_{\text{eff}}) \tau}{h} \quad (2)$$

where $\tilde{\mathcal{E}} \equiv \text{sgn}(\vec{\mathcal{E}} \cdot \hat{z})$, τ is the spin precession time, and $\mu_B g$ is the magnetic moment (15) of the $H, J = 1$ state where $g = -0.0044 \pm 0.0001$ is the gyromagnetic ratio and μ_B is the Bohr magneton. The sign of the EDM term, $\tilde{N} \tilde{\mathcal{E}}$, arises from the relative orientation between $\vec{\mathcal{E}}_{\text{eff}}$ and the electron spin, as illustrated in Fig. 1B.

After the spin precesses as each molecule travels over a distance of $L \approx 22$ cm ($\tau \approx 1.1$ ms), we measure ϕ by optically pumping on the same $H \rightarrow C$ transition with the state readout laser. The laser polarization alternates between \hat{X} and \hat{Y} every 5 μs , and we record the modulated fluorescence signals S_X and S_Y from the decay of C to the ground state (fig. S1A). This procedure amounts to a projective measurement of the spin onto \hat{X} and \hat{Y} , which are defined such that \hat{X} is at an angle θ with respect to \hat{x} in the xy plane (Fig. 1A). To cancel the effects of fluctuations in molecule number, we normalize the spin precession signal by computing the asymmetry

$$\mathcal{A} \equiv \frac{S_X - S_Y}{S_X + S_Y} = \mathcal{C} \cos[2(\phi - \theta)] \quad (3)$$

(10), where the contrast \mathcal{C} is $94 \pm 2\%$ on average. We set $|\mathcal{B}_z|$ and θ such that $\phi - \theta \approx (\pi/4)(2n + 1)$ for integer n , so that the asymmetry is linearly proportional to small changes in ϕ and is maximally sensitive to the EDM. We measure

\mathcal{C} by dithering θ between two nearby values that differ by 0.1 rad, denoted by $\theta = \pm 1$.

We perform this spin precession measurement repeatedly under varying experimental conditions to (i) distinguish the EDM energy shift from background phases and (ii) search for and monitor possible systematic errors. Within a “block” of data (fig. S1C) taken over 40 s, we perform measurements of the phase for each experimental state derived from four binary switches, listed from fastest (0.5 s) to slowest (20 s): the molecule alignment \tilde{N} , the \mathcal{E} -field direction $\tilde{\mathcal{E}}$, the readout laser polarization dither state $\tilde{\theta}$, and the \mathcal{B} -field direction $\tilde{\mathcal{B}}$. For each $(\tilde{N}, \tilde{\mathcal{E}}, \tilde{\mathcal{B}})$ state of the experiment, we measure \mathcal{A} and \mathcal{C} , from which we can extract ϕ . Within each block, we form “switch parity components” of the phase, ϕ^u , which are combinations of the measured phases that are odd or even under these switch operations (13). We denote the switch parity of a quantity with a superscript, u , listing the switch labels under which the quantity is odd; it is even under all unlabeled switches. For example, the EDM contributes to a phase component $\phi^{\tilde{N}\tilde{\mathcal{E}}} = -d_e \mathcal{E}_{\text{eff}} \tau / h$. We extract the mean precession time τ from $\phi^{\tilde{\mathcal{B}}} = -\mu_B g |\mathcal{B}_z| \tau / h$ and compute the frequencies, $\omega^u \equiv \phi^u / \tau$. The EDM value is obtained from $\omega^{\tilde{N}\tilde{\mathcal{E}}}$ by $d_e = -h \omega^{\tilde{N}\tilde{\mathcal{E}}} / \mathcal{E}_{\text{eff}}$.

On a slower time scale, we perform additional “superblock” binary switches (fig. S1D) to suppress some known systematic errors and to search for unknown ones. These switches, which occur on time scales of 40 to 600 s, are the excited-state parity addressed by the state readout lasers, $\tilde{\mathcal{P}}$; a rotation of the readout polarization basis by $\theta \rightarrow \theta + \pi/2$, $\tilde{\mathcal{R}}$; a reversal of the leads that supply the electric fields, $\tilde{\mathcal{L}}$; and a global polarization rotation of both the state preparation and readout laser polarizations, $\tilde{\mathcal{G}}$. The $\tilde{\mathcal{P}}$ and $\tilde{\mathcal{R}}$ switches interchange the role of the \hat{X} and \hat{Y} readout beams and hence reject systematic errors associated with small differences in power, shape, or pointing. The two $\tilde{\mathcal{G}}$ state angles are chosen to suppress systematics that couple to unwanted ellipticity imprinted on the polarizations by birefringence in the electric field plates. The $\tilde{\mathcal{L}}$ switch rejects systematics that couple to an offset voltage in the electric field power supplies. We extract the EDM from $\omega^{\tilde{N}\tilde{\mathcal{E}}}$ after a complete

set of the 2^8 block and superblock states. The value of $\omega^{\tilde{N}\tilde{\mathcal{E}}}$ is even under all of the superblock switches.

The total data set consists of $\sim 10^4$ blocks of data taken over the course of ~ 2 weeks (fig. S1, E and F). During data collection, we also varied, from fastest (hours) to slowest (a few days), the \mathcal{B} -field magnitude, $|\mathcal{B}_z| \approx 1, 19$, or 38 mG (corresponding to $|\phi| \approx 0, \pi/4$, or $\pi/2$, respectively); the \mathcal{E} -field magnitude, $|\mathcal{E}_z| \approx 36$ or 141 V/cm; and the pointing direction of the lasers, $\hat{k} \cdot \hat{z} = \pm 1$. Figure 2B shows measured EDM values obtained when the data set is grouped according to the states of $|\mathcal{B}_z|$, $|\mathcal{E}_z|$, $\hat{k} \cdot \hat{z}$, and each superblock switch. All of these measurements are consistent within 2σ .

We computed the 1σ standard error in the mean and used standard Gaussian error propagation to obtain the reported statistical uncertainty. The reported upper limit was computed using the Feldman-Cousins prescription (20) applied to a folded normal distribution. To prevent experimental bias, we performed a blind analysis by adding an unknown offset to $\omega^{\tilde{N}\tilde{\mathcal{E}}}$. The mean, statistical error, systematic shifts, and procedure for calculating the systematic error were determined before unblinding. Figure 2A shows a histogram of EDM measurements. The asymmetry \mathcal{A} obeys a ratio distribution, which has large non-Gaussian tails in the limit of low signal-to-noise ratio (21). We applied a photon count rate threshold cut so that we included only data with a large signal-to-noise ratio, resulting in a statistical distribution that closely approximates a Gaussian. When the EDM measurements are fit to a constant value, the reduced χ^2 is 0.996 ± 0.006 . On the basis of the total number of detected photoelectrons (~ 1000 per pulse) that contributed to the measurement, the statistical uncertainty is 1.15 times that from shot noise (15).

To search for possible sources of systematic error, we varied more than 40 separate parameters (table S1) and observed their effects on $\omega^{\tilde{N}\tilde{\mathcal{E}}}$ and many other components of the phase correlated with \tilde{N} , $\tilde{\mathcal{E}}$, or $\tilde{\mathcal{B}}$. These parameters were intentionally applied tunable imperfections, such as transverse magnetic fields or laser detunings. These systematic checks were performed concurrently with the 8 block and superblock switches.

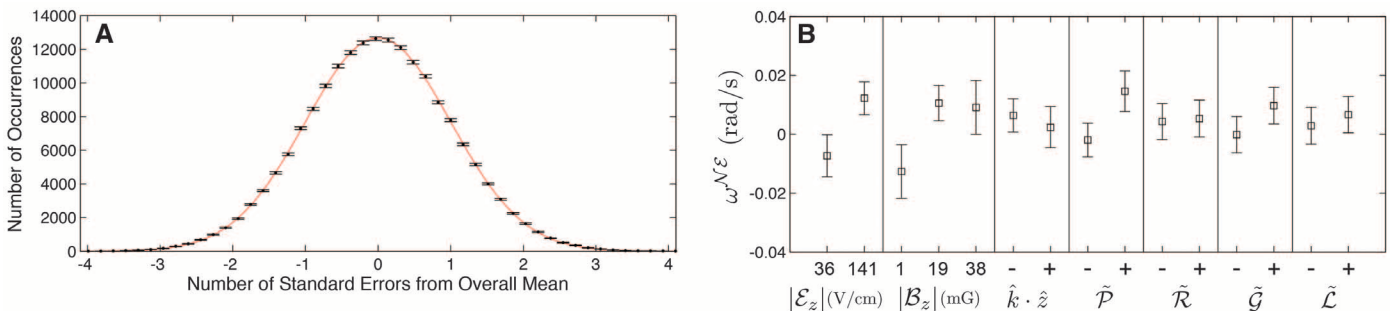


Fig. 2. Statistical spread of $\omega^{\tilde{N}\tilde{\mathcal{E}}}$ measurements. (A) Histogram of $\omega^{\tilde{N}\tilde{\mathcal{E}}}$ measurements for each time point (within the molecule pulse) and for all blocks. Error bars represent expected Poissonian fluctuations in each histogram bin. (B) Measured $\omega^{\tilde{N}\tilde{\mathcal{E}}}$ values grouped by the states of $|\mathcal{B}_z|$, $|\mathcal{E}_z|$, $\hat{k} \cdot \hat{z}$, and each superblock switch, before systematic corrections, with 1σ statistical error bars.

We assume that $\omega^{N\mathcal{E}}$ depends linearly on each parameter P , so that the possible systematic shift and uncertainty of $\omega^{N\mathcal{E}}$ is evaluated from the measured slope, $S = \partial\omega^{N\mathcal{E}}/\partial P$, and the parameter value during normal operation (obtained from auxiliary measurements). If S is not monitored throughout the data set, we do not apply a systematic correction but simply include the measured upper limit in our systematic error budget. Data taken with intentionally applied parameter imperfections are used only for determination of systematic shifts and uncertainties. Table 1 lists all contributions to our systematic error.

We identified two parameters that systematically shift the value of $\omega^{N\mathcal{E}}$ within our experimental resolution. Both parameters couple to the ac Stark shift induced by the lasers. The molecules are initially prepared in the dark state with a spin orientation dependent on the laser polarization. If there is a polarization gradient along the molecular beam propagation direction, the molecules acquire a small bright-state amplitude.

Away from the center of a Gaussian laser profile, the laser can be weak enough that the bright-state amplitude is not rapidly pumped away; it acquires a phase relative to the dark state due to the energy splitting between the bright and dark states, given by the ac Stark shift. An equivalent phase is acquired in the state readout laser. This effect changes the measured phase by $\phi_{ac}(\Delta, \Omega_r) \approx (\alpha\Delta + \beta\Omega_r)$, where Δ and Ω_r are the detuning from the $H \rightarrow C$ transition and the transition's Rabi frequency, respectively. The constants α and β are measured directly by varying Δ and Ω_r , and their values depend on the laser's spatial intensity and polarization profile. These measurements are in good agreement with our analytical and numerical models.

A large ($\sim 10\%$) circular polarization gradient is caused by laser-induced thermal stress birefringence (22) in the electric field plates. The laser beams are elongated perpendicular to the molecular beam axis, which creates an asymmetric thermal gradient and defines the axes for the

resulting birefringence gradient. By aligning the laser polarization with the birefringence axes, the polarization gradient can be minimized. We have verified this both with polarimetry (23) and through the resulting ac Stark shift systematic (Fig. 3A).

Such ac Stark shift effects can cause a systematic shift in the measurement of $\omega^{N\mathcal{E}}$ in the presence of an $\tilde{N}\tilde{\mathcal{E}}$ -correlated detuning, $\Delta^{N\mathcal{E}}$, or Rabi frequency, $\Omega_r^{N\mathcal{E}}$. We observed both.

The detuning component $\Delta^{N\mathcal{E}}$ is caused by a nonreversing \mathcal{E} -field component, \mathcal{E}^{nr} , generated by patch potentials and technical voltage offsets, which is small relative to the reversing component, $|\mathcal{E}_z|\mathcal{E}$. The \mathcal{E}^{nr} creates an $\tilde{N}\tilde{\mathcal{E}}$ -correlated dc Stark shift with an associated detuning $\Delta^{N\mathcal{E}} = D\mathcal{E}^{nr}$, where D is the H state electric dipole moment. We measured \mathcal{E}^{nr} via microwave spectroscopy (Fig. 3B), two-photon Raman spectroscopy, and the $\tilde{N}\tilde{\mathcal{E}}$ -correlated contrast.

The Rabi frequency component, $\Omega_r^{N\mathcal{E}}$, arises from a dependence of Ω_r on the orientation of the molecular axis, $\hat{n} \approx \tilde{N}\tilde{\mathcal{E}}\hat{z}$ with respect to the laser propagation direction, \hat{k} . This $\hat{k} \cdot \hat{z}$ dependence can be caused by interference between E1 and M1 transition amplitudes on the $H \rightarrow C$ transition. Measurements of a nonzero $\tilde{N}\tilde{\mathcal{E}}$ -correlated fluorescence signal, $S^{N\mathcal{E}}$, and an $\tilde{N}\tilde{\mathcal{E}}\mathcal{B}$ -correlated phase, $\phi^{N\mathcal{E}\mathcal{B}}$ —both of which changed sign when we reversed \hat{k} —provided evidence for a nonzero $\Omega_r^{N\mathcal{E}}$. The $\phi^{N\mathcal{E}\mathcal{B}}$ channel, along with its linear dependence on an artificial $\Omega_r^{N\mathcal{E}}$ generated by an $\tilde{N}\tilde{\mathcal{E}}$ -correlated laser intensity, allowed us to measure $\Omega_r^{N\mathcal{E}}/\Omega_r = (-8.0 \pm 0.8) \times 10^{-3}(\hat{k} \cdot \hat{z})$, where Ω_r is the uncorrelated (mean) Rabi frequency (see supplementary materials).

By intentionally exaggerating these parameters, we verified that both \mathcal{E}^{nr} and $\Omega_r^{N\mathcal{E}}$ couple to ac Stark shift effects to produce a false EDM. For the EDM data set, we tuned the laser polarization for each \tilde{G} state to minimize the magnitude of the systematic slope $\partial\omega^{N\mathcal{E}}/\partial\mathcal{E}^{nr}$ (Fig. 3A). The correlations $\partial\omega^{N\mathcal{E}}/\partial\mathcal{E}^{nr}$ and $\partial\omega^{N\mathcal{E}}/\partial\Omega_r^{N\mathcal{E}}$ were monitored at regular intervals throughout data collection (fig. S1E). The resulting systematic corrections to $\omega^{N\mathcal{E}}$ were all <1 mrad/s.

For a subset of our data, the \tilde{N} -correlated phase ϕ^N was nonzero and drifted with time. We identified the cause of this behavior as an \tilde{N} -correlated laser pointing $\hat{k}^N \cdot \hat{x} \approx 5 \mu\text{rad}$ present in our optical frequency switching setup. We eliminated this effect with improved optical alignment; however, we were not able to determine the precise mechanism by which \hat{k}^N coupled to ϕ^N , and so we chose to include ϕ^N variations in our systematic error budget. The slope $\partial\omega^{N\mathcal{E}}/\partial\phi^N$ (consistent with zero) and the mean value of ϕ^N established a systematic uncertainty limit of ~ 1 mrad/s on $\omega^{N\mathcal{E}}$.

To be cautious, we included in our systematic error budget possible contributions from the following parameters that caused a nonzero EDM shift in experiments similar to ours: stray \mathcal{B} -fields $\mathcal{B}_{x,y,z}^{nr}$ and \mathcal{B} -field gradients (13); an $\tilde{\mathcal{E}}$ -correlated phase, $\phi^{\mathcal{E}}$, caused by leakage current, $\vec{v} \times \vec{\mathcal{E}}$, and geometric phase effects (4); and laser detunings and

Fig. 3. The \mathcal{E}^{nr} systematic.

(A) Tuning out laser polarization gradient and $\partial\omega^{N\mathcal{E}}/\partial\mathcal{E}^{nr}$ (see text for details). Red and black data points were taken with the polarization misaligned and aligned, respectively, with the birefringence axes of the electric field plates. Error bars represent 1σ statistical uncertainties. **(B)** Microwave spectroscopic measurement of \mathcal{E}^{nr} during normal operation along the molecule beam axis, x , with 1σ statistical error bars.

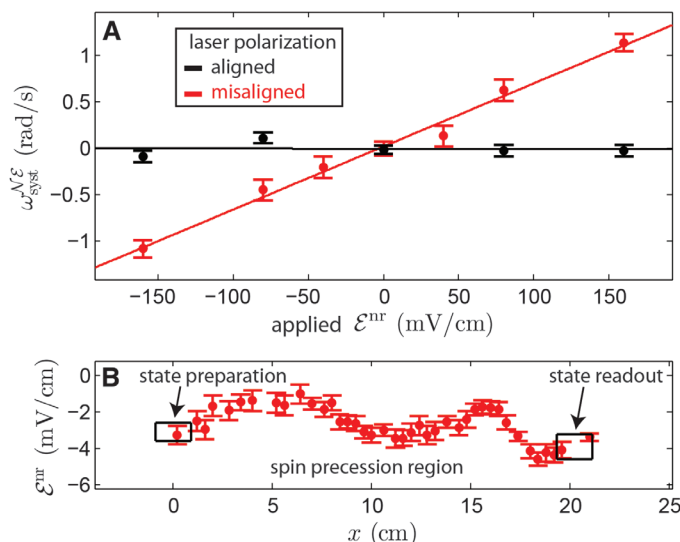


Table 1. Summary of systematic errors. Systematic and statistical errors for $\omega^{N\mathcal{E}}$, in units of mrad/s. All uncertainties are added in quadrature and are derived from Gaussian 1σ (68%) confidence intervals. In EDM units, $1.3 \text{ mrad/s} \approx 10^{-29} \text{ e} \cdot \text{cm}$.

Parameter	Shift	Uncertainty
\mathcal{E}^{nr} correction	-0.81	0.66
$\Omega_r^{N\mathcal{E}}$ correction	-0.03	1.58
$\phi^{\mathcal{E}}$ -correlated effects	-0.01	0.01
ϕ^N correlation		1.25
Nonreversing \mathcal{B} -field (\mathcal{B}_z^{nr})		0.86
Transverse \mathcal{B} -fields ($\mathcal{B}_x^{nr}, \mathcal{B}_y^{nr}$)		0.85
\mathcal{B} -field gradients		1.24
Prep./read laser detunings		1.31
\tilde{N} -correlated detuning		0.90
\mathcal{E} -field ground offset		0.16
Total systematic	-0.85	3.24
Statistical		4.80
Total uncertainty		5.79

\mathcal{E} -field ground offsets (5). We obtained direct $\omega^{N\mathcal{E}}$ systematic limits of $\lesssim 1$ mrad/s for each. We simulated the effects that contribute to $\phi^{\mathcal{E}}$ by deliberately correlating B_z with $\tilde{\mathcal{E}}$, which allowed us to place a $\sim 10^{-2}$ mrad/s limit on their combined effect. Because of our slow molecular beam, relatively small applied \mathcal{E} -fields, and small magnetic dipole moment, we do not expect any of these effects to systematically shift $\omega^{N\mathcal{E}}$ above the 10^{-3} mrad/s level (10, 11).

The result of this first-generation ThO measurement,

$$d_e = (-2.1 \pm 3.7_{\text{stat}} \pm 2.5_{\text{sys}}) \times 10^{-29} e \cdot \text{cm} \quad (4)$$

comes from $d_e = -\hbar\omega^{N\mathcal{E}}/\mathcal{E}_{\text{eff}}$ using $\mathcal{E}_{\text{eff}} = 84$ GV/cm (8, 9) and $\omega^{N\mathcal{E}} = (2.6 \pm 4.8_{\text{stat}} \pm 3.2_{\text{sys}})$ mrad/s. This sets a 90% confidence limit,

$$|d_e| < 8.7 \times 10^{-29} e \cdot \text{cm} \quad (5)$$

that is smaller than the previous best limit by a factor of 12 (4, 5)—an improvement made possible by the use of the ThO molecule and of a cryogenic source of cold molecules for this purpose. If we were to take into account the roughly estimated 15% uncertainty on the calculated \mathcal{E}_{eff} (8) and assume that this represents a 1σ Gaussian distribution width, the d_e limit stated above would increase by about 5%. Because paramagnetic molecules are sensitive to multiple time reversal (T)-violating effects (24), our measurement should be interpreted as $\hbar\omega^{N\mathcal{E}} = -d_e\mathcal{E}_{\text{eff}} - W_S C_S$, where C_S is a T-violating electron-nucleon coupling and W_S is a molecule-specific constant (8, 25). For the d_e limit above, we assume $C_S = 0$. Assuming instead that $d_e = 0$ yields $C_S = (-1.3 \pm 3.0) \times 10^{-9}$, corresponding to a 90% confidence limit $|C_S| < 5.9 \times 10^{-9}$ that is smaller than the previous limit by a factor of 9 (26).

A measurably large EDM requires new mechanisms for T violation, which is equivalent to combined charge-conjugation and parity (CP) violation, given the CPT invariance theorem (2). Nearly every extension to the Standard Model (27, 28) introduces new CP-violating phases ϕ_{CP} . It is difficult to construct mechanisms that systematically suppress ϕ_{CP} , so model builders typically assume $\sin(\phi_{\text{CP}}) \sim 1$ (29). An EDM arising from new particles at energy Λ in an n -loop Feynman diagram will have size

$$\frac{d_e}{e} \sim \kappa \left(\frac{\alpha_{\text{eff}}}{4\pi} \right)^n \left(\frac{m_e c^2}{\Lambda^2} \right) \sin(\phi_{\text{CP}}) (\hbar c) \quad (6)$$

where α_{eff} (about $4/137$ for electroweak interactions) encodes the strength with which the electron couples to the new particles, m_e is the electron mass, and $\kappa \sim 0.1$ to 1 is a dimensionless prefactor (2, 30, 31). In models where 1- or 2-loop diagrams produce d_e , our result typically sets a bound on CP violation at energy scales $\Lambda \sim 3$ TeV or 1 TeV, respectively (27–29, 31). Hence, within the context of many models, our EDM limit constrains

CP violation up to energy scales similar to, or higher than, those explored directly at the Large Hadron Collider.

References and Notes

- P. G. H. Sandars, *Phys. Lett.* **14**, 194–196 (1965).
- I. B. Khriplovich, S. K. Lamoreaux, *CP Violation Without Strangeness* (Springer, New York, 1997).
- E. D. Commins, D. DeMille, in *Lepton Dipole Moments*, B. L. Roberts, W. J. Marciano, Eds. (World Scientific, Singapore, 2010), chap. 14, pp. 519–581.
- B. Regan, E. Commins, C. Schmidt, D. DeMille, *Phys. Rev. Lett.* **88**, 071805 (2002).
- J. J. Hudson *et al.*, *Nature* **473**, 493–496 (2011).
- D. M. Kara *et al.*, *New J. Phys.* **14**, 103051 (2012).
- M. A. Player, P. G. H. Sandars, *J. Phys. B* **3**, 1620–1635 (1970).
- L. V. Skripnikov, A. N. Petrov, A. V. Titov, *J. Chem. Phys.* **139**, 221103 (2013).
- E. R. Meyer, J. L. Bohn, *Phys. Rev. A* **78**, 010502 (2008).
- A. C. Vutha *et al.*, *J. Phys. B* **43**, 074007 (2010).
- A. C. Vutha *et al.*, *Phys. Rev. A* **84**, 034502 (2011).
- S. Bickman, P. Hamilton, Y. Jiang, D. DeMille, *Phys. Rev. A* **80**, 023418 (2009).
- S. Eckel, P. Hamilton, E. Kirilov, H. W. Smith, D. DeMille, *Phys. Rev. A* **87**, 052130 (2013).
- W. C. Campbell *et al.*, EPJ Web of Conferences **57**, 02004 (2013).
- E. Kirilov *et al.*, *Phys. Rev. A* **88**, 013844 (2013).
- S. E. Maxwell *et al.*, *Phys. Rev. Lett.* **95**, 173201 (2005).
- N. R. Hutzler *et al.*, *Phys. Chem. Chem. Phys.* **13**, 18976 (2011).
- N. R. Hutzler, H.-I. Lu, J. M. Doyle, *Chem. Rev.* **112**, 4803–4827 (2012).
- H. R. Gray, R. M. Whitley, C. R. Stroud Jr., *Opt. Lett.* **3**, 218–220 (1978).
- G. J. Feldman, R. D. Cousins, *Phys. Rev. D* **57**, 3873–3889 (1998).
- J. H. Curtiss, *Ann. Math. Stat.* **12**, 409–421 (1941).
- S. Eisenbach, H. Lotem, *Proc. SPIE* **1972**, 19 (1993).
- H. G. Berry, G. Gabrielse, A. E. Livingston, *Appl. Opt.* **16**, 3200–3205 (1977).
- M. G. Kozlov, L. N. Labzowsky, *J. Phys. At. Mol. Opt. Phys.* **28**, 1933–1961 (1995).
- V. A. Dzuba, V. V. Flambaum, C. Harabati, *Phys. Rev. A* **84**, 052108 (2011).
- W. C. Griffith *et al.*, *Phys. Rev. Lett.* **102**, 101601 (2009).
- S. Barr, *Int. J. Mod. Phys. A* **08**, 209–236 (1993).
- M. Pospelov, A. Ritz, *Ann. Phys.* **318**, 119–169 (2005).
- J. Engel, M. J. Ramsey-Musolf, U. van Kolck, *Prog. Part. Nucl. Phys.* **71**, 21–74 (2013).
- N. Fortson, P. Sandars, S. Barr, *Phys. Today* **56**, 33 (2003).
- W. Bernreuther, M. Suzuki, *Rev. Mod. Phys.* **63**, 313–340 (1991).

Acknowledgments: Supported by NSF and the Precision Measurement Grants Program of the National Institute of Standards and Technology. We thank M. Reece and M. Schwartz for discussions and S. Cotreau, J. MacArthur, and S. Sansone for technical support. P.W.H. was supported in part by the Office of Science Graduate Fellowship Program, U.S. Department of Energy. The authors declare no competing financial interests.

Supplementary Materials

www.sciencemag.org/content/343/6168/269/suppl/DC1
Materials and Methods
Fig. S1
Table S1
References (32–36)

7 November 2013; accepted 9 December 2013
Published online 19 December 2013;
10.1126/science.1248213

Single-Crystal Linear Polymers Through Visible Light-Triggered Topochemical Quantitative Polymerization

Letian Dou,^{1,2,3} Yonghao Zheng,^{1,4} Xiaoqin Shen,¹ Guang Wu,⁵ Kirk Fields,⁶ Wan-Ching Hsu,^{2,3} Huanping Zhou,^{2,3} Yang Yang,^{2,3}† Fred Wudl^{1,4,5,*}†

One of the challenges in polymer science has been to prepare large-polymer single crystals. We demonstrate a visible light-triggered quantitative topochemical polymerization reaction based on a conjugated dye molecule. Macroscopic-size, high-quality polymer single crystals are obtained. Polymerization is not limited to single crystals, but can also be achieved in highly concentrated solution or semicrystalline thin films. In addition, we show that the polymer decomposes to monomer upon thermolysis, which indicates that the polymerization-depolymerization process is reversible. The physical properties of the polymer crystals enable us to isolate single-polymer strands via mechanical exfoliation, which makes it possible to study individual, long polymer chains.

Obtaining single-crystalline materials is of importance in chemistry, physics, and materials science because it enables not only a fundamental understanding of the nature of the materials through structure-function correlations but also provides a wide range of advanced applications (1–3). Different from inorganic compounds or organic small molecules, polymers tend to form amorphous or semicrystalline phases because of entanglements of the long and flexible backbone (4, 5). Preparing large-size polymer single crystals remains a challenge in polymer

science (6–8). Topochemical polymerization, a process whereby the confinement and preorganization of the solid state forces a chemical reaction to proceed with a minimum amount of atomic and molecular movement, has provided a promising solution (9, 10). Hasegawa *et al.* reported topochemical polymerization reactions of diolefin-related compounds (11, 12) and Wegner discovered the polymerization of the 1,4-disubstituted-1,3-diacetylene single crystals by heating or high-energy photon irradiation (13). It was found that, if the reactive monomers are

preorganized at a distance commensurate with the repeat distance in the final polymer, polymerization ensued (13, 14). Numerous studies have been carried out to understand the mechanism and explore applications (15–19). The metallic and superconducting polymer (SN)_x was prepared through the thermal polymerization of S₂N₂ crystals. (20). More recently, the topochemical polymerization of diene (21–23) and quinodimethane (24, 25) compounds were

studied by Matsumoto *et al.* and Itoh *et al.*, respectively.

Although ultraviolet (UV) light-mediated reversibility of polymerization has been reported (26), in most cases, a reversible polymerization–thermal depolymerization process cannot be directly observed, and more important, polymerization is not quantitative. It is not possible to form large single crystals under irradiation because the just-formed polymer at the crystal surface layer prevents penetration of light through the bulk. In addition, most of the reaction can happen only in crystals where the monomers are aligned perfectly (9–26).

We demonstrate a topochemical polymerization reaction of two conjugated dye molecules based on [2,2'-bi-1H-indene]-1,1'-dione-3,3'-diyl dialkylcarboxylate. The alkyl side chains are found to play an important role in the molecular packing and, hence, topochemical reactivity. Because of the relatively small optical bandgap of the precursor solids (~2.2 eV), visible light can be used to induce the polymerization (27–29). The polymerization occurs, not only in the single

crystalline state but also in highly concentrated solution or semicrystalline thin films. Moreover, the topochemical polymerization-decomposition process is reversible under certain conditions.

The dye molecule [2,2'-bi-1H-indene]-3,3'-dihydroxy-1,1'-dione (BIT-OH₂) was synthesized and characterized in 1898 by Gabriel and Leupold (30), using inexpensive starting materials via a simple one-step reaction. In more recent times, this dye has not been widely investigated, and only few derivatives that showed liquid crystallinity and photochromism have been reported (31–33). In this work, we functionalize the BIT-OH₂ with a series of alkylcarboxylates on the hydroxyl groups in the 3 and 3' positions and demonstrate that topochemical polymerization occurs under exposure to visible light. The synthetic routes for four derivatives—namely, BIT-Ac₂, BIT-Hep₂, BIT-Non₂, and BIT-EH₂ (acetate, heptanoate, nonanoate, and 2-ethylhexanoate side chains, respectively)—and their corresponding polymers (PBIT-Hep₂ and PBIT-Non₂) are shown in Fig. 1A. BIT-OH₂ was synthesized according to Gabriel and Leupold (30). All the side

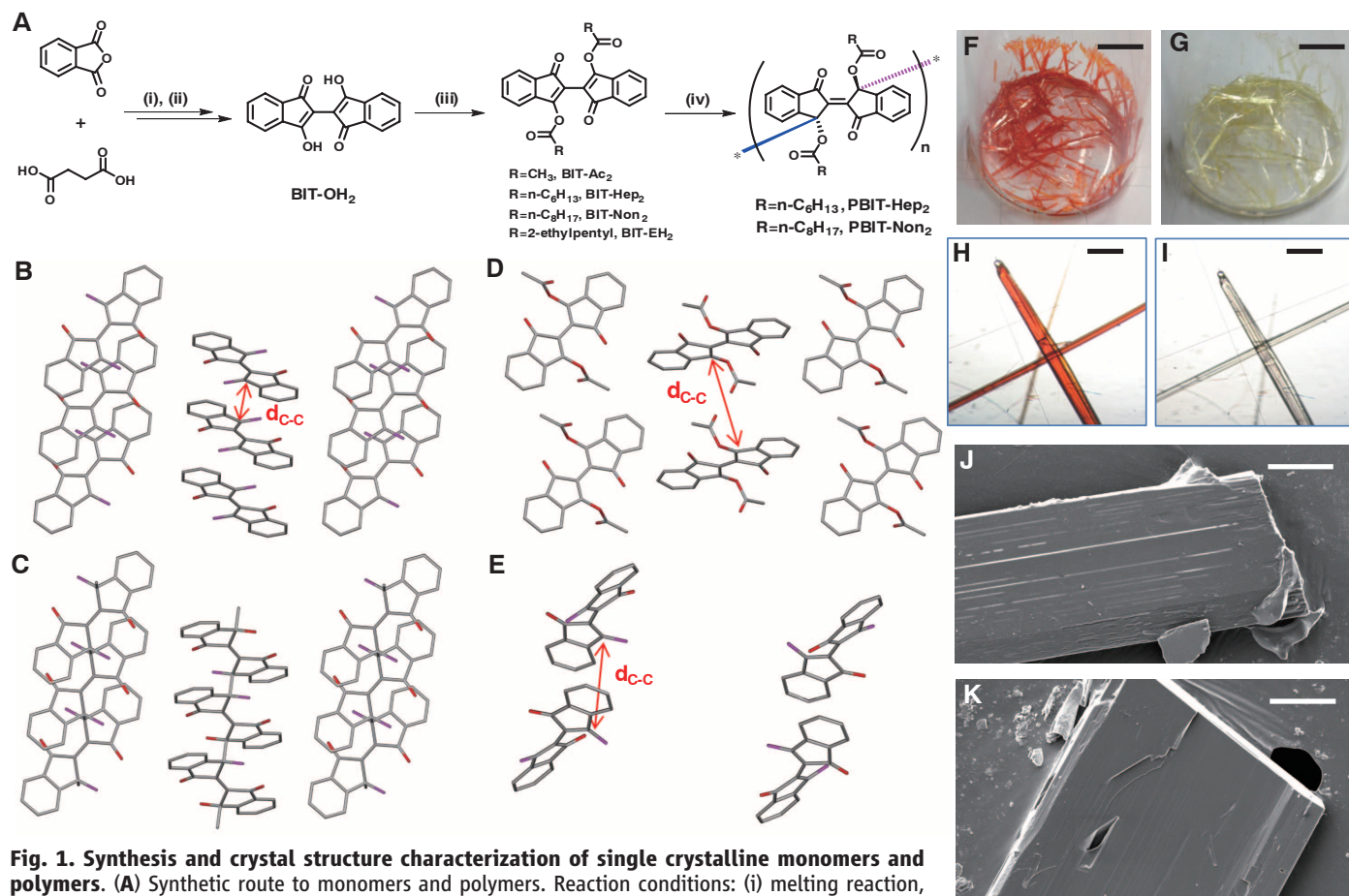


Fig. 1. Synthesis and crystal structure characterization of single crystalline monomers and polymers. (A) Synthetic route to monomers and polymers. Reaction conditions: (i) melting reaction, potassium acetate, 220°C, 2 hours; (ii) methanol, sodium, 60°C, 30 min; (iii) acyl chloride, triethyl amine, dichloromethane, 0°C to room temperature, 3 hours; and (iv) where h is Planck's constant, ν is the frequency, and λ is the wavelength of the photon's radiation, $h\nu, \lambda \sim 500$ nm. (B) Crystal structure of BIT-Hep₂. (C) Crystal structure of PBIT-Hep₂. (D) Crystal structure of BIT-Ac₂. (E) Crystal structure of BIT-EH₂. Long side chains and hydrogen atoms are removed for clarity. The oxygen atoms at 3 and 3' position are labeled using purple color to distinguish them from the one at 1 and 1' positions. (F) Image of BIT-Hep₂ (scale bar, 1.0 cm). (G) Image of PBIT-Hep₂ (scale bar, 1.0 cm). (H) Optical microscope image of BIT-Hep₂ (scale bar, 0.5 mm). (I) Optical microscope image of PBIT-Hep₂ (scale bar, 0.5 mm). (J) SEM image of BIT-Hep₂ (scale bar, 20 μm). (K) SEM image of PBIT-Hep₂ (scale bar, 20 μm).

Table 1. Single-crystal x-ray diffraction data of monomers and polymers (see table S2). Values in parentheses for cell lengths and cell angles are estimated standard deviations.

Monomers and polymers	Space group	Cell lengths (Å)	Cell angles (°)	Cell volume (Å ³)	d_{C-C} (Å)	$d_{\pi-\pi}$ (Å)	R factor (%)
BIT-Ac ₂	C 2/c	a 17.940 (7) b 4.8376 (17) c 19.458 (7)	α 90.00 β 98.650 (10) γ 90.00	1669.5 (11) (Z = 4)	6.612	4.498	4.1
BIT-Hep ₂	P 21/c	a 14.014 (2) b 4.8850 (7) c 19.589 (3)	α 90.00 β 100.086 (11) γ 90.00	1320.3 (3) (Z = 2)	3.228	3.400	6.0
PBIT-Hep ₂	P 21/c	a 14.177 (5) b 4.8325 (17) c 19.159 (7)	α 90.00 β 104.422 (9) γ 90.00	1271.2 (8) (Z = 1)	1.590	3.229	5.2
BIT-Non ₂	P 21/c	a 15.949 (3) b 4.9529 (8) c 19.403 (3)	α 90.00 β 93.527 (5) γ 90.00	1529.9 (5) (Z = 2)	3.258	3.387	4.0
PBIT-Non ₂	P 21/c	a 16.259 (2) b 4.8471 (6) c 19.078 (3)	α 90.00 β 98.974 (6) γ 90.00	1485.1 (3) (Z = 1)	1.599	3.200	4.8
BIT-EH ₂	Pnna	a 7.0782 (6) b 28.764 (2) c 14.618 (11)	α 90.00 β 90.00 γ 90.00	2976.2 (4) (Z = 4)	5.561	3.306	16.7
BIT-OH ₂	P2(1)2(1)2(1)	a 3.6817 (8) b 12.291 (3) c 27.527 (6)	α 90.00 β 90.00 γ 90.00	1245.6 (5) (Z = 4)	5.201	3.368	4.1

chains were added by using the same conditions, and all the monomers (BIT-Ac₂, BIT-Hep₂, BIT-Non₂, and BIT-EH₂) were obtained in ~60% yield. The detailed synthesis and molecular structure characterization can be found in figs. S1 and S2 (34). All the monomers are orange in solution, as well as in the solid state, and exhibit similar absorption onset at ~550 nm [ultraviolet-visible (UV-vis) absorption spectra of the monomers are shown in fig. S3]. The absorption band from 350 to 550 nm is due to the π -electron delocalization and intramolecular donor-acceptor interactions (the alkylcarboxylate groups at 3,3' positions are weak donors, and carbonyl groups at 1,1' positions are strong acceptors). Single crystals of monomers were obtained from dichloromethane (DCM)-ethanol solutions by slow evaporation. The orange crystals of BIT-Hep₂ and BIT-Non₂ (with long linear side chains) turned to light yellow crystals when exposed to sun light (in ~1 hour) or irradiated under a high-pressure sodium lamp (in ~10 min) and became insoluble in all common organic solvents.

X-ray diffraction analysis of the light yellow crystals revealed the solids to be polymer single crystals. The crystal structure characterization of monomers and polymers is shown in Fig. 1, B to K, and Table 1. Because BIT-Hep₂ and BIT-Non₂ have the same space group, have similar unit cells, and have similar reactivity toward polymerization, only BIT-Hep₂ is shown. The packing of BIT-Hep₂ and PBIT-Hep₂ in the crystals is shown in Fig. 1, B and C, respectively (side chains are removed for clarity). It can be seen that, after polymerization, the carbon atoms in the 3,3' positions changed from sp² to sp³ hybridization, and there is a single bond formed

between the 3 and 3' positions of adjacent monomers. The length of the bond is 1.590 Å, slightly larger than that of a conventional C – C single bond (~1.54 Å) (35). The polymer crystal shares the same space group with the monomer, slightly larger cell angle β (104.422 versus 100.086 degrees), slightly smaller cell volume and slightly smaller $\pi - \pi$ stacking distance ($d_{\pi-\pi}$). The perfect alignment of the monomers in the crystals and the short distance of the two active carbon atoms (d_{C-C} , ~3.2 to ~3.3 Å) are necessary to ensure that topochemical reaction will occur with concomitant high-quality polymer crystal formation (R factor of ~5%) for both BIT-Hep₂ and BIT-Non₂. As shown in Fig. 1, D and E, the crystal packing and space group of BIT-Ac₂, with very short side chains, and BIT-EH₂ with long and branched side chains, are very different from BIT-Hep₂ or BIT-Non₂. For BIT-Ac₂, the shortest side chains lead to the largest d_{C-C} of 6.6 Å and $d_{\pi-\pi}$ of 4.5 Å. For BIT-EH₂, the 2-ethylhexyl groups lead to significant steric hindrance to close packing, which results in a ~30° twisting of the normally coplanar pentagon planes. After many trials, only low-quality crystals (R factor of 16.8%) were obtained for BIT-EH₂. Because BIT-Ac₂ and BIT-EH₂ show larger d_{C-C} than the typical value for topochemical polymerization (~4 to 5 Å) (9, 10), no polymerization reaction is observed. BIT-OH₂ with two hydroxyl groups is also inactive, probably because of the unfavorable packing (see Table 1 and supplementary materials for the crystal structure data) (34). The self-assembly effect of non-aromatic alkyl side chains plays a critical role in determining the molecular packing and reactivity. Oak Ridge Thermal Ellipsoid Plots (ORTEP) of BIT-Hep₂, BIT-Non₂, PBIT-Hep₂, and PBIT-Non₂

are shown in fig. S4. The carbon atoms at 3,3' positions in polymers have smaller thermal displacement, probably because they are bonded to four atoms in the polymers, whereas they bond only three atoms in the monomers (the polymer increases the rigidity of the atoms in question) (34).

In a study of the wavelength dependence of the reaction, the monomer crystals (BIT-Hep₂ and BIT-Non₂) were irradiated with 254-, 365-, and 500-nm light for 1 hour. The results showed that 356- and 500-nm light effected polymerization. It was also found that heating the orange crystals in the dark (from room temperature to 200°C) did not initiate polymerization. Therefore, the absorption band from 350 to 550 nm is responsible for the topochemical reactivity. The polymerization mechanism is believed to be similar to that reported for the diene and the quinodimethane compounds (21–25), except that the relatively long-lived excited state is created by visible and not UV light. At the same time, attempted polymerization by a free radical initiator, azobisisobutyronitrile, in a concentrated toluene solution in the dark, afforded only ~5% yield. This result, coupled with the result of photolysis of concentrated solution demands that the polymerization proceeds through a diradical and is not a simple free radical polymerization. This situation would be analogous to diacetylene polymerization where the propagating species is a carbene (14, 16) and not a free radical. We examined the yield of the reaction by extraction of the polymer crystals with DCM, as well as chloroform, for several hours. Evaporation of the solvent afforded no residue. This is in contrast to most previous cases (11–26, 36). The polymerization process described here is quantitative (>99% yield) for

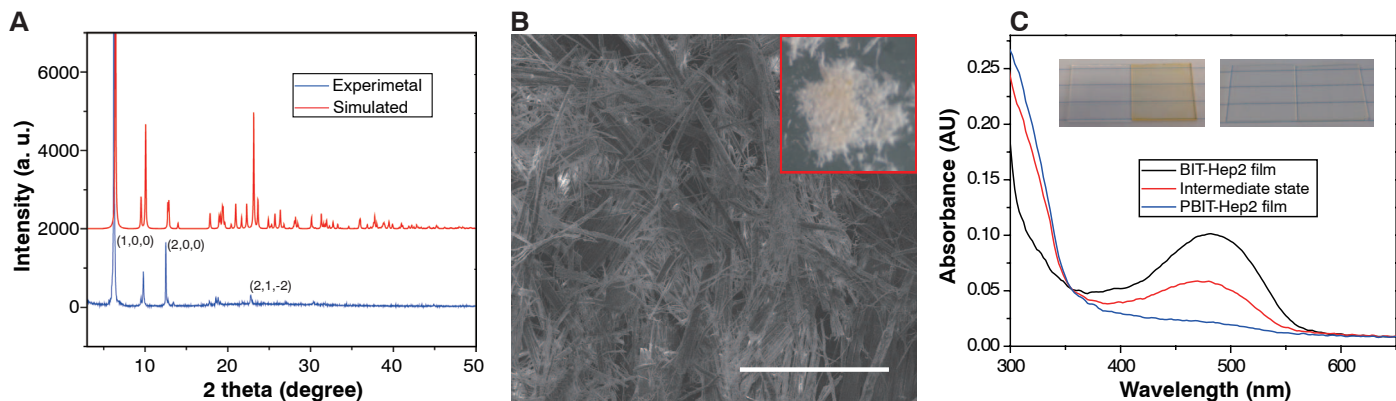


Fig. 2. Characterization of PBIT-Hep₂ synthesized from concentrated solution and thin film. (A) Powder x-ray diffraction data from experiments and simulation. a.u., arbitrary units. **(B)** SEM image (scale bar, 100 μm)

and optical microscope image (inset). **(C)** UV-vis absorption spectra of BIT-Hep₂ and PBIT-Hep₂ in thin films and corresponding real images (inset). AU, absorbance units.

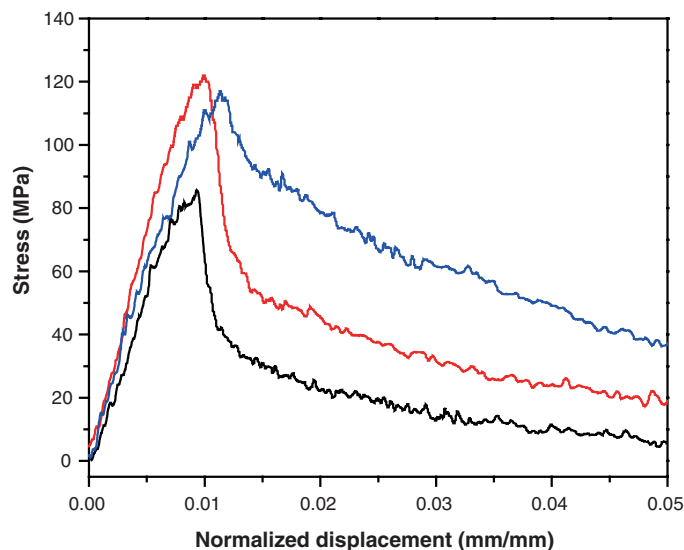
both BIT-Hep₂ and BIT-Non₂. The excellent conversion yield is attributed to the high reactivity of the monomer crystals and the fact that the polymers do not absorb the wavelength (450 to 550 nm) that is required for the reaction.

Images of the BIT-Hep₂ crystals (orange) and PBIT-Hep₂ crystals (light yellow) are shown in Fig. 1, F and G, respectively. The average length is about 1.5 cm (maximum ~ 1.9 cm), and the average width is about 0.6 mm (maximum ~ 1.1 mm). Optical microscope images of the same crystals before and after polymerization are shown in Fig. 1, H and I. The gross morphology of the polymers is the same as the monomers. The scanning electron microscope (SEM) images of a BIT-Hep₂ and PBIT-Hep₂ crystal are shown in Fig. 1, J and K, respectively. The monomer and polymer show long and narrow straight domains along the crystal but no obvious “grain boundary” in the long-axis direction. The surface morphology of the polymer crystal is smoother than that of the monomer crystal, probably because of the slight changes of molecular orientation in the crystals. SEM images of the same crystal before and after polymerization can be found in fig. S5. The orientation of the polymer backbone is determined to be along the long axis of the crystal (see fig. S6 for more details), and the molecular mass is estimated to be extremely large.

For example, an ideal 5-mm-long polymer in the crystal contains $\sim 10^7$ monomers (the distance between two monomers is ~ 5 Å) and the molecular mass is $\sim 6 \times 10^9$ daltons (37). A closer examination of Fig. 1C and fig. S6 reveals that, in the polymerization process, two asymmetric centers per monomer unit are created. Further, the two asymmetric centers are of opposite configuration. As a result, each monomer unit is of *meso* configuration and the polymer is not expected to be optically active (38).

Because of the high reactivity of BIT-Hep₂, other polymerization conditions, including solution and thin film, were examined with the aim of synthesizing PBIT-Hep₂ with different dimensions

Fig. 3. Representative tensile strain-stress curves of polymer single crystals. The initial length of the tested crystals (between two gauge length markers) is ~ 3.0 mm. Average yield strength = 102 MPa. Average tensile strength = 118 MPa. Estimated elastic strain = 0.8%. Estimated average Young's modulus = 15 GPa.



and morphology. For the reaction in solution, a concentrated toluene solution (~ 350 mg/ml) of BIT-Hep₂ was heated to 50°C (to keep it fully dissolved) under a high-pressure sodium lamp and stirred for 6 hours. Powderlike fine crystals of PBIT-Hep₂ were obtained with an isolated yield of $\sim 60\%$. The experimental and simulated x-ray powder diffraction profiles of the solution-generated polymers are shown in Fig. 2A (simulation is based on single-crystal x-ray diffraction data). Several peaks such as (1,0,0), (2,0,0), and (2,1,-2) in the experimental data match well with the simulated profile. The flat background in the experimental profile indicates the crystallinity is very high for the solution-generated polymers. The SEM image and optical microscope image (inset) of the powderlike polymers are collected in Fig. 2B. Different from highly ordered single crystals (Fig. 1J), disordered tiny fibers with diameters of ~ 1 to ~ 10 μm can be seen. The highly crystalline polymer nanocrystal fibers obtained here represent an interesting morphological feature.

The topochemical polymerization of BIT-Hep₂ in thin film was examined to demonstrate the solution processability that is needed for use in flexible plastic electronics. A thin layer of BIT-Hep₂ (~ 60 nm) was spin-cast on a glass substrate from chloroform solution. The orange-colored thin film was irradiated with a high-pressure sodium lamp, which resulted in a colorless film in 10 min. The UV-vis absorption spectra of the thin films before and after polymerization, as well as the images of the orange-colored monomer film and colorless polymer film, are shown in Fig. 2C. After polymerization, the absorption band in the visible range disappeared, and the absorption below 350 nm became stronger. As shown in fig. S7, the x-ray diffraction profile of the polymer thin film consists of broader and weaker peaks than the signal of the polymer powders generated from solution. The average size of the crystallites in the thin film was calculated to be around 40 nm (using the Scherrer equation), much smaller than the polymer powders shown in Fig. 2B. These results indicate that it is possible to coat high-

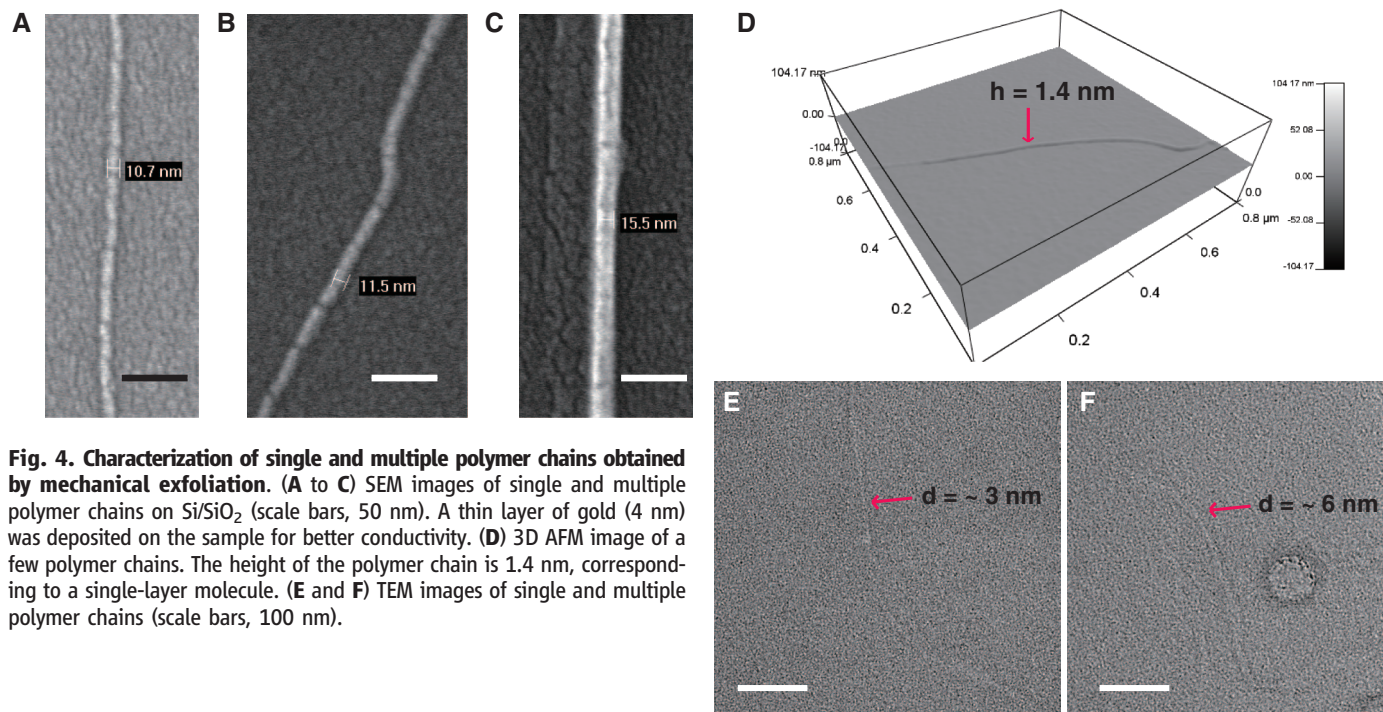


Fig. 4. Characterization of single and multiple polymer chains obtained by mechanical exfoliation. (A to C) SEM images of single and multiple polymer chains on Si/SiO₂ (scale bars, 50 nm). A thin layer of gold (4 nm) was deposited on the sample for better conductivity. (D) 3D AFM image of a few polymer chains. The height of the polymer chain is 1.4 nm, corresponding to a single-layer molecule. (E and F) TEM images of single and multiple polymer chains (scale bars, 100 nm).

quality monomer thin films by solution processing and then convert them to nanocrystalline polymer thin films with visible light.

The reaction is thermally reversible. The optical microscope and polarized optical microscope (POM) images of PBIT-Hep₂ crystals on a hot stage are shown in fig. S8 (34). When the polymer was heated to 195°C, it turned back to orange, and the orange crystal melted at 205°C (fig. S8, A, B, and C). The highly orientated crystals show bright colors in the POM images (fig. S8, D and E), but the isotropic liquid is dark (fig. S8F). The two processes at 195°C and 205°C are endothermic, as determined by differential scanning calorimetry (see fig. S9). When the orange crystals obtained at 195°C were exposed to visible light, however, they changed back to light yellow, which meant that the reaction is multiply reversible (see fig. S10 for the optical microscope images of the reversibility). The molecular structure of the monomer recovered by decomposition of the polymer was confirmed by nuclear magnetic resonance, and the result is shown in fig. S11. The decomposition process of a polymer crystal to monomer crystal is shown in fig. S8, G to J. It was found that the decomposition happens along the crystal length, which further confirms that the polymer backbone is along the crystal long-axis direction. The thermal decomposition of the polymers is probably due to the relatively longer carbon-carbon single-bond length (~ 1.59 Å) between two adjacent monomers, compared with the conventional bond length (the polymer chains are under slight tensile stress). Therefore, the bond should be easier to break at elevated temperature or under high-energy photon irradiation. Thermogravimetric analysis of the monomer BIT-Hep₂ shows that it decomposes

at, or above, 200°C (see fig. S12). Therefore, fig. S8C shows the decomposed monomer instead of the pure melt. A summary of the polymerization and decomposition conditions can be found in table S1.

Preliminary investigations show that the mechanical properties are dominated by very weak interchain van der Waals attraction. During the tensile stress-strain measurements (see fig. S13 for experimental set-up) (34), it was found that the polymer crystals behave as a unidirectional, fiber-reinforced composite, with extreme strength in the fiber direction and basically none in the transverse direction. This behavior resulted in the specimens splitting into individual strands in the grips, sliding with respect to each other. At maximum stress, no final “fracture” occurred. After the point of maximum stress, individual strands failed similar to the way rope fails, such that the stress decreased as the number of failed strands climbed (see fig. S14 and movie S1 for details). This behavior yields a stress-strain curve that exhibits a “toughening” of the material. Despite many difficulties during the measurements (see supplementary materials), the average Young’s modulus could be estimated to be around 15 GPa for several polymer crystal samples. The stress-strain curves of three representative samples are shown in Fig. 3. The result is lower than a typical polydiacetylene polymer (39). One possible reason is, again, the larger carbon-carbon single-bond length (~ 1.59 Å) between bonded monomers. Another possibility is that the value is underestimated because of the sliding effect (along the crystal long axis) between the polymer chains because the intermolecular interactions are very weak (which leads to overestimated strain). Based on these properties, we are able to isolate a single and/or multi-

ple unentangled rigid polymer chain by simple mechanical exfoliation (similar to graphene).

To characterize the mechanically exfoliated polymer chains, several microscopy technologies, such as SEM, atomic force microscopy (AFM), and transmission electron microscopy (TEM) were used, and the results are shown in Fig. 4, A to C; D; and E and F, respectively). Some very tiny polymer fibers with diameters around 10 to 15 nm are shown in Fig. 4, A to C. The thinnest one that we can find is 10.7 nm. Considering that ~ 4 -nm-thick gold was deposited on the sample (to ensure good conductivity for SEM measurements), the 10-nm one should contain only one, at most two, polymer chains. The three-dimensional (3D) AFM image of few polymer chains is shown in Fig. 4D. The height of the observed chain is measured to be 1.4 nm, which is in accordance with the thickness of one polymer layer. TEM images of several polymer chains are shown in Fig. 4, E and F. The diameters of the chains labeled are around 3 and 6 nm, which indicates single and double polymer chains, respectively. The mechanical exfoliation relies on the highly ordered alignment of the polymer chains in the single crystal and the weak interchain interactions.

We demonstrated selective visible light-triggered topochemical polymerization in single crystals, concentrated solutions, and thin films, as well as the reverse process—topochemical decomposition from polymers to monomers, of two bi-indene-dione derivatives. The simple and cost-effective chemistry presented here suggests that dihydroxy-bi-indene-dione is a versatile platform for further study. The properties of a polymeric solid consisting entirely of nonentangled, straight, infinitely long chains are influenced by

the absence of entanglements and relatively weak van der Waals attractive interactions. Just as graphite is made up of two-dimensional graphene sheets held together by weak van der Waals forces, PBIT-Hep₂ and PBIT-Non₂ are made up of one-dimensional chains held together by the same weak forces, mechanically, but not electronically, akin to “one-dimensional graphite.”

References and Notes

- E. M. Landau, M. Levanon, L. Leiserowitz, M. Lahav, J. Sagiv, *Nature* **318**, 353–356 (1985).
- Y. Yin *et al.*, *Science* **304**, 711–714 (2004).
- S. Mann, G. A. Ozin, *Nature* **382**, 313–318 (1996).
- P. J. Flory, *J. Chem. Phys.* **10**, 51–61 (1942).
- M. L. Huggins, *J. Chem. Phys.* **9**, 440 (1941).
- E. W. Fischer, G. F. Schmidt, *Angew. Chem. Int. Ed. Engl.* **1**, 488–499 (1962).
- X. Liu *et al.*, *Science* **307**, 1763–1766 (2005).
- J. Xu, Y. Ma, W. Hu, M. Rehahn, G. Reiter, *Nat. Mater.* **8**, 348–353 (2009).
- M. Hasegawa, *Chem. Rev.* **83**, 507–518 (1983).
- K. Biradha, R. Santra, *Chem. Soc. Rev.* **42**, 950–967 (2013).
- M. Hasegawa, Y. Suzuki, *J. Polym. Sci. Part B* **5**, 813–815 (1967).
- M. Hasegawa, *Adv. Phys. Org. Chem.* **30**, 117–171 (1995).
- G. Wegner, *Z. Naturforsch. B* **24**, 824–832 (1969).
- G. Wegner, *Pure Appl. Chem.* **49**, 443–454 (1977).
- D. Bloor, L. Koski, G. C. Stevens, *J. Mater. Sci.* **10**, 1689–1696 (1975).
- H. Eichele, M. Schwoerer, R. Huber, D. Bloor, *Chem. Phys. Lett.* **42**, 342–346 (1976).
- Y. Lu *et al.*, *Nature* **410**, 913–917 (2001).
- J. W. Lauher, F. W. Fowler, N. S. Goroff, *Acc. Chem. Res.* **41**, 1215–1229 (2008).
- A. Sun, J. W. Lauher, N. S. Goroff, *Science* **312**, 1030–1034 (2006).
- A. G. MacDiarmid *et al.*, *J. Chem. Soc. Chem. Commun.* **1975**, 476–477 (1975).
- A. Matsumoto, T. Matsumura, S. Aoki, *Macromolecules* **29**, 423–432 (1996).
- A. Matsumoto, T. Odani, K. Sada, M. Miyata, K. Tashiro, *Nature* **405**, 328–330 (2000).
- A. Matsumoto *et al.*, *J. Am. Chem. Soc.* **124**, 8891–8902 (2002).
- T. Itoh *et al.*, *Angew. Chem. Int. Ed.* **41**, 4306–4309 (2002).
- S. Nomura *et al.*, *J. Am. Chem. Soc.* **126**, 2035–2041 (2004).
- P. Johnston, C. Braybrook, K. Saito, *Chem. Sci.* **3**, 2301–2306 (2012).
- So far, only a few topochemical polymerization reactions can be induced by visible light. For example, the distyryl pyrazine derivatives are sensitive to purple light. See references (28) and (29) for details.
- M. Hasegawa, Y. Suzuki, F. Suzuki, H. Nakanishi, *J. Polym. Sci. A1* **7**, 743–752 (1969).
- J. Swiatkiewicz, P. N. Prasad, *J. Polym. Sci., Polym. Phys. Ed.* **22**, 1417–1429 (1984).
- S. Gabriel, E. Leupold, *Ber. Dtsch. Chem. Ges.* **31**, 1159–1174 (1898).
- V. Khodorkovsky, A. Ellern, O. Neilands, *Tetrahedron Lett.* **35**, 2955–2958 (1994).
- K. Tanaka, F. Toda, *J. Chem. Soc., Perkin Trans. 1* **1**, 873–874 (2000).
- J. Han *et al.*, *New J. Chem.* **31**, 543–548 (2007).
- Materials and methods are available as supplementary materials on Science Online.
- R. T. Morrison, R. N. Boyd, R. K. Boyd, *Organic Chemistry* (Benjamin Cummings, Redwood City, CA, ed. 6, 1992).
- Although sometimes it is claimed that polymerizations of diacetylenes go to completion, the resulting solids are always extracted after polymerization, and substantial amounts of monomer and other low-molecular-weight material are isolated from the extracts.
- Because of the insolubility of the polymers, we were not able to measure the molecular masses using conventional methods. Because we did not observe “grain boundaries” along the crystals in the SEM images, and for purposes of estimation, we assumed the length of the polymer is equal to the length of the crystal.
- We thank the editorial staff for bringing up the question of stereochemistry.
- C. Galiotis, R. J. Young, *Polymer* **24**, 1023–1030 (1983).

Acknowledgments: L.D. was supported by NSF (grant no. DMR-1210893) and the Link Foundation Energy Fellowship. Y.Z. and X.S. were supported by the Center for Energy Efficient Materials, an Energy Frontier Research Center funded by the U.S. Department of Energy, Office of Science, Office of Basic Energy Sciences under award number DE-SC0001009 and Department of Energy (grant no. DE-FG02-08ER46535). We thank M. Cornish and W. Cui at University of California, Santa Barbara, for the help with SEM and nuclear magnetic resonance measurements, respectively. We thank Y. Liu, C.-C. Chen, and C.-J. Hsu at University of California, Los Angeles, for the help with AFM, absorption, and thermogravimetric analysis measurements, respectively. Metrical parameters for the structures of BIT-Ac₂, BIT-EH₂, BIT-Hep₂, BIT-Non₂, BIT-OH₂, PBIT-Hep₂, and PBIT-Non₂ are available free of charge from the Cambridge Crystallographic Data Centre under reference numbers CCDC-976926, 976927, 976928, 976929, 976930, 976931, and 976932, respectively.

Supplementary Materials

www.sciencemag.org/content/343/6168/272/suppl/DC1
Materials and Methods
Figs. S1 to S14
Tables S1 and S2
References
Movie S1

12 September 2013; accepted 16 December 2013
10.1126/science.1245875

Nonenzymatic Sugar Production from Biomass Using Biomass-Derived γ -Valerolactone

Jeremy S. Luterbacher, Jacqueline M. Rand, David Martin Alonso, Jeehoon Han, J. Tyler Youngquist, Christos T. Maravelias, Brian F. Pfleger, James A. Dumesic*

Widespread production of biomass-derived fuels and chemicals will require cost-effective processes for breaking down cellulose and hemicellulose into their constituent sugars. Here, we report laboratory-scale production of soluble carbohydrates from corn stover, hardwood, and softwood at high yields (70 to 90%) in a solvent mixture of biomass-derived γ -valerolactone (GVL), water, and dilute acid (0.05 weight percent H₂SO₄). GVL promotes thermocatalytic saccharification through complete solubilization of the biomass, including the lignin fraction. The carbohydrates can be recovered and concentrated (up to 127 grams per liter) by extraction from GVL into an aqueous phase by addition of NaCl or liquid CO₂. This strategy is well suited for catalytic upgrading to furans or fermentative upgrading to ethanol at high titers and near theoretical yield. We estimate through preliminary techno-economic modeling that the overall process could be cost-competitive for ethanol production, with biomass pretreatment followed by enzymatic hydrolysis.

Biomass is emerging as a possible renewable alternative to petroleum-based resources in light of increasing environmental, economic, and political difficulties associated with fossil fuel extraction and use. Accordingly,

biomass-derived sugars have been presented as intermediates for the production of renewable fuels (1–3) and chemicals (4–6). However, producing water-soluble carbohydrates from lignocellulosic biomass requires cleaving ether bonds in hemicellulose (primarily xylan) and cellulose (glucan) chains while minimizing further degradation of the resulting C₅ and C₆ sugars (primarily xylose and glucose) to insoluble degradation

products. Unfortunately, in aqueous solutions containing low acid concentrations [<10 weight percent (wt %)] the high rate of sugar degradation reactions compared with polysaccharide depolymerization necessitates impractical reaction protocols for conversion of solid biomass, such as short residence times (10 ms to 1 min) at high temperatures (520 to 670 K), to obtain high yields of glucose (7). Because of the recalcitrance of crystalline cellulose to deconstruction, high yields at lower reaction temperatures can only be obtained by using concentrated mineral acid and/or ionic liquids (8, 9). However, recovery of the mineral acid is critical to the economics of the process, and the cost of ionic liquids can be prohibitive (8–10). Similarly, cellulase enzymes operating at temperatures of 320 K can achieve high glucose yields when converting cellulose rendered accessible by thermochemical pretreatment. However, the costs associated with producing these enzymes can be substantial compared with the value of the final product [with estimates of \$0.32 to \$1.47 per gallon of lignocellulose-derived ethanol (11, 12)].

Decoupling the residence times of the solid carbohydrate polymer from its soluble counterpart by flowing a solvent through a heated packed bed of biomass can minimize sugar degradation when using low acid concentrations (13). These systems are typically limited by their ability to produce concentrated soluble carbohydrate solutions (for example, 45 to 55% glucose yields

Department of Chemical and Biological Engineering, University of Wisconsin–Madison, Madison, WI 53706, USA.

*Corresponding author. E-mail: dumesic@engr.wisc.edu

when producing a 2 to 4 wt % sugar solution using 1 wt % H_2SO_4 in water) (13). In recent work, we have shown that liquid solutions of gamma-valerolactone (GVL) and water containing dilute concentrations of mineral acids ($<0.1 \text{ M H}_2\text{SO}_4$) can completely dissolve lignocellulosic biomass (negligible amounts of solids are recovered with filtration by using a 0.22- μm filter or with centrifugation) and be used to produce levulinic acid and furfural (6, 14). In this work, we report a processing strategy that uses GVL/water solutions for producing soluble carbohydrates—a more versatile biomass platform—from corn stover, hardwood, and softwood in a flow-through reactor using a progressive temperature increase from 430 to 490 K (Fig. 1). In addition, we demonstrate the effective separation of these sugars from GVL into a concentrated aqueous phase that is compatible with subsequent upgrading by chemical or biological processes.

The results in Fig. 2, A and B, show the concentrations of soluble carbohydrate achieved in the GVL/water solvent as a function of solvent volume flowed through the reactor packed with corn stover (fig. S1), for a mixture containing 80 wt % GVL and 20 wt % water (80/20 GVL/water), and for another mixture containing 90 wt % GVL and 10 wt % water (90/10 GVL/water). Both solutions contain a low concentration of mineral acid: 5 mM H_2SO_4 ($\sim 0.05 \text{ wt } \%$). In comparison, dilute acid pretreatment of biomass is typically carried out with at least 0.5 to 2 wt % H_2SO_4 (15). In both cases, the concentrations of C_5 (xylose and xylo-oligomer) and C_6 sugars (glucose and gluco-oligomer) reach maxima at temperatures between 430 and 470 K [where oligomers are defined as soluble carbohydrate species with more than one glucan or xylan monomer (supplementary materials)]. In contrast, when water is used as a solvent (Fig. 2C) the C_6 concentration increases continuously with increasing temperature up to 490 K and potentially beyond. When an alternate organic solvent such as ethanol is used in place of GVL, the C_6 sugar concentration shows a similar profile to that obtained with GVL, but lower by a factor of three (Fig. 2D). Therefore, the presence of GVL promotes cellulose deconstruction, most of which occurs below 480 K.

Increased deconstruction of biomass in the presence of GVL can be attributed to the complete solubilization of biomass solids, including the lignin fraction, observed during these experiments and previous work (6). In addition to providing a soluble lignin stream with potential as a feedstock for future upgrading, GVL prevents reprecipitation of lignin by-products on the surface of cellulose, which is a known phenomenon in water that decreases accessibility to the reactive cellulose surface (16). Water-insoluble solids corresponding to 95 and 84% of the original lignin were recovered for experiments conducted with 80/20 and 90/10 GVL/water, respectively (fig. S2). In addition, it appears that the presence of GVL plays a role in disrupting cellulose crystallinity—as suggested by x-ray diffraction

measurements of pure cellulose solids isolated after treatment with GVL—showing an increased fraction of more reactive amorphous cellulose (fig. S3).

Biomass conversion in the GVL/water solvent system leads to a significant increase in the overall sugar yields as compared with that of conversion with water or water/ethanol as the solvent. Specifically, C_5 recovery increases by 5 to 20 percentage points, and overall recovery of C_6 sugars increases by two- to fourfold (Fig. 2E). These C_5 and C_6 yields of 89 and 80%, respectively, are similar to those achievable by using ionic liquids or enzymes, rather than those obtainable with water (9, 17, 18). With 80/20 GVL/water, 90 to 95% of polysaccharides are recovered as known soluble products when dehydration products such as furfural, 5-hydroxymethylfurfural (5-HMF), and levulinic acid [all potential GVL precursor molecules (6)] are included (fig. S4). In comparison, conversion in water leaves 50% of the C_6 and 30% of the C_5 fractions as unidentified solid products (fig. S4). Unlike reports of enzymatic processes (15), we found that C_5 and C_6 sugar yields in GVL/water are insensitive to biomass type because they are comparable for corn stover, maple wood, and loblolly pine (Fig. 2E). Furthermore, when using GVL/water as a solvent it is possible to recover $>80\%$ of the C_5 and C_6 sugars in separate volume fractions without additional separation processes (fig. S5). Depending on economic factors, producing separate C_5 and C_6 sugar streams can provide opportunities to implement separate upgrading processes.

Decreasing the temperature ramp duration from 2 hours to 30 min increases the concentrations of carbohydrates by reducing the volume of solvent flowed through the biomass by 70% while reducing sugar yields by less than 10% (Fig. 2F). When a 20 wt % biomass solution in 80/20 GVL/water with 0.15 M H_2SO_4 is treated for 1 hour at 390 K, most of the C_5 sugars and

lignin are solubilized, and the remaining solids can be placed in the flow-through reactor where the same 0.5-hour temperature ramp with 80/20 GVL/water and 5 mM H_2SO_4 is used. This approach decreases the solvent-to-solids ratio by $>50\%$ while maintaining similar C_6 yields and lowering C_5 yields by only 15% (Fig. 2F). Accordingly, the concentration of soluble C_6 sugars is doubled as compared with that of our standard treatment. Moreover, when furfural is taken into account the overall conversion of xylan to known products remains above 90% for this biomass processing strategy (table S1).

The aqueous phase can be separated along with 75 to 91% of the carbohydrates from GVL/water solvent systems by addition of NaCl (Fig. 3A) (14) or liquid CO_2 (Fig. 3B). This separation yields a total soluble carbohydrate concentration of up to 112 g/liter, depending on the ramp time and method used. In the case of GVL extraction by CO_2 , $>70\%$ of the nonextracted carbohydrates that remain in the organic phase can be recovered in a single reextraction from the organic phase after water addition (0.1 g water per g of extracted GVL) (fig. S6). Furthermore, if CO_2 -extracted GVL is recycled, then any recycled sugars will contribute to increased concentrations after biomass conversion. We have shown that GVL remains stable during recycle (supplementary materials). Subsequent extractions of the separated aqueous phase with CO_2 lower the GVL concentration in water below 2 wt % while removing less than 4% of the carbohydrates and increasing their concentration to a total of 127 g/liter (Fig. 3B). This concentration corresponds to 65 to 85% of the highest concentrations obtained by enzymatic hydrolysis (150 to 200 g/liter) (17, 18) and is more than 8 times higher than concentrations that could have been obtained with pure water as a solvent ($<15 \text{ g/liter}$). Moreover, the concentrated monomer solutions obtained from salt separation and CO_2 extraction are clear (fig. S7), as opposed

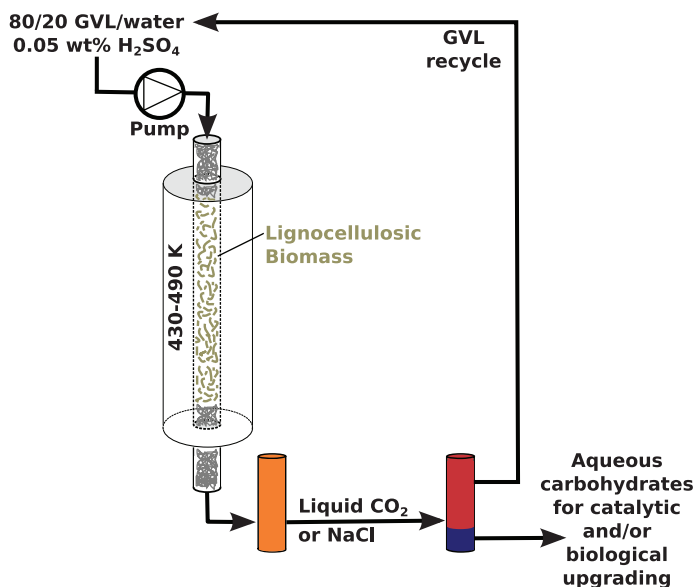


Fig. 1. Overview of the aqueous-phase soluble-sugar production using GVL as a solvent.

to the slurries obtained by using enzymatic hydrolysis or acidic-aqueous processing.

The C₅ and C₆ sugars recovered in the aqueous phase can be upgraded through catalytic dehydration to furfural and HMF (4). Furan selectivity is increased when these hydrophobic compounds are continuously extracted into an organic phase, such as 2-s-butyl-phenol (SBP) (19). Aqueous-phase modifiers such as NaCl (present by default in our salt-separated aqueous carbohydrate

stream) and a Lewis acid catalyst such as AlCl₃ further promote selectivity to furans by increasing their partitioning toward the organic phase and catalyzing carbohydrate isomerization, respectively (4, 19). Shown in Fig. 4A are the yields of furfural and 5-HMF obtained as a function of reaction time at 443 K through conversion of the soluble carbohydrates (monomers and oligomers) produced from corn stover by using the 2-hour temperature ramp. The separated aqueous phase

was used without further treatment, except for the addition of AlCl₃ and the presence of the SBP organic phase. The yields of 60 and 70% (Fig. 4A) for production of 5-HMF and furfural (>94% recovered in the SBP), respectively, are within 5% of yields reported from pure glucose and xylose, despite the presence of oligomers and other biomass by-products (19, 20).

Using liquid CO₂ to extract GVL eliminates the use of salt and reduces the GVL concentration,

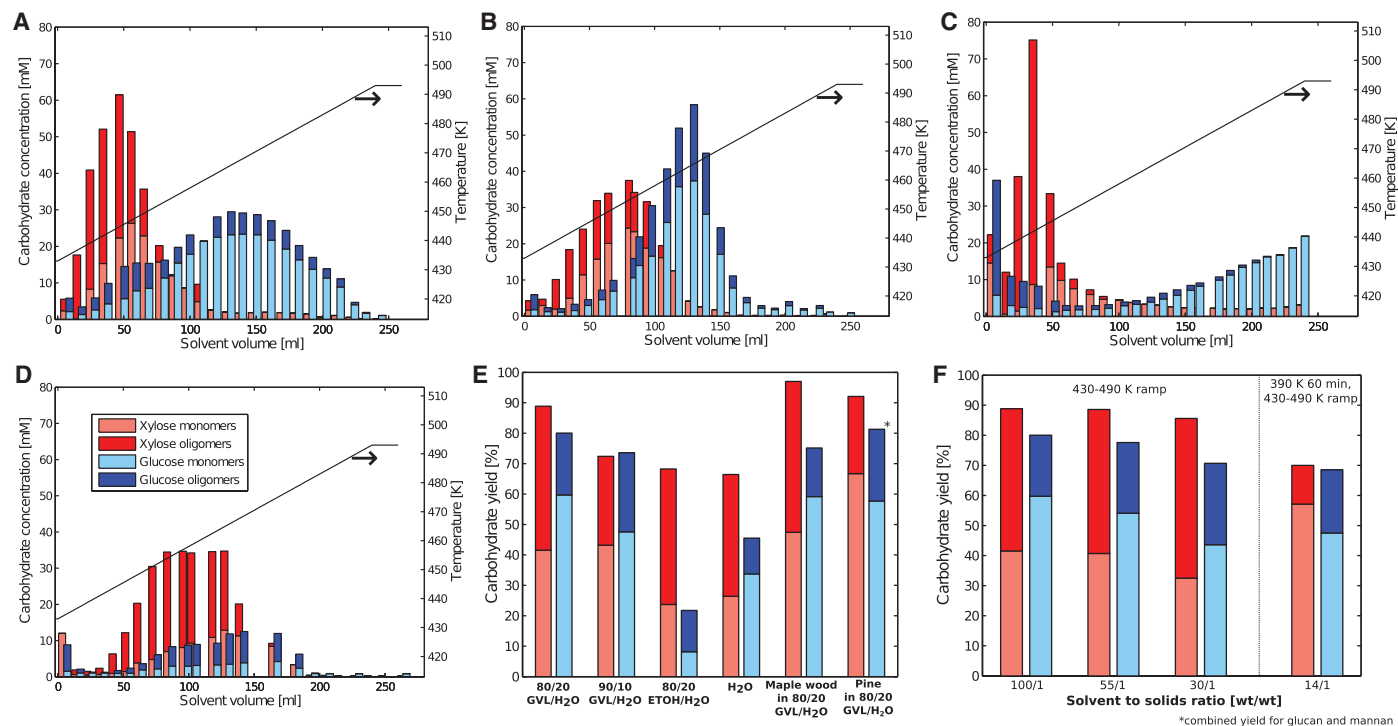
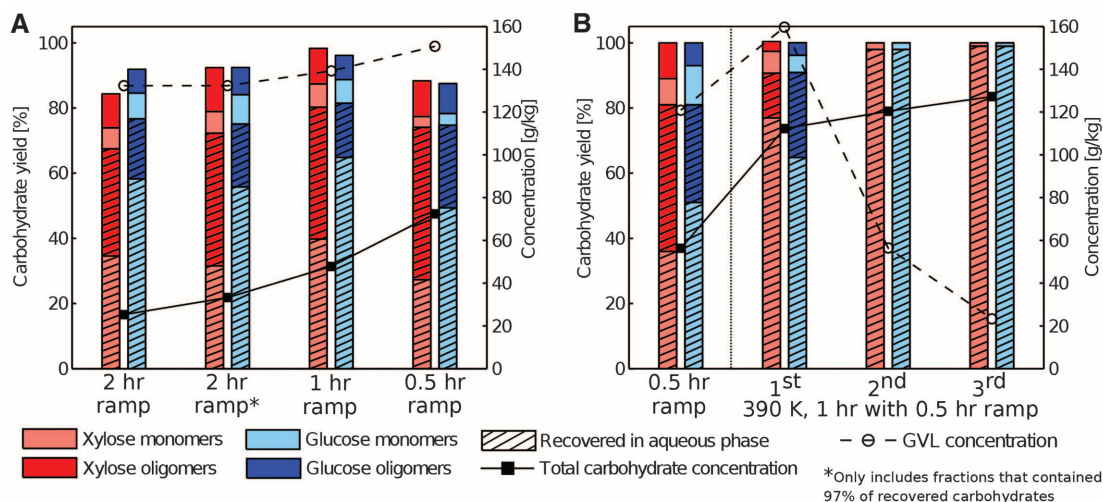


Fig. 2. Soluble carbohydrates produced by progressive heating of corn stover in a packed-bed flow-through reactor. Carbohydrate concentrations were measured in sequential volume fractions for solvent consisting of 5 mM H₂SO₄ in (A) 80 wt % GVL, 20 wt % water; (B) 90 wt % GVL, 10 wt % water; (C) water; and (D) 80 wt % ethanol, 20 wt % water. (E) Total yields of

soluble carbohydrates in different solvents from corn stover, maple wood, and loblolly pine. (F) Total yields of soluble carbohydrate from corn stover by using 80 wt % GVL and 20 wt % water as a function of solvent-to-solids ratio. The solid line in (A) to (C) represents the increasing temperature within the reactor. The legend in (D) applies to (A) to (F).

Fig. 3. Separation of 80 wt % GVL and 20 wt % water mixtures. (A) Separation using 12 wt %_{aq} NaCl (salt content is given as mass fraction of the salt and water mixture). Separated solutions were all derived from corn stover by using a 0.5- to 2-hours temperature ramp. Total yields differ slightly from 100% because of experimental error. (B) Separation using one to three subsequent CO₂ extractions. The separated solution was derived from corn stover either by a 0.5-hour temperature ramp or by initial treatment at 390 K for 1 hour followed by the 0.5-hour ramp. The aqueous phase was heated to 413 K to produce monomers after the first extraction (fig. S13).



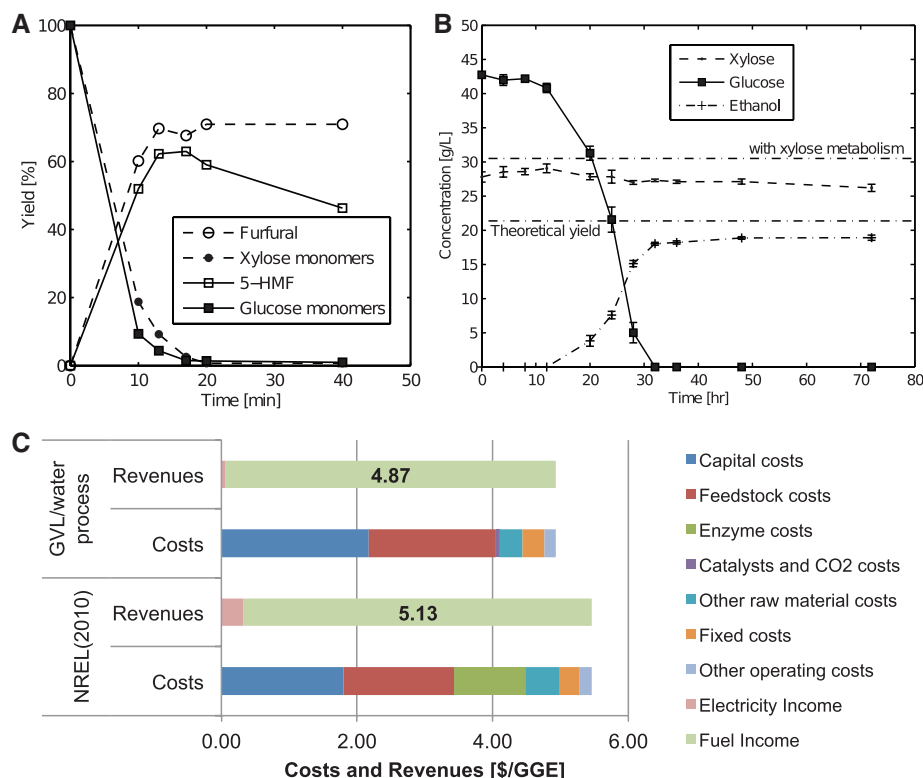


Fig. 4. Product yields for carbohydrate upgrading. (A) Production of furans as a function of time at 443 K. Yields include products analyzed in both phases. (B) Fermentation of CO₂-extracted feed. Theoretical ethanol yield is represented for glucose, and a potential ethanol yield is represented assuming that xylose is metabolized and converted similarly to glucose. Error bars represent SD of triplicate runs. (C) Comparison of costs and revenues for the GVL/water process with the lignocellulosic ethanol production process modeled by NREL (22).

both of which can inhibit microbial growth (fig. S8). In addition, the oligomers present in the recovered aqueous phase (Fig. 3) can be converted into monomers (preferable starting products for biological upgrading) in the acidic aqueous environment present in the aqueous phase (supplementary materials). In an aqueous monomer solution produced by using CO₂ extraction and the 0.5-hour temperature ramp and then diluted by 75%, we observed robust growth of *Saccharomyces cerevisiae* PE2 (PE2), a nonevolved industrial yeast strain, with minimal media, and we achieved a yield of ethanol from glucose corresponding to 87% of the theoretical value (Fig. 4B). Ethanol yields that were 95% of theoretical, as well as fatty acid production, were both achieved by using more dilute salt-extracted feed (figs. S9 and S10). Because PE2 does not metabolize xylose, the ethanol titer obtained by using this CO₂-extracted feed (19 g/liter) was below that of a potential titer of 31 g/liter that could be achieved if xylose had been converted at a similar yield [which has been demonstrated by using engineered yeast strains (21)] (Fig. 4B). Using a similar dilution of the more concentrated feed containing 127 g/liter carbohydrates, ethanol titers of 29 g/liter (86% yield) were obtained from glucose after 6 days of fermentation. Assuming xylose conversion at similar yields, a potential titer of 48 g/liter would

have been reached. Efforts are currently underway to study new strains and/or evolve one to grow robustly in the corresponding undiluted hydrolysate, which could lead to ethanol concentrations of 60 g/liter. An industrial scenario recently published by the National Renewable Energy Laboratory (NREL) assumed ethanol titers ~50 g/liter (22). Using our current carbohydrate recovery yields and assuming that an undiluted carbohydrate stream can be used for fermentation, a preliminary techno-economic model suggests that such a process could produce ethanol at a minimum selling price (MSP) of \$4.87/gallon of gasoline equivalent (GGE), versus \$5.13/GGE for the NREL scenario (Fig. 4C) (22). Most of the savings are related to the absence of enzymes (a description of the model and further discussion on the effect of enzyme cost and fermentation titers are available in the supplementary materials). Using more optimistic estimates of enzyme costs and 10% higher overall ethanol yields from biomass (12) leads to a decrease in the MSP of ethanol to \$4.06/GGE (details are available in the supplementary materials), which is slightly below our estimate for the GVL process. Although these preliminary economic comparisons are dependent on various assumptions, the results suggest that our proposed approach could become an economically competitive al-

ternative to current biomass-derived carbohydrates production schemes.

References and Notes

1. E. L. Kunkes *et al.*, *Science* **322**, 417–421 (2008).
2. P. Anbarasan *et al.*, *Nature* **491**, 235–239 (2012).
3. J. T. Youngquist, J. P. Rose, B. F. Pfleger, *Appl. Microbiol. Biotechnol.* **97**, 5149–5159 (2013).
4. Y. Román-Leshkov, J. N. Chheda, J. A. Dumesic, *Science* **312**, 1933–1937 (2006).
5. D. R. Dodds, R. A. Gross, *Science* **318**, 1250–1251 (2007).
6. D. M. Alonso, S. G. Wettstein, M. A. Mellmer, E. I. Gurbuz, J. A. Dumesic, *Energy Environ. Sci.* **6**, 76–80 (2012).
7. A. A. Peterson *et al.*, *Energy Environ. Sci.* **1**, 32–65 (2008).
8. M. von Sivers, G. Zacchi, *Bioresour. Technol.* **51**, 43–52 (1995).
9. J. B. Binder, R. T. Raines, *Proc. Natl. Acad. Sci. U.S.A.* **107**, 4516–4521 (2010).
10. K. Skill *et al.*, *Biotechnol. Bioeng.* **108**, 511–520 (2011).
11. D. Klein-Marcuschamer, P. Oleskowicz-Popiel, B. A. Simmons, H. W. Blanch, *Biotechnol. Bioeng.* **109**, 1083–1087 (2012).
12. D. Humbird *et al.*, "Process Design and Economics for Biochemical Conversion of Lignocellulosic Biomass to Ethanol," National Renewable Energy Laboratory report TP-5100-47764 (2011).
13. Y. Y. Lee, P. Iyer, R. W. Torget, in *Recent Progress in Bioconversion of Lignocellulosics, Advances in Biochemical Engineering/Biotechnology*, P. D. G. T. Tsao *et al.*, Eds. (Springer, Berlin, 1999), pp. 93–115.
14. S. G. Wettstein, D. M. Alonso, Y. Chong, J. A. Dumesic, *Energy Environ. Sci.* **5**, 8199–8203 (2012).
15. N. Mosier *et al.*, *Bioresour. Technol.* **96**, 673–686 (2005).
16. M. J. Selig *et al.*, *Biotechnol. Prog.* **23**, 1333–1339 (2007).
17. J. S. Luterbacher, Q. Chew, Y. Li, J. W. Tester, L. P. Walker, *Energy Environ. Sci.* **5**, 6990–7000 (2012).
18. D. B. Hodge, M. N. Karim, D. J. Schell, J. D. McMillan, *Bioresour. Technol.* **99**, 8940–8948 (2008).
19. Y. J. Pagán-Torres, T. Wang, J. M. R. Gallo, B. H. Shanks, J. A. Dumesic, *ACS Catal.* **2**, 930–934 (2012).
20. E. I. Gürbüz *et al.*, *Angew. Chem. Int. Ed. Engl.* **52**, 1270–1274 (2013).
21. M. W. Lau, B. E. Dale, *Proc. Natl. Acad. Sci. U.S.A.* **106**, 1368–1373 (2009).
22. F. K. Kazi *et al.*, *Fuel* **89**, S20–S28 (2010).

Acknowledgments: This work was supported by the Great Lakes Bioenergy Research Center (www.glbc.org), supported by the U.S. Department of Energy, through Cooperative Agreement DE-FC02-07ER64494 between the Board of Regents of the University of Wisconsin System and the U.S. Department of Energy and the National Science Foundation (CBET-1149678). J.S.L. acknowledges support from the Swiss National Science Foundation. The authors thank S. Ralph (Forests Products Laboratory) for providing loblolly pine. Patents have been filed by the Wisconsin Alumni Research Foundation (WARF) involving the use of GVL as a solvent for biomass processing (application nos. 13/736550 and 13/918097), and D.M.A. and J.A.D. are involved with a start-up company (Glucan Biorenewables) that is working in this area.

Supplementary Materials

www.sciencemag.org/content/343/6168/277/suppl/DC1
Materials and Methods
Supplementary Text
Figs. S1 to S15
Tables S1 to S7
References (23–28)

2 October 2013; accepted 27 November 2013
10.1126/science.1246748

Atomic-Scale Variability and Control of III-V Nanowire Growth Kinetics

Y.-C. Chou,^{1,2} K. Hillerich,³ J. Tersoff,⁴ M. C. Reuter,⁴ K. A. Dick,^{3,5} F. M. Ross^{4*}

In the growth of nanoscale device structures, the ultimate goal is atomic-level precision. By growing III-V nanowires in a transmission electron microscope, we measured the local kinetics in situ as each atomic plane was added at the catalyst-nanowire growth interface by the vapor-liquid-solid process. During growth of gallium phosphide nanowires at typical V/III ratios, we found surprising fluctuations in growth rate, even under steady growth conditions. We correlated these fluctuations with the formation of twin defects in the nanowire, and found that these variations can be suppressed by switching to growth conditions with a low V/III ratio. We derive a growth model showing that this unexpected variation in local growth kinetics reflects the very different supply pathways of the V and III species. The model explains under which conditions the growth rate can be controlled precisely at the atomic level.

The self-assembly of III-V semiconductors into nanowires via a catalytic particle provides rich opportunities for the formation of structures that are difficult to grow by more conventional techniques: heterostructures composed of highly mismatched materials (1, 2), metastable crystal structures (3), and new configurations such as nanowires with regularly arranged defects (4, 5). Precise control over this vapor-liquid-solid growth process, which takes place bilayer-by-bilayer at the catalyst-nanowire (111) interface (6, 7), is key to the formation of such structures and their development for new electronic and optical applications. Variability in the growth process can complicate the formation of precisely controlled individual structures or arrays of identical structures, but may also provide new pathways for understanding growth and developing new crystal configurations.

We used in situ transmission electron microscopy to provide a direct view of the addition of each atomic bilayer to Au-catalyzed GaP nanowires. Under typical growth conditions, where P is supplied in excess, we found marked changes in growth rate from one atomic layer to the next. The observed variability was much greater than expected from nucleation statistics (8) and was found to be correlated with the formation of defects in the nanowire. The variability can be suppressed by reducing the P supply relative to Ga. This dependence on growth conditions can be understood via a simple model as resulting from the very different transport mechanisms for the two species.

Nanowire growth was carried out in an ultrahigh-vacuum transmission electron microscope (UHV TEM) capable of flowing reactive gases over a heated sample (9). III-V growth has not been

widely studied in the TEM (10, 11) because of the complications involved with handling the necessary precursor gases. However, by flowing trimethylgallium (TMGa) and phosphine (PH₃) at 10⁻⁵ torr over samples heated to ~440°C, we were able to grow GaP nanowires from Au at rates of 0.1 to 3 nm min⁻¹. Because these rates are low, we used samples on which nanowire “stubs” ~1 μm in length and 30 to 50 nm in diameter had been grown ex situ from Au aerosol particles

(12), and observed the continued growth at the tips. Movies of growth were recorded using dark-field imaging conditions. We identified the instant at which each atomic layer adds to the nanowire by measuring the configuration of the catalyst-nanowire interface: Each change in the geometry at the trijunction indicates the moment at which a bilayer adds to the nanowire (11). Simultaneously, changes in image contrast indicate the formation of twin defects in the nanowire (see supplementary text). The observations therefore clarify the relationship among layer-by-layer growth kinetics, nanowire structure, pressure, and temperature. We quantified GaP nanowire growth for temperatures of 400° to 440°C. This temperature is within the range used in conventional metal-organic chemical vapor deposition (MOCVD) of GaP nanowires (13). The TMGa pressure ranged from 10⁻⁸ to 10⁻⁶ torr; the PH₃ pressure was 10⁻⁷ to 10⁻⁵ torr. MOCVD growth of GaP is usually carried out in the presence of H₂ carrier gas and with V/III ratios typically 500 or greater (13–15). In situ, there was no H₂ but our V/III ratios ranged from close to this value (100 to 300, referred to as “high”) to much smaller values (down to ~10). The growth rate examined here, 0.1 to 3 nm min⁻¹, is lower than for conventional MOCVD

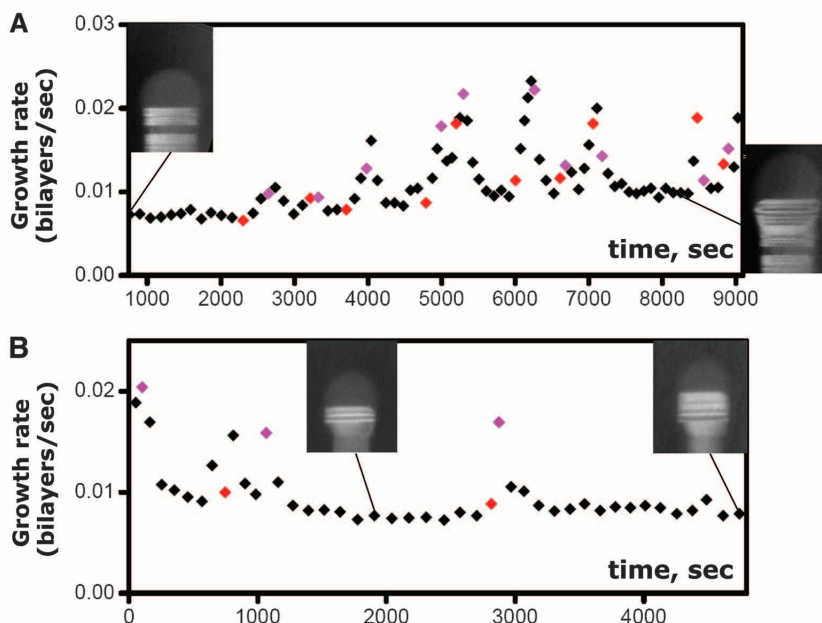


Fig. 1. Growth kinetics of GaP nanowires under conditions of high V/III ratio. The instantaneous growth rate is calculated from the interval between the addition of each bilayer. Inset are images of the nanowires at the times indicated. Imaging is in the $\langle 110 \rangle$ zone axis so that twin contrast is visible. The two twin variants appear as bright and dark bands in the image. Bilayers that were added with a twin orientation are indicated by colored data points. Red points are transitions from the bright to dark twin variant; purple points are transitions from dark to bright. (A) GaP nanowire (diameter 40 nm) showing frequent twin planes, one every 5 to 10 nm. The growth rate fluctuates by a factor of almost 3. During growth the temperature was 440°C, PH₃ pressure varied between 8×10^{-6} and 1×10^{-5} torr, and TMGa pressure varied between 4×10^{-8} and 8×10^{-8} torr. Time is given in seconds since gas exposure began. (B) GaP nanowire (diameter 28 nm) showing increases in growth rate by a factor of 2 associated with the presence of more widely spaced twin pairs. Growth took place at 440°C with PH₃ = 1.0×10^{-5} torr and TMGa = 5×10^{-8} torr. Time is given in seconds since imaging began.

¹Center for Functional Nanomaterials, Brookhaven National Laboratory, 735 Brookhaven Avenue, Upton, NY 11973, USA.

²Department of Electrophysics, National Chiao Tung University, 1001 University Road, Hsinchu City, Taiwan 300, R.O.C. ³Solid State Physics, Lund University, Box 118, S-221 00 Lund, Sweden. ⁴IBM Research Division, T. J. Watson Research Center, Yorktown Heights, NY 10598, USA. ⁵Polymer & Materials Chemistry, Lund University, Box 124, S-221 00 Lund, Sweden.

*Corresponding author. E-mail: fmross@us.ibm.com

but is at the low end of the range for molecular beam epitaxy of GaP (16–19).

Figure 1 and movies S1 and S2 show examples of nanowire growth kinetics measured during GaP growth at 440°C with typical high V/III ratios: TMGa = 5×10^{-8} to 10×10^{-8} torr, PH₃ = 1.0×10^{-5} torr, and V/III ratio = 100 to 200. Growth under these conditions produced nanowires with twinned zinc blende structure, as expected from ex situ growth (15, 20, 21). The graphs show the instantaneous growth rate, calculated from the time interval between addition of successive bilayers to the nanowire. The most striking feature of the data is that GaP nanowires do not grow at a uniform rate, even when the source gas pressures remain constant. At intervals the growth rate increases over a clear baseline rate by as much as a factor of 3 to 4, with the accelerated growth persisting for several bilayers. Moreover, the accelerated growth periods are generally correlated with the appearance of planar defects in the nanowire. These defects may be single twin planes or a closely spaced pair of twin planes. The time at which each defect plane forms is estimated from the image contrast (see supplementary text) and indicated in Fig. 1.

To determine the growth kinetics as a function of pressure, we varied the pressures of TMGa and PH₃ individually while still maintaining a high V/III ratio. The results show no strong dependence of growth rate on PH₃. This is unsurprising because group V is supplied in excess, as in conventional MOCVD. The growth rate also shows no strong dependence on TMGa pressure (fig. S2), although this was hard to quantify because of the fluctuations.

When we reduced the V/III ratio below ~100, we found radically different growth kinetics. GaP growth with a V/III ratio of 20 to 60 took place with a large and hence Ga-rich droplet (Fig. 2). The addition of bilayers occurred at remarkably regular intervals (Fig. 2, A and B). The lower V/III ratios produced relatively fewer twins than were seen in the high-V/III regime, with only one occurrence in Fig. 2. Examining a broader set of data that includes several twin defects, we consistently find no measurable change in growth rate when a twin defect forms. Furthermore, the growth rate also appears insensitive to the TMGa pressure. This is shown in Fig. 2C, where varying TMGa pressure by a factor of 4 does not affect the growth rate measurably. Instead, the key parameter determining growth rate in this regime is the PH₃ pressure. In Fig. 3, we show that the growth rate is directly proportional to the PH₃ pressure. PH₃-limited regimes are known from ex situ studies (22).

The local measurements therefore demonstrate two different regimes: (i) at low V/III ratios, a growth rate proportional to PH₃ but with no dependence on TMGa or on crystal defects; and (ii) at high V/III ratios (above ~60 to 100 at the temperature used here), a rate insensitive to PH₃ but with strong local variability that correlates with the formation of twins in the structure.

To derive a compact model that can provide an overview of growth under a broad set of conditions, we neglect discrete aspects of growth such as the nucleation event for each layer (5, 8, 23) and the changing morphology at the growth interface (11, 24). Instead we focus on the well-known differences in transport mechanisms for group III and V atoms (25, 26). A brief outline is given here, with the full derivation and a discussion of nucleation and growth rate in the supplementary text. For simplicity, we consider the limit of fast diffusion of Ga along the surface and into the catalyst, and negligible surface diffusion of P due to its rapid evaporation. As discussed below, the key qualitative conclusions are expected to hold even under more realistic assumptions and should be equally relevant to GaAs and similar III-V nanowire systems. We take the growth rate as proportional to the supersaturation in the catalyst relative to the crystal. Because P diffusion is negligible, the supply of P to the catalyst is proportional to the PH₃ pressure, p_V , and the catalyst loses excess P by evaporation as well as incorporation into the crystal. In contrast, although the supply of Ga to the surface is proportional to the TMGa pressure p_{III} , much of this Ga reacts with P on the surface. As a result, the surface acts as a reservoir at chemical potential $\mu_{Ga} = kT \ln(\alpha p_{III}/p_V)$, where α is a surface rate constant (see supplementary text). Thus, the effective Ga supply reflects the V/III

ratio rather than the TMGa pressure. We then calculate the growth rate, finding

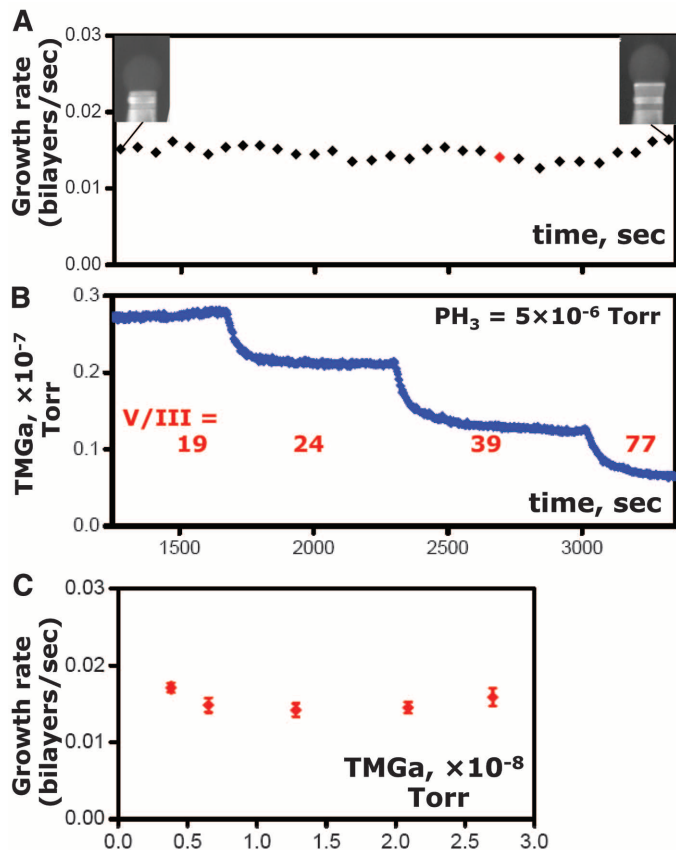
$$v = v_0 \left[\ln \left(\beta p_V - \frac{v}{v_0} \right) - \ln(\beta p_V) + \ln(\gamma p_{III}) - \frac{\mu_x}{kT} \right] \quad (1)$$

where v is the growth velocity, p_{III} and p_V are the pressures of Ga and P precursors, and μ_x is the chemical potential of the nanowire (per two-atom unit, up to an additive constant). The temperature-dependent parameters v_0 , β , and γ are not known, but we can already see one important point: The growth rate does not depend on the TMGa pressure and nanowire properties independently, but only in the specific combination $\ln(\gamma p_{III}) - \mu_x/kT$. Thus, a regime that is insensitive to one of these terms should also be insensitive to the other.

We can quickly see the essentials of the growth behavior by solving Eq. 1 and plotting v/v_0 versus βp_V and $\ln(\gamma p_{III}) - \mu_x/kT$. Figure 4 shows qualitatively distinct regimes depending on the gas pressures.

For high group V flux, the growth becomes independent (27) of p_V . This agrees with the experimental observation that in the high-V/III regime, the GaP growth rate is independent of PH₃ pressure. Instead, the growth rate depends linearly on $\ln(p_{III}) - \mu_x/kT$ (upper part of Fig. 4).

Fig. 2. Growth kinetics of a GaP nanowire (diameter 34 nm) under conditions of lower V/III ratio. Growth took place at 435°C with steady PH₃ = 5×10^{-6} torr and varying TMGa. (A) Instantaneous growth rate, with inset images showing the nanowire structure. The wire has a few twins, about one every 20 to 30 nm. During this experiment only one twin defect forms, and it has no effect on the growth rate. Time is given in seconds since imaging began. (B) TMGa pressure, as measured by mass spectrometer during growth. The V/III ratio is indicated. The TMGa pressure varies by a factor of 4 without measurably affecting the growth rate in (A). (C) Average growth rate as a function of TMGa pressure. The values shown were obtained from the data in (A) and other measurements on the same nanowire at a higher TMGa pressure. Error bars denote SD of the measurements of instantaneous growth rate at each TMGa pressure.



The first term suggests a weak dependence on TMGa pressure in the model; the second term leads to a dependence of growth rate on crystal defects.

In general, any defect or change in local crystal structure will alter the nanowire chemical po-

tential μ_x , as will other factors such as any change in diameter, any change in sidewall surface energy, or any change in the angle the sidewalls make with the growth direction. This latter effect arises because of changes in the capillary forces applied by the droplet and the sidewall (28) (supplemen-

tary text). Ex situ observations (15) show that untwinned GaP nanowires grow with {211} sidewalls parallel to the growth direction, and that twins are associated with changes in both nanowire cross-sectional shape and sidewall structure inclination (15). In particular, after a twin, the nanowire grows for a certain length with inclined {111} sidewalls (15, 29). It is difficult to disentangle the effects on μ_x of all the changes that occur upon twinning, and indeed our model does not address which feature of the defective crystal changes μ_x and hence the growth rate. However, the data in Figs. 1 and 2 do provide some clues. An obvious possibility would be the twin plane itself. However, because the growth rate enhancement persists for several layers, it is unlikely to be an effect of the buried twin plane alone. Indeed, the data in Fig. 1A hint that when there is a pair of twin planes, the first twin is associated with an increasing growth rate, whereas after the second twin plane the growth rate decreases back to the baseline. In (15), when a pair of twins occurs, sidewalls with the opposite inclination form after the second twin, returning the cross section to its original shape. We therefore speculate that upon twinning, μ_x and hence the growth rate may be dominated by changes in sidewall energy and/or inclination angle. (We have not confirmed the cross section or inclined facets in our experiments because of the limited resolution of the in situ imaging.)

For high group III flux, the model gives a growth rate that is linear in p_V . This low-V/III regime is seen at the lower right corner of Fig. 4. The linearity holds as long as p_V is much greater than the evaporation rate. Most important, in this high p_{III} pressure limit, the growth rate becomes independent of both p_{III} and crystal defects or morphological changes. These predictions match well with the observations in Figs. 2 and 3. In this low-V/III regime, the surface is acting as a reservoir of Ga at high chemical potential, with which the catalyst is near equilibrium. Thus, any P arriving at the catalyst is efficiently captured and the growth rate is determined by direct impingement of P atoms, and is therefore insensitive to other factors. The growth rate in this regime would remain linear in p_V and insensitive to defects even if we included an atomistic nucleation process in the model (see supplementary text).

Although the model is highly simplified, its most important conclusions remain valid under more realistic assumptions and are equally applicable to other III-V nanowire systems. The key requirements to explain the qualitative behavior are only the standard and well-supported assumptions [e.g., (24–26)] that group V diffusion is unimportant relative to direct impingement and evaporation, whereas group III comes primarily from rapid diffusion over a relatively large area.

A third distinct regime is visible at the far left of Fig. 4: If the pressures become too low, the velocity becomes negative as the wire decomposes. However, even our low-pressure experimental conditions appear far from this regime, as evidenced by Fig. 3C.

Fig. 3. Effect of group V pressure on nanowire growth kinetics.

(A) Growth kinetics for the same GaP nanowire shown in Fig. 2, but now with varying PH_3 and steady TMGa = 2.7×10^{-7} torr. Inset images show the nanowire structure. One twin forms during the experiment and does not affect the growth rate. Time is given in seconds since imaging began. (B) PH_3 pressure as measured by mass spectrometer during growth. The V/III ratio is indicated. Note the strong correlation of the growth rate in (A) with PH_3 pressure. (C) Average growth rate as a function of PH_3 pressure. Error bars denote SD of the measurements of instantaneous growth rate at each PH_3 pressure. The dotted line indicates that the growth rate is proportional to the PH_3 pressure until the PH_3 pressure rises to values where presumably it is no longer small relative to the TMGa pressure.

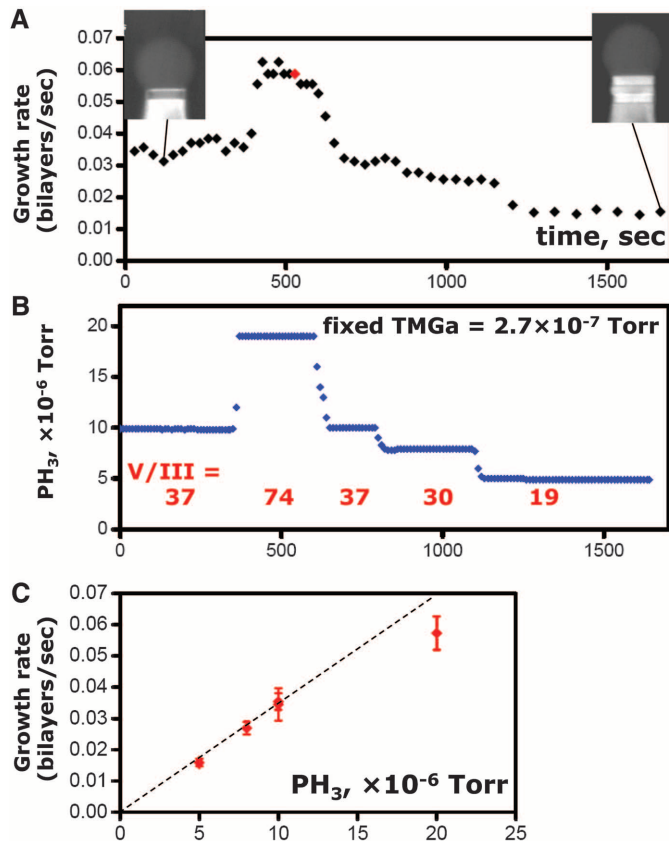
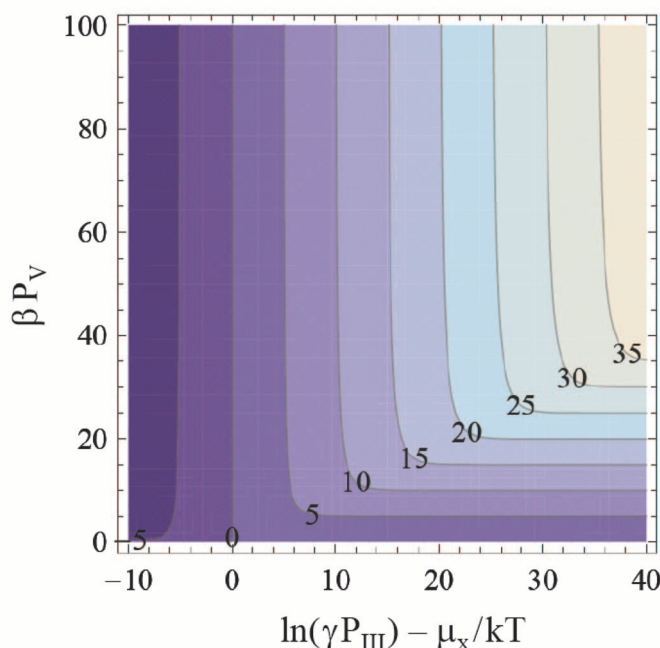


Fig. 4. Dependence of nanowire growth velocity on gas pressures and nanowire chemical potential μ_x , from Eq. 1. Note the linear scale for group V pressure p_V and logarithmic scale for group III pressure p_{III} . Contours of constant velocity are labeled, with velocity increasing from lower left to upper right. In the upper region, corresponding to high V/III ratios, the growth rate becomes independent of p_V and varies logarithmically with p_{III} and linearly with μ_x . At lower right, corresponding to low V/III ratios, the growth rate becomes independent of p_{III} and μ_x and varies linearly with p_V .



The relationship between local growth kinetics and atomic structure, obtained through in situ measurements during GaP nanowire growth over a range of parameters, provides insights into understanding the growth mechanism and the requirements for the most precise control over growth. A high V/III ratio is commonly used, but we find local variations in growth rate by as much as a factor of 4. These variations appear to be correlated with changes in the crystal structure associated with twin defects, and we suggest that changes in sidewall configuration are an important factor. The key implication is that the growth rate is very sensitive to perturbations, and such sensitivity must be suppressed to achieve the ultimate control over structure. We find that this sensitivity is absent when growing at low V/III ratios, creating a highly regular regime that may be optimal for growth of complex materials that include features such as narrow quantum wells or arrays of identical nanowires. We can explain the differences between regimes by considering the asymmetry in the pathways by which the two species arrive at the growth front. We expect our conclusions to apply to other III-V nanowire materials such as GaAs, InAs, and InP. The assumptions underlying the model (surface diffusion, evaporation, and solubility in Au) are common for a range of V and III species. In addition, the crystal structure and defect formation in all four materials are affected in the same way by V/III

ratio (30), suggesting that the effects controlling crystal structure must be general.

References and Notes

1. P. Caroff *et al.*, *Nanotechnology* **20**, 495606 (2009).
2. M. T. Björk *et al.*, *Nano Lett.* **2**, 87–89 (2002).
3. J. Johansson, J. Bolinsson, M. Ek, P. Caroff, K. A. Dick, *ACS Nano* **6**, 6142–6149 (2012).
4. P. Caroff *et al.*, *Nat. Nanotechnol.* **4**, 50–55 (2009).
5. R. E. Algra *et al.*, *Nature* **456**, 369–372 (2008).
6. S. Hofmann *et al.*, *Nat. Mater.* **7**, 372–375 (2008).
7. C.-Y. Wen *et al.*, *Science* **326**, 1247–1250 (2009).
8. F. Glas, J.-C. Harmand, G. Patriarche, *Phys. Rev. Lett.* **104**, 135501 (2010).
9. F. Glas, *Rep. Prog. Phys.* **73**, 114501 (2010).
10. R. E. Diaz, R. Sharma, K. Jarvis, Q. Zhang, S. Mahajan, *J. Cryst. Growth* **341**, 1–6 (2012).
11. C.-Y. Wen *et al.*, *Phys. Rev. Lett.* **107**, 025503 (2011).
12. K. A. Dick *et al.*, *Nano Lett.* **7**, 1817–1822 (2007).
13. K. A. Dick, K. Deppert, T. Mårtensson, W. Seifert, L. Samuelson, *J. Cryst. Growth* **272**, 131–137 (2004).
14. J. Johansson, C. P. T. Svensson, T. Mårtensson, L. Samuelson, W. Seifert, *J. Phys. Chem. B* **109**, 13567–13571 (2005).
15. R. E. Algra *et al.*, *Nano Lett.* **10**, 2349–2356 (2010).
16. J. P. Boulanger, R. R. Lapierre, *Semicond. Sci. Technol.* **27**, 035002 (2012).
17. J. P. Boulanger, R. R. Lapierre, *J. Cryst. Growth* **332**, 21–26 (2011).
18. F. Jabeen, G. Patriarche, F. Glas, J.-C. Harmand, *J. Cryst. Growth* **323**, 293–296 (2011).
19. J. P. Boulanger, thesis, McMaster University (2013).
20. G. Zhang, K. Tateno, T. Sogawa, H. Nakano, *J. Appl. Phys.* **103**, 014301 (2008).
21. J. Johansson *et al.*, *Nat. Mater.* **5**, 574–580 (2006).
22. M. A. Verheijen, G. Immink, T. de Smet, M. T. Borgström, E. P. A. M. Bakkers, *J. Am. Chem. Soc.* **128**, 1353–1359 (2006).
23. H. J. Joyce, J. Wong-Leung, Q. Gao, H. H. Tan, C. Jagadish, *Nano Lett.* **10**, 908–915 (2010).
24. P. Krogstrup *et al.*, *J. Phys. D* **46**, 313001 (2013).
25. V. G. Dubrovskii *et al.*, *Phys. Rev. B* **79**, 205316 (2009).
26. C. Colombo, D. Spirkoska, M. Frimmer, G. Abstreiter, A. Fontcuberta i Morral, *Phys. Rev. B* **77**, 155326 (2008).
27. One might expect a logarithmic dependence on p_V , but this dependence is cancelled by the effect of p_V on the group III supply.
28. K. W. Schwarz, J. Tersoff, *Nano Lett.* **11**, 316–320 (2011).
29. Because the twinning exchanges A and B planes, inclined sidewalls allow the cross section to change gradually to a trigonal hexagon in which wide and narrow sidewalls are also exchanged.
30. S. Lehmann, J. Wallentin, D. Jacobsson, K. Deppert, K. A. Dick, *Nano Lett.* **13**, 4099–4105 (2013).

Acknowledgments: Supported by the Center for Functional Nanomaterials, Brookhaven National Laboratory, which is supported by the U.S. Department of Energy, Office of Basic Energy Sciences, under contract DE-AC02-98CH10886 (Y.-C.C.); NSF grant DMR-0907483; and the Nanometer Structure Consortium at Lund University, the Swedish Research Council, the Swedish Foundation for Strategic Research, and the Knut and Alice Wallenberg Foundation. Y.-C.C. and K.H. performed experiments and data analysis, J.T. developed the growth model, M.C.R. developed the experimental techniques, and K.A.D. and F.M.R. designed the experiments and coordinated the analysis.

Supplementary Materials

www.sciencemag.org/content/343/6168/281/suppl/DC1
Supplementary Text
Figs. S1 and S2
Movies S1 and S2
References (31–35)

13 August 2013; accepted 11 December 2013
10.1126/science.1244623

Temporal Constraints on Hydrate-Controlled Methane Seepage off Svalbard

C. Berndt,^{1*} T. Feseker,² T. Treude,¹ S. Krastel,^{1†} V. Liebetrau,¹ H. Niemann,³ V. J. Bertics,^{1‡} I. Dumke,¹ K. Dünnebier,^{1§} B. Ferré,⁴ C. Graves,⁵ F. Gross,¹ K. Hissmann,¹ V. Hühnerbach,^{5||} S. Krause,¹ K. Lieser,¹ J. Schauer,¹ L. Steinle³

Methane hydrate is an icelike substance that is stable at high pressure and low temperature in continental margin sediments. Since the discovery of a large number of gas flares at the landward termination of the gas hydrate stability zone off Svalbard, there has been concern that warming bottom waters have started to dissociate large amounts of gas hydrate and that the resulting methane release may possibly accelerate global warming. Here, we corroborate that hydrates play a role in the observed seepage of gas, but we present evidence that seepage off Svalbard has been ongoing for at least 3000 years and that seasonal fluctuations of 1° to 2°C in the bottom-water temperature cause periodic gas hydrate formation and dissociation, which focus seepage at the observed sites.

Large quantities of methane, a powerful greenhouse gas, are present in the continental margin west off Svalbard, where they are stored as marine gas hydrate (1–3). Because hydrate stability is temperature-dependent, Arctic warming is a potentially major threat to both the environment and the global economy. If even a fraction of the methane contained in Arctic hydrates were released to the atmosphere, the effect on climate could be dramatic (4, 5).

Water-column temperature measurements and mooring data suggest a 1°C bottom-water temperature warming for the past 30 years (6, 7). Numerical modeling of hydrate stability predicts that such warming would result in the dissociation of hydrates in the shallowest sediments (6–9). Therefore, the discovery of numerous gas flares—that is, trains of gas bubbles in the water column precisely at the water depth where gas hydrate is expected to dissociate—was interpreted as the

onset of submarine Arctic gas hydrate dissociation in response to global warming, which may potentially lead to large-scale escape of methane into the water column and ultimately into the atmosphere (6). In order to assess the consequences of methane venting on ocean and atmosphere composition, it is necessary to establish how the rates of methane emissions from hydrate systems change through time (10).

The margin of Svalbard (Fig. 1) can be considered a model system to study a temperature-related gas hydrate destabilization scenario, because water temperature in the Fram Strait oceanographic gateway will be more affected by changes in global atmospheric temperature than elsewhere in the Arctic; therefore, any corresponding changes to a hydrate system should be

¹GEOMAR Helmholtz Centre for Ocean Research Kiel, 24148 Kiel, Germany. ²MARUM Center for Marine Environmental Sciences and Faculty of Geosciences, University of Bremen, 28359 Bremen, Germany. ³Department of Environmental Sciences, University of Basel, 4056 Basel, Switzerland. ⁴CAGE (Centre for Arctic Gas Hydrate, Environment, and Climate), Department of Geology, University of Tromsø, 9037 Tromsø, Norway. ⁵National Oceanography Centre, Southampton SO14 3ZH, UK.

*Corresponding author. E-mail: cberndt@geomar.de

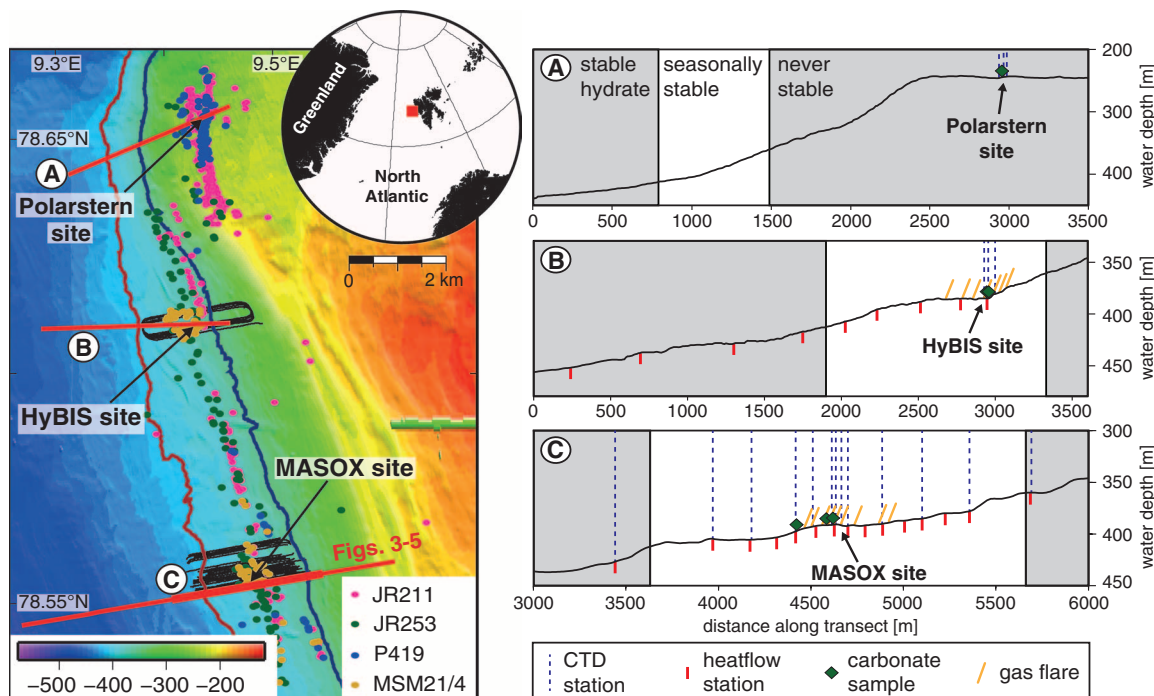
†Present address: Institute of Geosciences, University of Kiel, 24118 Kiel, Germany.

‡Deceased.

§Present address: Institut für Angewandte Geowissenschaften, Technische Universität Berlin, 10587 Berlin, Germany.

||Present address: GEOMAR Helmholtz Centre for Ocean Research Kiel, 24148 Kiel, Germany.

Fig. 1. The Svalbard gas hydrate province is located on the western margin of the Svalbard archipelago (inset). At water depths shallower than 398 m, numerous gas flares have been observed in the water column (color-coded dots for different surveys) by using EK60 echo sounders and high-resolution side scan sonar. The gas flares are located between the contour lines at which gas hydrate is stable in the sub-surface at 3° (brown) and 2° (blue) C average bottom-water temperature. The black lines show the location of PARASOUND profiles with 40-m separation, that is, complete coverage, for flare mapping. The black arrows point to the location of submarine dives discussed in the text. The red line shows the location of the modeling transect (bold section shown in Fig. 3). The large cluster of seeps at the northern limit of the gas flare line at a water depth of 240 to 260 m can be explained by the presence of an



elsewhere-absent glacial debris flow deposit that is deviating gas laterally within the prograding debris flow deposits and cannot have anything to do with gas hydrate dynamics (16, 23). CTD, conductivity, temperature, and depth.

easier to observe here than elsewhere (11). The continental margin of Svalbard is characterized by abundant contourite deposits (12) that consist of fine-grained sediments with high water content, which cover most of the margin between water depths of 800 and 3000 m. It is likely that these contourites are underlain by Miocene sediments with 3% (by weight) of total organic carbon as found at Ocean Drilling Project site 909 (13) and that the emanating gas was produced by these sediments. Proximally, that is, shallower than 700- to 800-m water depth, Pleistocene and Pliocene highly heterogeneous, terrigenous glacial deposits overlie the contourites (14, 15). In the glacial deposits, there is only limited evidence for free gas and no clear geophysical evidence for gas hydrate, such as a bottom simulating reflector. Yet, seismic evidence for gas hydrate occurrence is conclusive for the contourite deposits farther west (16), where gas hydrate has also been sampled at a vent site in ~900-m water depth (17).

Several oceanographic expeditions were able to corroborate the location of the gas flares discovered in 2008. During the MSM21/4 survey in August 2012, we collected a series of PARASOUND 18-kHz parametric echosounder profiles with 40-m spacing around the site of the MASOX (Monitoring Arctic Seafloor–Ocean Exchange) observatory (Fig. 1). An ~40-m footprint of the PARASOUND system at 390-m water depth allowed us to obtain a complete coverage of the flare locations within the area of this survey, which means these data were no longer biased by selection of ship tracks as in previous surveys. Our results show that the gas flares align between

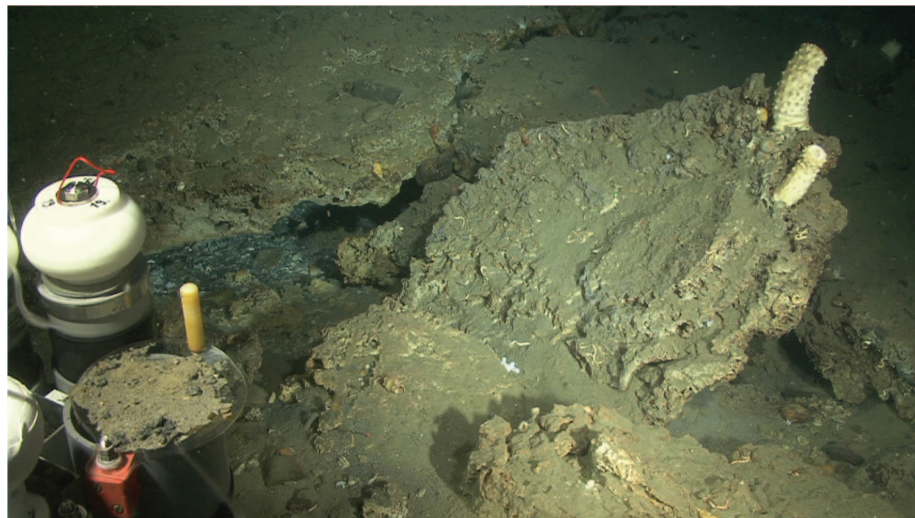


Fig. 2. Photograph of the massive authigenic carbonate crusts observed at the HyBIS site in 385-m water depth. For scale, the total length of the larger white sessile ascidia (white stalklike animal on the crest of the uplifted carbonate plate) is about 15 cm. Carbonate crusts such as these take at least several hundred years to develop through anaerobic oxidation of methane.

380- and 400-m water depths, which corresponds to the upper limit of the gas hydrate stability zone (GHSZ) considering present-day bottom-water temperature of around 3°C (16). Geological structures that may focus gas from deeper parts of the plumbing system are absent (16). Thus, we interpret this match of gas flare origination depth and the calculated landward termination of the gas hydrate stability zone in the sediments as strong circumstantial evidence for a link between gas hydrate dynamics and gas seepage. At the gas flares,

substantial amounts of methane are liberated into the water column, leading to bottom-water CH_4 concentrations of up to 825 nM and a net flux of methane to the atmosphere (18).

One objective of this study was to deduce a minimum age for the onset of marine methane release from the sea floor. For detailed sampling of the gas seeps, we carried out 10 dives with the manned submersible JAGO. Our observations substantiate the presence of more than 5-m-wide and typically more than 20- to 40-cm-thick outcropping

carbonate crusts at the Polarstern (246 m) and the HyBIS (385 m) (Fig. 2) sites; small carbonate nodules at the MASOX site (395 m) were found in gravity cores. We analyzed carbonates from the HyBIS and the MASOX site. The mineralogical composition of the carbonates was heterogeneous and admixed with high amounts of detrital silicates. They were characterized by low $\delta^{13}\text{C}$ isotope values between -27.1 and -41.4 per mil (‰) Vienna pee dee belemnite (V-PDB) (17). Consequently, these carbonates can be regarded as an archive of microbially induced, methane-related authigenic precipitation processes (19). The most reliable single-age data were obtained from aragonite-dominated surface samples. U/Th isotope measurements and resulting minimum seepage age for the MASOX site imply that significant methane-related precipitation was already occurring at 3000 years before the present (yr B.P.) (18). For comparison, the derived ages for the HyBIS site are overlapping or older, for example, sample SV-2 (8200 ± 500 yr B.P.) or sample SV-3 (4600 ± 500 yr B.P.). The youngest isochron-based age of ~ 500 yr B.P. was deduced from carbonates that were found in sediments at the MASOX site at 40- to 50-cm depth below the sea floor. Because of changes in the path of methane-bearing fluids, inclusion of impurities, and alteration of sample material, it was not possible to decipher potential on/off stages or chemical variation of the seeping fluids beyond the results presented in this paper. Hence, it is possible that seepage strength and transport of methane from the sediment to the water column and atmosphere varied over time.

We propose that carbonate formation in this area continues until today, because surface sediments (0- to 10-cm depth below sea floor) at gas vents at both the HyBIS and the MASOX sites were characterized by high rates of anaerobic oxidation of methane (AOM; maximum of $11.3 \mu\text{mol CH}_4 \text{ cm}^{-3} \text{ day}^{-1}$), which is the driver for carbonate precipitation at methane seeps (19). AOM correlated with high concentrations of methane (max $14,800 \text{ nM}$), sulfide (maximum of $11,000 \text{ nM}$), and total alkalinity (maximum of 29 meq l^{-1}) in the sediment. Chemosynthetic communities (sulfur bacteria mats and frenalate tubeworms) were present at both sites (18).

Observations of old carbonate crusts imply that seepage must have been ongoing at all three sites for more than 500 years. Detailed paleoceanographic reconstructions for the Svalbard area (11) show a pronounced warming since the end of the 19th century. However, even this 100-year time span seems too short to explain the observed thicknesses. The ages of the recovered carbonate crusts, which are all significantly older than 100 years, support this conclusion. Thus, it is unlikely that an anthropogenic decadal-scale bottom-water temperature rise is the primary reason for the origin of the observed gas flares, although this temperature rise may contribute to keeping gas pathways open longer and further.

During the cruise, we recovered the MASOX observatory, which had been deployed twice for

a total of 22 months within a cluster of flares between 390- and 400-m water depth. The observatory contained a bottom-water temperature sensor sampling every 15 min during both deployments. The recorded time series revealed fluctuations of bottom-water temperature between 0.6°C and 4.9°C , with lowest temperatures between April and June and highest temperatures between November and March (Fig. 3). In both years, the temperature difference between spring and fall/winter was around 1.5°C , but during the second year the average bottom-water temperature was generally about 0.5° higher than that recorded during the first deployment. The time series implies that there is a strong seasonal change of sea floor temperature.

In order to obtain better constraints on the heat exchange between the sediment and the bottom water, we conducted in situ sediment temperature and thermal conductivity measurements by using a 6-m-long heat flow probe along transects down the slope. Between 500- and 360-m water depths, our measurements revealed a landward increase in thermal conductivity from 1.5 to $2.6 \text{ W m}^{-1} \text{ K}^{-1}$,

with a maximum around the position of the MASOX observatory. High sediment thermal conductivity, large temporal variability in bottom-water temperature, and possibly formation and dissociation of gas hydrates resulted in very irregular sediment temperature profiles, which made it difficult to determine the heat flow along the transect line from our data. On the basis of our measurements at 500-m water depth, we estimate the regional heat flow to be around 0.05 W m^{-2} . Given the comprehensive evidence for seepage, this value is likely modulated by convective heat transport.

On the basis of the recorded bottom-water temperature time series and the acquired thermal conductivity data, we developed a two-dimensional model of the evolution of the GHSZ along the transect line. As illustrated in Fig. 3, the seasonal changes in bottom water temperature are accompanied by large lateral shifts of the GHSZ at least within the top 5 m of surface sediments. During the cycle of a year in which bottom-water temperature varies as observed in 2011 and 2012, the volume of the GHSZ varied between a maximum

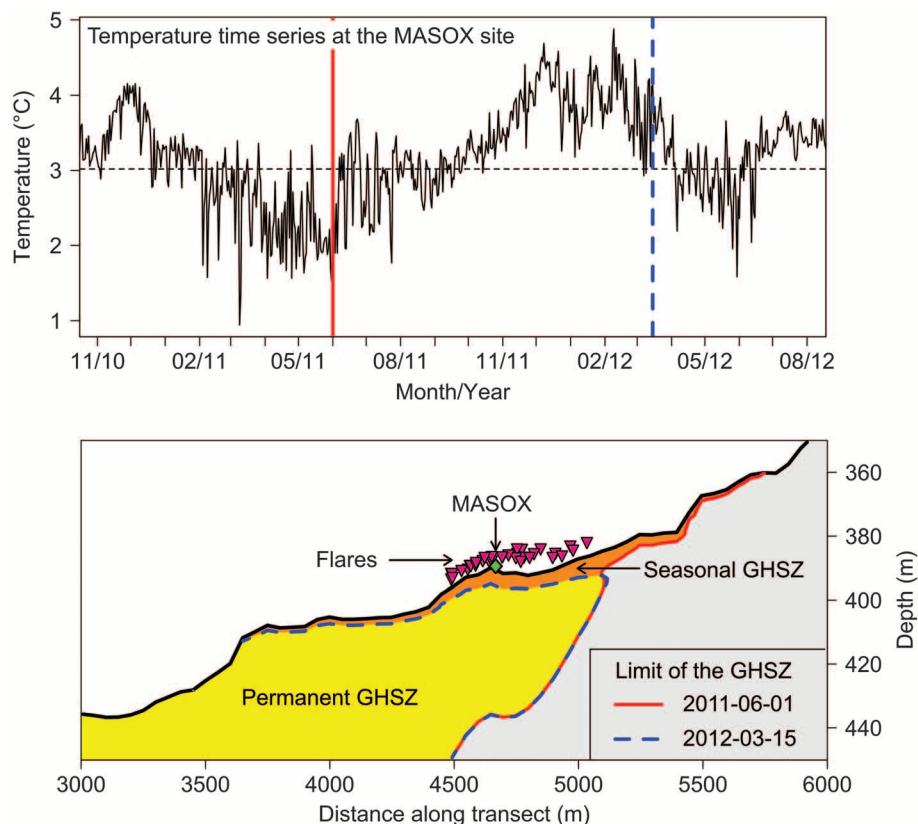


Fig. 3. Temperature and the GHSZ. (Top) Daily means of bottom-water temperature recorded by the MASOX observatory. The times when the extent of the GHSZ was at its maximum and minimum are marked by solid red and dashed blue lines, respectively. **(Bottom)** The seasonal dynamics of the GHSZ. Driven by changes in bottom-water temperature, the GHSZ advances and retreats in the course of the year. The solid red lines and the dashed blue lines indicate maximum and minimum extents of the GHSZ, respectively. The area in which gas hydrates are stable in the long-term is shaded in yellow. The difference between maximum and minimum extents of the hydrate stability zone is shaded in orange and corresponds to the seasonal GHSZ, in which gas hydrate dissociation and formation alternate periodically. The triangles filled in magenta represent the projected locations of all flares detected within 1000 m of the transect line. The green diamond shows the position of the MASOX observatory. An animated illustration of the modeling results is provided in the supplementary materials.

value in summer and a minimum value in winter. During the time period covered by our measurements, the GHSZ was at its maximum in June 2011, when it extended to a 360-m water depth. Increasing bottom-water temperatures from June until December were accompanied by a retreat of the GHSZ at the seafloor to more than 410-m water depth. In the subsurface, the GHSZ retreated further until it reached its minimum in March 2012.

The modeling shows that persistent supply of dissolved methane from below the GHSZ in this section of the slope would lead to the formation of hydrate from winter until summer. The newly formed hydrate would dissociate again during the second half of the year and thus augment methane emissions from the seabed both by opening pathways to gas ascending from underneath and by releasing gas from the hydrate phase. The total volume of sediment that was affected by seasonal shifts of the GHSZ amounted to between 3000 and 5000 m³ per meter of the margin. Assuming a gas hydrate concentration of 5% of the pore space and a porosity of 50%, the seasonal GHSZ has the potential to periodically store and release between 9 and 15 tons of CH₄ per meter of the margin. However, these amounts represent the upper limits of the seasonal buffering capacity, because the latent heat of hydrate kinetics was not included in the simulation. Depending on the concentration and distribution of gas hydrates in the sediment, alternating formation and dissociation would dampen the oscillation of the GHSZ and thus reduce its volume.

Although the modeling shows that seasonal bottom-water temperature variations are capable of modulating the observed gas emissions, we found no direct evidence in the heat flow data that would suggest that the slope sediments experienced decadal-scale warming. The combined data demonstrate that hydrate is playing a fundamental role in modulating gas seeps between 380- and 400-m water depth at the upper limit of the GHSZ, whereas ascending gas would be trapped or deviated up along the base of the GHSZ further seaward. Long-term variations in seepage may exist, but presently available data are insufficient to document annual, decadal, or centennial changes in seepage. Our data suggest that shallow hydrate accumulations are sensitive to bottom-water temperature changes and therefore that significant anthropogenic warming will affect the shallow parts of the hydrate system. This sensitivity demonstrates the need for quantifying the total amount of gas hydrate in the shallowest part of the gas hydrate stability zone if climate feedback mechanisms are to be assessed beyond simple global models (20, 21). Our observations show that methane seepage west off Svalbard has been ongoing for much longer than anthropogenic warming. Therefore, observations of large contemporary emissions reported in other studies cannot be considered proof of accelerating hydrate destabilization, although neither do they prove that catastrophic destabilization is not accelerating.

References and Notes

1. G. K. Westbrook et al., *Mar. Pet. Geol.* **25**, 744–758 (2008).
2. A. Chabert et al., *J. Geophys. Res.* **116**, B12102 (2011).
3. J. M. Carcione, D. Gei, G. Rossi, G. Madrusani, *Geophys. Prospect.* **53**, 803–810 (2005).
4. G. Whiteman, C. Hope, P. Wadhams, *Nature* **499**, 401–403 (2013).
5. E. Post et al., *Science* **325**, 1355–1358 (2009).
6. G. K. Westbrook et al., *Geophys. Res. Lett.* **36**, L15608 (2009).
7. B. Ferré, J. Mienert, T. Feseker, *J. Geophys. Res. Oceans* **117**, C10017 (2012).
8. M. T. Reagan, G. J. Moridis, *Geophys. Res. Lett.* **36**, L23612 (2009).
9. K. E. Thatcher, G. K. Westbrook, S. Sarkar, T. A. Minshall, *J. Geophys. Res. Solid Earth* **118**, 22–38 (2013).
10. G. R. Dickens, *Clim. Past* **7**, 831–846 (2011).
11. R. F. Spielhagen et al., *Science* **331**, 450–453 (2011).
12. O. Eiken, K. Hinz, *Sediment. Geol.* **82**, 15–32 (1993).
13. J. Knies, U. Mann, *Mar. Pet. Geol.* **19**, 811–828 (2002).
14. T. O. Vorren, E. Lebesbye, K. Andreassen, K. B. Larsen, *Mar. Geol.* **85**, 251–272 (1989).
15. A. Solheim, E. S. Andersen, A. Elverhøi, A. Fiedler, *Global Planet. Change* **12**, 135–148 (1996).
16. S. Sarkar et al., *J. Geophys. Res.* **117**, B09102 (2012).
17. R. E. Fisher et al., *Geophys. Res. Lett.* **38**, L21803 (2011).
18. See online supplementary materials.
19. R. Luff, K. Wallmann, G. Aloisi, *Earth Planet. Sci. Lett.* **221**, 337–353 (2004).
20. D. Archer, B. A. Buffett, *Geochim. Geophys. Geosyst.* **6**, Q03002 (2005).
21. A. Biastoch et al., *Geophys. Res. Lett.* **38**, L08602 (2011).
22. P. Wessel, W. H. F. Smith, *EOS* **72**, 441 (1991).
23. A. Rajan, J. Mienert, S. Bünz, *Mar. Pet. Geol.* **32**, 36–49 (2012).

Acknowledgments: This manuscript is dedicated to the memory of our beloved colleague and friend Victoria Bertics. We are grateful to K. Bergmann and the officers and crew of R/V *Maria S. Merian* for their help at sea. The German Research Foundation (DFG), the Swiss National Science Foundation, and the Cluster of Excellence “The Future Ocean” supported the project financially. Further support came from the ESONET project (European Seas Observatory NETWORK), the PERGAMON project (European Cooperation in Science and Technology), and the Alexander von Humboldt Foundation. Figure 1 was drafted by using Generic Mapping Tools (22). Supplementary data are available at <http://dx.doi.org/10.1594/PANGAEA.824947>.

Supplementary Materials

www.sciencemag.org/content/343/6168/284/suppl/DC1
Materials and Methods
Fig. S1 to S4
Tables S1 and S2
Movie S1
References (24–44)

23 September 2013; accepted 16 December 2013
Published online 2 January 2014;
10.1126/science.1246298

Conserved Class of Queen Pheromones Stops Social Insect Workers from Reproducing

Annette Van Oystaeyen,^{1*} Ricardo Calieri Oliveira,^{1*} Luke Holman,^{2*} Jelle S. van Zweden,¹ Carmen Romero,³ Cintia A. Oi,¹ Patrizia d'Ettorre,⁴ Mohammadreza Khalesi,⁵ Johan Billen,¹ Felix Wäckers,⁶ Jocelyn G. Millar,³ Tom Wenseleers^{1†}

A major evolutionary transition to eusociality with reproductive division of labor between queens and workers has arisen independently at least 10 times in the ants, bees, and wasps. Pheromones produced by queens are thought to play a key role in regulating this complex social system, but their evolutionary history remains unknown. Here, we identify the first sterility-inducing queen pheromones in a wasp, bumblebee, and desert ant and synthesize existing data on compounds that characterize female fecundity in 64 species of social insects. Our results show that queen pheromones are strikingly conserved across at least three independent origins of eusociality, with wasps, ants, and some bees all appearing to use nonvolatile, saturated hydrocarbons to advertise fecundity and/or suppress worker reproduction. These results suggest that queen pheromones evolved from conserved signals of solitary ancestors.

Eusocial insects exhibit a remarkable reproductive division of labor between queens and largely sterile workers. Mechanistically, pheromones emitted by the queen are thought to play a key role in suppressing worker reproduction (1). However, for most species, the identity of these pheromones remains unknown. In fact, decades of research have resulted in the successful identification of only a few, structurally unrelated, sterility-inducing queen pheromones in the domestic honeybee, *Lasius* ants, and one termite species (1–5). This paucity of data is unfortunate, because insights into the evolution of queen pheromones could contribute greatly to our understanding of the evolution of sociality.

In the present study, we test whether a structurally related class of queen pheromones might be biologically active across three independently evolved eusocial lineages. We hypothesized that long-chain hydrocarbons, which recently have been found to act as queen pheromones in *Lasius* ants (3, 4) and which are thought to advertise fertility in diverse groups of social insects (6–10), could play such a role. We searched for sterility-inducing queen pheromones in representative species of wasps, bees, and ants—namely, the common wasp, *Vespa vulgaris*; the buff-tailed bumblebee, *Bombus terrestris*; and the desert ant, *Cataglyphis iberica*. Candidate queen pheromones were selected by comparing the cuticular

chemical profiles of queens and workers and ranking the components according to their queen-caste specificity [for details see (11) and table S1]. Subsequently, synthetic samples of several putative queen pheromones were tested for their ability to inhibit worker reproduction in nests from which the mother queen had been removed, after which all workers were dissected and their ovaries classified as undeveloped, developed, or regressed.

¹Laboratory of Socioecology and Social Evolution, Zoological Institute, University of Leuven, Naamsestraat 59—Box 2466, 3000 Leuven, Belgium. ²Division of Ecology, Evolution, and Genetics, Research School of Biology, Australian National University, Canberra, ACT 0200, Australia. ³Departments of Entomology and Chemistry, University of California, Riverside, CA 92521, USA. ⁴Laboratory of Experimental and Comparative Ethology (LEEC), University of Paris 13, Sorbonne Paris Cité, 93430 Villetaneuse, France. ⁵Centre for Food and Microbial Technology, Department of Microbial and Molecular Systems (MS), University of Leuven, Kasteelpark Arenberg 33—Box 2463, 3001 Heverlee, Belgium. ⁶Lancaster Environment Centre, Farrer Avenue, Lancaster, Lancashire LA1 4YQ, UK.

*These authors contributed equally.

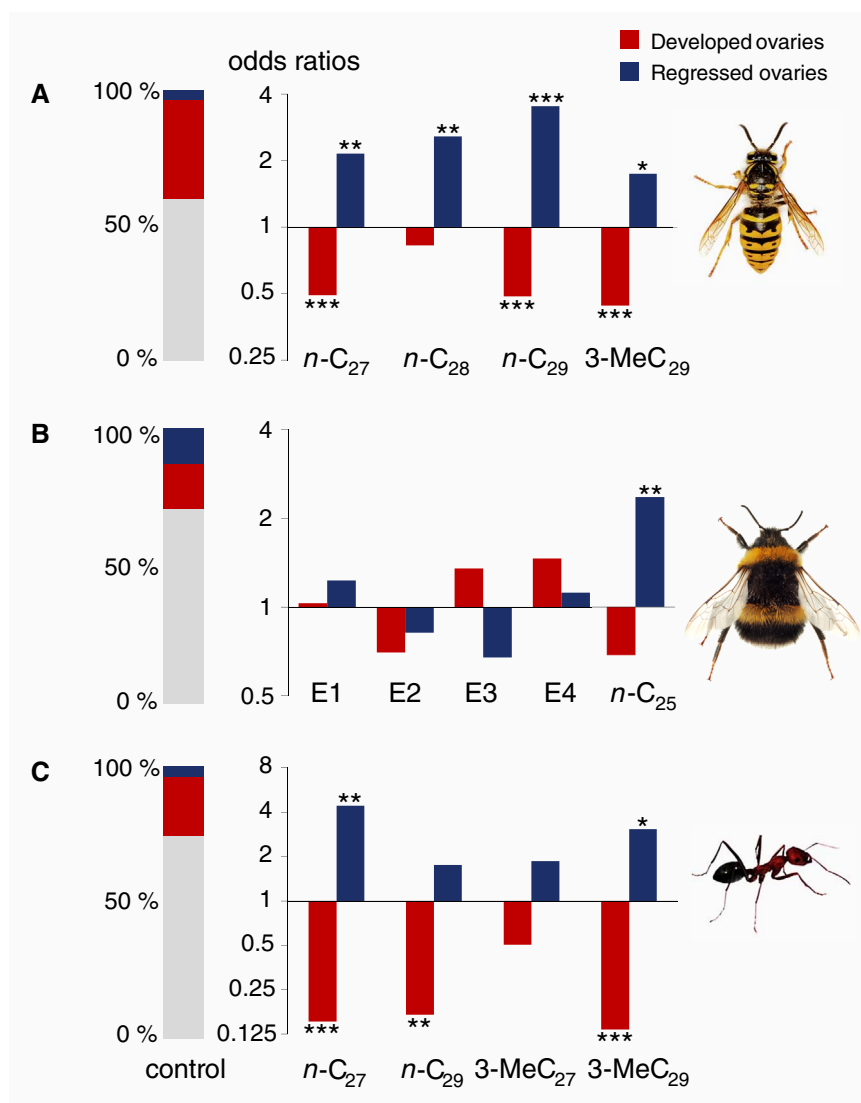
†Corresponding author. E-mail: tom.wenseleers@bio.kuleuven.be (T.W.); annette.vanoystaeyen@bio.kuleuven.be (A.V.O.)

Our results support the hypothesis that, in all three species, long-chain linear and methyl-branched saturated hydrocarbons are used to stop workers from reproducing (Fig. 1 and table S2). This reproductive inhibition occurred via two distinct physiological processes: (i) by preventing workers from activating their ovaries and (ii) by causing secondary oocyte resorption (regression). Live queens have also been shown to induce both of these effects, with queen-induced ovary regression being particularly well documented in bumblebees (table S2). Hence, the application of synthetic pheromones closely mimicked the effect of the presence of a live queen. Three of the same compounds that induced sterility in the common wasp—the linear alkanes $n\text{-C}_{27}$ and $n\text{-C}_{29}$ and the methylalkane 3-MeC₂₉—also did so in the desert ant (Fig. 1). Furthermore, the sterility-inducing queen pheromones of all three species were structural homologs of the previously identified queen pheromone of *Lasius* ants, 3-MeC₃₁ (5, 6), and the fertility signal $n\text{-C}_{25}$ isolated from the ant *Aphaenogaster cockerelli* (8). The linear alkane $n\text{-C}_{25}$ also induced strong ovary

regression in the bumblebee, whereas four queen-specific esters had no effect on worker ovary development (Fig. 1). Thus, saturated hydrocarbons appear to act as a conserved class of queen pheromones in bumblebees, ants, and wasps, even though these taxa derive from separate, ancient origins of eusociality (12). These results do not necessarily imply that there is perfect conservation at the level of individual compounds. For example, the linear alkane $n\text{-C}_{29}$, which was active in both *Vespula* wasps and *Cataglyphis* ants, is most likely not biologically active in bumblebees, given that this compound is not overproduced in *Bombus terrestris* queens. In addition, we cannot exclude the possibility that other, as-yet-unidentified compounds act in synergy with the pheromones identified here.

To further investigate the extent to which sterility-inducing queen pheromones might be conserved at the level of chemical families across distantly related species, we conducted a systematic review of the chemicals that are overproduced by fertile individuals (mainly queens) relative to infertile individuals (workers) (table S3).

Fig. 1. Queen pheromone bioassays. The results demonstrate that long-chain cuticular hydrocarbons act as a conserved class of sterility-inducing queen pheromones in three independently evolved social insect lineages, represented by the wasp *V. vulgaris* (A), the bumblebee *B. terrestris* (B), and the ant *C. iberica* (C). Treatment of queenless worker groups with the linear alkanes $n\text{-C}_{27}$ and $n\text{-C}_{29}$ and the methyl alkane 3-MeC₂₉ caused a two- to sevenfold reduction in the odds of workers having fully developed ovaries in the common wasp and the Iberian ant (bar charts, red bars) relative to a pentane-treated control (left, stacked bar charts) (significance levels based on binomial mixed models: * $P < 0.05$, ** $P < 0.01$, and *** $P < 0.001$; see table S2 for detailed statistics). Furthermore, the probability of workers having regressed ovaries (blue bars) was increased ~two- to four-fold by treating colonies with $n\text{-C}_{27}$, $n\text{-C}_{28}$, $n\text{-C}_{29}$, and 3-MeC₂₉ in the common wasp, $n\text{-C}_{25}$ in the bumblebee, and $n\text{-C}_{27}$ and 3-MeC₂₉ in the Iberian ant. Decreased worker ovary development mimicked the effect of the presence of a live queen, as did the increased worker ovary regression observed in the bumblebee (table S2). By contrast, none of four queen-specific esters tested (E1 to E4: eicosyl, docosyl, tetracosyl, and hexacosyl oleate) significantly influenced worker ovary development in the bumblebee. Colony size and the number of males present were included in the model whenever they had a significant effect (table S2).



Based on data from 90 published studies, we reconstructed the evolutionary history of putative fertility or queen signals across 64 hymenopteran species comprising five independent origins of

eusociality [ants, halictine bees, corbiculate bees, stenogastrine wasps, and polistine and vespine wasps (12)]. This comparative analysis demonstrates that saturated hydrocarbons are the single

most common class of chemicals overproduced by queens or fertile individuals (Fig. 2). In fact, our ancestral state reconstruction shows that saturated hydrocarbons were most likely used as fertility

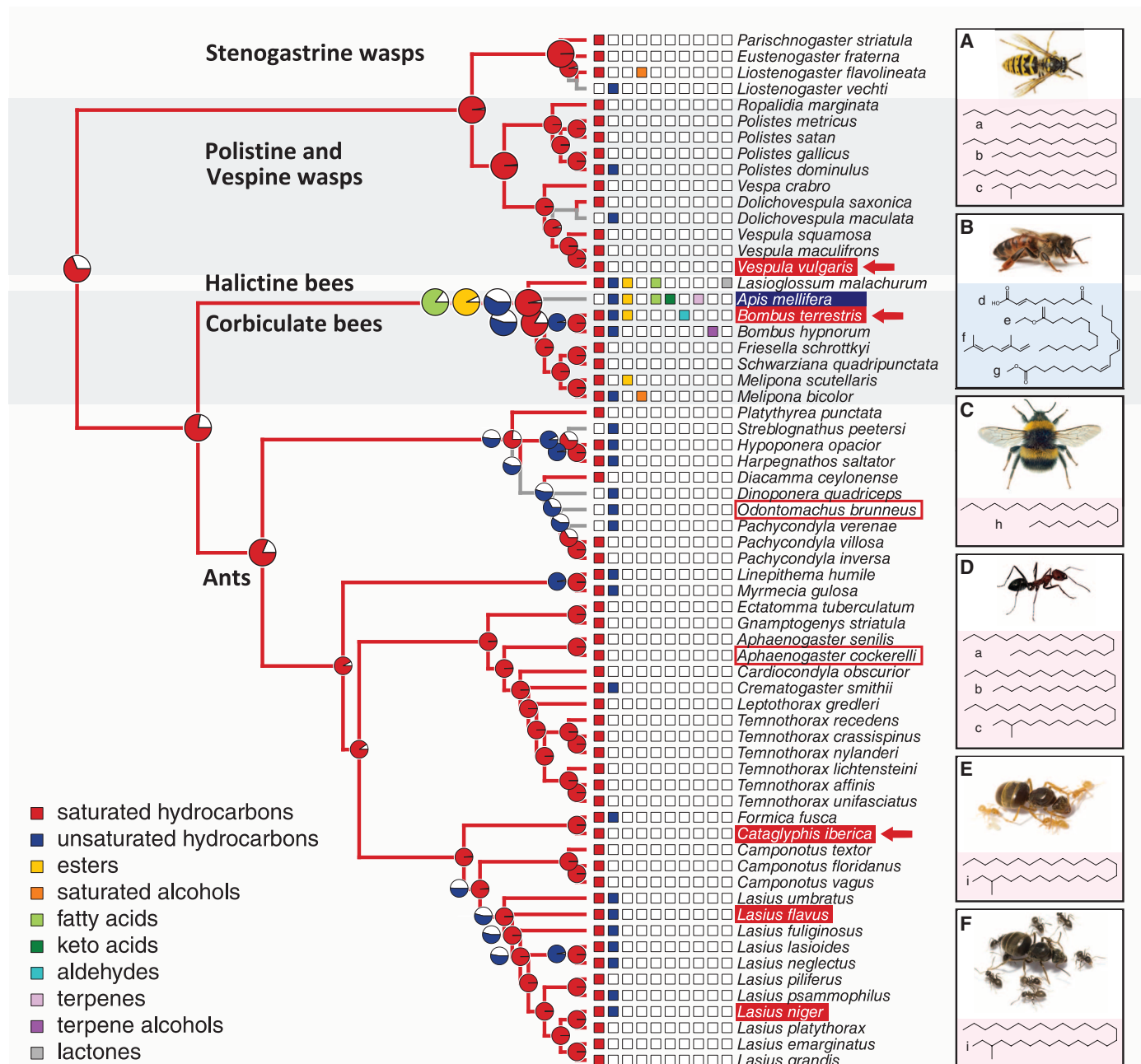


Fig. 2. The evolutionary history of queen and fertility signals across major clades of social hymenopteran insects. Each alternately shaded clade indicates an independent origin of eusociality (12). The pie charts show the likelihoods of different compound classes being used as queen or fertility signals as inferred from a maximum likelihood ancestral state reconstruction under a single-rate evolutionary model. Saturated hydrocarbons (linear and methyl-branched alkanes) receive very high support for being used as conserved queen or fertility signals across several independent origins of eusociality (red pie charts, see likelihood values in table S5; branches with likelihood of >50% are highlighted in red). By contrast, the use of other compound classes, such as the keto acid (E)-9-oxo-2-decenoic acid (2) (dark green) and the esters ethyl palmitate and methyl linoleate (19) in *A. mellifera* honeybees (yellow) or the alkene (Z)-9-nonacosene in

Odontomachus ants (9) (blue), appear to be either derived or highly taxon-specific (pie charts of maximum likelihood reconstructions of particular compound classes are shown when likelihood values are >50%). Data are based either on the overrepresentation of particular compound classes on queens relative to workers or on direct experimental evidence for specific pheromones being used to suppress worker reproduction (solid highlights indicate direct physiological inhibition; open boxes indicate aggression-mediated inhibition) (table S3). Species tested in the present study are marked with arrows. The main active compounds are shown in the insets (A) *V. vulgaris* and (D) *C. iberica*: a = heptacosane, b = nonacosane, c = 3-methylnonacosane. (B) *A. mellifera*: d = (E)-9-oxo-2-decenoic acid, e = ethyl palmitate, f = (E)- β -ocimene, g = methyl linoleate. (C) *B. terrestris*: h = pentacosane. (E) *L. flavus* and (F) *L. niger*: i = 3-methylhentriacontane.

cues in the common solitary ancestor of all ants, bees, and wasps, which lived ~145 million years ago (13). Furthermore, the use of other compound classes as queen pheromones in all cases appears to be derived (Fig. 2). These secondary changes could be explained by minor biochemical alterations in pheromone biosynthesis. For example, up-regulation of desaturases could result in a shift from the use of saturated to unsaturated hydrocarbons (14, 15). In addition, selection for other, more volatile, compound classes could be favored when queen pheromones serve multiple functions. In the honeybee, for example, the more volatile queen pheromone blend not only stops workers from reproducing but also induces long-range mate attraction and worker retinue behavior (16).

In conclusion, the results of our bioassays and comparative analyses demonstrate that structurally related compounds act as queen pheromones across several independent origins of eusociality. This finding implies that social insect queen pheromones likely evolved from preexisting fertility signals directed at males, e.g., in the context of mate choice or mate attraction (14, 15). This theory is supported by the fact that, in both social and solitary insects, specific hydrocarbons are produced as direct or indirect by-products of ovary development and that some of these compounds function as mate attractants in solitary species (14, 15). In the house fly, for example, ovary development re-

sults in the release of 20-hydroxyecdysone, which causes the production of the cuticular hydrocarbon sex pheromone (Z)-9-tricosene (14). Hence, our data provide important new support for the hypothesis that many traits in social insects are derived directly from a preexisting ground plan of solitary ancestors (17, 18).

References

1. Y. Le Conte, A. Hefetz, *Annu. Rev. Entomol.* **53**, 523–542 (2008).
2. S. E. R. Hoover, C. I. Keeling, M. L. Winston, K. N. Slessor, *Naturwissenschaften* **90**, 477–480 (2003).
3. L. Holman, C. G. Jørgensen, J. Nielsen, P. d'Ettorre, *Proc. Biol. Sci.* **277**, 3793–3800 (2010).
4. L. Holman, R. Lanfear, P. d'Ettorre, *J. Evol. Biol.* **26**, 1549–1558 (2013).
5. K. Matsuura et al., *Proc. Natl. Acad. Sci. U.S.A.* **107**, 12963–12968 (2010).
6. A. Endler et al., *Proc. Natl. Acad. Sci. U.S.A.* **101**, 2945–2950 (2004).
7. T. Monnin, *Ann. Zool. Fenn.* **43**, 515–530 (2006).
8. A. A. Smith, B. Hölldobler, J. Liebig, *Curr. Biol.* **19**, 78–81 (2009).
9. A. A. Smith, J. G. Millar, L. M. Hanks, A. V. Suarez, *Behav. Ecol. Sociobiol.* **66**, 1267–1276 (2012).
10. J. Liebig, in *Insect Hydrocarbons: Biology, Biochemistry, and Chemical Ecology*, G. J. Blomquist and A. G. Bagnères, Eds. (Cambridge Univ. Press, Cambridge, 2010), pp. 282–324.
11. Material and methods are available as supplementary material on Science Online.
12. B. J. Fischman, S. H. Woodard, G. E. Robinson, *Proc. Natl. Acad. Sci. U.S.A.* **108** (suppl. 2), 10847–10854 (2011).
13. J. S. Wilson, C. D. von Dohlen, M. L. Forister, J. P. Pitts, *Evol. Biol.* **40**, 101–107 (2013).

14. G. J. Blomquist, R. G. Vogt, *Insect Pheromone Biochemistry and Molecular Biology: The Biosynthesis and Detection of Pheromones and Plant Volatiles* (Elsevier Academic Press, Amsterdam, 2003).
15. G. J. Blomquist, A. G. Bagnères, *Insect Hydrocarbons: Biology, Biochemistry, and Chemical Ecology* (Cambridge Univ. Press, Cambridge, 2010).
16. K. N. Slessor, M. L. Winston, Y. Le Conte, *J. Chem. Ecol.* **31**, 2731–2745 (2005).
17. G. V. Amdam, K. Norberg, M. K. Fondrk, R. E. Page Jr., *Proc. Natl. Acad. Sci. U.S.A.* **101**, 11350–11355 (2004).
18. J. H. Hunt, G. V. Amdam, *Science* **308**, 264–267 (2005).
19. A. Mohammadi, A. Paris, D. Crauser, Y. Le Conte, *Naturwissenschaften* **85**, 455–458 (1998).

Acknowledgments: We thank the Research Foundation Flanders (FWO), KU Leuven Centre of Excellence PF/2010/007 and the Erasmus Mundus Master in Evolutionary Biology (MEME) for funding, X. Cerdá and A. Lenoir for help with collecting the *Cataglyphis* ants, and M. Ayasse and R. Gadagkar for comments. P.d.E. was supported by a European Union Grant (FP7-MC-ERG-2009-256524) and C.A.O. and R.C.O. by scholarships from CNPq-Brazil (201959/2012-7 and 238127/2012-5). We are also grateful to G. Derdelinckx and K. Vestrepen for allowing access to their Shimadzu gas chromatograph–mass spectrometer. Our data are available from the Dryad Repository: <http://dx.doi.org/10.5061/dryad.cg4qp>.

Supplementary Materials

www.sciencemag.org/content/343/6168/287/suppl/DC1
Materials and Methods
Tables S1 to S5
References (20–161)

19 August 2013; accepted 26 November 2013
10.1126/science.1244899

Identification of a Plant Receptor for Extracellular ATP

Jeongmin Choi,^{1,*} Kiwamu Tanaka,^{1*} Yangrong Cao,¹ Yue Qi,² Jing Qiu,² Yan Liang,¹ Sang Yeol Lee,³ Gary Stacey^{1†}

Extracellular adenosine 5'-triphosphate (ATP) is an essential signaling molecule that is perceived in mammals by plasma membrane P2-type purinoceptors. Similar ATP receptors do not exist in plants, although extracellular ATP has been shown to play critical roles in plant growth, development, and stress responses. Here, we identify an ATP-insensitive *Arabidopsis* mutant, *dorn1* (Does not Respond to Nucleotides 1), defective in lectin receptor kinase 1.9 (*Arabidopsis* Information Resource accession code At5g60300). DORN1 binds ATP with high affinity (dissociation constant of 45.7 ± 3.1 nanomolar) and is required for ATP-induced calcium response, mitogen-activated protein kinase activation, and gene expression. Ectopic expression of *DORN1* increased the plant response to physical wounding. We propose that DORN1 is essential for perception of extracellular ATP and likely plays a variety of roles in plant stress resistance.

Adenosine 5'-triphosphate (ATP), the universal energy currency in all organisms, also acts as an extracellular signaling molecule (1). The first report that ATP could play

an extracellular signaling role was viewed with skepticism (2). This skepticism disappeared when the plasma membrane receptors for extracellular ATP were identified in mammals (3, 4). These receptors are of two general types: ligand-gated ion channel P2X and G protein-coupled P2Y receptors (5, 6). The various members of these two receptor classes show distinct ligand binding affinity. Spatial and temporal expression patterns of these receptors support their postulated roles in the regulation of a broad range of mammalian physiology, including neurotransmission, muscle contraction, inflammation, and cell growth and death (5).

In contrast, relatively little is known about the role of ATP as an extracellular signal in plants, and some skepticism exists as to the role this molecule may play in plants. However, a number of papers have suggested a role for extracellular ATP in plant growth (7, 8), development (9, 10), and stress responses (11–13). Furthermore, the presence of extracellular ATP was visualized at actively growing root hair tips (7). ATP is actively released from plant cells in response to abiotic stresses (14), fungal elicitors (7, 15), and mechanical stimuli (16). Some plant cellular responses to ATP are similar to those seen in mammals (17), for example, cytoplasmic calcium increase, production of reactive oxygen species and nitric oxide, and the role of ecto-apyrases that regulate extracellular ATP homeostasis. However, efforts to identify plant ATP receptors through their genomic sequence homology to animal purinoceptors failed to identify any suitable candidate proteins.

To identify genes involved in extracellular ATP recognition in plants, we performed a forward genetic screen for *Arabidopsis thaliana* mutants impaired in their ability to respond to ATP treatment. Exogenously applied ATP triggers cytoplasmic calcium influx in wild-type *Arabidopsis* seedlings expressing the calcium reporter protein, aequorin (18, 19). We screened 50,000 ethylmethanesulfonate (EMS)-mutagenized seedlings for the ATP-induced calcium response (fig. S1) and identified two mutants lacking a cytoplasmic calcium response to ATP addition (Fig. 1A and fig. S2). As described below, these mutants also failed

¹Divisions of Biochemistry and Plant Sciences, Christopher S. Bond Life Sciences Center, University of Missouri, Columbia, MO 65211, USA. ²Department of Statistics, 1341 Middlebush Hall, University of Missouri, Columbia, MO 65211, USA. ³Plant Molecular Biology and Biotechnology Research Center (PMBBRC), Gyeongsang National University, Bd.6-421, Jinjudaero 501, Jinju, Gyeongsangnam-do 660-701, Korea.

*These authors contributed equally to this work.

†Corresponding author. E-mail: staceyg@missouri.edu

to respond to a variety of other nucleotides, except pyrimidine nucleotides, that is, cytosine triphosphate (CTP) (Fig. 2 and fig. S2). The two mutants were found to be allelic (fig. S3), and, therefore, we named them Does not Respond to Nucleotides 1-1 (*dorn1-1*) and *dorn1-2*. Addition of ATP to *dorn1-1* plants failed to trigger phosphorylation of mitogen-activated protein kinase 3 (MPK3) and MPK6 as seen in wild-type plants (Fig. 1B).

To define the transcriptional response to ATP, we performed microarray analysis in wild-type and *dorn1-1* mutant seedlings after the addition of ATP. In wild-type plants, 332 and 242 genes were significantly up- and down-regulated in response to ATP, respectively (Fig. 1C). However, none of these genes responded to ATP in the *dorn1-1* mutant. Quantitative reverse transcriptase–polymerase chain reaction (qRT-PCR) confirmed the ATP-induced gene expression of *WRKY domain transcription factor 40* (*WRKY40*) and *calcium-dependent protein kinase 28* (*CPK28*) in the wild-type but not in the mutant (fig. S4). The Gene-Ontology enrichment test showed that stress-responsive genes and signal transduction-related genes were overrepresented in the list of up-regulated genes, whereas cell-wall organization genes were specifically down-regulated (fig. S5).

We identified the gene responsible for the ATP-insensitive phenotype in the *dorn1* mutants by map-based cloning and whole-genome sequencing. Map-based cloning initially showed genetic linkage to a 615-kb interval at the bottom of chromosome 5 (fig. S6). We compared whole-genome sequences in wild-type, *dorn1-1*, and *dorn1-2* and found independent point mutations in the gene, At5g60300, predicted to encode a lectin receptor kinase-I.9 (*LecRK-I.9*). *LecRK-I.9* consists of an extracellular legume-type lectin domain, a single transmembrane domain, and an intracellular kinase domain (fig. S7). The muta-

tions in *dorn1-1* and *dorn1-2* resulted in the conversion of amino acid Asp⁵⁷² and Asp⁵²⁵ to Asn in subdomain X and in the DxWxxG motif (where D indicates Asp; x, any amino acid; W, Trp; and G, Gly) in subdomain IX, respectively, each of which is important for phosphorylation of the activation loop or stabilization of the catalytic loop of the kinase (20, 21). In vitro kinase assays demonstrated that the kinase domain of *dorn1-1* and *dorn1-2* is completely inactive (fig. S8). The identification of the *LecRK-I.9* gene allowed isolation of a *dorn1* transferred DNA (T-DNA) insertion (*Arabidopsis* Biological Resource Center accession code Salk_042209; *dorn1-3*), which has reduced transcript levels (fig. S9). The phenotype of the *dorn1-3* mutant was identical to that of *dorn1-1* and *dorn1-2* in that the mutant did not show an increase in intracellular calcium concentration or gene induction upon the addition of ATP (Fig. 1A and fig. S10). In addition, ectopic expression of the wild-type version of *LecRK-I.9* in *dorn1-2* plants reinstated normal calcium influx in response to ATP (fig. S11).

If *DORN1* encodes the essential receptor for extracellular ATP, then *dorn1* mutants should not show defects in signaling processes other than the response to ATP. Indeed, the intracellular calcium responses of the *dorn1* mutants to various biotic (flg22, chitin, elf26, and pep1) and abiotic (NaCl, mannitol, and cold water) calcium elicitors were identical to those of wild-type plants (Fig. 2). The T-DNA insertion line, *dorn1-3*, consistently showed a normal response to various calcium elicitors despite some variation observed in EMS mutants, possibly because of the secondary mutations.

Some animal P2Y receptors recognize other nucleotides, for example, adenosine diphosphate (ADP) and uridine triphosphate (UTP), in addition to ATP (5, 6). Therefore, we tested the calcium response of *dorn1* mutants to other nucleotides.

All of the *dorn1* mutant seedlings showed strong defects in the calcium response to ADP and slowly hydrolyzable forms, ATPγS and ADPβS, and also to other purine nucleotides, guanosine triphosphate (GTP) and UTP. In contrast, the response to a pyrimidine nucleotide, CTP, was comparable to the level of wild-type plants (Fig. 2). We also tested the nucleotide-induced calcium responses in the *DORN1* ectopic expression line (*oxDORN1*). These plants showed a much stronger response to most of nucleotides tested, for example, ~20-fold higher response to ATP in comparison to wild type. The relative calcium responses of the *oxDORN1* line showed a rank order of ligand and potency of ATP > GTP > inosine triphosphate (ITP) > thymidine triphosphate (TTP) = UTP > CTP (fig. S12), identical to that of wild-type plants (18). Our observation that the *dorn1* mutants retain sensitivity to CTP (Fig. 2 and fig. S2) is consistent with evidence for an independent recognition system for CTP (18). Collectively, our results suggest that *DORN1* is a key player in the recognition of various nucleotides with a preference for purine nucleotides over pyrimidine nucleotides.

Localization of the *LecRK-I.9* protein to the plasma membrane (22, 23) is consistent with a role in the recognition of an extracellular ligand. Therefore, we measured ATP binding to the extracellular domain of the *DORN1* recombinant protein by using radiolabeled ATP (Fig. 3A). The *DORN1* protein exhibited a typical saturation curve for ATP binding with relatively high affinity [dissociation constant = 45.7 ± 3.1 nM, maximum binding capacity = 488.0 ± 6.3 pmol/mg of protein]. If *DORN1* is the receptor responsible for the plant response to nucleotides, then the protein should also bind to those nucleotides shown to be biologically active with the same relative specificity as the cellular response. We assessed the ability of various unlabeled nucleotides to compete with binding of radiolabeled ATP. The

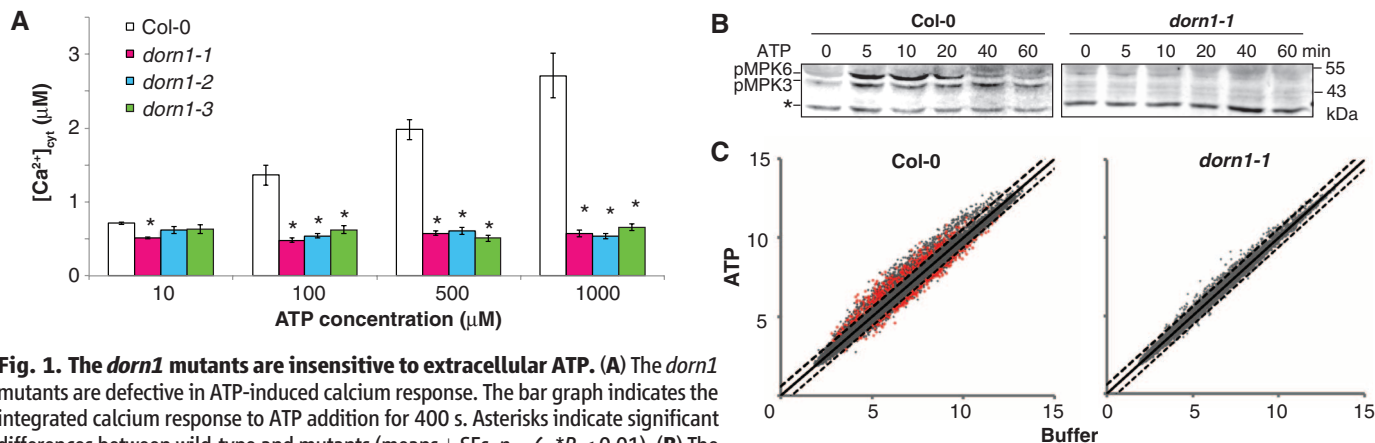


Fig. 1. The *dorn1* mutants are insensitive to extracellular ATP. (A) The *dorn1* mutants are defective in ATP-induced calcium response. The bar graph indicates the integrated calcium response to ATP addition for 400 s. Asterisks indicate significant differences between wild-type and mutants (means \pm SEs, $n = 6$, $*P < 0.01$). (B) The *dorn1-1* mutant did not phosphorylate MPK3 and MPK6 in response to 100 μ M of ATP. Phosphorylation of MPK3 and MPK6 was detected by using antibody against phospho-p44/p42 mitogen-activated protein kinase. The nonspecific band was used (*) as a loading control. (C) Microarray analysis of ATP-induced gene expression in wild-type (Col-0) and the *dorn1-1* mutant plants. Red dots show the genes significantly altered 30 min after treatment with 100 μ M ATP (false discovery rate < 0.05, fold change ≥ 1.5). The data were based on three replicates for each treatment. Normalized probe intensities (log₂ scale) were compared for ATP treatment (y axis) and buffer control (x axis). Black hatched line indicates the same intensity between two treatments, whereas black dash lines indicate 1.5-fold change.

results showed that unlabeled ATP and ADP were the best competitors for binding with radiolabeled ATP, with less competition by ITP, GTP, and UTP and little or no competition by other nucleotides, e.g., CTP and adenosine (Fig. 3B). This ligand specificity reflects the order of magnitude of the

calcium response in the wild-type *Arabidopsis* (18) and the substrate potency seen with the transgenic line ectopically expressing *DORN1* (Fig. 2 and fig. S12). Collectively, our results demonstrate that DORN1 is a nucleotide-binding protein with preferred affinity for ATP. Next, we conducted

an in planta ATP-binding assay using *Arabidopsis* protoplasts (Fig. 3C). The extracellular domain including transmembrane domain of DORN1 was cross-linked with biotinylated 8-azido-ATP and was precipitated by streptavidin beads. Biotinylated 8-azido-ATP cross-linking to DORN1 was

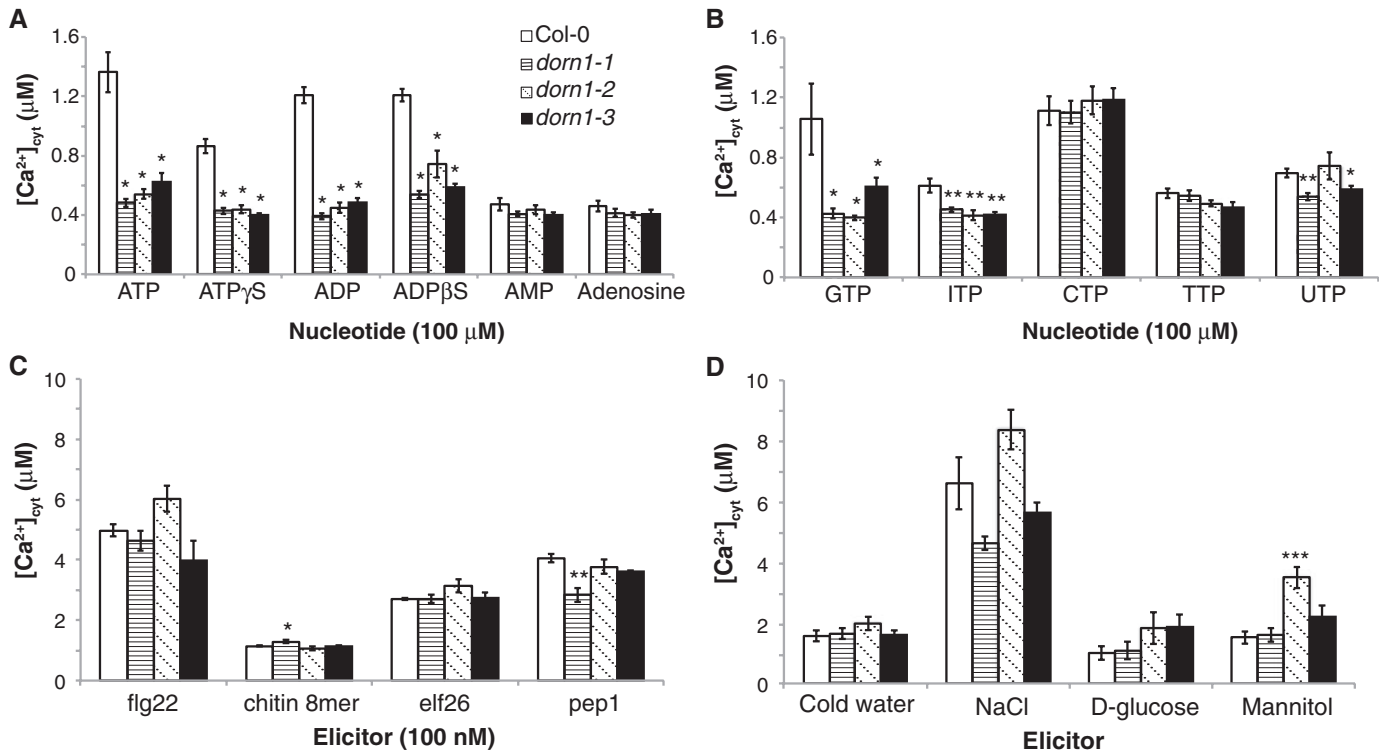
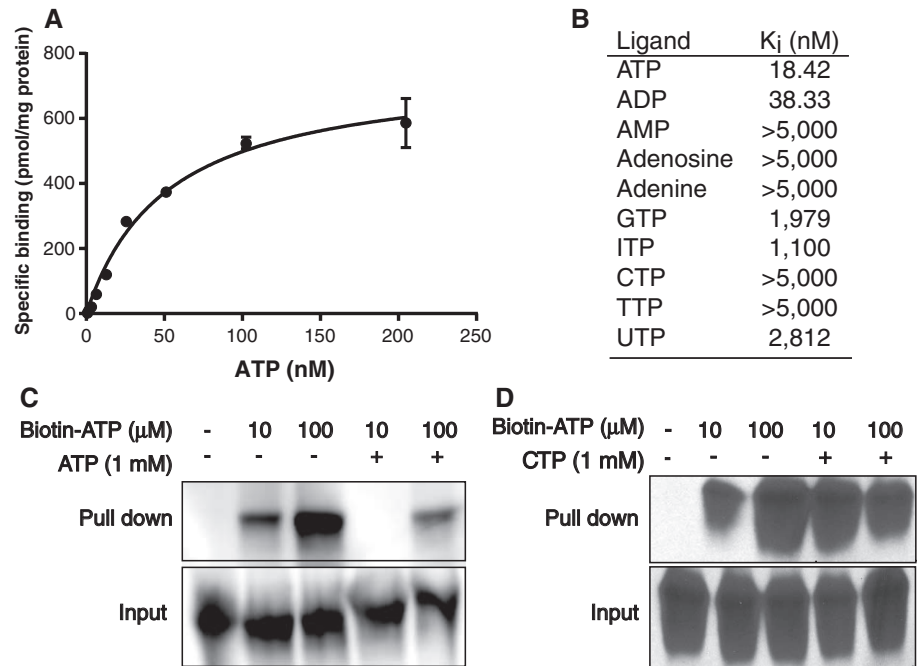


Fig. 2. The *dorn1* mutants show defects in the calcium responses to various nucleotides. (A) Calcium responses to adenine nucleotides and its slowly hydrolyzable derivatives were absent in the *dorn1* mutants. (B) Calcium responses to CTP were normal in the *dorn1* mutants. (C and D) Biotic (C) and

abiotic stress reagents (D, 300 mM NaCl, 4% D-glucose and 300 mM mannitol)–induced calcium responses in the *dorn1* mutants were comparable to those of wild type (Col-0). All data represented as means \pm SEs, $n = 6$ (* $P < 0.05$, ** $P < 0.01$, *** $P < 0.001$).

Fig. 3. DORN1 binds ATP. (A) Saturation binding assay for DORN1. The extracellular domain of DORN1 was incubated with the indicated concentrations of radiolabeled ATP for 30 min. Bound radiolabeled ATP was separated from free ATP by gel filtration chromatography. Data were plotted as a specific binding with SE of three replicates. (B) Competitive binding assay for DORN1. Samples containing 25 nM radiolabeled ATP in the presence of 10 nM to 10 mM of the unlabeled nucleotides were assayed for specific binding of labeled ATP. Inhibition constant (K_i) values were calculated after the data points were fitted by the one-site competition model using GraphPad Prism 5, www.graphpad.com. (C and D) DORN1 binds ATP in planta. Protoplasts expressing hemagglutinin (HA)–tagged extracellular domain of DORN1 with its transmembrane domain were ultraviolet cross-linked with biotinylated 8-azido-ATP followed by precipitation with streptavidin beads. DORN1 was detected with antibody against HA. Unlabeled 1 mM ATP (C) or CTP (D) was used as a competitor.



abolished by competition with unlabeled ATP (Fig. 3C), whereas CTP had no effect (Fig. 3D). Thus, DORN1 binds extracellular ATP at the cell surface.

Lectin domains are typically associated with proteins that bind carbohydrates or oligosaccharides (24). However, the legume-type lectin domain found in DORN1 lacks the conserved Ca^{2+} and Mn^{2+} binding residues that are critical for monosaccharide binding (25). Early studies of legume lectins made note of their ability to bind adenine, a component of ATP (26, 27). However, adenine was not able to compete with ATP for binding to DORN1 (Fig. 3B). Therefore, the exact ATP binding site in DORN1 remains to be determined.

Although ATP can be released from plant cells by vesicle fusion with the plasma membrane

(7, 16), the levels released in this way appear to be quite low, that is, nanomolar levels (16). In contrast, ATP concentrations as high as 40 μM were recorded in the fluid released at sites of physical wounding (13). Therefore, we compared the transcriptional response to ATP (Fig. 1C) to the response to wounding (28). Sixty percent of the ATP-induced genes were also induced by wounding, with 90% of these genes responding very early to wounding (Fig. 4A). For example, out of 332 ATP-induced genes, 112 were up-regulated 15 min after wounding (Fig. 4B). Expression of selected genes after wounding was much higher in the *oxDORN1* plants and notably reduced in the *dorn1-3* plants (Fig. 4C). This is consistent with the gene expression pattern when ATP was applied to these plants (Fig. 4D). The data suggest that ATP is released during physical damage as a

danger signal, which is then recognized by the DORN1 receptor.

Genomic sequence-based surveys for canonical P2X and P2Y receptors in plants failed to detect any likely candidates for an ATP receptor. This is now explained by the fact that the ATP receptor in *Arabidopsis*, DORN1, has a very different molecular structure from the known animal receptors. Given this unique structure, we propose the name P2K (K for kinase) for this previously unknown family of purinoreceptors, with DORN1 (P2K₁) being the founding member. The P2K family is likely to be plant-specific because animals appear to lack lectin receptor kinases (29). On the basis of the phylogenetic occurrence of lectin receptor kinases, P2K receptors may be found in primitive plants (e.g., mosses) through higher plants but not in green algae. Indeed, at least one P2X receptor-like receptor has been identified in green algae (30). Given the variety of roles that extracellular ATP has been shown to play in animal systems, it is likely that further biological functions will also be found for this interesting signal molecule in plants.

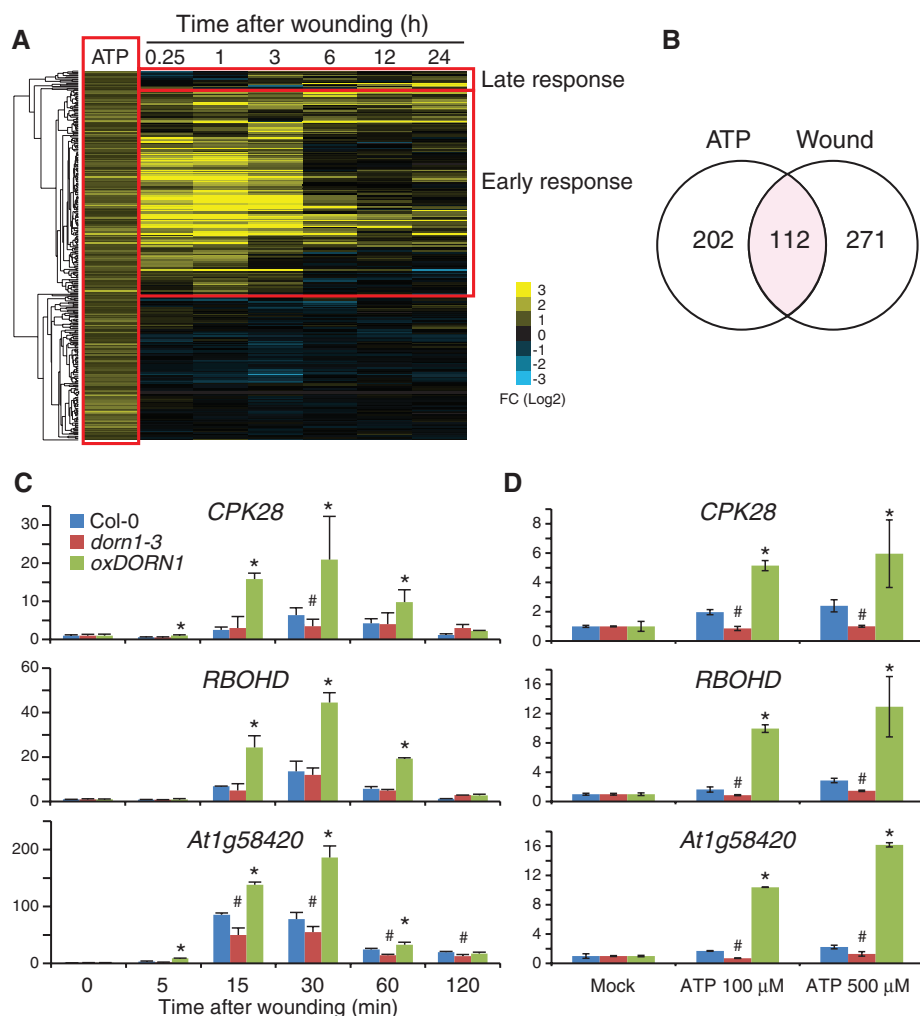


Fig. 4. ATP and wounding induce a common set of genes. (A and B) ATP up-regulated genes (Fig. 1C) were compared with transcriptome data from wounded rosette leaves (28). (A) Hierarchical clustering of ATP-induced genes with genes regulated over a time course after wounding of rosettes. Note that the majority of ATP-induced genes respond early to wounding. FC, fold change. (B) Venn diagram shows the number of ATP up-regulated genes and wound-induced genes (15 min). (C and D) Gene expression of coregulated genes by ATP and wounding in *dorn1* and *oxDORN1* plants. Locally wounded rosettes (C) or ATP-treated whole seedlings (D) were subjected to qRT-PCR analysis. Histograms show means with SEs as values relative to those of untreated controls. Symbols show statistically significant differences ($P < 0.05$) between wildtype (*Col-0*) and *dorn1-3* (#) or *oxDORN1* (*).

References and Notes

1. G. Burnstock, *Pharmacol. Rev.* **24**, 509–581 (1972).
2. G. Burnstock, *Bioessays* **34**, 218–225 (2012).
3. T. E. Webb et al., *FEBS Lett.* **324**, 219–225 (1993).
4. K. D. Lustig, A. K. Shiao, A. J. Brake, D. Julius, *Proc. Natl. Acad. Sci. U.S.A.* **90**, 5113–5117 (1993).
5. V. Ralevic, G. Burnstock, *Pharmacol. Rev.* **50**, 413–492 (1998).
6. M. P. Abbracchio et al., *Pharmacol. Rev.* **58**, 281–341 (2006).
7. S. Y. Kim, M. Sivaguru, G. Stacey, *Plant Physiol.* **142**, 984–992 (2006).
8. R. R. Lew, J. D. W. Dearnaley, *Plant Sci.* **153**, 1–6 (2000).
9. S. A. Reichler et al., *J. Exp. Bot.* **60**, 2129–2138 (2009).
10. I. Steinebrunner, J. Wu, Y. Sun, A. Corbett, S. J. Roux, *Plant Physiol.* **131**, 1638–1647 (2003).
11. S. Chivasa et al., *Plant J.* **60**, 436–448 (2009).
12. C. R. Jeter, W. Tang, E. Henaff, T. Butterfield, S. J. Roux, *Plant Cell* **16**, 2652–2664 (2004).
13. C. J. Song, I. Steinebrunner, X. Wang, S. C. Stout, S. J. Roux, *Plant Physiol.* **140**, 1222–1232 (2006).
14. A. Dark, V. Demidchik, S. L. Richards, S. Shabala, J. M. Davies, *Plant Signal. Behav.* **6**, 1855–1857 (2011).
15. S. J. Wu, Y. S. Liu, J. Y. Wu, *Plant Cell Physiol.* **49**, 617–624 (2008).
16. R. R. Weerasinghe et al., *FEBS Lett.* **583**, 2521–2526 (2009).
17. K. Tanaka, S. Gilroy, A. M. Jones, G. Stacey, *Trends Cell Biol.* **20**, 601–608 (2010).
18. K. Tanaka, S. J. Swanson, S. Gilroy, G. Stacey, *Plant Physiol.* **154**, 705–719 (2010).
19. O. Shimomura, F. H. Johnson, Y. Saiga, *J. Cell. Comp. Physiol.* **59**, 223–239 (1962).
20. P. R. Romano et al., *Mol. Cell. Biol.* **18**, 2282–2297 (1998).
21. P. W. Schenk, B. E. Snaar-Jagalska, *Biochim. Biophys. Acta* **1449**, 1–24 (1999).
22. K. Bouwmeester et al., *PLOS Pathog.* **7**, e1001327 (2011).
23. K. Bouwmeester et al., *Plant Biotechnol. J.* n/a (2013).
24. S. H. Barondes, *Trends Biochem. Sci.* **13**, 480–482 (1988).
25. C. Hervé et al., *Plant Mol. Biol.* **39**, 671–682 (1999).
26. D. D. Roberts, I. J. Goldstein, *J. Biol. Chem.* **258**, 13820–13824 (1983).
27. D. D. Roberts, I. J. Goldstein, *Prog. Clin. Biol. Res.* **138**, 131–141 (1983).
28. J. Kilian et al., *Plant J.* **50**, 347–363 (2007).

29. M. D. Lehti-Shiu, C. Zou, K. Hanada, S. H. Shiu, *Plant Physiol.* **150**, 12–26 (2009).
 30. S. J. Fountain, L. Cao, M. T. Young, R. A. North, *J. Biol. Chem.* **283**, 15122–15126 (2008).

Acknowledgments: We thank M. R. Knight (Durham University) for providing aequorin-expressing transgenic *Arabidopsis*; S. C. Peck and J. C. Anderson (University of Missouri) for technical advice on charge-coupled device camera imaging; G. A. Weisman (University of Missouri) for critical comments on the manuscript; and M. R. Dixon (University of Dallas), A. J. Witte (University of Missouri), and Y. Tanaka (Columbia, MO) for

support during the mutant screening. This work was supported by the Division of Chemical Sciences, Geosciences, and Biosciences, Office of Basic Energy Sciences of the U.S. Department of Energy through grant DE-FG02-08ER15309 and the Next-Generation BioGreen 21 Program Systems and Synthetic Agrobiotech Center, Rural Development Administration, Republic of Korea (grant no. PJ009068) to G.S. The accession number of the microarray discussed in this manuscript is GSE52610 in Gene Expression Omnibus. J.C., K.T., and G.S. are co-inventors on a provisional patent application titled, “Novel extracellular ATP receptor, lectin receptor kinase I.9 and its application to develop plants more stress resistant to bacterial disease and wound

damage.” The authors declare that there are no competing financial interests.

Supplementary Materials

www.sciencemag.org/content/343/6168/290/suppl/DC1
 Materials and Methods
 Figs. S1 to S12
 Table S1
 References (31–42)

30 September 2013; accepted 12 December 2013
 10.1126/science.343.6168.290

Btk29A Promotes Wnt4 Signaling in the Niche to Terminate Germ Cell Proliferation in *Drosophila*

Noriko Hamada-Kawaguchi,¹ Beston F. Nore,^{2,3} Yusuke Kuwada,¹
 C. I. Edvard Smith,² Daisuke Yamamoto^{1*}

Btk29A is the *Drosophila* ortholog of the mammalian Bruton's tyrosine kinase (Btk), mutations of which in humans cause a heritable immunodeficiency disease. Btk29A mutations stabilized the proliferating cystoblast fate, leading to an ovarian tumor. This phenotype was rescued by overexpression of wild-type Btk29A and phenocopied by the interference of Wnt4- β -catenin signaling or its putative downstream nuclear protein Piwi in somatic escort cells. Btk29A and mammalian Btk directly phosphorylated tyrosine residues of β -catenin, leading to the up-regulation of its transcriptional activity. Thus, we identify a transcriptional switch involving the kinase Btk29A/Btk and its phosphorylation target, β -catenin, which functions downstream of Wnt4 in escort cells to terminate *Drosophila* germ cell proliferation through up-regulation of *piwi* expression. This signaling mechanism likely represents a versatile developmental switch.

Stem cell maintenance and differentiation are not entirely autonomic, but instead are under strict control by supporting cells that

form the “niche” (fig. S1A) (1, 2). Recent studies in *Drosophila* have shown that the dynamics of Piwi and its associated piRNAs, a protein-RNA

complex for gene silencing, are required in not only germ cells but also distinct niche-forming somatic cells—escort cells—for germ cell development (3, 4); however, their regulatory mechanisms remain largely unknown. Here we identify a transcriptional switch involving the factor Bruton's tyrosine kinase (Btk) and its phosphorylation target, β -catenin, operating downstream of Wnt4 in escort cells to terminate *Drosophila* germ cell proliferation through modulation of *piwi* expression.

Drosophila Btk29A type 2 is the ortholog of human BTK (fig. S1B) (5). The type 1 isoform is present and the type 2 is absent in *Btk29A^{ficP}* mutants (fig. S1G) (5). Germ stem cells (GSCs) and transit amplifying cystoblasts (CBs) are localized

¹Department of Developmental Biology and Neurosciences, Tohoku University Graduate School of Life Sciences, Sendai 980-8577, Japan. ²Karolinska Institutet, Clinical Research Center, Department of Laboratory Medicine, Karolinska University Hospital Huddinge, SE-141 86 Huddinge, Sweden. ³Department of Biochemistry, School of Medicine, Faculty of Medical Sciences, University of Sulaimani, Post Office Box Sulaimani 438, Kurdistan Region, Iraq.

*Corresponding author. E-mail: daichan@m.tohoku.ac.jp

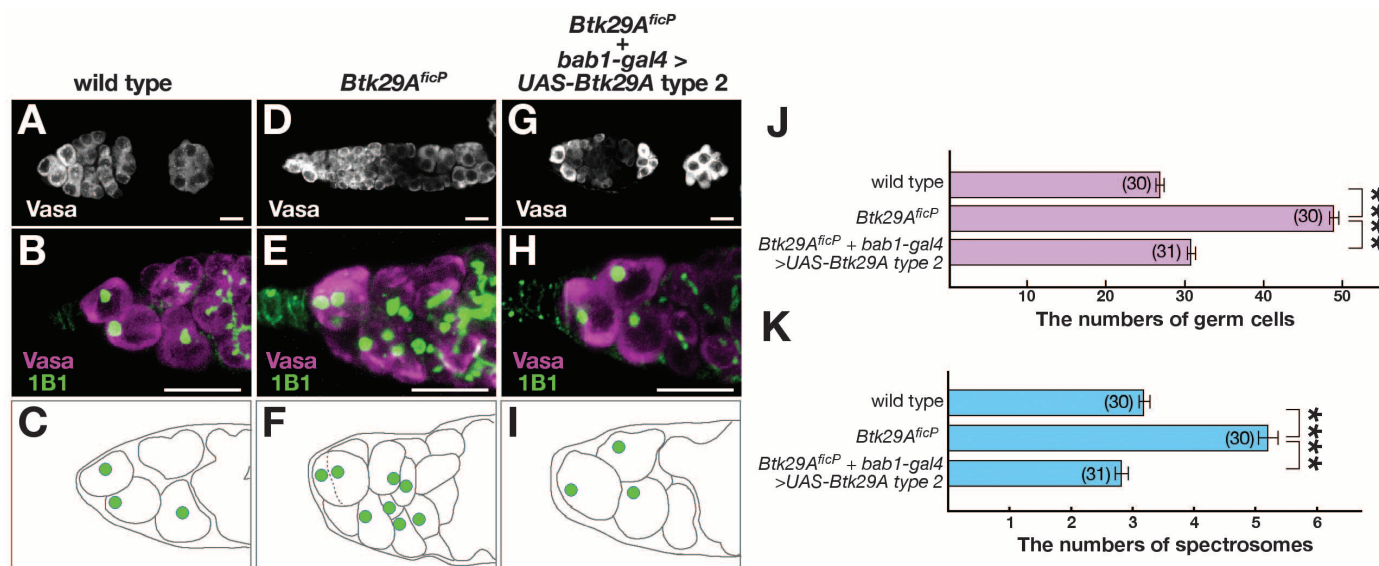


Fig. 1. Deficiency of Btk29A in niche cells impairs germ cell development. (A to I) The germaria of flies of the indicated genotypes doubly stained with anti-Vasa and monoclonal antibody (mAb) 1B1. Cells with spectroosomes observed in (B), (E), and (H) are schematically drawn in (C), (F), and (I). (J and K) The number of germ cells (J) and spectroosomes (K) in the region anterior to region 2 (indicated in fig. S1A, bottom) of the germaria of the indicated fly genotypes. In (J), the number of germ cells

was estimated by counting the number of Vasa-expressing cells present on the single optical section that gave the largest surface area among all horizontal sagittal sections from a germarium. In (K), the numbers of spectroosomes contained in a stack image of a whole germarium are shown. Values are presented as the mean \pm SEM. The number of germaria examined is indicated in parentheses. Statistical differences were evaluated by Student's *t* test (***P* < 0.01).

in the germarium situated at the anterior tip of an ovariole, posteriorly flanked by region 2, in which each CB divides twice and differentiates into cystocytes. The 16 cystocytes originating from a single CB remain interconnected by the fibrous structure fusome, a derivative of the spectrosome. GSCs and CBs both carry the spectrosome, a round, tubulin-enriched structure. The *Btk29A* mutant germarium contains significantly more germ cells than does the wild-type germarium (Fig. 1, A to J, and fig. S1, C to F). Although we observed supernumerary cells with spectrosomes in the *Btk29A^{ficP}* germarium (Fig. 1, A to K), many of the excess cells appear to be cystocytes, as they were accompanied by a branched fusome structure (Fig. 1E). A large excess of cystocytes in grossly deformed ovarioles has been observed in female *Drosophila* that are mutant for *mei-P26* (6), a gene encoding a TRIM-NHL (tripartite motif and Ncl-1, HT2A, and Lin-41 domain) protein that binds to the argonaute protein Ago-1 for microRNA regulation. In *mei-P26* mutants, an ovarian tumor “cystocytoma” is formed because cystocytes regain the ability to self-renew after they enter the differentiation path (6). This suggests that *mei-P26* normally terminates CB proliferation. Intriguingly, the following phenotypes of *mei-P26* were recapitulated in *Btk29A^{ficP}*. First, phospho-histone H3–positive mitotic germline cells, which were restricted to the anterior tip of the wild-type ger-

marium (fig. S1O), were detected throughout the ovarioles (fig. S1P). Second, the expression of Bam, a protein that induces differentiation of GSCs into CBs in the wild type, was markedly increased in CB-like GSC daughters (fig. S1, Q and R). Third, ool18 RNA-binding protein (Orb) remained expressed in multiple cells in a cyst (fig. S1, S and T), contrasting to a wild-type cyst, where Orb expression becomes restricted to an oocyte.

The reduction in *mei-P26* transcription in *Btk29A^{ficP}* (Fig. 2, A and B) places *mei-P26* downstream of *Btk29A*. Notably, *mei-P26* functions cell-autonomously in germ cells (6, 7). However, the almost complete rescue of germ cell defects in *Btk29A^{ficP}* was attained by overexpression of *Btk29A⁺* type 2 via *bab1-Gal4* (Fig. 1, G to K), which showed high levels of expression in terminal filament cells and cap cells (TF and CPC in fig. S1A, respectively) and lower levels of expression in escort cells (EC in fig. S1A). *bab1-Gal4* was effective in inducing germ cell overproduction when used to knockdown *Btk29A* (Fig. 2I and fig. S1, J and K). We also used *hh-Gal4* with expression in the terminal filament cells and cap cells and *c587-Gal4* with expression in escort cells to target *UAS-Btk29ARNai* expression; *c587-Gal4*, but not *hh-Gal4*, led to the overproduction of spectrosome-bearing cells (Fig. 2, C to F and I, and fig. S1, L and M), and therefore, the escort cells were considered as likely sites of *Btk29A* action. These observations

imply that *Btk29A* is required in the escort cells for soma-to-germ signaling to control the switch from proliferation to differentiation in germ cells, where *mei-P26* functions as a core component of the switch (fig. S6).

Bone morphogenetic protein (BMP) signaling and *piwi*-dependent signaling compose two different pathways in the niche to control proliferation and differentiation of GSCs and their daughters (1, 8, 9). BMPs are secreted morphogens, and *Piwi* is an argonaute protein regulating gene expression. The *Btk29A^{ficP}* mutation abrogated *piwi* expression with little effect on *decapentaplegic* (*dpp*) or *glass bottom boat* (*gbb*) expression, two BMPs operating in the germarium (Fig. 2, A and B), and the BMP downstream component Mothers against Dpp (*Mad*) was normally phosphorylated in *Btk29A^{ficP}* GSCs (fig. S1, H and I). Furthermore, somatic *piwi* knockdown mimicked the *Btk29A^{ficP}* ovarian phenotypes (Fig. 2, G to J, and fig. S2, E to J).

Immunohistochemistry revealed that the *Btk29A^{ficP}* mutation or somatic *Btk29A* knockdown abrogated *Piwi* expression in the niche, but not in germ cells (Fig. 2K; see also fig. S1N). This reduction in *Piwi* expression was reversed by the somatic *Btk29A⁺* overexpression (Fig. 2K). Furthermore, the loss-of-function *piwi* allele dominantly enhanced the *Btk29A* mutant phenotype (Fig. 3A and fig. S2, K to T). Moreover, somatic overexpression of *piwi⁺* in *Btk29A^{ficP}* alleviated

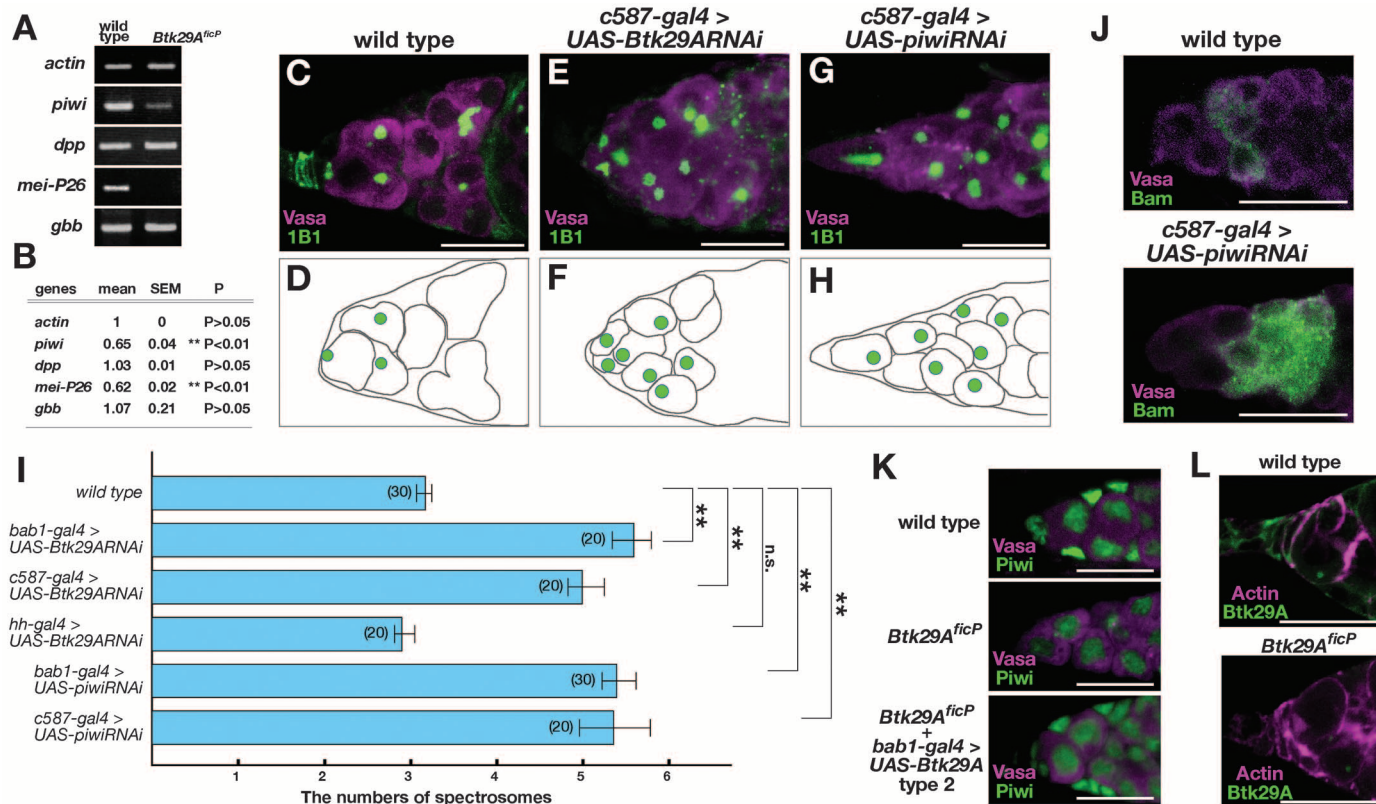


Fig. 2. Effect of somatic knockdown of *Btk29A* or *piwi*. (A and B) Reverse transcriptase–polymerase chain reaction analysis of *piwi*, *dpp*, *mei-P26*, and *gbb*. *actin* served as a control. The number of ovaries used for the analysis was standardized to yield equivalent *actin* signals in both the wild-type flies and mutants. (C to H) Germaria of flies of the indicated genotypes. The flies with

Btk29A type 2 RNAi (RNA interference) carried also a copy of *UAS-Dcr2*. (I) The number of spectrosomes of flies of the indicated genotypes. Values represent mean \pm SEM (** $P < 0.01$, Student's *t* test); ns, not significant. (J) Bam expression in germ cells was increased by somatic knockdown of *piwi*. (K and L) Localization of *Piwi* (K) or *Btk29A* type 2 (L) as revealed by immunostaining. Scale bar: 10 μ m.

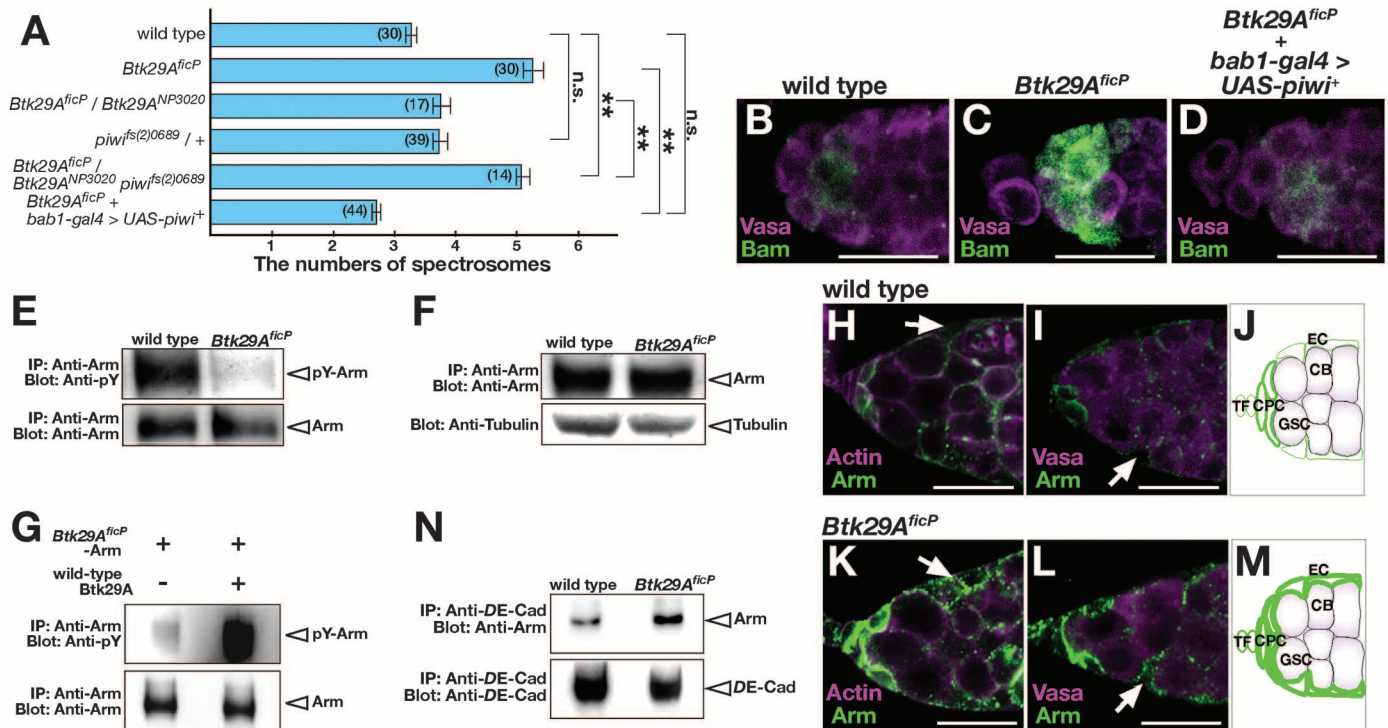


Fig. 3. Genetic interactions between *Btk29A* and *piwi* and tyrosine phosphorylation of Arm by *Btk29A*. (A) The number of spectroscopy units in the indicated fly groups. Values represent mean \pm SEM (** $P < 0.01$, Student's *t* test); ns, not significant. (B to D) Bam protein expression. (E to G, N) Western analysis of the immunoprecipitates of ovarian lysates with antibodies (indicated as IP) was probed with the same or other antibodies (indicated as Blot) (19). β -Tubulin served as a loading control. (G) In vitro phospho-

rylation (19) of Arm immunoprecipitated from *Btk29A^{ficP}*. mAb-Btk29A(COM), which recognizes both the type 1 and type 2 isoforms of Btk29A, was used in immunoprecipitation. (H to M) Anti-Arm staining. Escort cells are indicated by arrows. Scale bar: 10 μ m. [(J) and (M) are schematic drawings of the germarium; TF: terminal filament cell, CPC: cap cell, GSC: germ stem cell, CB: cystoblast, EC: escort cell.] (N) The amount of Arm coimmunoprecipitated with DE-cadherin was greater in *Btk29A^{ficP}* than in the wild type.

the germ cell hypertrophy (fig. S2, U and V) and reduced Bam expression to the normal level (Fig. 3, B to D). We therefore consider that Btk29A regulates the Piwi-dependent pathway in the niche to control germ cell proliferation.

Piwi and piRNAs constitute a major transposon-silencing pathway (10–12). Somatic knockdown of *Btk29A* resulted in an increase in the expression of *gypsy-lacZ* (13) that monitored the activity of the *gypsy* transposon (fig. S3, A and B). Also, transcript levels of the *ZAM*, *DM412*, and *mdg1* transposons were significantly increased in *Btk29A^{ficP}* (fig. S3C). We conclude that the Piwi deficiency due to the impairment of Btk29A results in de-repression of transposon activities.

Genome instability associated with transposon mobilization may lead to the activation of a DNA double-strand break (DSB) checkpoint (14, 15). We found that a mutation in DSB signaling, *mmk*, did not ameliorate the germ cell hypertrophy induced by somatic *Btk29A* knockdown (fig. S3, D to H), indicating that the germ cell hypertrophy by the Btk29A deficiency is not a consequence of the DSB checkpoint activation.

Next, we searched for potential substrates of Btk29A in the niche. Btk29A type 2 was enriched in the interface between cells (Fig. 2L), where *Drosophila melanogaster* epithelial (DE)-cadherin and associated Arm, the β -catenin ortholog, are the major structural components (16). We found no

sign of tyrosine phosphorylation of Arm (fig. S4, F and G), whereas Arm contained a high level of phosphotyrosine (Fig. 3, E and F), which was almost entirely absent from *Btk29A^{ficP}* ovaries (Fig. 3E). However, Arm immunoprecipitated from *Btk29A^{ficP}* was strongly phosphorylated in vitro by the exposure of Arm to active Btk29A protein that had been immunoprecipitated from wild-type ovaries (Fig. 3G). These results demonstrate that Btk29A mediates the tyrosine phosphorylation of Arm in vivo.

The anti-Arm labeling intensity of cell adhesion sites was stronger in *Btk29A^{ficP}* (Fig. 3, K to M) than in the wild type (Fig. 3, H to J). Immunoprecipitation assays revealed that the relative amount of Arm associated with DE-cadherin was greater in *Btk29A^{ficP}* than in the wild type (Fig. 3N), suggesting that the tyrosine phosphorylation of Arm facilitates its release from the membrane to the cytoplasm, as in mammalian cells (17).

Mammalian β -catenin is tyrosine-phosphorylated at residues Y86, Y142, and Y654 (fig. S4A). When transfected into mammalian Cos7 cells, *Drosophila* Btk29A type 2 phosphorylated all these tyrosine residues of β -catenin (fig. S4, B to D). Moreover, the antibodies against phosphorylated Y142 (anti-pY142) and anti-pY654 recognized Arm phosphorylated at the conserved site Y150 and Y667, respectively, in the immunoprecipitates from ovarian lysates (Fig. 4A).

Expression of unphosphorylatable Arm-Y150F in the escort cells via *c587-GAL4* or *bab1-GAL4*, but not *hh-Gal4*, induced germ cell hypertrophy (fig. S5I), whereas another unphosphorylatable mutant, Y667F, or wild-type Arm exerted little effect (Fig. 4, B to E and J, and fig. S5, E to H). In addition, somatic *arm* knockdown resulted in an increase in spectroscopy-containing cells (Fig. 4J and fig. S5, C and D), reduced *piwi* expression in escort cells (Fig. 4F), and increased Bam expression in germ cells (Fig. 4G). Considering these results together, we propose that Btk29A acts on Arm, which in turn regulates *piwi* in the niche.

Arm functions in the canonical Wnt pathway (18). We therefore examined the ovaries of *wg*, *Wnt2*, *Wnt4*, and *Wnt5* mutants; the germ cell overproduction was detected only in *Wnt4* (fig. S5J). Somatic knockdown of *Wnt4* aided by *bab1-GAL4* resulted in a reduction in the expression of Piwi (Fig. 4H), accompanied by an accumulation of germ cells carrying spectroscopy (Fig. 4J and fig. S5, K to Q) with an increase in germline Bam expression (Fig. 4I). These findings support the hypothesis that Arm in the escort cells regulates germ cell proliferation under the control of Wnt4, which was likely derived from somatic cells other than cap cells and terminal filament cells, as *hh-GAL4* selective for these cells was least effective to induce germ cell overproduction when used to drive *Wnt4RNAi* expression (fig. S5, K to Q).

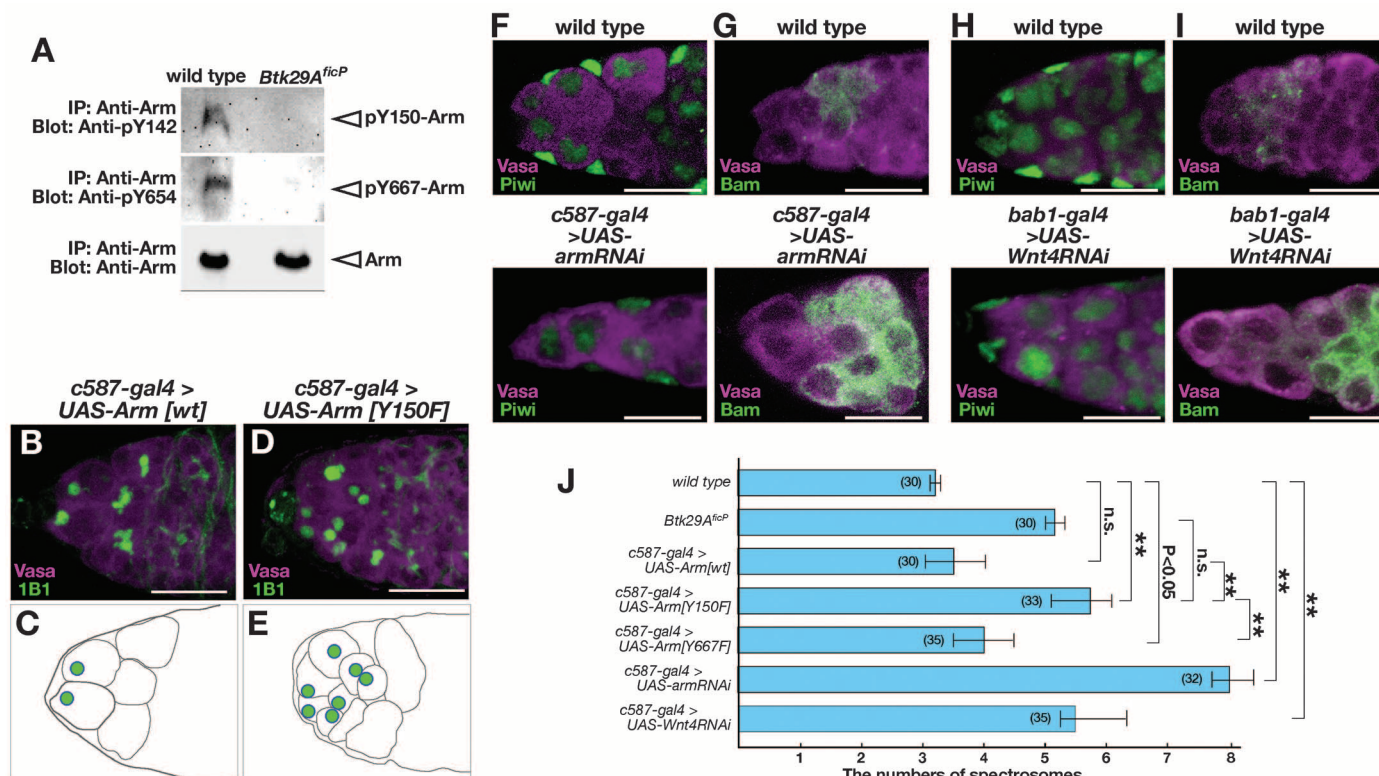


Fig. 4. Btk29A/Btk-dependent tyrosine phosphorylation of Arm/β-catenin. (A) Western blotting of anti-Arm immunoprecipitates of ovarian lysates probed with anti-pY142 or anti-pY654. (B to I) Germaria of flies of the indicated

genotypes. (F to I) Piwi expression (F and H) or Bam expression (G and I) in germaria of flies of the indicated genotypes. (J) The number of spectrosomes. Values represent mean + SEM (***P* < 0.01, Student's *t* test); ns, not significant.

To evaluate the ability of Arm to activate transcription, we used T cell factor (TCF) reporter assays with Cos7 cells transiently transfected with human *Btk* (hBtk) (fig. S3L). The wild-type hBtk alone was sufficient to induce phosphorylation at Y142 and Y654 of β-catenin (fig. S4E), whereas the kinase-dead hBtk (Btk-K430E) was not (fig. S4E). Tyrosine phosphorylation of β-catenin was completely blocked by two antagonists of hBtk (fig. S4E). Similarly, Btk29A type 2 phosphorylated Y142 and Y654 of mammalian β-catenin (fig. S4, B to D). Notably, the TCF reporter activity was six times as high when hBtk was transfected into Cos7 cells (fig. S3L) compared with the mock-transfected control, indicating that hBtk modulates the TCF-dependent transcriptional activation mechanism, in which Arm-β-catenin is involved as a coactivator (18).

We then examined the expression of an *arm*-dependent *Ubx-lacZ* reporter in the embryonic midgut. *Btk29A* knockdown abrogated the expression of this reporter (fig. S3, I to K), demonstrating that Btk29A supports Arm-dependent transcription in vivo.

We showed that Btk29A phosphorylates Arm-β-catenin on conserved tyrosine residues, one of which (Arm-Y150) is pivotal for the niche function to prevent GSC daughters from overproliferating (Fig. 4, D E, and J). Notably, most GSCs in *Btk29A* mutants do not express Bam (fig. S1R). This suggests that the presumptive Btk29A-Arm-Piwi pathway selectively regulates

the proliferation of differentiating GSC daughters without interfering with GSC maintenance. Without Btk29A type 2, cystoblasts fail to exit the cell cycle, leading to the overproduction of germ cells, many of which are unable to complete differentiation and contribute to the genesis of an ovarian tumor. The model to explain how somatic Btk29A controls the switch from proliferation to differentiation in germ cells is shown in fig. S6.

β-Catenin exerts multiple functions through its promiscuous binding abilities in cell-to-cell interactions and transcription (18). This protein plays critical roles in stem cell biology, and β-catenin malfunction results in a variety of cancers (1). Our findings add a new dimension to the study of β-catenin by highlighting the pivotal role of the tyrosine phosphorylation of β-catenin in the control of transcription in the nucleus, in addition to the regulated control of the stability and motility of cell adhesion (17).

References and Notes

1. T. Xie, A. C. Spradling, *Cell* **94**, 251–260 (1998).
2. V. P. Losick, L. X. Morris, D. T. Fox, A. C. Spradling, *Dev. Cell* **21**, 159–171 (2011).
3. P. Rangan et al., *Curr. Biol.* **21**, 1373–1379 (2011).
4. X. Wang et al., *PLOS Genet.* **7**, e1002426 (2011).
5. K. Baba et al., *Mol. Cell. Biol.* **19**, 4405–4413 (1999).
6. R. A. Neumüller et al., *Nature* **454**, 241–245 (2008).
7. Y. Li, J. Z. Maines, O. Y. Tastan, D. M. McKearin, M. Buszczak, *Development* **139**, 1547–1556 (2012).
8. H. Lin, A. C. Spradling, *Development* **124**, 2463–2476 (1997).
9. D. Chen, D. McKearin, *Curr. Biol.* **15**, 179–184 (2005).

10. M. C. Siomi, K. Sato, D. Pezic, A. A. Aravin, *Nat. Rev. Mol. Cell Biol.* **12**, 246–258 (2011).
11. G. Sienski, D. Döntert, J. Brennecke, *Cell* **151**, 964–980 (2012).
12. N. V. Rozhkov, M. Hammell, G. J. Hannon, *Genes Dev.* **27**, 400–412 (2013).
13. E. Sarot, G. Payen-Groschène, A. Bucheton, A. Pélissier, *Genetics* **166**, 1313–1321 (2004).
14. S. Takada, S. Kwak, B. S. Koppetsch, W. E. Theurkauf, *Development* **134**, 1737–1744 (2007).
15. C. Navarro, S. Bullock, R. Lehmann, *Proc. Natl. Acad. Sci. U.S.A.* **106**, 9691–9696 (2009).
16. X. Song, C. H. Zhu, C. Doan, T. Xie, *Science* **296**, 1855–1857 (2002).
17. J. Tominaga, Y. Fukunaga, E. Abelardo, A. Nagafuchi, *Genes Cells* **13**, 67–77 (2008).
18. H. Clevers, R. Nusse, *Cell* **149**, 1192–1205 (2012).
19. B. F. Nore et al., *Eur. J. Immunol.* **30**, 145–154 (2000).

Acknowledgments: We thank M. Asaoka, M. Bienz, J. J. Buggy, D. Drummond-Barbosa, P. Lasko, D. McKearin, K. Mochizuki, A. Nagafuchi, Y. Niki, M. Ote, A. Pélissier, K. Sato, H. Siomi, T. Tabata, Y. Tamori, R. Ueda, T. Uemura, H. White-Cooper, Bloomington Stock Center and Drosophila Genetic Resource Center for reagents, M. Suyama for secretarial assistance, and M. O. Gustafsson for technical help. This work was supported by Grant-in-Aids for Scientific Research (nos. 1802012, 23220007, and 24113502) from the Ministry of Education, Culture, Sports, Science, and Technology (Japan) to D.Y. B.F.N., and C.I.E.S. received support from the Swedish Cancer Society, the Swedish Research Council, and the Stockholm County Council (ALF).

Supplementary Materials

www.sciencemag.org/content/343/6168/294/suppl/DC1
Materials and Methods
Figs. S1 to S6
References (20–25)

9 August 2013; accepted 13 December 2013
10.1126/science.1244512

Changes in rRNA Transcription Influence Proliferation and Cell Fate Within a Stem Cell Lineage

Qiao Zhang, Nevine A. Shalaby, Michael Buszczak*

Ribosome biogenesis drives cell growth and proliferation, but mechanisms that modulate this process within specific lineages remain poorly understood. Here, we identify a *Drosophila* RNA polymerase I (Pol I) regulatory complex composed of Under-developed (Udd), TAF1B, and a TAF1C-like factor. Disruption of *udd* or *TAF1B* results in reduced ovarian germline stem cell (GSC) proliferation. Female GSCs display high levels of ribosomal RNA (rRNA) transcription, and Udd becomes enriched in GSCs relative to their differentiating daughters. Increasing Pol I transcription delays differentiation, whereas reducing rRNA production induces both morphological changes that accompany multicellular cyst formation and specific decreased expression of the bone morphogenetic protein (BMP) pathway component Mad. These findings demonstrate that modulating rRNA synthesis fosters changes in the cell fate, growth, and proliferation of female *Drosophila* GSCs and their daughters.

Lineage-specific stem cell populations help to maintain tissues that experience high rates of cell turnover (1). Self-renewal and differentiation must be finely tuned to replace cells lost under normal physiological conditions and to rapidly compensate for acute cell loss. Although external cues from niches influence stem cell-based homeostasis (2–4), the intrinsic mechanisms that regulate differential growth and proliferation within stem cell lineages remain poorly understood.

We isolated the *Drosophila* recessive mutation *under-developed*¹ (*udd*¹) on the basis of its

sterile phenotype. Staining for the germline markers Vasa and Hts (5, 6) revealed that *udd*¹ mutants exhibit germ cell loss in ovaries and testes (figs. S1 and S2). Noncomplementation tests, reverse transcription–polymerase chain reaction (RT-PCR), and cDNA rescue experiments indicated that *udd*¹ disrupts the expression of a divergent gene *CG18316*, referred to as *udd* hereafter (figs. S1 to S3). *udd*^{null} homozygotes exhibited embryonic lethality, which was rescued by expression of the *udd* open reading frame (fig. S2 and S3). Mosaic analysis revealed that *udd*¹ and *udd*^{null} homozygous clones displayed egg-chamber degeneration similar to that of *udd*¹/*udd*¹ and *udd*¹/*udd*^{null} mutants (fig. S1). Over time, *udd*¹ and *udd*^{null} mutant GSCs became less proliferative and were eventually lost from the cap cell niche (Fig. 1).

Costaining with Modulo (Mod) (7) revealed that Udd protein exhibits ubiquitous expression and localizes to the nucleoli of nondividing cells ($n > 100$ cells) (Fig. 2A and fig. S3). Tandem purification and mass spectrometry (fig. S4), followed by coimmunoprecipitation (Fig. 2B and fig. S4), revealed that Udd associates with two proteins, CG6241 and CG10496. CG6241 shares homology with human TATA box-binding protein-associated factor RNA polymerase I subunit B (TAF1B) and yeast Rm7 (8, 9) (fig. S5), whereas CG10496 resembles human TAF1C on the basis of sequence and secondary-structure analyses (fig. S6). CG6241 and CG10496 will hereafter be referred to as TAF1B and TAF1C-like, respectively. Human TAF1B and TAF1C are components of the selectivity factor 1 (SL1) complex, which promotes RNA polymerase I (Pol I) transcription (10–12). *Drosophila* TAF1B and the TAF1C-like factor localized to nucleoli (Fig. 2, C and D, and fig. S4), and TAF1B was required for the localization and stability of Udd (fig. S7). Udd and TAF1B associated with the Pol I-specific subunit Rpl135 (13) (fig. S4), and knockdown of *TAF1B* in the germ line resulted in phenotypes similar to that of *udd*¹ (fig. S7).

To determine whether the Udd, TAF1B, and TAF1C-like complex promotes ribosomal RNA (rRNA) generation, we performed bromouridine-triphosphate (BrUTP) in situ run-on transcription assays to label nascent rRNA in *udd*^{null} clonal ovaries. BrUTP pulse-labeling revealed colocalization between nascent rRNA and Udd protein in control cells, but little BrUTP incorporation in homozygous *udd*^{null} mutant cells (Fig. 2E and figs. S8 and S9). RNA interference (RNAi) knockdown of TAF1B also reduced the synthesis of rRNA (fig. S7). Northern blot analysis (14) showed that *udd* mutants displayed a reduction in both pre-rRNA and processed rRNA inter-

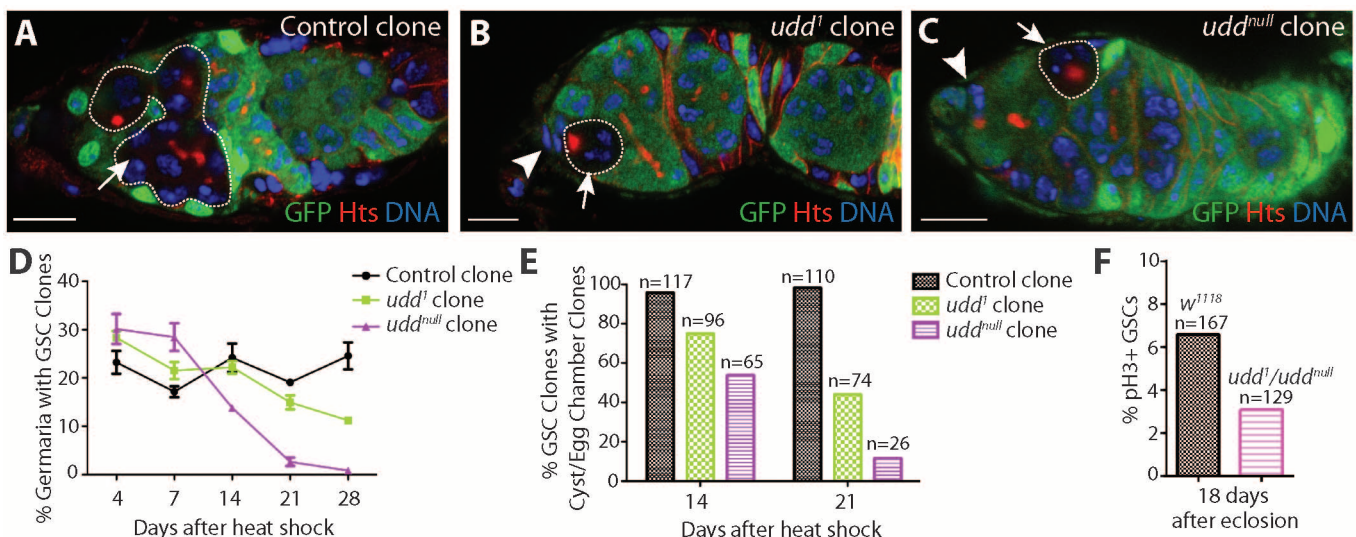


Fig. 1. Disruption of *udd* results in reduced GSC proliferation and loss. Negatively marked (A) control, (B) *udd*¹ and (C) *udd*^{null} clones (white dotted lines) dissected 21 days after clone induction stained for GFP (green), Hts (red), and DNA (blue). Arrowheads mark cap cells. (D)

Percentage of germaria with GSC clones over time. Error bars indicate SD. (E) Percentage of GSC clones that produce a differentiating cyst over time. (F) Percentage of GSCs positive for the mitotic marker phospho-histone H3 (pH3). Scale bars: 10 μ m.

mediates (Fig. 2F and fig. S9). Chromatin immunoprecipitation (ChIP) experiments revealed that Udd associates with the rDNA promoter (Fig. 2G and fig. S9). Together these data indicate that the Udd, TAF1B, and TAF1C-like complex likely functions in a manner analogous to that of the human SL1 complex to promote Pol I transcription (fig. S7). As expected, disruption of Pol I transcription impeded ribosome production based on the nuclear accumulation of green fluorescent protein (GFP)-tagged RpS2 in *udd¹/udd^{null}* mutant cells (fig. S9).

GSCs exhibited higher levels of rRNA synthesis and nucleolar Udd relative to their immediate progeny (Fig. 3A and fig. S10). These differences correlated with the expression of Bam, a key differentiation factor (15–17) (Fig. 3B and fig. S10). Wicked, a component of the rRNA processing U3 small nucleolar ribonucleoprotein (snoRNP) complex, becomes enriched in cytoplasmic particles that asymmetrically segregate to presumptive GSCs during mitosis (18). To determine whether Udd also becomes asymmetrically enriched within GSCs, we performed immunofluorescence analysis of endogenous Udd and time-lapse microscopy using a rescuing GFP-tagged Udd genomic transgene (Fig. 3C, figs. S11 and S12, and movies S1 to S8). Live imaging showed discrete Udd-GFP localization during

prophase. Udd-GFP dispersed during metaphase and anaphase, but a small amount of endogenous Udd remained associated with chromosomes through most of mitosis (fig. S11). At the end of telophase, GFP-tagged and endogenous Udd re-coalesce within the nucleoli of newly formed GSCs more quickly and at higher levels relative to their sibling cells oriented away from the cap cells (Fig. 3C and fig. S11). By contrast, Udd appeared evenly distributed in multicellular cyst nucleoli immediately after mitosis (fig. S12).

Udd and rRNA synthesis did not decrease in *bam^{Δ86}* mutant germ cells (Fig. 3D and fig. S10), suggesting that persistently low levels of Pol I transcription during early cyst differentiation correlate with the developmental state of these cells and not with their position relative to the niche. To further explore this idea, we overexpressed an inducible *bam* transgene in a *bam^{Δ86}* mutant background. Following *bam* expression, the germ cells differentiated into multicellular cysts, and both nucleolar Udd and nascent rRNA production levels decreased (Fig. 3E and fig. S10).

To examine the functional significance of reduced rRNA transcription in early differentiating cells, we crossed the *udd¹* mutation into a *bam^{Δ86}* mutant background. Although *bam^{Δ86}* mutant cells remained as single cells with round fusomes (Fig. 4A and fig. S13), *udd¹ bam^{Δ86}*

double-mutant germaria (94.7%; $n = 94$) contained many four- and eight-cell cysts with branched fusomes and ring canals (Fig. 4B and fig. S13). Mature 16-cell cysts were not observed. RNAi knockdown of *TAF1B* in a *bam^{RNAi}* background also resulted in multicellular cyst formation (fig. S13). Consistent with the idea that reduced translation promotes morphological changes that accompany early germline differentiation, knockdown of an rRNA processing factor, ribosomal proteins, and a translation initiation factor in a *bam* loss-of-function background also resulted in multicellular cyst formation (fig. S13). *udd¹ bam^{Δ86}* double-mutant germ cells maintain nucleolar fibrillar and fail to down-regulate sex-lethal and up-regulate A2bp1 despite forming multicellular cysts (figs. S14 and S15).

The *udd bam* double-mutant phenotype suggested that attenuation of Pol I activity promotes some of the early steps of germ cell differentiation. We speculated that increasing rRNA transcription in stem cell daughters exiting the niche might delay their ability to initiate cyst formation. Overexpression of TIF-IA, a conserved factor that bridges divergent Pol I regulatory factors with the Pol I transcriptional complex, results in greater rRNA transcription (19). Although we could not drive robust TIF-IA expression (fig. S16), low levels of TIF-IA overexpression

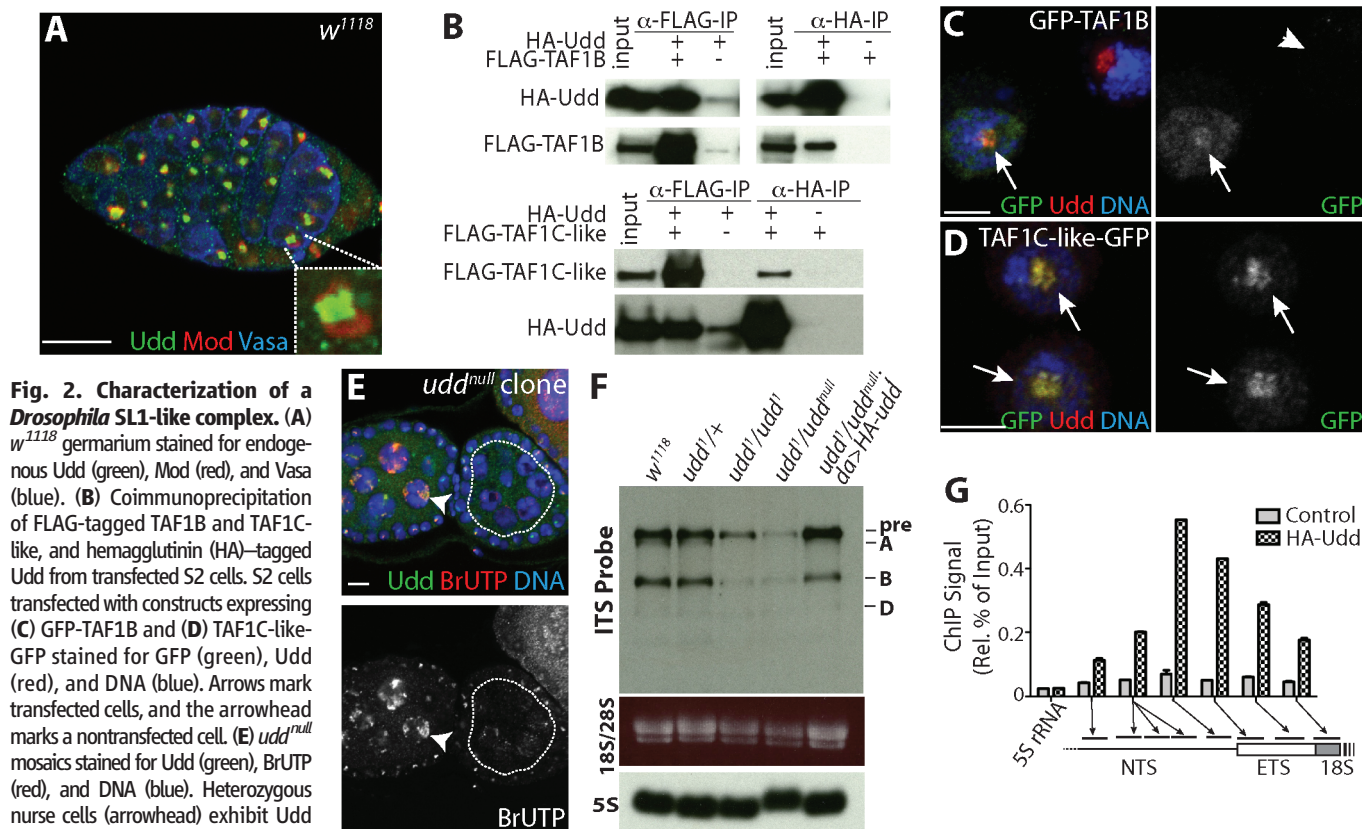


Fig. 2. Characterization of a *Drosophila* SL1-like complex. (A) *w¹¹¹⁸* germarium stained for endogenous Udd (green), Mod (red), and Vasa (blue). (B) Coimmunoprecipitation of FLAG-tagged TAF1B and TAF1C-like, and hemagglutinin (HA)-tagged Udd from transfected S2 cells. S2 cells transfected with constructs expressing (C) GFP-TAF1B and (D) TAF1C-like-GFP stained for GFP (green), Udd (red), and DNA (blue). Arrows mark transfected cells, and the arrowhead marks a nontransfected cell. (E) *udd^{null}* mosaics stained for Udd (green), BrUTP (red), and DNA (blue). Heterozygous nurse cells (arrowhead) exhibit Udd expression and BrUTP incorporation, whereas *udd^{null}* mutant cells (white-dotted line) show little BrUTP labeling. (F) Northern blot of total ovarian RNA isolated from the indicated genotypes probed with a fragment of internal transcribed spacer (ITS). Ethidium bromide-stained mature 28S and 18S rRNA. 5S rRNA was used as a loading control. (G) ChIP–

quantitative PCR analysis of *da>HA-udd* ovaries reveals that Udd associates with specific sites within the rRNA promoter and external transcribed spacer (ETS), as indicated by arrows and bars. Control represents anti-HA immunoprecipitation from the *da-gal4* background. Error bars represent SD. Scale bars: 10 μ m (A and E); 5 μ m (C and D).

resulted in a modest but significant increase in the number of single germ cells with round fusomes within germaria and the percentage of germaria containing over five single undifferentiated cells (Fig. 4, C to E). These cells continued to express *Dad-LacZ*, a hallmark of bone morphogenetic protein (BMP) signal transduction and GSC identity (20) (Fig. 4, F to H). We compared the levels of two downstream components of the

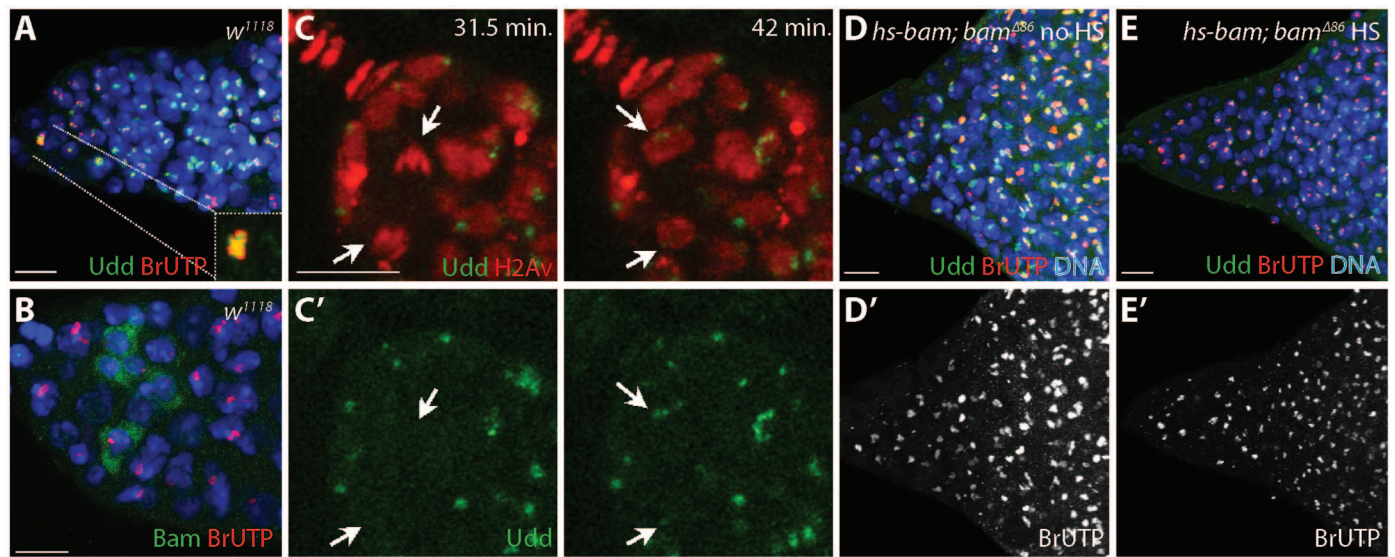


Fig. 3. GSCs and undifferentiated cells maintain high levels of Udd. (A) Control germarium stained for Udd (green), BrUTP (red), and DNA (blue). GSCs (inset) exhibit high levels of BrUTP labeling and Udd. (B) *w¹¹¹⁸* germarium stained for Bam (green), BrUTP (red), and DNA (blue). (C and C') Still images from live-cell imaging (movies S1 and S2) showing GFP-tagged Udd (green) and monomeric red fluorescent protein (mRFP)-tagged histone H2Av (red) in a dividing GSC at the times indicated. Arrows point to the dividing GSC and resulting daughters. (D) No heat-shock (no HS) control *hs-bam; bam^{Δ86}* mutant germarium and (E) heat-shocked (HS) *hs-bam; bam^{Δ86}* mutant germarium 36 hours after *bam* induction stained for Udd (green), BrUTP (red) and DNA (blue). (D' and E') BrUTP labeling alone. Scale bars: 10 μm.

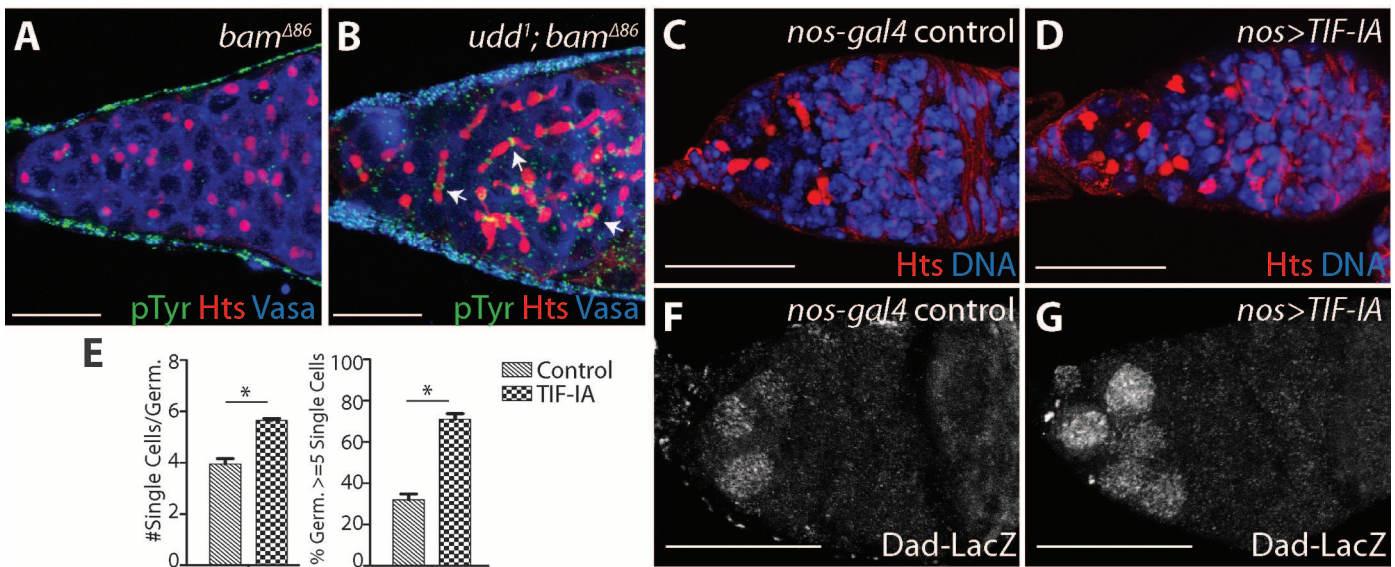


Fig. 4. Modulating rRNA synthesis influences cyst development and BMP signaling in the germ line. (A) *bam^{Δ86}* and (B) *udd1; bam^{Δ86}* double-mutant germaria stained for phosphotyrosine (pTyr) (green), Hts (red), and DNA (blue). Arrows point to cysts with branched fusomes. (C) *nos-gal4* and (D) *nos>Tif-IA* stained for Hts (red) and DNA (blue). (E) Quantification of the number of single cells with round fusomes per germarium (germ) upon *Tif-IA* overexpression. (F) *nos-gal4* and (G) *nos>TIF-IA* stained for *Dad-LacZ*. (H) Quantification of *Dad-LacZ*-positive cells upon *Tif-IA* overexpression. (I) Western blots of *bam^{Δ86}* and *udd1; bam^{Δ86}* ovarian extracts probed for Mad, Medea, and histone H2B proteins. (C to H) Two copies of *nos-gal4* were present. (E and H) Error bars represent SEM. Scale bars: 20 μm. **P* < 0.0001.

BMP pathway, Mad and Medea (21), in *bam*^{Δ86} and *udd¹ bam*^{Δ86} double mutants. Disruption of *udd* resulted in reduced levels of Mad but not Medea or histone H2B, indicating that modulation of rRNA transcription affects the expression of specific proteins that regulate cell-fate decisions within the GSC lineage (Fig. 4I and fig. S16). Down-regulation of Mad in response to reduced rRNA transcription likely acts in concert with other mechanisms that extinguish BMP signaling in GSC daughters displaced away from the stem cell niche (22, 23).

Besides TIF-1A and dMyc (19, 24), few regulators of *Drosophila* Pol I have been characterized. The identification of a *Drosophila* SL1-like complex provides insights into the mechanisms that regulate rRNA transcription in a developmental context (fig. S16D). Seminal work has shown that specific cellular structures asymmetrically segregate during stem cell divisions in *Drosophila* and mice (18, 25–27). Results presented here indicate that rRNA transcriptional machinery also partitions unevenly during certain cell divisions. These data reveal that distinct levels of ribosome biogenesis, once considered a generally constitutive process, modulate the expression of specific proteins that direct cell fate decisions, growth, and proliferation within an in vivo stem cell lineage more rapidly or to a greater extent than others. Notably, the direction of asymmetric en-

richment of ribosome biogenesis factors may be reversed in other lineages, especially in those stem cells destined to enter a quiescent state. These findings may have important implications for human ribosome-related diseases (28, 29).

References and Notes

1. A. Spradling, D. Drummond-Barbosa, T. Kai, *Nature* **414**, 98–104 (2001).
2. S. J. Morrison, A. C. Spradling, *Cell* **132**, 598–611 (2008).
3. M. de Cuevas, E. L. Matunis, *Development* **138**, 2861–2869 (2011).
4. D. Kirilly, T. Xie, *Cell Res.* **17**, 15–25 (2007).
5. H. Lin, L. Yue, A. C. Spradling, *Development* **120**, 947–956 (1994).
6. M. de Cuevas, A. C. Spradling, *Development* **125**, 2781–2789 (1998).
7. L. Perrin *et al.*, *J. Cell Sci.* **111**, 2753–2761 (1998).
8. B. A. Knutson, S. Hahn, *Science* **333**, 1637–1640 (2011).
9. S. Naidu, J. K. Friedrich, J. Russell, J. C. Zomerdijs, *Science* **333**, 1640–1642 (2011).
10. J. C. Zomerdijs, H. Beckmann, L. Comai, R. Tjian, *Science* **266**, 2015–2018 (1994).
11. L. Comai *et al.*, *Science* **266**, 1966–1972 (1994).
12. L. Comai, N. Tanese, R. Tjian, *Cell* **68**, 965–976 (1992).
13. W. Seifarth *et al.*, *Mol. Gen. Genet.* **228**, 424–432 (1991).
14. E. Giordano, I. Peluso, S. Senger, M. Furia, *J. Cell Biol.* **144**, 1123–1133 (1999).
15. B. Ohlstein, D. McKearin, *Development* **124**, 3651–3662 (1997).
16. D. M. McKearin, A. C. Spradling, *Genes Dev.* **4**, 2242–2251 (1990).
17. D. McKearin, B. Ohlstein, *Development* **121**, 2937–2947 (1995).
18. P. Fichelson *et al.*, *Nat. Cell Biol.* **11**, 685–693 (2009).
19. S. S. Grewal, J. R. Evans, B. A. Edgar, *J. Cell Biol.* **179**, 1105–1113 (2007).
20. X. Song *et al.*, *Development* **131**, 1353–1364 (2004).
21. D. J. Sutherland, M. Li, X. Q. Liu, R. Stefancsik, L. A. Rafferty, *Development* **130**, 5705–5716 (2003).
22. R. E. Harris, M. Pargett, C. Sutcliffe, D. Umulis, H. L. Ashe, *Dev. Cell* **20**, 72–83 (2011).
23. L. Xia *et al.*, *Cell* **143**, 978–990 (2010).
24. S. S. Grewal, L. Li, A. Orian, R. N. Eisenman, B. A. Edgar, *Nat. Cell Biol.* **7**, 295–302 (2005).
25. J. Cheng *et al.*, *Nature* **456**, 599–604 (2008).
26. Y. M. Yamashita, A. P. Mahowald, J. R. Perlman, M. T. Fuller, *Science* **315**, 518–521 (2007).
27. X. Wang *et al.*, *Nature* **461**, 947–955 (2009).
28. K. M. Hannan, E. Sanij, L. I. Rothblum, R. D. Hannan, R. B. Pearson, *Biochim. Biophys. Acta* **1829**, 342–360 (2013).
29. J. M. Liu, S. R. Ellis, *Blood* **107**, 4583–4588 (2006).

Acknowledgments: We thank L. Rafferty, Z. Chen, A. Spradling, J. Pradel, N. Perrimon, the Bloomington Stock Center, and the Iowa Developmental Studies Hybridoma Bank for providing reagents. J. Huynh and P. R. Hiesinger provided imaging advice. N. Conrad, J. Jiang, and P. R. Hiesinger provided comments. Supported by NIH (R01GM086647 and R01GM045820) and E.E. and Greer Garson Fogelson Endowment (University of Texas Southwestern Medical Center).

Supplementary Materials

www.sciencemag.org/content/343/6168/298/suppl/DC1
Materials and Methods
Figs. S1 to S16
References (30–41)
Movies S1 to S8

24 September 2013; accepted 11 December 2013
10.1126/science.1246384

Lenalidomide Causes Selective Degradation of IKZF1 and IKZF3 in Multiple Myeloma Cells

Jan Krönke,¹ Namrata D. Udeshi,² Anupama Narla,¹ Peter Grauman,¹ Slater N. Hurst,¹ Marie McConkey,¹ Tanya Svinkina,² Dirk Heckl,¹ Eamon Comer,² Xiaoyu Li,² Christie Ciarlo,² Emily Hartman,² Nikhil Munshi,³ Monica Schenone,² Stuart L. Schreiber,² Steven A. Carr,² Benjamin L. Ebert^{1,2*}

Lenalidomide is a drug with clinical efficacy in multiple myeloma and other B cell neoplasms, but its mechanism of action is unknown. Using quantitative proteomics, we found that lenalidomide causes selective ubiquitination and degradation of two lymphoid transcription factors, IKZF1 and IKZF3, by the CRBN-CRL4 ubiquitin ligase. IKZF1 and IKZF3 are essential transcription factors in multiple myeloma. A single amino acid substitution of IKZF3 conferred resistance to lenalidomide-induced degradation and rescued lenalidomide-induced inhibition of cell growth. Similarly, we found that lenalidomide-induced interleukin-2 production in T cells is due to depletion of IKZF1 and IKZF3. These findings reveal a previously unknown mechanism of action for a therapeutic agent: alteration of the activity of an E3 ubiquitin ligase, leading to selective degradation of specific targets.

Lenalidomide is a highly effective drug for the treatment of multiple myeloma (1) and has activity in other B cell lymphomas. In addition, lenalidomide and its analogs thalidomide

and pomalidomide have multiple additional biological effects, including teratogenicity, stimulation of interleukin-2 (IL-2) production by T cells (2), and inhibition of tumor necrosis factor production by monocytes (3), but the molecular basis of these pleiotropic activities is unknown.

Using an immobilized derivative of lenalidomide in combination with SILAC (stable isotope labeling of amino acids in cell culture)-based quan-

titative mass spectrometry (MS), we found that lenalidomide binds DDB1 and CRBN that, together with CUL4 and ROC1, form an E3 ubiquitin ligase (CRBN-CRL4) (fig. S1). The same target has recently been reported to bind thalidomide and has been implicated in the teratogenic effects of thalidomide (4). The finding that CRBN-DDB1 binds both lenalidomide and thalidomide in independent proteomic studies provides powerful evidence that this ubiquitin ligase complex is a major direct protein-binding partner for this class of molecules.

We hypothesized that the pleiotropic effects of lenalidomide might be caused by altered ubiquitination of target proteins. Specificity of the CRL4 ubiquitin ligase is mediated by an interchangeable substrate receptor, but no targets have been identified for CRBN, a putative substrate receptor (4–6). To characterize lenalidomide-induced modulation of CRBN-CRL4 ubiquitin ligase activity, we used SILAC-based quantitative MS studies to characterize changes in the ubiquitinome and proteome in the MM1S multiple myeloma cell line. Ubiquitination profiling was completed through the enrichment of formerly ubiquitinated peptides with an antibody to K-e-GG (Fig. 1A) (7, 8). Two proteins, Ikaros (IKZF1) and Aiolos (IKZF3), scored at the top of the lists of proteins regulated by lenalidomide at both the protein and ubiquitin-site level (Fig. 1, B and C). Lenalidomide decreased the abundance of IKZF3 (log₂ ratio –2.09) and IKZF1 (log₂ ratio –1.54). Whereas increased ubiquitination would be expected to be associated with decreased protein abundance,

¹Brigham and Women's Hospital, Boston, MA 02115, USA.

²Broad Institute of MIT and Harvard, Cambridge, MA 02142, USA. ³Dana-Farber Cancer Institute, Boston, MA 02115, USA.

*Corresponding author. E-mail: bebert@partners.org

we observed a decrease in ubiquitination of multiple lysine residues of IKZF1 and IKZF3 after treating cells with lenalidomide for 12 hours before addition of the proteasome inhibitor MG132. A likely interpretation of these results is that IKZF1 and IKZF3 are rapidly ubiquitinated, targeting them for degradation and resulting in a decrease in abundance of both ubiquitinated and absolute levels of these proteins. IKZF1 and IKZF3 also scored at the top of the list of thalidomide-regulated proteins, which is consistent with the similar biological activity of the molecules (fig. S2).

In parallel, we examined the landscape of lenalidomide-dependent CRBN protein interactions (fig. S3). We found that binding of IKZF1 and IKZF3 to the putative CRBN substrate receptor that was enhanced in the presence of lenalidomide (Fig. 1D and fig. S3). As expected, we pulled down all of the members of the CRBN-CRL4 ubiquitin ligase and proteins known to interact with DDB1, including subunits 1 to 8 of the COP9 signalosome complex, in both, untreated, or lenalidomide-treated cells. No other known substrate receptors for DDB1 were coimmunoprecipitated, indicating that CRBN is a substrate receptor and precludes binding of alternative receptors to DDB1. In aggregate, the proteomic data suggest that lenalidomide increases the binding of IKZF1 and IKZF3 to the CRBN-DDB1 ubiquitin ligase complex, leading to increased ubiquitination and consequent degradation.

To validate this putative mechanism, we analyzed whether lenalidomide causes posttranscriptional regulation of IKZF1 and IKZF3 protein abundance. The cDNAs of candidate genes, fused to firefly luciferase (FFluc), were expressed in 293T cells (9). IKZF1 and IKZF3 conferred a lenalidomide-regulated decrease in luciferase activity. In contrast, luciferase levels were not altered after lenalidomide treatment when FFluc was fused to RAB28, a protein that decreased in abundance after lenalidomide treatment but did not bind to CRBN. Similarly, lenalidomide did not alter the abundance of FFluc fused to three other transcription factors of the Ikaros family, Helios (IKZF2), Eos (IKZF4), and Pegasus (IKZF5); IRF4, a protein implicated in lenalidomide activity (10); or the transcription factors HOXA9 and Myc (Fig. 2A). We confirmed that in MM1S cells stably expressing hemagglutinin (HA)-IKZF1 or HA-IKZF3, lenalidomide caused a dose-dependent reduction of both proteins (fig. S5). Taken together, these results demonstrate the selective regulation of IKZF1 and IKZF3 levels in response to lenalidomide.

We next examined endogenous protein expression in response to lenalidomide. Lenalidomide strongly decreased the abundance of IKZF1 and IKZF3 in a dose-dependent manner in cell lines (Fig. 2B and fig. S4A) as well as in primary multiple myeloma samples (Fig. 2E), as did thalidomide and pomalidomide (fig. S4C). Depletion of these proteins was evident in as little as 3 hours after lenalidomide treatment (Fig. 2C). In contrast, *IKZF1* and *IKZF3* mRNA levels were not altered by lenalidomide treatment (Fig. 2D and fig. S4B).

Lenalidomide induced ubiquitination of HA-tagged IKZF1 and IKZF3 expressed in MM1S (Fig. 2F) and 293T cells as well as endogenous IKZF1 and IKZF3 (fig. S6). Cullin-RING ubiquitin ligase (CRL) activity depends on NEDDylation (11), and treatment with the Nedd8 enzyme inhibitor MLN-4924 prevented the lenalidomide-induced decrease of IKZF1 and IKZF3 (fig. S5). These experiments demonstrate that lenalidomide-induced degradation of IKZF1 and IKZF3 involves ubiquitination by a cullin-based E3 ubiquitin ligase.

We next sought to determine whether lenalidomide-induced ubiquitination of IKZF1 and IKZF3 is caused by altered binding of these proteins to CRBN, as observed in our proteomic studies. We confirmed that more IKZF1 and IKZF3 coimmunoprecipitated with endogenous CRBN in cells treated with lenalidomide (Fig. 3A). If CRBN is essential for lenalidomide-induced degradation of IKZF1 and IKZF3, then loss or mutation of CRBN would inhibit the effect of the drug. Knockdown of CRBN by short hairpin RNAs

(shRNAs) as well as expression of the CRBN^{YWAA} mutant (4) that does not bind lenalidomide abrogated degradation of IKZF1 and IKZF3 and conferred lenalidomide resistance to MM1S cells (fig. S7), which is consistent with previous studies that have shown CRBN to be essential for lenalidomide activity in multiple myeloma (12, 13). IKZF3 was ubiquitinated in vitro when coimmunoprecipitated with CRBN from 293T cells, demonstrating that IKZF3 is an enzymatic substrate of the CRBN complex (Fig. 3B). These studies demonstrate that lenalidomide causes increased binding of IKZF1 and IKZF3 to CRBN and promotes their ubiquitination and degradation.

In order to identify a degen sequence in IKZF3 responsible for lenalidomide sensitivity, we generated a series of deletion mutants and identified a 59-amino acid sequence that is sufficient for lenalidomide sensitivity, of which 30 amino acids are essential (Fig. 3, C and D, and fig. S8). The critical amino acid sequence lies within zinc finger domain 2, which is highly homologous be-

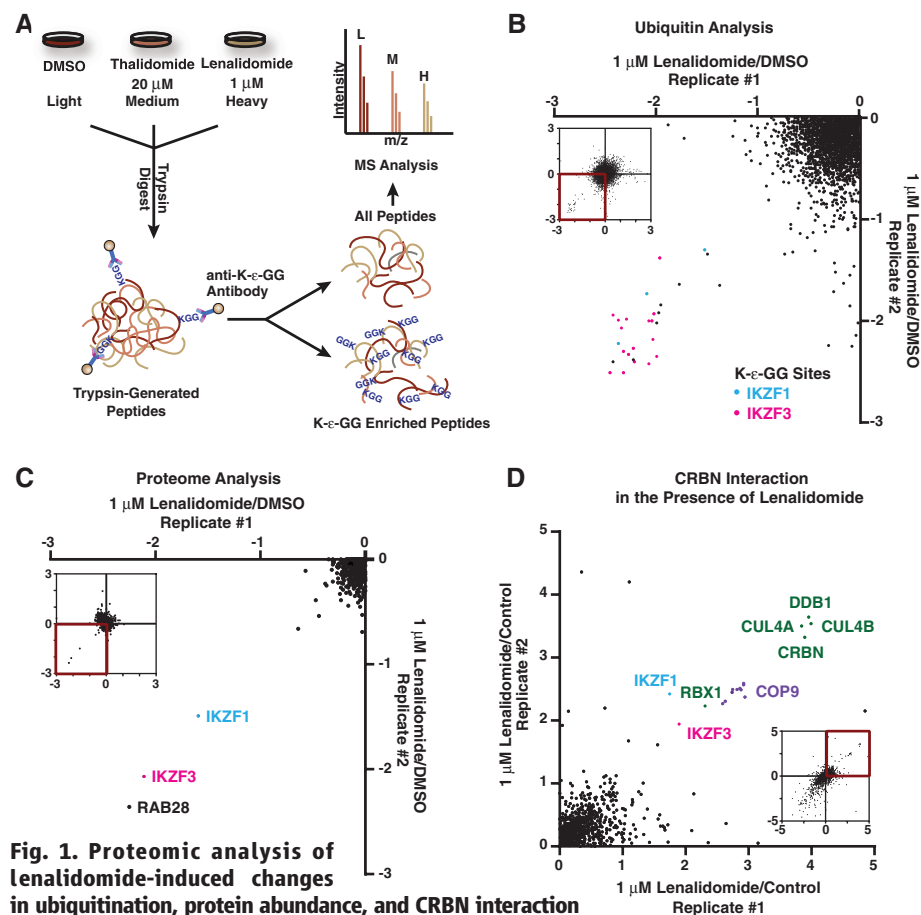


Fig. 1. Proteomic analysis of lenalidomide-induced changes in ubiquitination, protein abundance, and CRBN interaction in MM1S cells. (A) Experimental design for SILAC-based assessment of global changes in ubiquitination and protein levels. Cells were treated for 12 hours with dimethyl sulfoxide (DMSO), lenalidomide, or thalidomide. For ubiquitination analysis, 5 μM MG132 were added for the last 3 hours. (B) Log₂ ratios for individual K-ε-GG sites of lenalidomide- versus DMSO-treated cells for replicates 1 and 2. Each dot represents an individual K-ε-GG site. (C) Log₂ ratios of changes of protein abundance of lenalidomide- versus DMSO-treated cells. Each dot represents a distinct protein group. (D) CRBN interaction analysis in cells treated for 6 hours with 1 μM lenalidomide. Scatter plot shows log₂ changes of proteins pulled down by HA-CRBN in lenalidomide- versus DMSO-treated control cells.

tween Ikaros proteins. IKZF2 and IKZF4, which are not sensitive to lenalidomide, differ from IKZF1 and IKZF3 at only one position within

this critical region (Fig. 3D). Substitution of Q147 in IKZF3 with a histidine residue (*IKZF3*^{Q147H}), which is present at this corresponding site in IKZF2

and IKZF4, caused resistance to lenalidomide-induced degradation. (Single-letter abbreviations for the amino acid residues are as follows: H, His;

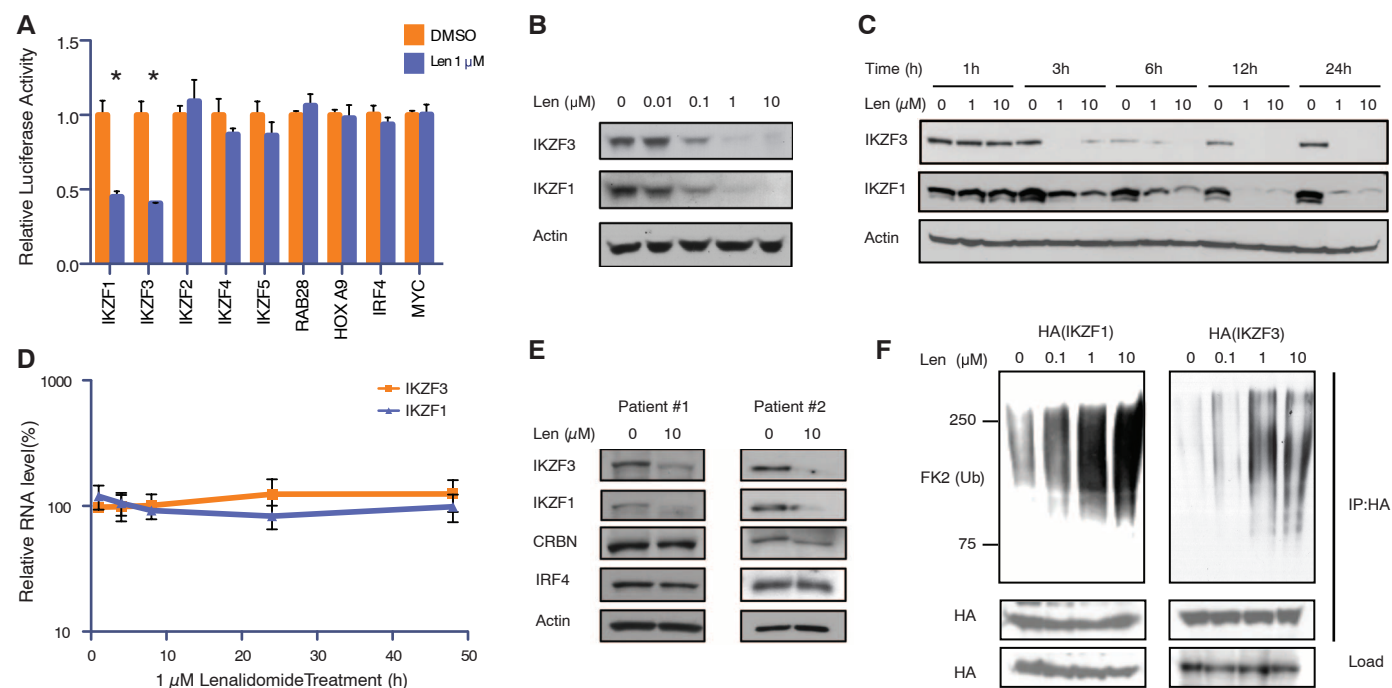


Fig. 2. Effect of lenalidomide on IKZF1 and IKZF3 protein levels. (A) 293T cells transfected with vectors expressing the indicated cDNA fused to firefly luciferase and control renilla luciferase were treated with DMSO or 1 μ M lenalidomide for 24 hours. Bars represent the firefly-to-renilla luciferase ratio, normalized to DMSO-treated cells. (B) Effects of lenalidomide on endogenous IKZF1 and IKZF3 in MM1S cells treated for 24 hours. (C) Time course of

lenalidomide treatment in MM1S cells for IKZF1 and IKZF3 protein levels and (D) mRNA levels. (E) Primary multiple myeloma samples were treated for 6 hours and analyzed by means of immunoblot. (F) In vivo ubiquitination analysis of HA-tagged IKZF1 and IKZF3 expressed in MM1S cells treated for 1.5 hours with 100 nM Epoxomicin and the indicated concentrations of lenalidomide. The FK2 antibody detects covalently linked ubiquitin.

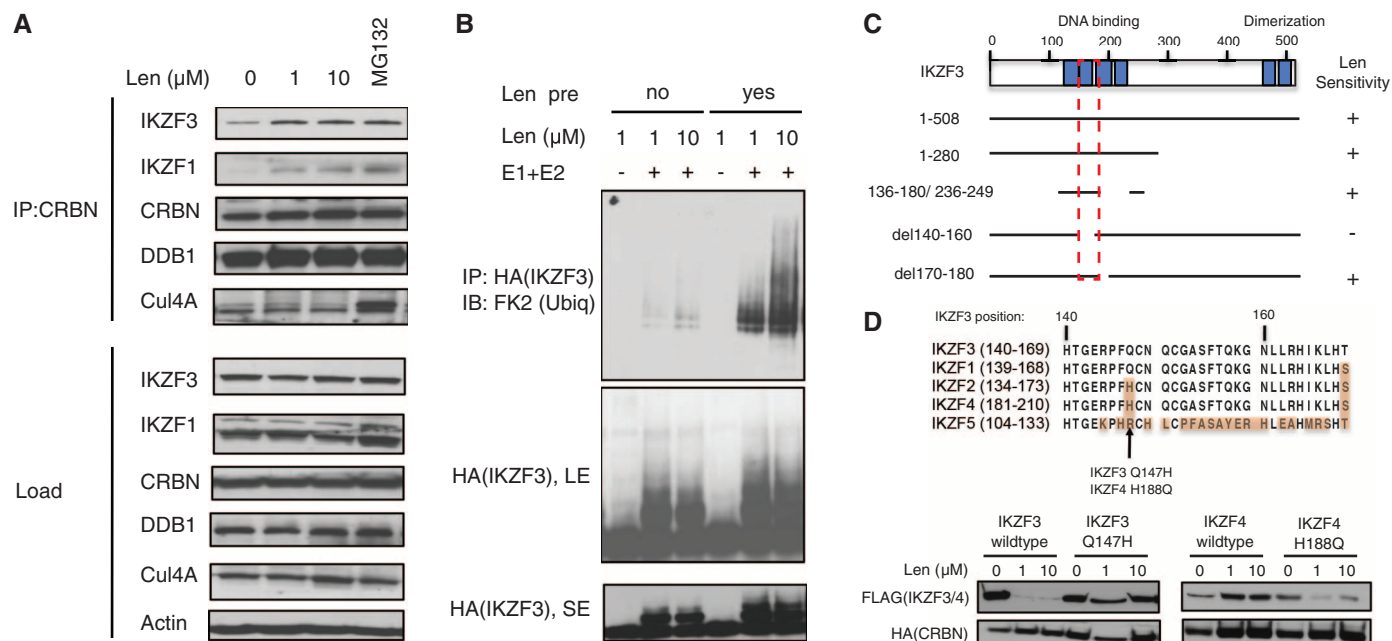


Fig. 3. CRBN is a substrate receptor for IKZF1 and IKZF3. (A) Immunoprecipitation of endogenous CRBN in MM1S cells treated for 1 hour with the indicated drugs. (B) In vitro ubiquitination reaction of HA-IKZF3 coimmunoprecipitated with FLAG-CRBN from 293T cells and incubated in the presence or absence of E1 and E2 ubiquitin-conjugating enzymes. (C) Mapping of the

degron that confers lenalidomide sensitivity. Blue boxes in the IKZF3 protein represent zinc finger domains. (D) Sequence alignment of the core lenalidomide region between the five Ikaros proteins. Western blots of 293T cells lysates 48 hours after cotransfection of FLAG-tagged IKZF3 or IKZF4 with HA-tagged CRBN and 24 hours of drug treatment.

Q, Gln.) In the mutants, other amino acids were substituted at certain locations; for example, Q147H indicates that glutamine at position 147 was replaced by histidine. Conversely, when the corresponding histidine (H188) in IKZF4 was changed to glutamine (*IKZF4*^{H188Q}), IKZF4 was degraded after lenalidomide treatment (Fig. 3D). Binding to CRBN in the presence of lenalidomide is decreased for IKZF3^{Q147H} as compared with wild-type IKZF3 (fig. S8C). This domain is therefore necessary and sufficient for lenalidomide-induced binding to CRBN and subsequent protein degradation, and amino acid changes in this region provide the basis for differential sensitivity to lenalidomide between Ikaros family members.

Having demonstrated that lenalidomide regulates IKZF1 and IKZF3 ubiquitination and abundance, we next sought to determine whether these proteins mediate specific biological and therapeutic effects of lenalidomide. IKZF1 and IKZF3 are essential transcription factors for terminal differentiation of B and T cell lineages (14, 15). Whereas IKZF1 is highly expressed in early lymphoid progenitors, IKZF3 is expressed at high levels in more mature B cell neoplasms (16, 17), and mouse studies have demonstrated that IKZF3 is required for the generation of plasma cells, which are the physiologic counterparts of multiple myeloma cells (18). Therefore, we examined the dependence of multiple myeloma cells on *IKZF1* and *IKZF3* expression by genetic silencing of these proteins using RNA interference. *IKZF1* and *IKZF3* shRNAs that effectively decrease expression of

the target proteins (fig. S11) inhibited growth of lenalidomide-sensitive multiple myeloma cell lines, whereas lenalidomide-insensitive cell lines were unaffected (Fig. 4A and fig. S9). Similarly, expression of a dominant negative IKZF3 isoform that lacks the complete DNA binding region resulted in depletion of MM1S cells (Fig. 4B). Overexpression of *IKZF3* conferred relative lenalidomide-resistance to MM1S cells when competed with MM1S cells infected with a control retrovirus (fig. S9B). Moreover, MM1S cells expressing the lenalidomide-resistant *IKZF3*^{Q147H} mutation were relatively resistant toward lenalidomide when competed against MM1S cells expressing wild-type *IKZF3* (Fig. 4B). These studies indicate that the antiproliferative effect of lenalidomide in multiple myeloma cells is mediated by depletion of IKZF1 and IKZF3.

The transcription factor IRF4 was previously reported to be an essential gene in multiple myeloma and was implicated in the activity of lenalidomide in this disease (10, 19). Although IRF4 protein levels were only slightly decreased in our proteomic analysis after 12 hours of treatment, we observed a decrease of *IRF4* mRNA and protein when cells were treated for 24 hours and longer. Knockdown of *IKZF3* also suppressed *IRF4* mRNA levels, suggesting that IRF4 is a transcriptional target of IKZF3 (fig. S10).

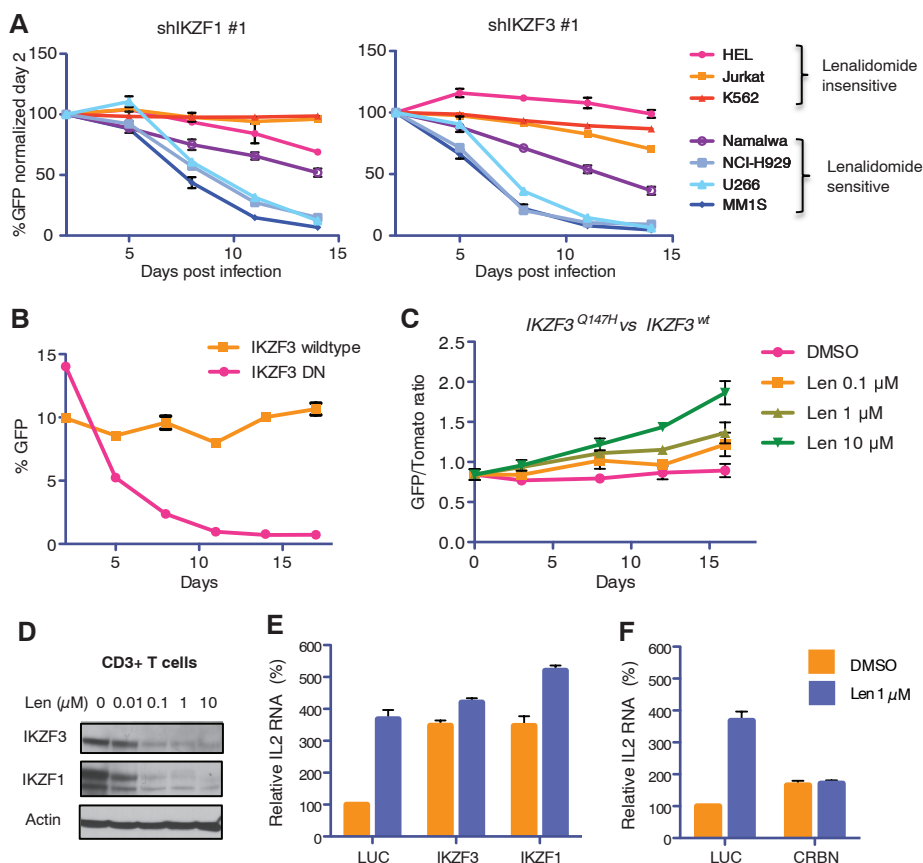
IKZF3 binds the *IL2* gene promoter and represses *IL2* transcription in T cells (20, 21). We therefore sought to determine whether lenalidomide regulates IL-2 levels by modulating IKZF3 expres-

sion. Both IKZF1 and IKZF3 protein levels decrease markedly in primary human T cells treated with lenalidomide (Fig. 4D). Lenalidomide induced *IL2* mRNA expression by 3.3-fold in T cells expressing a control shRNA. shRNA-mediated knockdown of *IKZF3* or *IKZF1* induced IL-2 expression and repressed further response to lenalidomide (Fig. 4E). Similarly, the effect of lenalidomide on *IL2* expression was abrogated by shRNA knockdown of *CRBN* (Fig. 4F). These studies demonstrate that induction of IL-2 is mediated by derepression of the IL-2 promoter by depletion of IKZF3.

In aggregate, our studies demonstrate that lenalidomide acts via a previously unknown mechanism of drug activity—enforced binding of the substrate receptor CRBN to IKZF1 and IKZF3—resulting in selective ubiquitination and degradation of the target proteins. IKZF1 and IKZF3 play central roles in the biology of B and T cells, and ablation of protein expression for these transcription factors explains the activity of lenalidomide in lymphoid cells. In particular, IKZF3 is critical for plasma cell development, and our data indicate that IKZF3 is essential in multiple myeloma, a plasma cell malignancy, providing a mechanistic basis for therapeutic efficacy in this disorder (18). Moreover, the activity of lenalidomide in other B cell neoplasms, including mantle cell lymphoma (22) and chronic lymphocytic leukemia (23), may be explained by high IKZF3 expression in these disorders (16). Somatic inactivation of *IKZF1* and *IKZF3* occurs in acute lympho-

Fig. 4. Biological role of IKZF1 and IKZF3 in multiple myeloma cell lines and T cells. (A)

Lenalidomide-sensitive and -insensitive cell lines were infected with lentivirus-expressing *IKZF1* or *IKZF3* shRNAs and green fluorescent protein (GFP). Relative depletion was assessed by means of flow cytometry and normalized to day 2 after infection. (B) MM1S cells were transduced with retrovirus expressing GFP and wild-type *IKZF3* or a dominant negative *IKZF3* isoform, with deletion of the complete DNA binding region. (C) MM1S cells were infected with retrovirus expressing *IKZF3*^{Q147H}/GFP or *IKZF3*^{wt}/dTomato and competed against each other in media containing DMSO or lenalidomide. (D) Human CD3⁺ T cells were stimulated with plate-bound antibody to CD3 and antibody to CD28 and treated with different concentrations of lenalidomide for 24 hours. (E and F) T cells were infected with lentiviral vectors expressing shRNAs targeting the indicated genes. After selection with puromycin, T cells were stimulated with antibody to CD3/CD28 Dynabeads and treated with DMSO or 1 μ M lenalidomide for 12 hours before lysis. *IL-2* RNA expression levels were analyzed by quantitative reverse transcription polymerase chain reaction by using glyceraldehyde-3-phosphate dehydrogenase expression as an internal control.



blastic leukemia, resulting in an accumulation of immature lymphoid progenitor cells, which is consistent with an essential role for these factors in lymphoid differentiation (24, 25). In T cells, ablation of IKZF3-mediated repression of IL-2 gene expression provides a mechanism for increased IL-2 production in response to lenalidomide. The teratogenicity of thalidomide and the efficacy of lenalidomide in myelodysplastic syndrome may be mediated by alternative substrates in different cellular lineages.

RING-based E3 ubiquitin ligases are characterized by a high specificity for their substrates and therefore represent promising drug targets (26). Our studies reveal that lenalidomide modulates the activity of the CRL4-CRBN complex to increase ubiquitination of two transcription factors, IKZF1 and IKZF3, which would otherwise be considered “undruggable.” A plant hormone, auxin, appears to act similarly, increasing the interaction between a ubiquitin ligase and a specific substrate, suggesting that this mechanism might be operative in additional biological contexts (27). Selective ubiquitination and degradation of specific targets provides a previously unidentified mechanism of therapeutic activity for proteins that are not otherwise amenable to small-molecule inhibition.

References and Notes

- S. V. Rajkumar *et al.*, *Blood* **106**, 4050–4053 (2005).
- P. A. Haslett, L. G. Corral, M. Albert, G. Kaplan, *J. Exp. Med.* **187**, 1885–1892 (1998).
- E. P. Sampaio, E. N. Sarno, R. Galilly, Z. A. Cohn, G. Kaplan, *J. Exp. Med.* **173**, 699–703 (1991).
- T. Ito *et al.*, *Science* **327**, 1345–1350 (2010).
- R. Groisman *et al.*, *Cell* **113**, 357–367 (2003).
- S. Angers *et al.*, *Nature* **443**, 590–593 (2006).
- N. D. Udeshi, P. Mertins, T. Svinkina, S. A. Carr, *Nat. Protoc.* **8**, 1950–1960 (2013).
- N. D. Udeshi *et al.*, *Mol. Cell. Proteomics* **12**, 825–831 (2013).
- P. Koivunen *et al.*, *Nature* **483**, 484–488 (2012).
- Y. Yang *et al.*, *Cancer Cell* **21**, 723–737 (2012).
- T. A. Soucy *et al.*, *Nature* **458**, 732–736 (2009).
- A. Lopez-Girona *et al.*, *Leukemia* **26**, 2326–2335 (2012).
- Y. X. Zhu *et al.*, *Blood* **118**, 4771–4779 (2011).
- K. Georgopoulos *et al.*, *Cell* **79**, 143–156 (1994).
- M. Cortes, E. Wong, J. Koipally, K. Georgopoulos, *Curr. Opin. Immunol.* **11**, 167–171 (1999).
- H. Nüchel *et al.*, *Br. J. Haematol.* **144**, 268–270 (2009).
- B. Morgan *et al.*, *EMBO J.* **16**, 2004–2013 (1997).
- M. Cortés, K. Georgopoulos, *J. Exp. Med.* **199**, 209–219 (2004).
- A. L. Shaffer *et al.*, *Nature* **454**, 226–231 (2008).
- R. Gandhi *et al.*, *Nat. Immunol.* **11**, 846–853 (2010).
- F. J. Quintana *et al.*, *Nat. Immunol.* **13**, 770–777 (2012).
- T. M. Habermann *et al.*, *Br. J. Haematol.* **145**, 344–349 (2009).
- A. Chanan-Khan *et al.*, *J. Clin. Oncol.* **24**, 5343–5349 (2006).
- C. G. Mullighan *et al.*, *Nature* **446**, 758–764 (2007).
- S. Winandy, P. Wu, K. Georgopoulos, *Cell* **83**, 289–299 (1995).
- R. J. Deshaies, C. A. Joazeiro, *Annu. Rev. Biochem.* **78**, 399–434 (2009).
- X. Tan *et al.*, *Nature* **446**, 640–645 (2007).

Acknowledgments: We thank Y.-T. Tai (Dana-Farber Cancer Institute) for technical assistance with primary multiple myeloma samples. This work was supported by funding from the NIH (R01HL082945, P01 CA108631), a Leukemia and Lymphoma Society Scholar Award, an Evans Foundation grant, and a grant from the Starr Cancer Consortium to B.L.E. In addition, the work was supported by a grant from the SPARC consortium and by an National Human Genome Research Institute (RL1- HG004671) initiative in genome-based drug discovery. J.K. was supported by the German Research Foundation (DFG, Kr-3886/1-1). D.H. was supported by the German Cancer Aid. B.L.E. and N.M. have received consulting fees from Celgene. The authors (J.K., N.D.U., S.A.C., and B.L.E.) and the Broad Institute have filed a patent application (number 61/902,066) pertaining to the prediction of therapeutic response to lenalidomide and related compounds.

Supplementary Materials

www.sciencemag.org/content/343/6168/301/suppl/DC1

Materials and Methods

Supplementary Text

Figs. S1 to S11

Table S1

References (28–31)

19 August 2013; accepted 12 November 2013

Published online 28 November 2013;

10.1126/science.1244851

The Myeloma Drug Lenalidomide Promotes the Cereblon-Dependent Destruction of Ikaros Proteins

Gang Lu,¹ Richard E. Middleton,^{1,2} Huahang Sun,^{1,2} MarkVic Naniong,^{1,2} Christopher J. Ott,¹ Constantine S. Mitsiades,¹ Kwok-Kin Wong,^{1,2} James E. Bradner,¹ William G. Kaelin Jr.^{1,3*}

Thalidomide-like drugs such as lenalidomide are clinically important treatments for multiple myeloma and show promise for other B cell malignancies. The biochemical mechanisms underlying their antitumor activity are unknown. Thalidomide was recently shown to bind to, and inhibit, the cereblon ubiquitin ligase. Cereblon loss in zebrafish causes fin defects reminiscent of the limb defects seen in children exposed to thalidomide in utero. Here we show that lenalidomide-bound cereblon acquires the ability to target for proteasomal degradation two specific B cell transcription factors, Ikaros family zinc finger proteins 1 and 3 (IKZF1 and IKZF3). Analysis of myeloma cell lines revealed that loss of IKZF1 and IKZF3 is both necessary and sufficient for lenalidomide's therapeutic effect, suggesting that the antitumor and teratogenic activities of thalidomide-like drugs are dissociable.

Fifty years ago, thalidomide was used for insomnia and morning sickness but was later banned because of its teratogenicity, manifest as profound limb defects. Thalidomide and the related drugs lenalidomide and pomalidomide (IMiDs) have regained interest, however, as im-

munomodulators and antineoplastics, especially for multiple myeloma and other B cell malignancies (1–3). Nonetheless, the biochemical mechanisms underlying their teratogenic and therapeutic activities, and whether they are linked, are unknown.

In this regard, thalidomide was recently shown to bind to cereblon, which is the substrate-recognition component of a cullin-dependent ubiquitin ligase, and to inhibit its autoubiquitination activity (4). Treatment of zebrafish with cereblon morpholinos or thalidomide caused fin defects (4), suggesting that IMiDs act by stabilizing cereblon substrates. However, myeloma

cells rendered IMiDs-resistant have frequently down-regulated cereblon (5–8). Conversely, high cereblon concentrations in myeloma cells are associated with increased responsiveness to IMiDs (9, 10). Collectively, these observations suggest that IMiDs are not simply cereblon antagonists but, instead, alter the substrate specificity of cereblon to include proteins important in myeloma.

To look for such proteins, we made a plasmid library encoding 15,483 open reading frames (ORFs) fused to firefly luciferase (Fluc), knowing that the stabilities of such fusions are usually influenced by the ubiquitin ligase(s) for the corresponding unfused ORF (11–13). Indeed, Elledge and co-workers used a green fluorescence protein (GFP)–ORF library to monitor the stabilities of thousands of ORFs after specific perturbations (13). Partly on the basis of their work, we inserted a renilla luciferase (Rluc) reporter into each ORF-luciferase cDNA for normalization purposes and placed both reporters under internal ribosome entry site (IRES) control (Fig. 1A and fig. S1).

In pilot experiments 293FT embryonic kidney cells grown in multiwell plates were transfected with the ORF-luciferase library (one ORF per well) and treated with the proteasome inhibitor MG132, the hydroxylase inhibitor dimethylxylglycine (DMOG), or vehicle. Fluc/Rluc values measured 36 to 48 hours later were stable over a wide range of input plasmid concentrations (fig. S2). As expected, MG132 stabilized many proteasomal substrates and DMOG stabilized HIF1 α , which is rapidly degraded when prolyl hydroxylated (fig. S3).

¹Department of Medical Oncology, Dana-Farber Cancer Institute, Boston, MA 02215, USA. ²Belfer Institute for Applied Cancer Science, Dana-Farber Cancer Institute, Boston, MA 02215, USA. ³Howard Hughes Medical Institute, Chevy Chase, MD 20815, USA.

*Corresponding author. E-mail: william_kaelin@dfci.harvard.edu

Next, we used this approach to identify changes in protein stability in 293FT cells treated with lenalidomide (Fig. 1A and fig. S4). A total of 2113 ORF-luciferase fusions produced luciferase signals that were undetectable or highly variable (>50% SD), leaving 13,370 for analysis. As expected, most ORFs were unaffected by lenalidomide (Fig. 1B, fig. S5, and table S1). The 107 ORFs that were >3 SDs from the mean (46 ORFs plus 61 ORFs displaying decreased or increased Fluc/Rluc ratios after lenalidomide treatment, respectively) were retested in secondary assays. One down-regulated ORF (IKZF3) and one up-regulated ORF (C11orf65) retested positively (table S2).

C11orf65 was unaffected by lenalidomide when fused to a hemagglutinin (HA) epitope tag instead of Fluc and so was not studied further (fig. S6). By contrast, lenalidomide down-regulated IKZF3 and its paralog IKZF1, which had fallen just outside the 3-SD cut-off in the primary screen, fused to either Fluc or HA (Fig. 1, B and C, and table S1). These effects were specific because lenalidomide did not affect exogenous IKZF2, IKZF4, IKZF5, or the B cell transcription factor IRF4 (Fig. 1C and fig. S7). Similar results were obtained with two common splice variants (V1 and V2) of IKZF1 and IKZF2 (Fig. 1C and fig. S7) and with pomalidomide (fig. S8). Down-regulation of exogenous IKZF1 was blocked by MG132 and by MLN4924,

which inhibits cullin-dependent ubiquitin ligases (Fig. 1D) (14, 15).

Consistent with these findings, lenalidomide down-regulated endogenous IKZF1 in U937 leukemia cells (fig. S9), which do not express IKZF3, and both IKZF1 and IKZF3 in MM1S and L363 myeloma cells (Fig. 1E) unless the cells were pretreated with MG132 or MLN4924 (Fig. 1E and fig. S9). Multiple IKZF1 bands were detected by immunoblot analysis, presumably due to alternative splicing. Lenalidomide did not alter IKZF1 and IKZF3 mRNA levels, consistent with it acting posttranscriptionally (fig. S10).

Down-regulation of cereblon in 293FT cells with a doxycycline-inducible short hairpin RNA (shRNA) prevented the destabilization of exogenous, HA-tagged, IKZF1, by lenalidomide (Fig. 2A and fig. S11). Similarly, cereblon shRNA blocked the down-regulation of endogenous IKZF1 by lenalidomide in U937 leukemia cells (U937) and myeloma cells (L363 and KMS34) (fig. S12, A to C). We also used clustered regularly interspaced short palindromic repeats (CRISPR)-based gene editing (16, 17) to generate *CRBN*^{-/-} 293FT cells, which were then transfected to produce IKZF1 fused to Fluc (Fig. 2B, top panel, and fig. S13) or HA (Fig. 2B, bottom panel). Exogenous IKZF1 was not down-regulated in *CRBN*^{-/-} 293FT cells (Fig. 2B and fig. S13). This defect was rescued by wild-type cereblon, but not a lenalidomide-resistant cereblon mutant (YWAA) (4) (Fig. 2B).

Similar results were obtained with a second *CRBN*^{-/-} 293FT subclone, but not in subclones with detectable amounts of cereblon (fig. S13). Moreover, endogenous IKZF1 and IKZF3 were not degraded by lenalidomide in two independent *CRBN*^{-/-} MM1S myeloma cell lines generated with CRISPR (Fig. 2, C and D).

Lenalidomide enhanced the binding of IKZF1 and IKZF3, but not IKZF2 and IKZF5, to the cereblon ubiquitin ligase in cotransfection experiments using MG132-treated 293FT cells (fig. S14, A and B). Next, we immunoprecipitated FLAG-tagged IKZF1 and IKZF2 from *CRBN*^{-/-} cells that were or were not treated with lenalidomide. The immobilized immunoprecipitates were then used to capture endogenous cereblon from *CRBN*^{+/+} cells (Fig. 3A) or exogenous cereblon from *CRBN*^{-/-} cells transfected to produce wild-type cereblon or the YWAA variant (Fig. 3B). In both cases, the cells producing cereblon were or were not treated with lenalidomide before lysis. Wild-type cereblon, but not the YWAA variant, bound specifically to IKZF1 provided that it was exposed to lenalidomide, consistent with lenalidomide binding directly to cereblon rather than to IKZF1 (Fig. 3, A and B, and fig. S15). Lenalidomide also promoted the binding of cereblon to exogenous IKZF1 (fig. S16) and to endogenous IKZF1 and IKZF3 (fig. S17) when added directly to binding assays performed with cell extracts. Moreover, wild-type cereblon, but not the YWAA variant, promoted

Fig. 1. Down-regulation of IKZF1 and IKZF3 by lenalidomide. (A) Vector schematic. (B) Distribution of fold change in Fluc/Rluc ratios after lenalidomide (LEN) (2 μ M) treatment. (C and D) Fluc/Rluc ratios (top panels) and immunoblots (bottom panels) of 293FT cells transfected to produce the indicated IKZF proteins fused to Fluc (top panels) or HA tag (bottom panels). Where indicated, cells were treated with lenalidomide (2 μ M), MLN4924 (1 μ M), or MG132 (10 μ M) for 12 hours. Fluc/Rluc ratios were normalized to corresponding dimethyl sulfoxide (DMSO)-treated cells. Data are presented as mean \pm SD ($n = 4$). (E) Immunoblot analysis of MM1S and L363 cells treated with LEN (2 μ M) and MLN4924 (1 μ M), as indicated, for 12 hours.

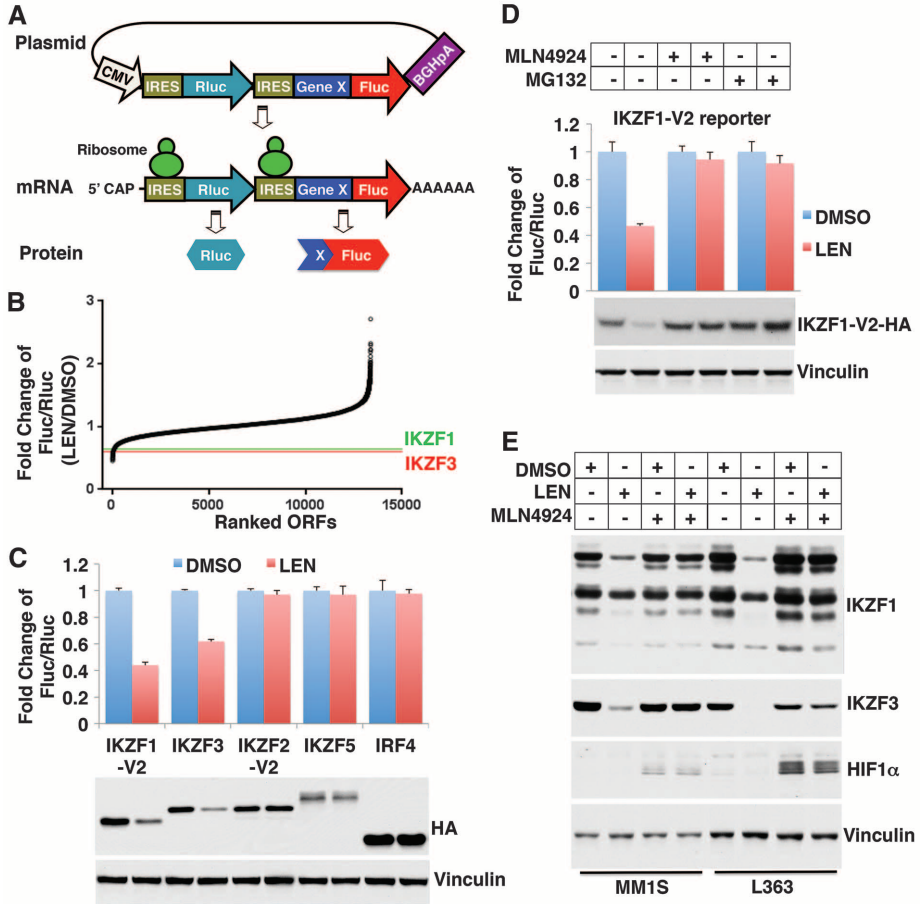


Fig. 2. Down-regulation of IKZF1 and IKZF3 by lenalidomide requires cereblon. (A) Immunoblot analysis of 293FT cells stably infected with lentiviral vectors expressing the indicated IKZF-HA proteins and a doxycycline-inducible *CRBN* shRNA. Where indicated, LEN (2 μ M) and doxycycline (Dox) (1 μ g/ml) were added for 12 and 60 hours, respectively. (B) Fluc/Rluc ratios (top panels) and immunoblots (bottom panels) of *CRBN*^{+/+} and *CRBN*^{-/-} 293FT cells transfected to produce IKZF1 fused to Fluc (top panel) or HA tag (bottom panels). Where indicated cells were treated with LEN (2 μ M) for 12 hours. Fluc/Rluc ratios were normalized to corresponding DMSO-treated cells. Data are presented as mean \pm SD ($n = 4$). (C and D) Immunoblot analysis of *CRBN*^{+/+} and *CRBN*^{-/-} MM1S myeloma cells. Where indicated, cells were treated with LEN (2 μ M) for 24 hours (C) or 1 hour before the addition of cyclohexamide (CHX) (100 μ g/ml) for the indicated periods (D).

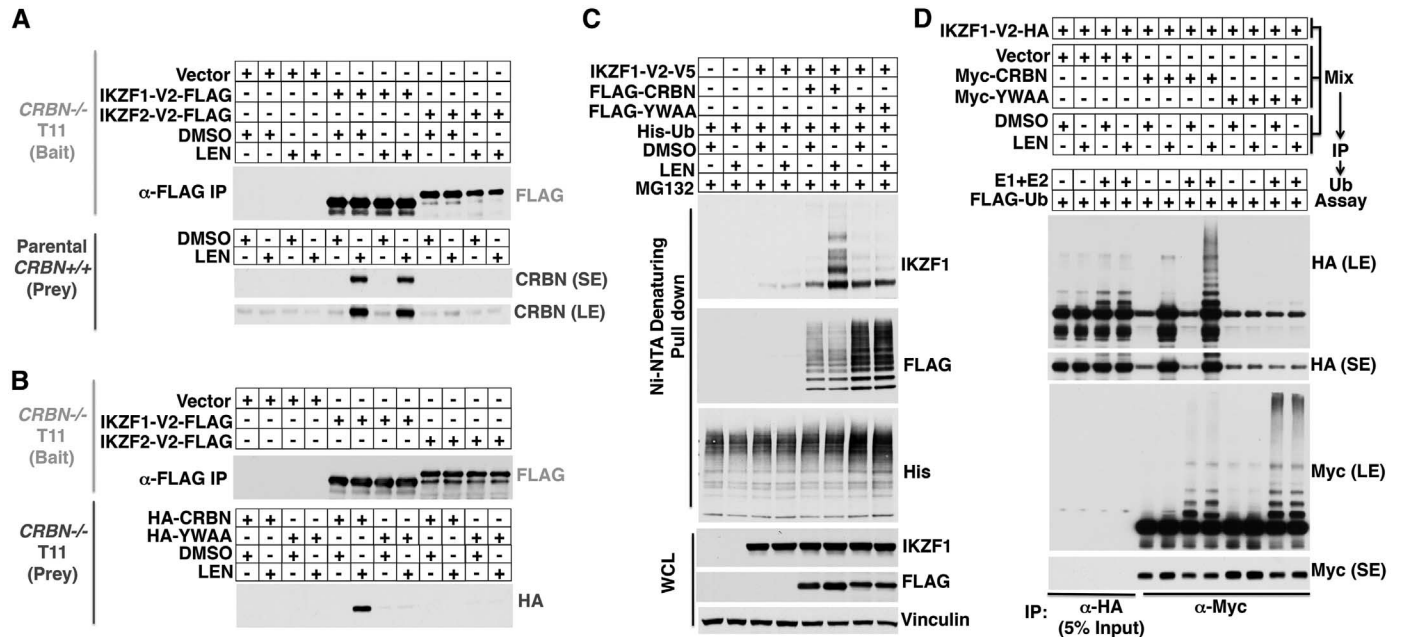
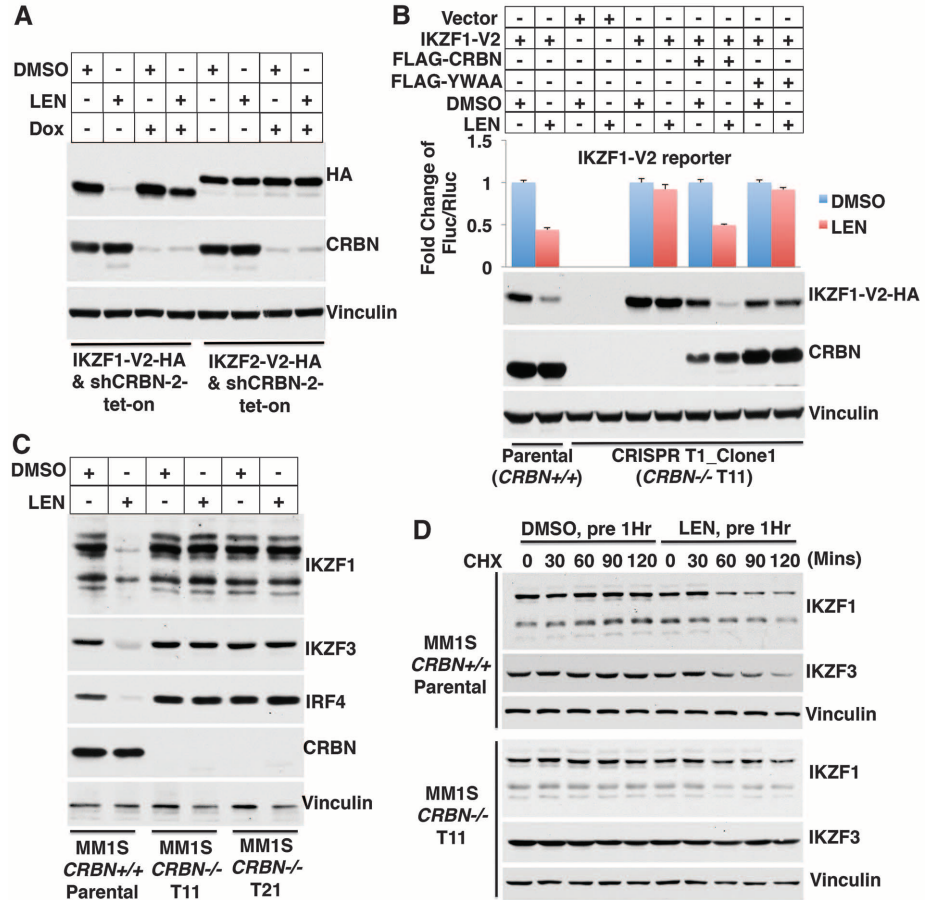


Fig. 3. Lenalidomide promotes ubiquitylation of IKZF1 and IKZF3 by cereblon. (A and B) FLAG-IKZF was immunoprecipitated from *CRBN*^{-/-} 293FT cells stably infected to produce the indicated IKZF proteins and used to capture cereblon from *CRBN*^{+/+} 293FT cells (A) or *CRBN*^{-/-} 293FT cells transfected to produce the indicated CRBN variants (B). Cells were treated with LEN (2 μ M) for 12 hours before lysis, as indicated. Bound proteins were detected by immunoblot analysis. (C) Immunoblot analysis of proteins captured with nickel Sepharose from

293FT cells transfected to produce the indicated FLAG-, His-, and V5-tagged proteins. The cells were treated with MG132 (10 μ M) and, where indicated, with LEN (2 μ M) for 12 hours. (D) *CRBN*^{-/-} 293FT cells were transfected to produce IKZF1-HA and the indicated Myc-cereblon variants and lysed. The extracts were mixed, treated with LEN (2 μ M) or DMSO, and immunoprecipitated with antibodies against HA (anti-HA) or anti-Myc. The immunoprecipitates were incubated with recombinant E1, E2, and ubiquitin (Ub) and subjected to immunoblot analysis.

the ubiquitylation of IKZF1 *in vivo* (Fig. 3C) and *in vitro* (Fig. 3D) after exposure to lenalidomide.

We analyzed a series of IKZF1/2 chimeras and determined that the region of IKZF1 corresponding to residues 108 to 197 of IKZF1(V2) mediated lenalidomide-dependent binding to cereblon (fig. S18). Within this region, there are only seven amino acid differences between IKZF1 and IKZF2 (fig. S19, A and B). Changing IKZF1 residue Q146 (or IKZF3 Q147) to the corresponding residue in IKZF2 (histidine) abrogated cereblon binding and lenalidomide-induced degradation (figs. S19C and S20). Conversely, the reciprocal change in IKZF2 rendered it partially sensitive to lenalidomide (fig. S19D).

Next, we tested six myeloma cell lines for their sensitivity to lenalidomide *in vitro* (Fig. 4, A and B). Previous studies showed that lenalidomide, at least indirectly, down-regulates IRF4 and linked this to its antimyeloma activity (5–8). MM1S, KMS34, and L363 cells were sensitive to lenalidomide *in vitro* whereas KMS11, RPMI8226, and OCImy5 cells were relatively resistant (Fig. 4B). In the three sensitive lines, IKZF1 and IKZF3 were down-regulated by lenalidomide (Fig. 4A). In two of these lines (MM1S and KMS34), loss of IKZF1 and IKZF3 was followed by a decrease in IRF4, consistent with IRF4 acting downstream of IKZF1 and/or IKZF3 in these cells (Fig. 4A and fig. S21A). Indeed, we confirmed decreased IRF4

mRNA and decreased binding of IKZF1 to the IRF4 locus by chromatin immunoprecipitation (ChIP) in MM1S cells treated with lenalidomide (fig. S21). The third sensitive cell line, L363, expressed high basal amounts of IRF4 that were unaffected by lenalidomide, providing evidence that the antiproliferative effects of this drug involves at least one target other than IRF4 (Fig. 4A and fig. S21A).

Two of the resistant lines had relatively high basal amounts of IKZF1 (OCImy5) or IKZF3 (KMS11) and corresponding low amounts of cereblon compared to the sensitive lines, and down-regulation of IKZF1 and IKZF3 by lenalidomide was attenuated in the third (RPMI8226) (Fig. 4A). IRF4 was not down-regulated by lenalidomide in the three resistant lines.

Next, we performed competition experiments with cells in which IKZF1 or IKZF3 was suppressed with shRNAs or enhanced through expression of lenalidomide-resistant versions of IKZF1 or IKZF3. Down-regulation of either IKZF1 or IKZF3 in the lenalidomide-sensitive cell lines MM1S and KMS34 markedly decreased cellular fitness compared to cells expressing a control shRNA and was associated with down-regulation of IRF4 (Fig. 4, C and D, and fig. S22). Notably, down-regulation of either IKZF protein led to loss of the other. Conversely, expression of the stabilized versions of IKZF1(Q146H) or IKZF3

(Q147H) conferred lenalidomide resistance to MM1S cells (Fig. 4, E and F, and fig. S23) and KMS34 cells (fig. S24). Ectopic expression of a T cell–specific Ikaros family member, IKZF2, which is naturally lenalidomide resistant (Fig. 1C), had similar effects (figs. S23G and S25). The effects of expressing IRF4 itself were much less pronounced, again suggesting that IKZF1 and IKZF3 have additional targets that are relevant for lenalidomide's antimyeloma activity (Fig. 4E and fig. S23H). It remains to be seen whether lenalidomide-resistance conferred by IKZF family members is due primarily to transcriptional activation of their target genes or to noncanonical functions.

Our findings link lenalidomide's antimyeloma activity to down-regulation of IKZF1 and IKZF3, two transcription factors that play critical roles in B cell development and are highly expressed in B cell malignancies, including myeloma (fig. S26) (18–21). There are many other examples of cancers that become addicted to transcription factors that specify cell lineage (22, 23). Although IKZF1 is a tumor suppressor in some other B cell malignancies (24), there is precedence for the same gene acting as either a tumor suppressor or an oncogene in different contexts.

Ikaros family members can serve as transcriptional activators or repressors in different settings. For example, IKZF1 and IKZF3 repress

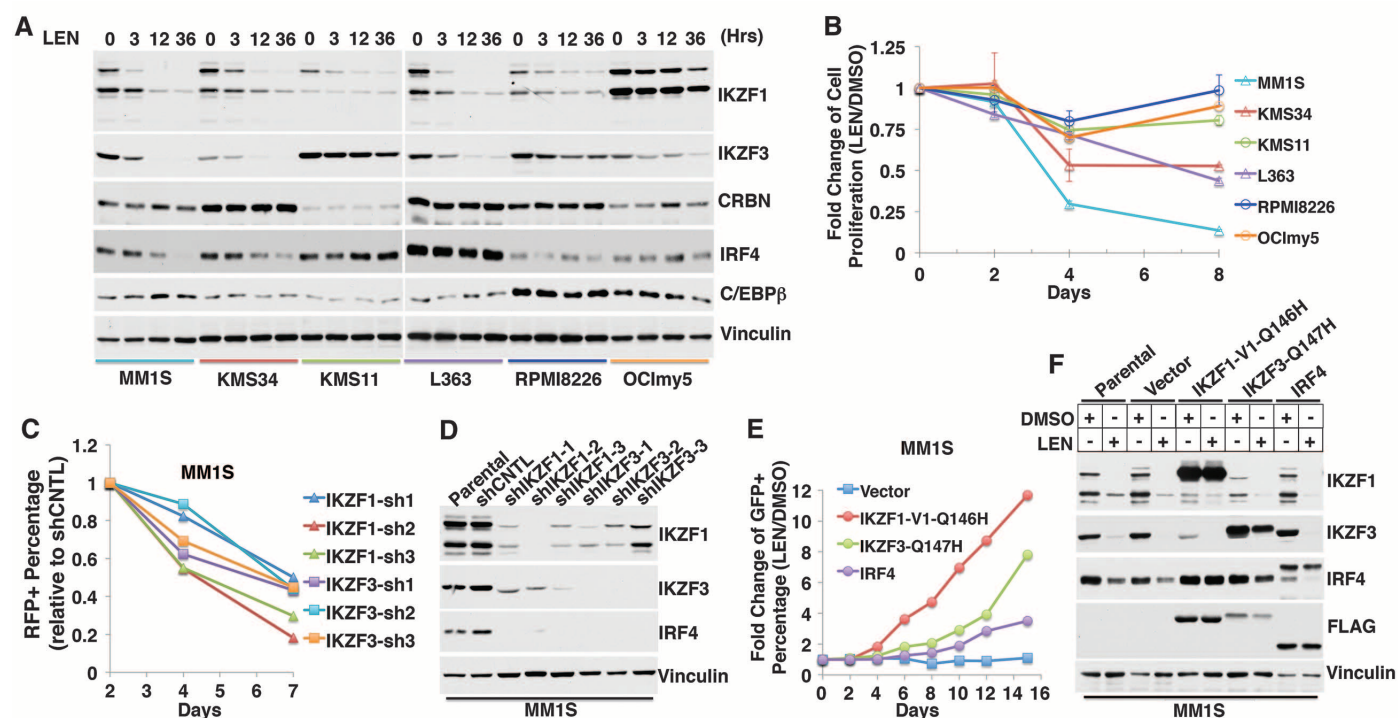


Fig. 4. Antimyeloma activity of lenalidomide linked to loss of IKZF1 and IKZF3. (A and B) Immunoblot analysis (A) and proliferation (B) of myeloma cell lines treated with LEN (2 μ M) for the indicated periods. In (B), data are presented as mean \pm SD ($n = 4$). (C) Change in % red fluorescent protein (RFP) positivity over time in MM1S cells infected with viruses encoding RFP and the indicated shRNAs. The day 2% RFP for each virus was normalized to 1, and subsequent values were expressed relative to cells infected with a

virus encoding RFP and a control (CNTL) shRNA. (D) Immunoblot analysis of MM1S cells transiently infected with lentiviruses expressing the indicated shRNAs for 72 hours. (E) MM1S cells were infected with lentiviral vectors encoding GFP and the indicated FLAG-tagged proteins. Shown for each protein is the percentage of GFP positivity for cells treated with LEN (2 μ M) for the indicated duration compared to DMSO. (F) Immunoblot analysis of MM1S cells infected as in (E) and treated with DMSO or LEN (2 μ M) for 24 hours.

interleukin-2 (IL-2) expression in T cells, thus explaining how IMiDs induce IL-2 production in vivo (19, 25, 26).

The proteasomal inhibitor bortezomib has antimyeloma activity, alone and in combination with lenalidomide, although the pertinent proteasomal substrates are debated (27, 28). This creates a paradox because proteasomal blockade prevents the destruction of IKZF1 and IKZF3 by lenalidomide. Proteasomal blockade by bortezomib is incomplete with therapeutic dosing, however, which might allow sufficient clearance of IKZF1 and IKZF3 while retaining bortezomib's other salutary effects. It is also possible that these two proteins, once polyubiquitinated, are inactive or dominant-negatives.

Earlier work suggested that thalidomide's teratogenic effects reflected cereblon inactivation, whereas our findings indicate that the therapeutic effects of the IMiDs reflect a cereblon gain of function. Notably, cereblon might have additional substrates that were not in our fusion library, could not be recognized as luciferase fusions, or require accessory proteins or signals absent in 293FT cells. Regardless, our findings create a path to uncouple the therapeutic and teratogenic activities of the IMiDs.

It is not yet clear whether lenalidomide's effect on cereblon is hypermorphic or neomorphic. Precedence for the latter is provided by rapamycin, which converts FKBP12 into a TORC1

kinase inhibitor and cyclosporine, which converts cyclophilin into a calcineurin antagonist (29). Perhaps oncoproteins currently deemed undruggable, such as c-Myc or β -catenin, could be destroyed by drugs that, like lenalidomide, repurpose ubiquitin ligases.

References and Notes

1. R. Martiniani, V. Di Loreto, C. Di Sano, A. Lombardo, A. M. Liberati, *Adv. Hematol.* **2012**, 842945 (2012).
2. E. Terpos, N. Kanellias, D. Christoulas, E. Kastiris, M. A. Dimopoulos, *Onco Targets Ther.* **6**, 531–538 (2013).
3. Y. X. Zhu, K. M. Kortuem, A. K. Stewart, *Leuk. Lymphoma* **54**, 683–687 (2013).
4. T. Ito et al., *Science* **327**, 1345–1350 (2010).
5. A. Lopez-Girona et al., *Leukemia* **26**, 2326–2335 (2012).
6. L. H. Zhang et al., *Br. J. Haematol.* **160**, 487–502 (2013).
7. Y. Yang et al., *Cancer Cell* **21**, 723–737 (2012).
8. Y. X. Zhu et al., *Blood* **118**, 4771–4779 (2011).
9. A. Broyl et al., *Blood* **121**, 624–627 (2013).
10. D. Heintel et al., *Br. J. Haematol.* **161**, 695–700 (2013).
11. G. J. Zhang et al., *Nat. Med.* **10**, 643–648 (2004).
12. M. Safran et al., *Proc. Natl. Acad. Sci. U.S.A.* **103**, 105–110 (2006).
13. H. C. Yen, Q. Xu, D. M. Chou, Z. Zhao, S. J. Elledge, *Science* **322**, 918–923 (2008).
14. T. A. Soucy et al., *Nature* **458**, 732–736 (2009).
15. M. Ohh et al., *EMBO Rep.* **3**, 177–182 (2002).
16. L. Cong et al., *Science* **339**, 819–823 (2013).
17. P. Mali et al., *Science* **339**, 823–826 (2013).
18. M. Merkenschlager, *FEBS Lett.* **584**, 4910–4914 (2010).
19. E. C. Thompson et al., *Immunity* **26**, 335–344 (2007).
20. I. Ferreirós-Vidal et al., *Blood* **121**, 1769–1782 (2013).
21. S. Monticelli, F. Sallusto, *Nat. Immunol.* **13**, 719–720 (2012).

22. L. A. Garraway, W. R. Sellers, *Nat. Rev. Cancer* **6**, 593–602 (2006).
23. S. P. Shah et al., *N. Engl. J. Med.* **360**, 2719–2729 (2009).
24. P. Kastner et al., *Am J Blood Res* **3**, 1–13 (2013).
25. F. J. Quintana et al., *Nat. Immunol.* **13**, 770–777 (2012).
26. N. Avitahl et al., *Immunity* **10**, 333–343 (1999).
27. J. Laubach, P. Richardson, K. Anderson, *Annu. Rev. Med.* **62**, 249–264 (2011).
28. P. G. Richardson et al., *J. Clin. Oncol.* **27**, 5713–5719 (2009).
29. G. R. Crabtree, S. L. Schreiber, *Trends Biochem. Sci.* **21**, 418–422 (1996).

Acknowledgments: We thank M. Vidal and A. MacWilliams at Dana-Farber Cancer Institute for the ORF cDNA collection and for help with recombination cloning. This work was supported by a grant (W.G.K.) and F32 fellowship (G.L.) from NIH. C.J.O. is supported by a Leukemia and Lymphoma Society Fellowship award, and J.E.B. and C.S.M. are supported by the Multiple Myeloma Research Foundation. W.G.K. is a Howard Hughes Medical Institute Investigator. C.S.M. has received consulting fees from Celgene, the manufacturer of lenalidomide and pomalidomide. The primary and secondary luciferase screen data are presented in the supplementary materials.

Supplementary Materials

www.sciencemag.org/content/343/6168/305/suppl/DC1
Materials and Methods
Figs. S1 to S26
Tables S1 and S2
References (30–34)

20 August 2013; accepted 12 November 2013
Published online 28 November 2013;
10.1126/science.1244917

Direct in Vivo RNAi Screen Unveils Myosin IIa as a Tumor Suppressor of Squamous Cell Carcinomas

Daniel Schramek,¹ Ataman Sandoel,¹ Jeremy P. Segal,^{1*} Slobodan Beronja,¹ Evan Heller,¹ Daniel Oristian,¹ Boris Reva,² Elaine Fuchs^{1†}

Mining modern genomics for cancer therapies is predicated on weeding out “bystander” alterations (nonconsequential mutations) and identifying “driver” mutations responsible for tumorigenesis and/or metastasis. We used a direct in vivo RNA interference (RNAi) strategy to screen for genes that upon repression predispose mice to squamous cell carcinomas (SCCs). Seven of our top hits—including *Myh9*, which encodes nonmuscle myosin IIa—have not been linked to tumor development, yet tissue-specific *Myh9* RNAi and *Myh9* knockout trigger invasive SCC formation on tumor-susceptible backgrounds. In human and mouse keratinocytes, myosin IIa's function is manifested not only in conventional actin-related processes but also in regulating posttranscriptional p53 stabilization. Myosin IIa is diminished in human SCCs with poor survival, which suggests that in vivo RNAi technology might be useful for identifying potent but low-penetrance tumor suppressors.

Squamous cell carcinomas of the head and neck (HNSCCs) are the sixth most common human cancer worldwide, with frequent, often aggressive recurrence and poor prognosis (1). Established genetic and epigenetic alterations include *EGFR* amplifications; *Trp53*, *H-RAS*, *NOTCH*, *PI3K/Akt*, and *BRCA1* mutations; and transforming growth factor- β (TGF- β) pathway repression (1). Recent whole-exome sequencing

efforts have revealed hundreds of additional “lower-penetrance” HNSCC mutations with unknown functional importance (2, 3).

To functionally test putative “driver mutations” that confer a selective advantage and contribute to tumor progression, researchers have used RNA interference (RNAi) followed by allografting of transduced cultured cancer cells. However, orthotopic transplantations necessitate immu-

nocompromised animals and generate wound responses, which can confound physiological relevance. We have circumvented these difficulties with noninvasive, ultrasound-guided in utero lentiviral-mediated RNAi delivery, selectively transducing single-layered surface ectoderm of living mouse embryos at embryonic day (E) 9.5 (4).

We first showed that mice transduced with *Brcal* short hairpin RNAs (shRNAs) that silence *BRCAL* expression recapitulate the *Brcal*-knockout phenotype and develop spontaneous skin and oral SCCs with long latency (5) (fig. S1). We accelerated tumor growth by testing hairpins in epithelial-specific, *TGF β -Receptor-II* conditional knockout (cKO) mice (*K14-Cre;T β RII^{flxed/flxed}*), which lose TGF- β signaling in skin, oral, and anogenital epithelia and display enhanced SCC susceptibility (6, 7). On this *T β RII*-cKO background, *Brcal* knockdown generated SCCs with increased frequency and a factor of 4 decrease in latency (fig. S1). Having validated our sensitized approach, we devised a pooled shRNA format to carry out

¹Howard Hughes Medical Institute, Laboratory of Mammalian Cell Biology and Development, The Rockefeller University, New York, NY 10065, USA. ²Department of Genetics and Genomic Science, Institute for Genomics and Multiscale Biology, Icahn School of Medicine at Mount Sinai, 1428 Madison Avenue, New York, NY 10029, USA.

*Present address: Department of Pathology, University of Chicago, Chicago, IL 60637, USA.

†Corresponding author. E-mail: fuchs@rockefeller.edu

an *in vivo* screen for additional putative suppressors of SCCs (Fig. 1A). We selected 1762 shRNA lentiviruses targeting 347 mouse genes that either (i) had human orthologs carrying recurring HNSCC somatic mutations (2, 3) or (ii) were deregulated by a factor of ≥ 2 in tumor-initiating stem cells purified from SCCs initiated by oncogenic *HRas* (8) (table S1). We also included positive (*Bcr1* shRNA) and negative (scrambled nontargeting shRNA) controls. After infecting E9.5 epidermis, we isolated E12.5 genomic DNA and verified by Illumina sequencing that shRNA representations correlated nicely with their individual abundance within our initial test pool (fig. S2).

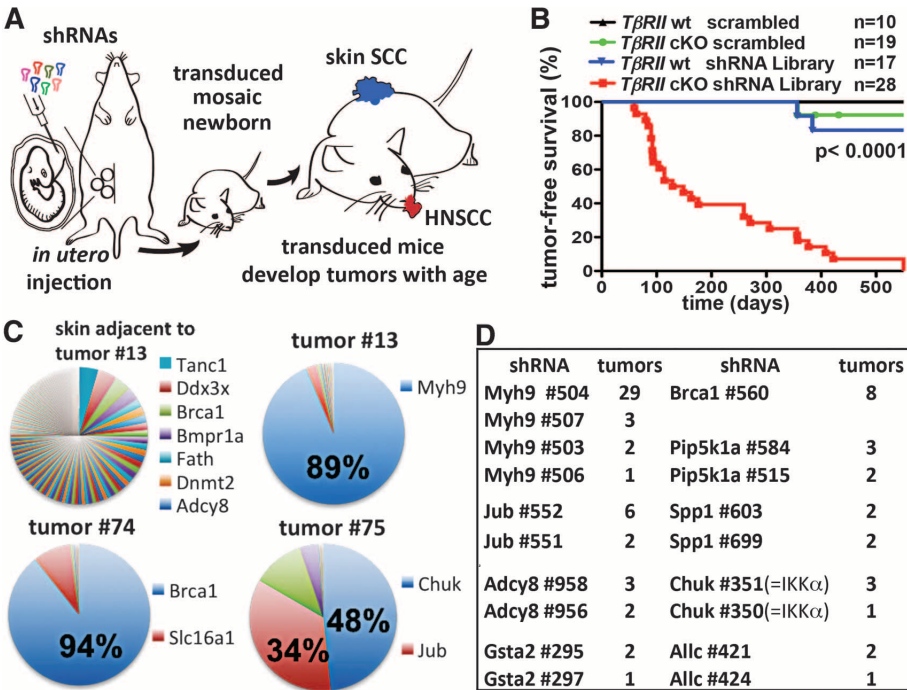


Fig. 1. Direct *in vivo* shRNA screen for HNSCC tumor suppressors. (A) Schematic of pooled shRNA screen. (B) Tumor-free survival of mice of the indicated genotype transduced at E9.5 with the shRNA library targeting putative HNSCC genes (n = number per group; $P < 0.0001$, log-rank test). (C) Representative pie charts showing percent representation of a particular shRNA within an individual tumor compared to surrounding healthy skin. (D) Top-scoring tumor suppressor candidates and corresponding numbers of tumors showing significant enrichment.

To ensure a coverage of >500 individual clones per shRNA, we infected 74 genotypically matched *TβRII*-cKO or *TβRII*^{fl/fl} control embryos with our lentivirus pool and monitored pups into adulthood. As expected (6), $\sim 5\%$ of the *TβRII*-cKO mice developed anogenital SCCs. Scrambled shRNA expression did not affect these statistics, nor did transduction with a “control pool” of 1000 random shRNAs. In contrast, all 28 library-transduced *TβRII*-cKO mice developed lesions within skin, the oral cavity, and/or mucocutaneous junctions at eyelids (Fig. 1B). These findings underscore the efficacy of our approach and document the enrichment of our test shRNA library for SCC tumor suppressors.

Most lesions displayed histopathological features of SCCs with varying degrees of differentiation and local invasion; a few were squamous papillomas or epidermal hyperplastic lesions (figs. S3 to S5). Sequencing revealed that most lesions harbored one or two shRNAs highly enriched relative to initial pool representation and to surrounding healthy skin; gratifyingly, this included the positive control *Bcr1* shRNA (Fig. 1C). Eight candidate tumor suppressors displayed highly enriched, multiple independent shRNAs in three or more tumors (Fig. 1D). Surprisingly, *Trp53* was not among them. Subsequent analyses revealed that the *Trp53* hairpins in our pool were inefficient, and when substituted with a more potent *Trp53* shRNA, SCCs developed in our assay (fig. S6).

About 40% of tumors were enriched for four out of five shRNAs against *Myh9*, encoding non-muscle myosin IIa heavy chain (Fig. 1, C and D). Tested individually, *Myh9* shRNAs markedly reduced myosin IIa protein, and efficiency correlated strongly with tumor multiplicity (fig. S7). *Myh9* shRNA-transduced *TβRII*-cKO mice displayed an “open eye at birth” phenotype and

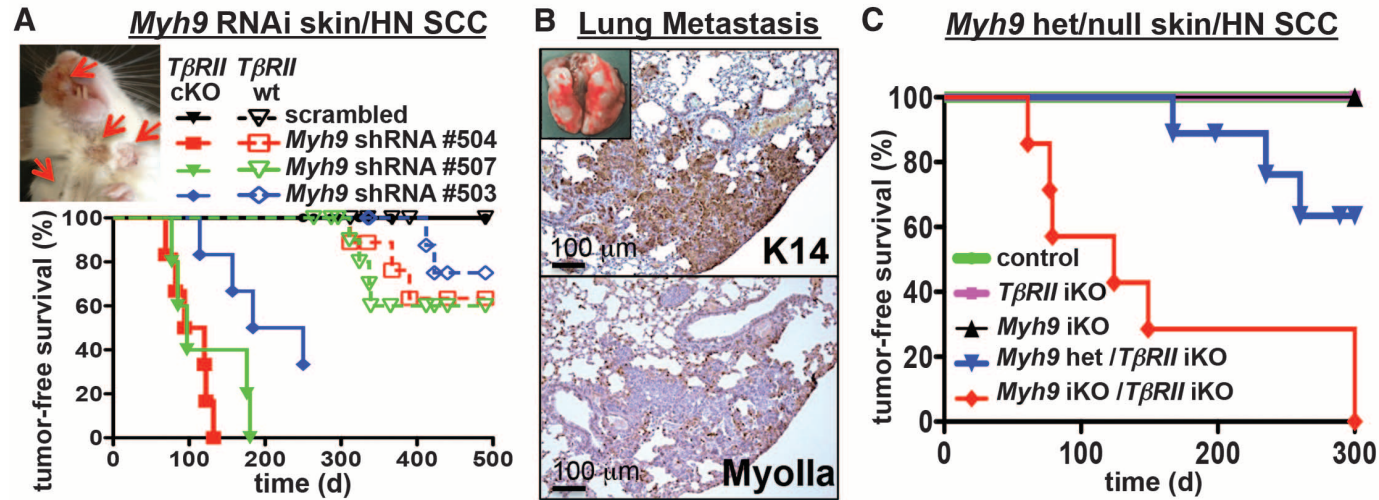


Fig. 2. Functional validation of *Myh9* as a bona fide tumor suppressor. (A) Tumor-free survival of mice of the indicated genotype and shRNA transduction ($n > 6$ for each genotype, $P < 0.0001$). Insert shows skin lesions (arrows) on 4-month-old *Myh9* shRNA-transduced *TβRII*-cKO mouse. (B) *Myh9* knock-

down results in pulmonary metastases in *TβRII*-cKO mice. Metastatic lesions are immunoreactive for epithelial keratin 14 and negative for myosin IIa. (C) Tumor-free survival of *Myh9*/*TβRII* inducible knockout (iKO) as well as *Myh9* heterozygous/*TβRII* iKO and control mice ($n = 6$, $P < 0.001$, log-rank test).

sparse hair coat, and although initially normal, signs of epidermal hyperproliferation appeared with age (fig. S8).

TβRII-cKO mice transduced with any of three different *Myh9* shRNAs developed multiple poorly differentiated myosin IIa-deficient skin SCCs and HNSCCs with median latencies of 3 to 7 months (Fig. 2A). Tumors displayed hallmarks of human SCCs, including invasion into subcutaneous fat, underlying muscle, and salivary glands as well as colonization to the draining lymph nodes (fig. S9). They even formed distant lung metastases

(Fig. 2B). Finally, ~30% of *TβRII*^{fl/fl} mice (no Cre) transduced with *Myh9* shRNAs but not scrambled shRNAs developed skin SCCs after 1 year, indicating that *Myh9* loss alone might be sufficient to promote spontaneous tumor development (Fig. 2A).

To further validate *Myh9* as an SCC tumor suppressor, we crossed *Myh9*^{fl/fl} mice to our epithelial-specific *K14-Cre* and tamoxifen-regulated *K14CreER* deleter strains. Embryologically, *Myh9*-cKO mice recapitulated the “open eye at birth” and hair phenotypes (fig. S10, A to C). In adult

mice, inducible deletion of even one *Myh9* allele concomitantly with *TβRII* ablation resulted in multiple invasive SCCs on the back, ears, and anal regions (Fig. 2C and fig. S10, C to E). Control littermates remained tumor-free during this time.

The pronounced invasion and distant metastases were linked to *Myh9* knockdown. Indeed, epithelial outgrowth from skin explants was markedly enhanced when *TβRII*^{fl/fl} or *TβRII*-cKO embryos were transduced with *Myh9* but not control shRNAs (fig. S11). Similar results were obtained in vitro with scratch-wound and transwell migration assays independent of TGF-β signaling status. Moreover, reducing *Myh9* levels profoundly affected invasion of cells through a Matrigel-coated filter (fig. S12).

These results were consistent with the well-established role for actin-myosin networks in regulating cellular movements. More puzzling was our discovery that, although *Myh9* knockdown accelerated tumor development and malignant progression upon *TβRII* ablation and under conditions favoring *HRas* mutations (fig. S13, A to E), it had very little effect on tumor latency or multiplicity in mice carrying an epithelial-specific *Trp53* gain-of-function mutation (Fig. 3A) (9). This context dependency raised the possibility that myosin IIa deficiency and *Trp53* mutations may partially overlap in function—a notion further supported by similar latencies and penetrance of spontaneous SCCs appearing in *Myh9* knockdown, *Trp53* mutant, and *Trp53* mutant-*Myh9* knockdown mice (fig. S13F). Such similarities were also observed when *Myh9* and *Trp53* knockdowns were tested on the SCC-susceptible *TβRII*-cKO background (fig. S13G).

To test for possible epistatic interactions, we treated primary keratinocytes with doxorubicin, which introduces double-strand DNA breaks, thereby triggering the DNA damage response (DDR) pathway and p53 activation (Fig. 3B) (10). Notably, expression of different *Myh9* shRNAs in keratinocytes significantly delayed and reduced p53 activation after doxorubicin treatment (Fig. 3B and fig. S14A). This was also true for *Myh9*^{fl/fl} keratinocytes transduced in vitro with lentiviral Cre and for epidermis from γ-irradiated *Myh9*-cKO and *Myh9* knockdown mice (Fig. 3, C and D, and fig. S14, B to D).

Relative to controls, *Myh9*-deficient keratinocytes also failed to induce p53-responsive genes such as *p21*, *Fas*, *Bax*, *Mdm2*, and *14-3-3σ* (Fig. 3, B, D, and E). These effects were specific to the p53 pathway, because control and *Myh9* knockdown keratinocytes responded equally to other stimuli such as epidermal growth factor (EGF) (fig. S15). Moreover, such effects were not observed with shRNAs against other non-muscle myosin II genes [*Myh10* (myosin IIb) and *Myh14* (myosin IIc)], nor were they dependent on TGF-β signaling (fig. S16).

Probing deeper, we discovered that the myosin II adenine triphosphatase (ATPase) inhibitor blebbistatin phenocopied *Myh9* loss-of-function effects on DDR-induced p53 activation

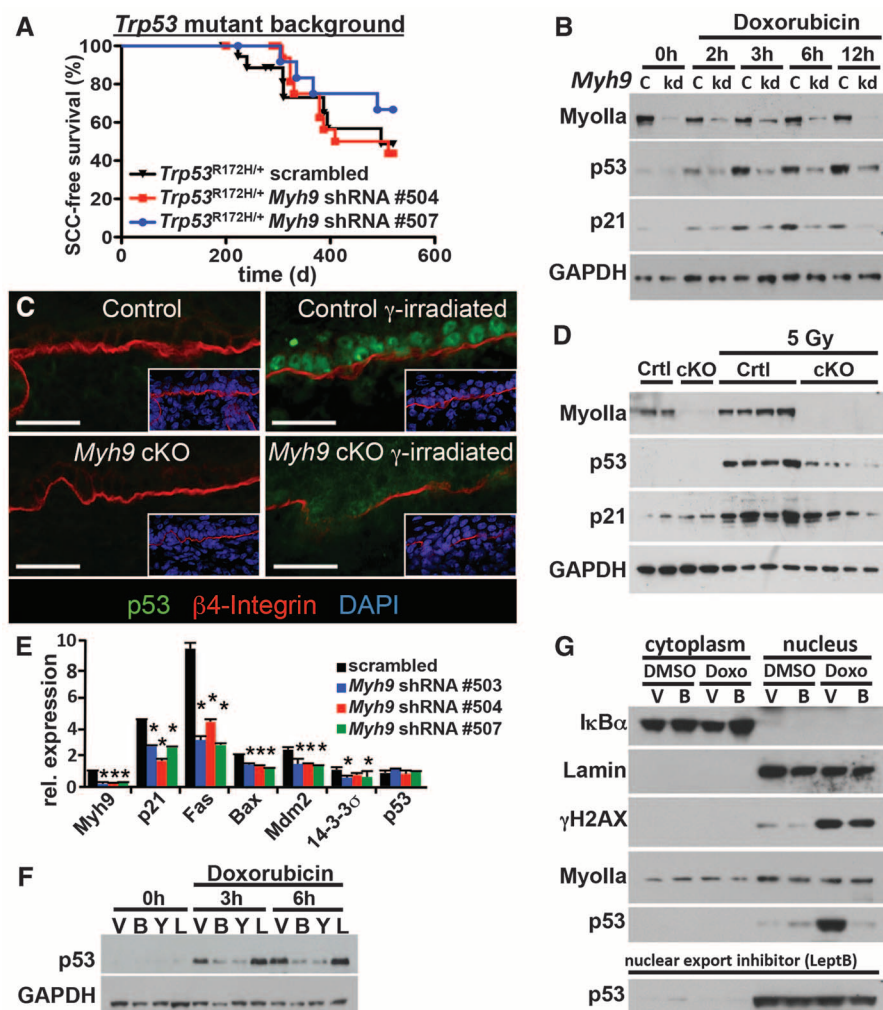


Fig. 3. A noncanonical role for myosin IIa in nuclear retention of activated p53. (A) Tumor-free survival of conditional *Trp53* mutant mice transduced with the indicated shRNA ($n > 6$ for each genotype; no significant survival change could be observed). (B) *Myh9* knockdown (kd) but not scrambled control shRNA (c) diminishes p53 and targets p21 (CDKN2) levels in response to the DDR inducer doxorubicin. Myosin IIa and GAPDH levels are shown as controls. (C and D) Lack of nuclear p53 in *Myh9*-cKO versus control (Ctrl) littermate skins 6 hours after γ irradiation (5 Gy). (C) Immunofluorescence (boxed regions show DAPI-stained nuclei in blue); (D) immunoblot analysis. Myosin IIa and GAPDH levels are shown as controls. (E) Quantitative polymerase chain reaction of p53 target genes illustrates the effects of *Myh9* knockdown on the p53 pathway. (F) p53 immunoblot of lysates from DDR-induced keratinocytes treated with vehicle (V), blebbistatin (B), Rho kinase inhibitor Y27632 (Y), or latrunculin B (L). GAPDH levels are shown as controls. (G) Nuclear p53 is not retained when DDR-induced *Myh9* knockdown primary keratinocytes are exposed to blebbistatin (B). Lamin A/C, IκBα, and γH2AX are controls for nuclear fraction, cytoplasmic fraction, and DDR, respectively. Nuclear export inhibitor leptomycin B rescues the ability of *Myh9*-deficient cells to retain p53 in the nucleus.

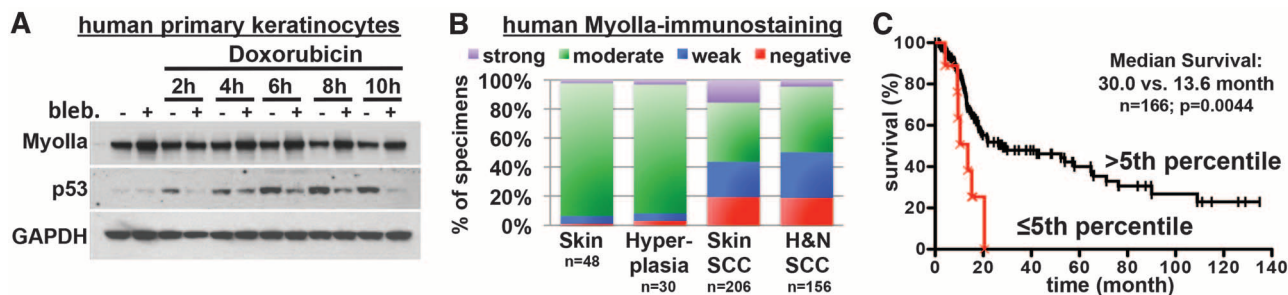


Fig. 4. *MYH9* is a bona fide tumor suppressor in human HNSCC. (A) p53 induction in primary human keratinocytes treated with the myosin ATPase inhibitor blebbistatin and with the DDR inducer doxorubicin. GAPDH levels are shown as loading control. **(B)** Myosin IIa quantifications on 362 samples of human healthy skin, skin SCCs, and HNSCCs. A substantial fraction of cases

show absent or reduced myosin IIa expression. **(C)** Decreased *MYH9* mRNA expression correlates with shortened survival. Kaplan-Meier analysis compares overall survival of TCGA HNSCC patients stratified according to the lowest (≤5th percentile) *MYH9* expression versus the rest (>5th percentile) ($n = 166$, $P = 0.0044$, log-rank test).

(Fig. 3F and fig. S17A). Consistent with a role for myosin IIa's ATPase function, inhibition of Rho kinase, an upstream regulator of myosin II's ATPase activity, similarly dampened the DNA damage-induced p53 response. However, latrunculin-mediated inhibition of F-actin polymerization did not elicit these effects, raising the tantalizing possibility that they may be independent of myosin IIa's conventional role (Fig. 3F and fig. S17B).

The initial steps of the DDR were unperturbed, as judged by stress-induced phosphorylation of the histone variant H2AX and activation of DNA checkpoint kinases Chk1 and Chk2 (fig. S17B). Additionally, *Myh9* ablation did not affect *Trp53* transcription (Fig. 3E). However, in the presence of proteasome inhibitor MG132, p53 protein levels were comparably induced by DDR in both *Myh9* knockdown and control keratinocytes (fig. S17C).

Seeking how myosin IIa deficiency might affect p53 stability, we discovered that p53's nuclear accumulation after DNA damage did not occur upon blebbistatin treatment (Fig. 3G). Inhibiting the nuclear export receptor Crm1 restored nuclear p53 accumulation as well as transactivation of p53 target genes such as p21 (Fig. 3G and fig. S17D). Thus, when myosin IIa is defective, even though the p53 pathway can be induced in response to DNA damage, it fails to do so because of an inability of p53 to remain and/or accumulate in the nucleus.

Given the possible clinical relevance of nuclear export inhibitors as a means to overcome p53 effects in myosin IIa-defective tumors, we verified that p53 activation is similarly compromised upon myosin IIa inhibition in primary human keratinocytes (Fig. 4A). We then surveyed myosin IIa's status in >350 human skin, HNSCC, and control tissues. In contrast to normal and hyperplastic skin, which consistently displayed strong immunolabeling, 24% of skin SCCs and 31% of HNSCCs showed weak or no immunolabeling (Fig. 4B and fig. S18A). Myosin IIa was diminished in a number of early-stage (grade I) SCCs, which suggests that its loss may constitute an early event in tumor progression (fig. S18B). Additionally, when skin SCCs were analyzed ac-

cording to *TβRII* and P-Smad2 status (6), a substantial fraction (~83%) of myosin IIa-negative tumors showed signs of concomitant loss of TGF-β signaling (fig. S18C). An initial analysis of The Cancer Genome Atlas (TCGA) showed that low *MYH9* mRNA expression significantly correlated with reduced survival of HNSCC patients (Fig. 4C), whereas patients with high *MYH9* mRNA expression or *MYH9* amplifications showed no survival changes (fig. S19, A to C). As larger patient cohorts are analyzed, it will be interesting to see whether this correlation proves diagnostically relevant.

Among 302 sequenced HNSCCs, 16 non-synonymous *MYH9* mutations surfaced. Computational analyses of evolutionary conservation patterns yielded a functional impact score (FIS), which assigns a probability that a specific amino acid mutation will alter protein function (11). Intriguingly, 15 out of 16 of these *MYH9* mutations gave a high or medium FIS score (fig. S20), and when all TCGA mutations were ranked according to FIS, *MYH9* ranked 16th among the ~15,000 genes mutated in HNSCCs ($P = 0.000026$, false discovery rate $q = 0.024$) and *MYH9* was found to be mutated above background also in some other cancers (fig. S21A and tables S2 and S3).

Although this cohort of cancer-associated *MYH9* mutations is relatively small, they showed statistically significant clustering to the highly conserved ATPase switch II region (fig. S20A; $P = 0.0015$). One conserved mutation (Ala⁴⁵⁴) was already known to compromise ATPase activity in *Dictyostelium* myosin II (12). Using site-directed point mutagenesis, we further corroborated the relevance of several other human mutants. Notably, although *MYH9* Glu⁴⁷⁵ → Lys and Glu⁵³⁰ → Lys mutants retained their ability to localize to stress fibers, they exerted dominant-negative effects on DDR-induced p53 activation (fig. S22).

Given that *Myh9* heterozygosity increased SCC susceptibility in mouse epithelia (Fig. 2C), it was also intriguing that ~15% of all HNSCCs showed hemizygous *MYH9* loss. Monoallelic *MYH9* loss was also common (~30%) in several other cancers (table S4). That said, no significant correlation existed between *MYH9* hemizygosity

or *MYH9* mutations and poor HNSCC prognosis (fig. S19, D and E). Hence, although provocative, these findings await further experimental and clinical evaluation.

Finally, contrary to our expectations, *MYH9* mutations in human HNSCCs were not mutually exclusive with *Trp53* mutations (mostly gain-of-function). Although such mutual exclusiveness with oncogenic alteration of established p53 regulators (e.g., MDM2 amplifications) can exist (e.g., among glioblastomas), this paradigm does not apply to HNSCCs (fig. S23). We speculate that in HNSCCs, p53 gain-of-function mutations could confer additional effects beyond inactivation of wild-type p53, such as metastasis promotion.

Like any RNAi screen, our strategy relied on knockdown efficiency and hence invariably missed some relevant genes (e.g., *Trp53*). It also missed such genes as *Notch1*, which functions nonautonomously in SCC progression (13). These caveats aside, this methodology evaluated function within the native environment, prior to gross perturbations in tissue architecture that invariably accompany cancer progression. This unearthed some lower-penetrance genes hitherto not associated with cancer. At first glance, the inverse relation between a well-known actin-based mechanosensitive motor and metastatic SCCs was puzzling, as dominant active Rho kinase and/or extracellular matrix stiffness can promote transformation in some cell lines and animal models (14). Although primary human cancer cells are considerably more pliable (15), and indeed our results document transforming potential, myosin IIa's most striking link to cancer appears to be in a newfound role in regulating p53 stabilization and nuclear retention. These findings highlight the utility of in vivo RNAi (16) to integrate cancer genomics and mouse modeling for rapid discovery, validation, and functional characterization of potent but low-penetrance tumor suppressors.

References and Notes

1. C. R. Leemans, B. J. Braakhuis, R. H. Brakenhoff, *Nat. Rev. Cancer* **11**, 9–22 (2011).
2. N. Stransky et al., *Science* **333**, 1157–1160 (2011).
3. N. Agrawal et al., *Science* **333**, 1154–1157 (2011).

4. S. Beronja, G. Livshits, S. Williams, E. Fuchs, *Nat. Med.* **16**, 821–827 (2010).
5. T. R. Berton *et al.*, *Oncogene* **22**, 5415–5426 (2003).
6. G. Guasch *et al.*, *Cancer Cell* **12**, 313–327 (2007).
7. S. L. Lu *et al.*, *Genes Dev.* **20**, 1331–1342 (2006).
8. M. Schober, E. Fuchs, *Proc. Natl. Acad. Sci. U.S.A.* **108**, 10544–10549 (2011).
9. C. Caulin *et al.*, *J. Clin. Invest.* **117**, 1893–1901 (2007).
10. D. Schramek *et al.*, *Nat. Genet.* **43**, 212–219 (2011).
11. B. Reva, Y. Antipin, C. Sander, *Nucleic Acids Res.* **39**, e118 (2011).
12. C. T. Murphy, R. S. Rock, J. A. Spudich, *Nat. Cell Biol.* **3**, 311–315 (2001).
13. S. Demehri, A. Turkoz, R. Kopan, *Cancer Cell* **16**, 55–66 (2009).
14. C. C. DuFort, M. J. Paszek, V. M. Weaver, *Nat. Rev. Mol. Cell Biol.* **12**, 308–319 (2011).
15. A. Fritsch *et al.*, *Nat. Phys.* **6**, 730–732 (2010).
16. S. Beronja *et al.*, *Nature* **501**, 185–190 (2013).

Acknowledgments: We thank members of the Fuchs laboratory for helpful discussions, especially C. Luxenburg for helpful experimental suggestions and S. Dewell for deep sequencing; S. Karlsson for TβRII^{fl/fl} mice; and T. Golub for sharing HNSCC data with us prior to publication. Special thanks go to the TCGA patients, the TCGA Program, and the cBio Portal for Cancer Genomics. D.S. is an Emerald Foundation Young Investigator. D.S. was supported by the American Association for Cancer Research and the Austrian Program for Advanced Research and Technology of the Austrian Academy of Sciences. D.S. and A.S. are fellows of the

Human Frontier Science Program Organization. E.F. is an Investigator of the Howard Hughes Medical Institute. Supported by NIH grant R37-AR27883 (E.F.) and Emerald Foundation Inc. The Rockefeller University has applied for a patent regarding the use of nuclear export inhibitors for the treatment of human squamous cell carcinomas, with D.S. and E.F. as inventors.

Supplementary Materials

www.sciencemag.org/content/343/6168/309/suppl/DC1
Materials and Methods

Figs. S1 to S23

Tables S1 to S4

References (17–41)

18 November 2013; accepted 13 December 2013

10.1126/science.1248627

Vaccine Activation of the Nutrient Sensor GCN2 in Dendritic Cells Enhances Antigen Presentation

Rajesh Ravindran,^{1*} Nooruddin Khan,^{1,2*} Helder I. Nakaya,^{1,3} Shuzhao Li,¹ Jens Loebbermann,¹ Mohan S. Maddur,¹ Youngja Park,⁴ Dean P. Jones,⁵ Pascal Chappert,^{6,7} Jean Davoust,^{6,7} David S. Weiss,⁸ Herbert W. Virgin,⁹ David Ron,¹⁰ Bali Pulendran^{1,3,†}

The yellow fever vaccine YF-17D is one of the most successful vaccines ever developed in humans. Despite its efficacy and widespread use in more than 600 million people, the mechanisms by which it stimulates protective immunity remain poorly understood. Recent studies using systems biology approaches in humans have revealed that YF-17D–induced early expression of general control nonderepressible 2 kinase (GCN2) in the blood strongly correlates with the magnitude of the later CD8⁺ T cell response. We demonstrate a key role for virus-induced GCN2 activation in programming dendritic cells to initiate autophagy and enhanced antigen presentation to both CD4⁺ and CD8⁺ T cells. These results reveal an unappreciated link between virus-induced integrated stress response in dendritic cells and the adaptive immune response.

Systems biological analysis of the immune response to the yellow fever vaccine in humans has identified early transcriptional signatures in the blood, which predict the magnitude of the later CD8⁺ T cell response to the vaccine (1). One of the genes contained within these signatures is the general control nonderepressible 2 kinase (GCN2)/EIF2AK4 (fig. S1), raising the possibility that GCN2 may be involved in the CD8⁺ T cell responses to YF-17D (1). GCN2 is a sensor of amino acid starvation in mam-

mals and orchestrates the so-called integrated stress response (2–4). During amino acid starvation, GCN2 regulates protein synthesis through phosphorylation of eukaryotic translation initiation factor 2α (eIF2α) at Ser⁵¹ (5). The phosphorylation of eIF2α attenuates assembly of the active preinitiation translational complex eIF2-GTP-tRNA^{Met} and polysome formation, resulting in stress granule formation (6). Recent work has also shown an antiviral effect of GCN2 against viruses (7–9) and in regulating the survival and proliferation of T cells (10, 11), but whether GCN2 mediates innate control of adaptive immunity is not clear. We have dissected the mechanisms through which GCN2 controls the antigen-specific T cell responses to YF-17D.

To determine whether YF-17D induces a stress response, we analyzed stress granule formation in human monocyte-derived dendritic cells (hMDCs) and baby hamster kidney (BHK) cells after YF-17D stimulation. Stress granules formed in response to YF-17D activation in vitro (Fig. 1, A and B). Further, Western blot analysis after culture with YF-17D revealed phosphorylation of eIF2α in mouse bone marrow–derived dendritic cells (BMDCs) (Fig. 1C) and phosphorylation of GCN2 (Fig. 1D) and eIF2α (Fig. 1D) in hMDCs after 1 hour. This rapid activation of GCN2 in vitro

is different from the kinetics (d7) of the transcriptional signature observed in YF-17D vaccines (fig. S1), which is likely caused by an acute viremia in vivo.

YF-17D–induced eIF2α phosphorylation was largely reduced by ultraviolet or heat inactivation of the virus, suggesting a requirement for live virus (fig. S2). Further, certain Toll-like receptor (TLR) ligands [CpG1826 and lipopolysaccharide (LPS), but not polyinosinic:polycytidylic acid] were capable of phosphorylating eIF2α (fig. S3). Myeloid differentiation primary response gene 88 (MyD88) is a universal adaptor for TLR activation. Because YF-17D signals via multiple TLRs (12), we determined whether TLR signaling was necessary for phosphorylation of eIF2α using *MyD88*^{−/−} mice. There was a partial reduction in eIF2α phosphorylation in DCs from *MyD88*^{−/−} mice compared with wild-type mice (fig. S4), suggesting that YF-17D induces eIF2α phosphorylation also independently of TLR.

Next, we analyzed whether GCN2 is necessary for the antigen-specific CD8⁺ T cell response to YF-17D using mice deficient in GCN2 (10). GCN2-deficient (*GCN2*^{−/−}) animals did not have any noticeable deficiencies in weight or appearance and had similar frequencies and numbers of immune-cell subsets (figs. S5 and S6). However, after vaccination with YF-17D the frequencies of interferon-γ (IFN-γ)–producing CD8⁺ T cells were substantially reduced in the liver and lung of *GCN2*^{−/−} mice (Fig. 2, A and B). In contrast to the robust responses in the liver and lung, responses were lower in the other organs but were nevertheless substantially reduced in *GCN2*^{−/−} mice, as assayed by a 4-day peptide restimulation culture (figs. S7 and S8). Furthermore, the kinetics of the responses was similar in wild-type and *GCN2*^{−/−} mice (fig. S8). In addition, the CD4⁺ T cell responses were also markedly reduced in *GCN2*^{−/−} mice (Fig. 2C and fig. S7), demonstrating a role for GCN2 in the induction of T cell immunity to YF-17D.

To determine whether GCN2 deficiency in the hematopoietic compartment resulted in impaired immune responses, we generated bone marrow chimeras. There was a substantial defect in antigen-specific CD8⁺ T cell response in wild-type animals reconstituted with *GCN2*^{−/−} bone marrow, as compared with those reconstituted

¹Emory Vaccine Center, Yerkes National Primate Research Center, Emory University, 954 Gatewood Road, Atlanta, GA 30329, USA. ²Department of Biotechnology, School of Life Sciences, University of Hyderabad, Hyderabad 500046, India. ³Department of Pathology and Laboratory Medicine, Emory University, Atlanta, GA 30322, USA. ⁴College of Pharmacy, Korea University, 339-700 Korea. ⁵Department of Medicine, Division of Pulmonary, Allergy and Critical Care, Emory University, Atlanta, GA 30322, USA. ⁶Institut National de la Santé et de la Recherche Médicale U1013, Paris, France. ⁷Université Paris Descartes, Sorbonne Paris Cité, Paris 75743 Paris Cedex 15, France. ⁸Department of Medicine, Division of Infectious Diseases, Emory University, Atlanta, GA 30329, USA. ⁹Department of Pathology and Immunology, Washington University School of Medicine, St. Louis, MO 63110, USA. ¹⁰University of Cambridge Metabolic Research Laboratories and NIHR Cambridge Biomedical Research Centre, Cambridge CB2 0QQ, UK.

*These authors contributed equally to this work.

†Corresponding author. E-mail: bpulend@emory.edu

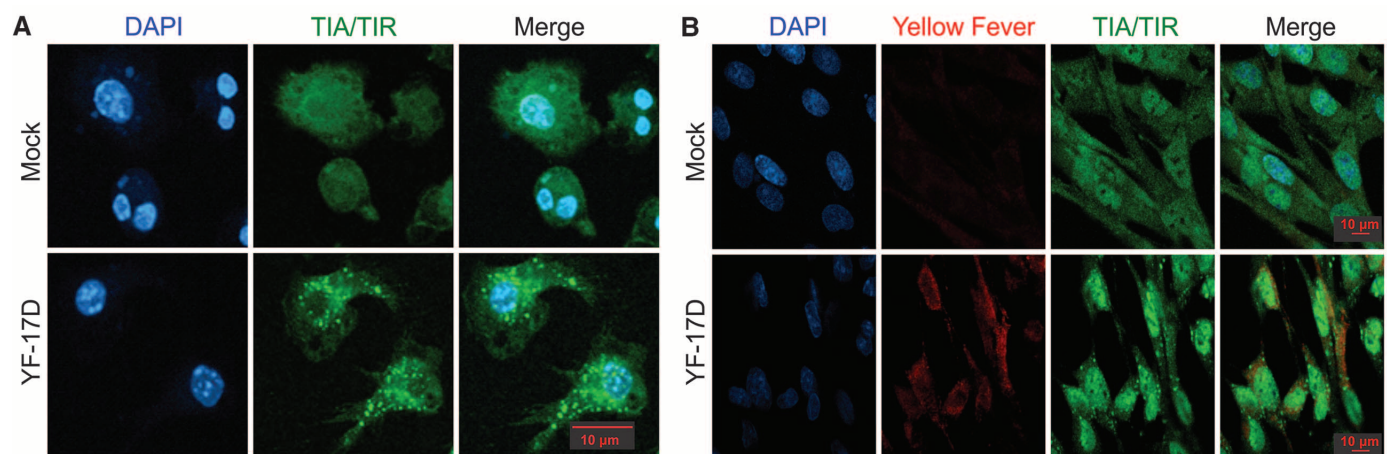


Fig. 1. YF-17D induces activation of the GCN2/eIF2 α -mediated stress response in DCs. (A) hmDCs or (B) BHK cells were mock-treated or cultured with YF-17D (24 hours), fixed, stained with TIA/TIR and 4',6-diamidino-2-phenylindole to visualize stress granule formation. Mouse BMDCs (C) or hmDCs (D) were mock-treated or cultured with YF-17D for the times indicated. "Media" represents cells not exposed to the virus. (C and D) Phosphorylation of GCN2 and eIF2 α was assessed by means of Western blotting.

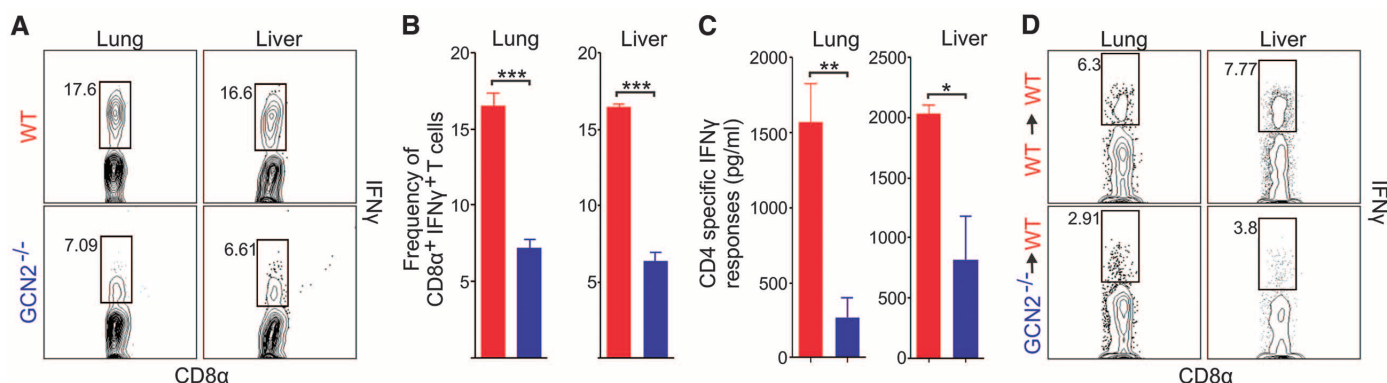
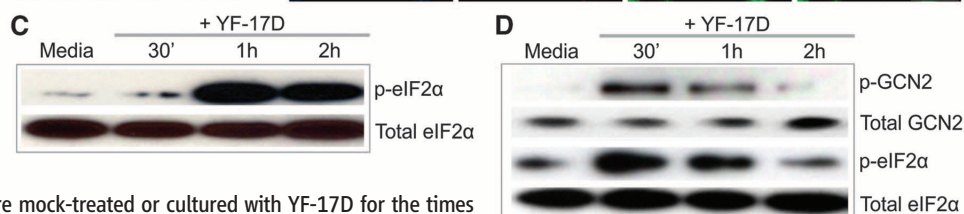
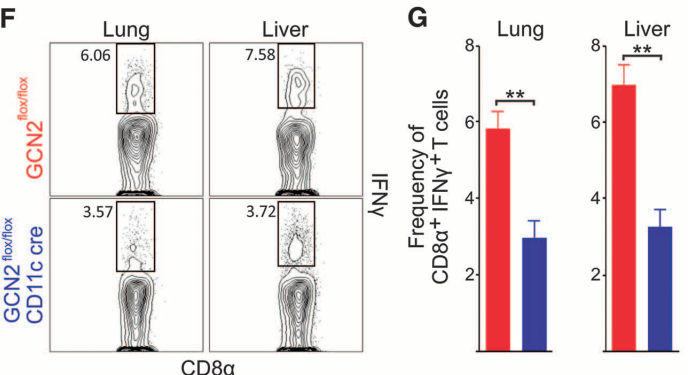


Fig. 2. Lack of GCN2 in dendritic cells leads to impaired CD8 $^{+}$ and CD4 $^{+}$ T cell responses to YF-17D. Mice were immunized subcutaneously with 2×10^6 plaque-forming units of YF-17D and euthanized on day 7. The magnitude of YF-17D-specific CD8 T cells was determined in the lung and liver with flow cytometry. (A and B) Representative fluorescence-activated cell sorting (FACS) plots (A) and frequencies (B) of CD8 $^{+}$ T cells producing IFN- γ in the lung and liver of wild-type versus *GCN2* $^{-/-}$ mice. (C) Assessment of YF-17D-specific CD4 $^{+}$ T cells producing IFN- γ in culture after 4-day ex vivo restimulation with class II restricted peptides from YF-17D. (D and E) Representative FACS plots gated on CD8 $^{+}$ T cells producing IFN- γ (D) and frequencies (E) of CD8 $^{+}$ T cells producing IFN- γ in the lung and liver of chimeric mice in which the hematopoietic compartment of wild-type mice was reconstituted with bone marrow from either wild-type or *GCN2* $^{-/-}$ mice. (F and G) Representative FACS plots gated on CD8 $^{+}$ T cells producing IFN- γ in the



lung and liver of *GCN2* $^{flx/flx} \times CD11c$ cre versus littermate control mice. In (E), (F), and (G), red indicates wild type, and blue indicates *GCN2* $^{-/-}$. The graphs represent the averages of CD8 $^{+}$ IFN- γ -producing cells in the liver and lung in 5 mice per group. Data are representative of four independent experiments. *** $P < 0.0005$; ** $P < 0.005$; * $P < 0.05$, calculated by Student's t test. Graphs show mean \pm SEM.

with wild-type bone marrow (Fig. 2, D and E, and fig. S9). To determine whether GCN2 expression in DCs is required for YF-17D-specific CD8⁺ T cell responses, we compared immunized GCN2^{fl/fl} CD11c-cre mice [in which GCN2 was ablated in DCs (fig. S10)] and observed reduced frequencies of IFN- γ -producing CD8⁺ T cells in the lung and liver, as compared with that of littermate controls (Fig. 2, F and G).

To investigate the mechanism by which GCN2 expression in DCs controls T cell responses, we

compared cytokine production by DCs from wild-type and GCN2^{-/-} mice, cultured in vitro with YF-17D. Induction of the inflammatory cytokines interleukin-6 (IL-6), tumor necrosis factor (TNF), IL-12, IL-1 β , or anti-inflammatory IL-10 (fig. S11) or antiviral IFN α (fig. S12) was unaffected by GCN2 deficiency. Furthermore, there was no difference in the induction of costimulatory molecules in vivo in response to vaccination with YF-17D (fig. S13) or in the uptake of soluble antigens (figs. S14 and S15).

Because GCN2 is a sensor of amino acid starvation (4), we determined whether YF-17D induced an amino acid starvation response in DCs. We used liquid chromatography/mass spectrometry (LC/MS) to analyze the intracellular concentration of free amino acids. Culture of hmDCs with YF-17D resulted in a rapid decrease of the intracellular concentration of free arginine and several other amino acids and a corresponding increase in citrulline (Fig. 3A). Arginine metabolism can lead to enhanced citrulline levels, a process catalyzed

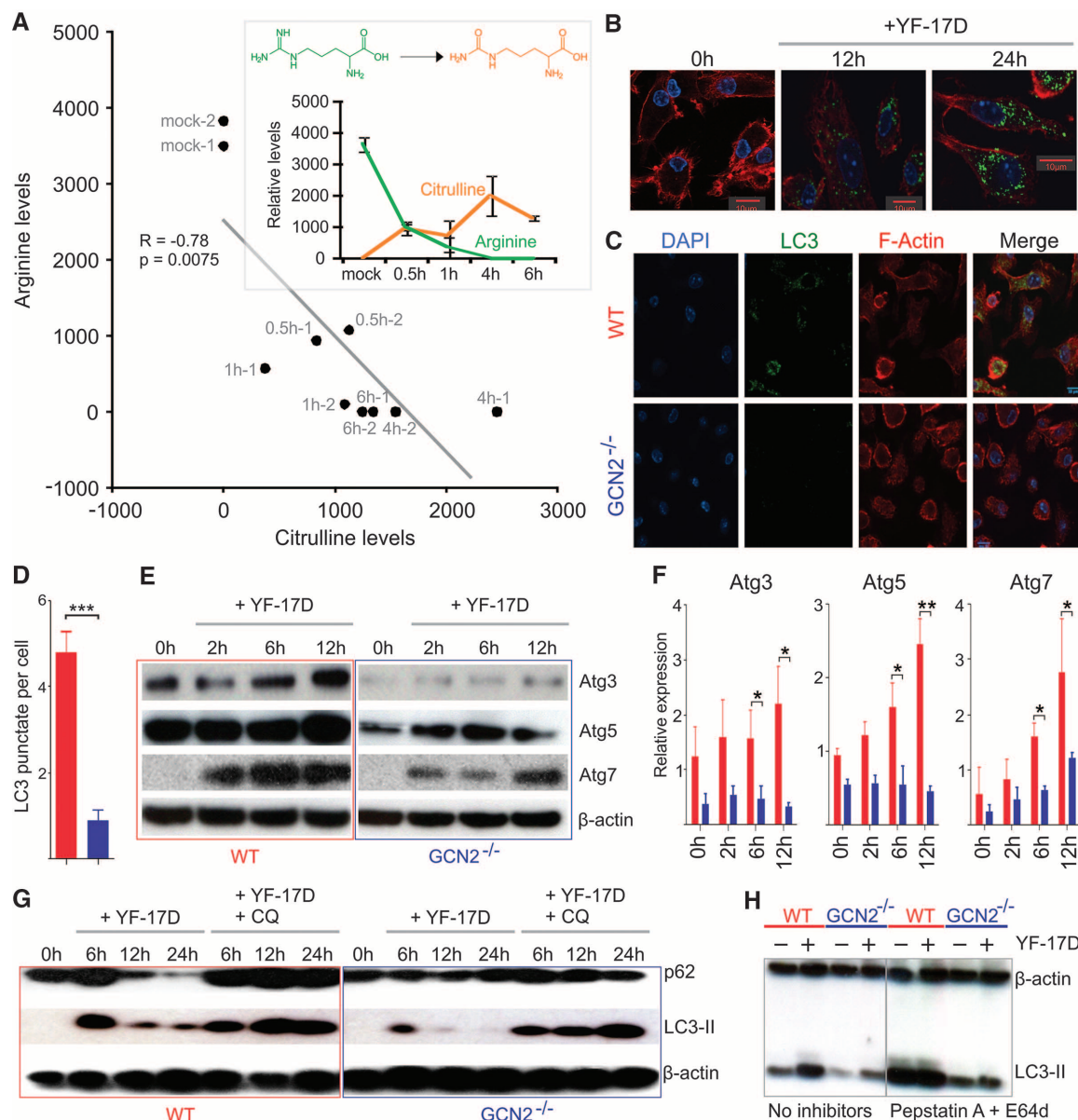


Fig. 3. YF-17D induces autophagy in dendritic cells via a mechanism dependent on GCN2. (A) Inverse correlation between the concentrations of free arginine and citrulline in hmDCs stimulated with YF-17D. Mock-treated DCs at 6 hours (without virus) are shown as controls. (Inset) Mean relative abundance \pm SD of arginine and citrulline. (B) Culture of hmDCs with YF-17D induces autophagy as visualized by means of confocal microscopy. (C) Comparison of autophagy (LC3 punctate staining) in mBMDs from wild-type or GCN2^{-/-} mice, cultured in vitro with YF-17D for 6 hours. (D) Counts of LC3 granules per cell. (E) Comparison of the autophagy proteins in BMDC from wild-type or GCN2^{-/-} mice

cultured in vitro with YF-17D. 0h represents 30 min after DCs are cultured in low volume of low fetal bovine serum medium with YF-17D. Basal levels of Atg5 and Atg7 in freshly isolated DC were similar in wild-type and GCN2^{-/-} mice (fig. S20). (F) Densitometric analysis of Western blots from three independent experiments. (G) Autophagy flux experiments depicting p62 and LC3II accumulation by chloroquine after culture with YF-17D. (H) Autophagy flux showing accumulation of LC3II 6 hours after YF-17D culture after treatment with lysosomal inhibitors (pepstatin and E64D). Data are representative of three independent experiments. * $P < 0.05$; ** $P < 0.005$, Student's t test. Error bars indicate mean \pm SEM

by nitric oxide synthase. Decreased intracellular concentrations of free amino acids, including arginine, leads to increased concentrations of uncharged transfer RNA molecules, which bind to the C terminus of GCN2 and induce its activation (13, 14). Consistent with changes in the concentrations of free amino acids, enzymes that are known to be important in amino acid metabolism were induced by YF-17D in DCs (fig. S16). Heat-killed or ultraviolet-irradiated YF-17D did not induce a noticeable reduction in amino acid concentrations, suggesting a requirement for live virus in this process.

Under conditions of amino acid deprivation, cells activate a homeostatic mechanism, called autophagy, that can effectively generate new amino acids and redirect the cell to use its limited amino acid supply specifically for the synthesis of essential proteins (15). GCN2 is a major sensor for amino acid deprivation in mammalian cells (4), and GCN2-deficient yeast are defective in induced autophagy (16). In this context, the expression of

genes encoding autophagy-related proteins in peripheral blood mononuclear cells from humans vaccinated with YF-17D (1) correlated with the magnitude of the later CD8⁺ T cell responses (fig. S17). Consistent with this, culture of hmDCs (Fig. 3B) or mBMDCs (Fig. 3C) with YF-17D induced autophagy, as evidenced with visualization of autophagic vesicles (punctate LC3 staining). Furthermore, YF-17D induced autophagy in mBMDCs from LC3-GFP mice [in which the gene encoding green fluorescent protein (GFP) is fused with the gene encoding LC3 autophagosome marker, the mammalian homolog of Atg8 (17)] (fig. S18, A and B). To address whether induction of autophagy was dependent on GCN2, we examined YF-17D-induced autophagy in wild-type versus *GCN2*^{-/-} mice (Fig. 3, C to H). In *GCN2*^{-/-} mBMDCs, induction of autophagy was reduced as compared with that in DCs from wild-type mice, as assessed with immunofluorescence (Fig. 3, C and D) or Western blot (Fig. 3, E and F).

In addition, reverse transcription polymerase chain reaction analyses revealed a marked reduction in the expression of genes encoding proteins involved in autophagy in *GCN2*^{-/-} DCs compared with wild-type DC stimulated from YF-17D (fig. S19). This was not due to baseline differences in autophagy proteins because basal expression of Atg5 and Atg7 in mBMDCs was identical in the absence of stimulation with YF-17D (fig. S20).

p62 and LC3-II accumulation are surrogate markers of autophagy because of their degradation after the fusion of the autophagosome to the lysosome (18). We therefore investigated the lysosomal turnover of endogenous p62 and LC3-II during virus-induced autophagy using either chloroquine (Fig. 3G) or the lysosomal protease inhibitors E64d plus pepstatin A, inhibitors of autophagy degradation (Fig. 3H). We observed greater accumulation of LC3-II (Fig. 3, G and H) and p62 (Fig. 3G) in the presence of these inhibitors in wild-type cells than in *GCN2*^{-/-} cells. Thus,

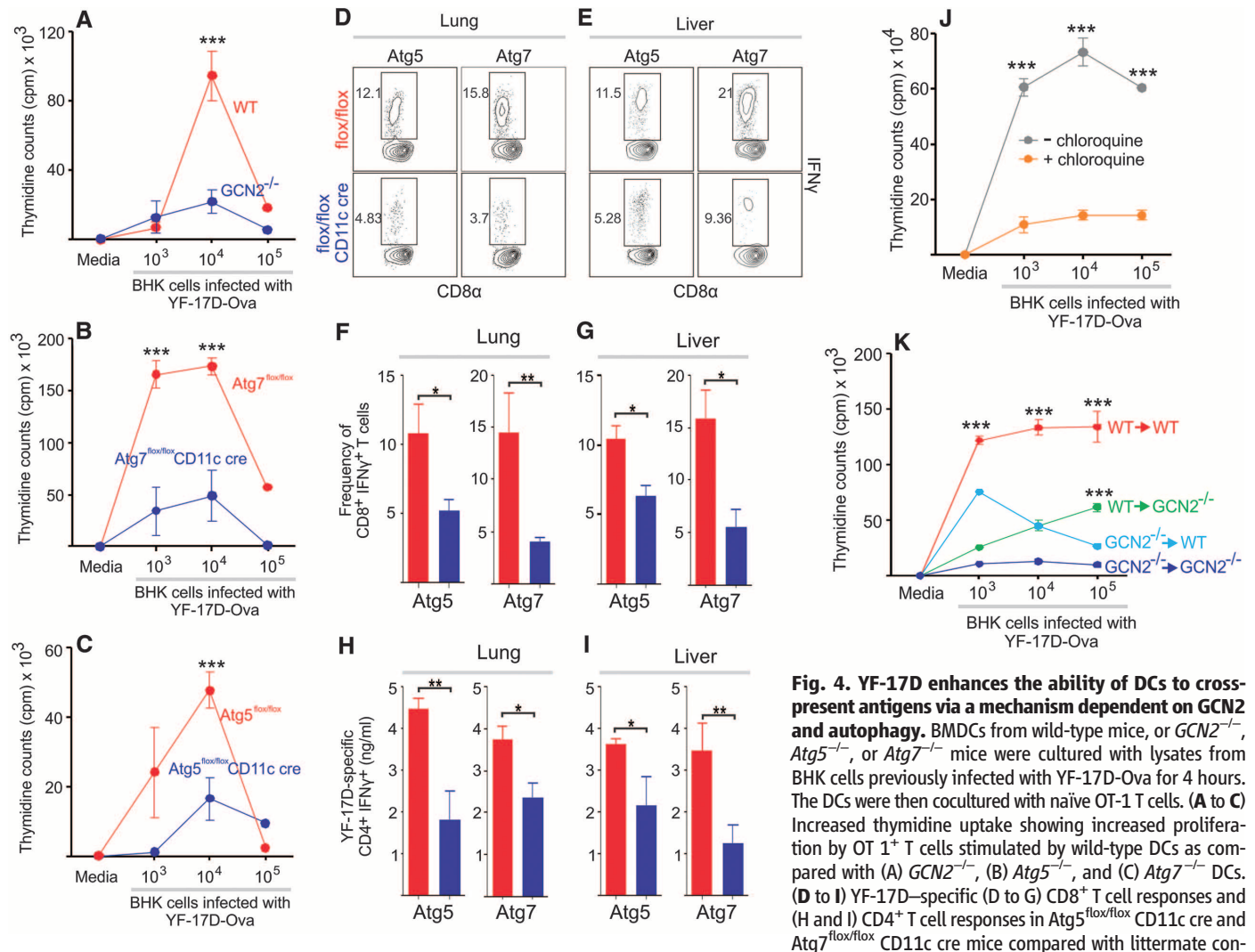


Fig. 4. YF-17D enhances the ability of DCs to cross-present antigens via a mechanism dependent on GCN2 and autophagy. BMDCs from wild-type mice, or *GCN2*^{-/-}, *Atg5*^{-/-}, or *Atg7*^{-/-} mice were cultured with lysates from BHK cells previously infected with YF-17D-Ova for 4 hours. The DCs were then cocultured with naïve OT-1 T cells. (A to C) Increased thymidine uptake showing increased proliferation by OT-1 T cells stimulated by wild-type DCs as compared with (A) *GCN2*^{-/-}, (B) *Atg5*^{-/-}, and (C) *Atg7*^{-/-} DCs. (D to I) YF-17D-specific (D to G) CD8⁺ T cell responses and (H and I) CD4⁺ T cell responses in *Atg5*^{flox/flox} CD11c cre and *Atg7*^{flox/flox} CD11c cre mice compared with littermate controls 7 days after vaccination with YF-17D. (J) Inhibition of autophagy by chloroquine results in impaired cross-presentation. (K) MEFs from either wild-type or *GCN2*^{-/-} mice were first infected with YF-17D-Ova and then irradiated and then cocultured with either wild-type or *GCN2*^{-/-} BMDCs. Then OT-1 T cells were added, and their proliferation was evaluated 72 hours later. Representative of three individual experiments. ****P* < 0.0005; ***P* < 0.005; **P* < 0.05, calculated by Student's *t* test. Graphs show mean ± SEM.

these data demonstrate that induction of autophagy by YF-17D in DCs is controlled by GCN2.

Autophagy is known to affect antigen presentation by DCs (19, 20). Effective priming of CD8⁺ T cells by viral antigens involves the pathways that are active in both direct presentation of endogenous antigens and cross presentation of exogenous antigens (21, 22). Recent reports have implicated a role for autophagy in antigen presentation via both class II (23, 24) and class I (19, 25, 26). We thus hypothesized that *GCN2*^{-/-} DCs that are defective in autophagy may be impaired in their capacity to present antigens to T cells. In particular, viral antigens are cross-presented by DCs to CD8⁺ T cells (22), and given the impaired CD8⁺ T cell immunity to YF-17D, we determined whether cross-presentation of YF-17D antigens was impaired in *GCN2*^{-/-} mice. For this, lysates from YF-17D-Ova-infected BHK cells were cultured with BMDCs (precultured for 2 hours in low amino acid medium in order to induce the stress response) from wild-type or *GCN2*^{-/-} mice. The DCs were then washed and cultured with naïve, antigen-specific CD8⁺ T cell receptor transgenic T cells from OT-1 mice. The proliferation of antigen-specific CD8⁺ T cells was monitored by their ability to divide and incorporate thymidine. *GCN2*^{-/-} DCs had a lower ability to induce T cell proliferation in vitro, indicating a critical role for GCN2 in cross presentation (Fig. 4A). Antigen-specific responses were similar when transgenic OT1 T cells were cultured with either wild-type or *GCN2*^{-/-} BMDCs pulsed with SIINFEKL peptide (fig. S21), suggesting that DCs from *GCN2*^{-/-} DCs were not intrinsically defective at presenting peptide antigens to CD8⁺ T cells. Furthermore, direct antigen presentation of endogenous antigens was unaffected by GCN2 deficiency in DCs (fig. S22).

Atg5 and Atg7 are essential proteins required for autophagosome formation (27, 28). To examine the DC intrinsic effects of Atg-5 and Atg-7 deficiency, we used DC-specific conditional knockouts (fig. S23, A and B). BMDCs isolated from these mice or littermate controls were initially cultured for 2 hours in low amino acid medium and then cocultured with lysates from BHK cells that had been previously infected with YF-17D-Ova (29). The BMDC loaded with YF-17D-Ova-infected BHK were then cultured with transgenic naïve OT-1 T cells, and proliferation was monitored by their ability to incorporate thymidine (Fig. 4, B and C). DCs from Atg-5- and Atg-7-deficient mice were impaired in their capacity to cross-present antigens (Fig. 4, B and C). Consistent with this, BMDCs from mice deficient in beclin-1—a protein necessary for Atg-5/Atg-7-dependent and independent-autophagy (30)—were impaired in their capacity to cross-present antigens from viral infected cells (fig. S24). A previous study demonstrates that Atg5 activity in DCs is not essential for cross-presentation of splenocytes coated with ovalbumin, in the absence of any viral stimulus or without any starvation (23). Consistent with our results, an analysis of the YF-17D-specific CD8⁺ and CD4⁺ T responses

in the Atg5- and Atg7-conditional knockout mice revealed lower immune responses as compared with that of littermate controls (Fig. 4, D to I), and inhibiting autophagy with chloroquine resulted in lower cross-presentation (Fig. 4J). The results indicate that Atg5 and Atg7 expression on DCs is critical to prime CD8⁺ T and CD4⁺ T cells under starvation conditions.

GCN2-mediated induction of autophagy could operate in DCs (the “cross-presenting” cells) or in neighboring cells that were infected by YF-17D (“donor” cells) and taken up by DCs (fig. S25). Enhanced autophagy on dying donor cells taken up by antigen-presenting cells can stimulate efficient cross-presentation (25). To dissect the putative roles of GCN2 in the donor versus cross-presenting cell, wild-type or *GCN2*^{-/-} DCs were cultured with cell lysates from wild-type or *GCN2*^{-/-} mouse embryonic fibroblasts (MEFs) infected with YF-17D-Ova and assayed for their ability to prime OT-1 T cells (Fig. 4K). The Ova-specific responses were the highest when both the MEFs and DCs are of wild-type origin. These responses were lower when either the MEFs or DCs were from the *GCN2*^{-/-} mice. The lowest proliferative responses were seen in the cocultures that had MEFs and DCs from the *GCN2*^{-/-} mice indicating a key role for GCN2 on both the dying and the phagocytosing cell. The results indicate that Atg5 and Atg7 expression on DCs is critical to prime CD8 T cells under starvation conditions. One caveat of these experiments is the use of YF-17D encoding a surrogate antigen rather than viral antigens.

These data suggest that GCN2-mediated activation of autophagy programs DCs to cross-present viral antigen to CD8⁺ T cells. Components of the autophagy machinery including Atg5 and Atg7 have recently been implicated in recognition and clearance of dead cells by a process known as LC3-associated phagocytosis (LAP) (31). It is likely that depletion of free amino acids induced by the initiation of viral replication or an innate response triggered by live viral entry leads to the activation of GCN2, which then induces autophagy and antigen presentation. Consistent with this, inactivated virus was unable to induce amino acid depletion. The question of how autophagy intersects the cross-presentation pathway at the cell biological level (such as through degradation of autophagosomal cargo or LAP or both) remains to be determined.

Last, in order to determine whether this mechanism was more generally relevant to other viruses or microbes, we analyzed the role of GCN2 in eliciting immune responses to other pathogens (fig. S26). We saw a role for GCN2 in antigen-specific CD8 T cell responses to the live attenuated influenza vaccine (fig. S27). We could not detect any differences between wild-type and *GCN2*^{-/-} mice in the immune responses to various other pathogens (fig. S26).

Taken together, these results demonstrate a role for GCN2 activation in DCs in modulating the adaptive immune response. This may have evolved as a mechanism of pathogen sensing that is capable of detecting “footprints” of a pathogen,

such as depleted amino acids in a local microenvironment in vivo. Furthermore, such a mechanism may be relevant in the induction of immunity against tumors, in which rapidly proliferating tumor cells may cause a depletion of amino acids in the local microenvironment. In addition, this mechanism may affect immunity to vaccination during amino acid malnutrition in humans. Last, vaccine adjuvants that activate the GCN2-autophagy pathway may be useful in inducing robust T cell responses in humans.

References and Notes

1. T. D. Querec *et al.*, *Nat. Immunol.* **10**, 116–125 (2009).
2. A. G. Hinnebusch, *Proc. Natl. Acad. Sci. U.S.A.* **81**, 6442–6446 (1984).
3. R. Sood, A. C. Porter, D. A. Olsen, D. R. Cavener, R. C. Wek, *Genetics* **154**, 787–801 (2000).
4. S. Hao *et al.*, *Science* **307**, 1776–1778 (2005).
5. J. Lu, E. B. O'Hara, B. A. Trieselmann, P. R. Romano, T. E. Dever, *J. Biol. Chem.* **274**, 32198–32203 (1999).
6. P. Anderson, N. Kedersha, *Cell Stress Chaperones* **7**, 213–221 (2002).
7. J. Krishnamoorthy, Z. Mounir, J. F. Raven, A. E. Koromilas, *Cell Cycle* **7**, 2346–2351 (2008).
8. J. J. Berlanga *et al.*, *EMBO J.* **25**, 1730–1740 (2006).
9. S. Won *et al.*, *J. Virol.* **86**, 1802–1808 (2012).
10. D. H. Munn *et al.*, *Immunity* **22**, 633–642 (2005).
11. S. P. Cobbald *et al.*, *Proc. Natl. Acad. Sci. U.S.A.* **106**, 12055–12060 (2009).
12. T. Querec *et al.*, *J. Exp. Med.* **203**, 413–424 (2006).
13. D. Ron, *J. Clin. Invest.* **110**, 1383–1388 (2002).
14. R. C. Wek, H. Y. Jiang, T. G. Anthony, *Biochem. Soc. Trans.* **34**, 7–11 (2006).
15. B. Levine, N. Mizushima, H. W. Virgin, *Nature* **469**, 323–335 (2011).
16. Z. Tallóczy *et al.*, *Proc. Natl. Acad. Sci. U.S.A.* **99**, 190–195 (2002).
17. N. Mizushima, A. Kuma, *Methods Mol. Biol.* **445**, 119–124 (2008).
18. D. J. Klionsky *et al.*, *Autophagy* **4**, 151–175 (2008).
19. L. English *et al.*, *Nat. Immunol.* **10**, 480–487 (2009).
20. V. L. Crotzer, J. S. Blum, *J. Immunol.* **182**, 3335–3341 (2009).
21. J. M. den Haan, M. J. Bevan, *Curr. Opin. Immunol.* **13**, 437–441 (2001).
22. M. J. Bevan, *Nat. Immunol.* **7**, 363–365 (2006).
23. H. K. Lee *et al.*, *Immunity* **32**, 227–239 (2010).
24. D. Schmid, M. Pypaert, C. Münz, *Immunity* **26**, 79–92 (2007).
25. M. Uhl *et al.*, *Cell Death Differ.* **16**, 991–1005 (2009).
26. S. K. Tey, R. Khanna, *Blood* **120**, 994–1004 (2012).
27. A. Kuma *et al.*, *Nature* **432**, 1032–1036 (2004).
28. M. Komatsu *et al.*, *J. Cell Biol.* **169**, 425–434 (2005).
29. A. McAllister, A. E. Arbetman, S. Mandl, C. Peña-Rossi, R. Andino, *J. Virol.* **74**, 9197–9205 (2000).
30. C. Münz, *Viruses* **3**, 1166–1178 (2011).
31. J. Martinez, K. Verbist, R. Wang, D. R. Green, *Cell Metab.* **17**, 895–900 (2013).

Acknowledgments: This work was supported by grants from the U.S. National Institutes of Health (grants R37 DK057665, R37 AI048638, U19 AI090023, U19 AI057266, U54 AI057157, N01 AI50019, and N01 AI50025) and from the Bill & Melinda Gates Foundation to B.P., a Wellcome Trust Principal Research Fellowship (084812/Z/08/Z) to D.R., and NIH grant U54 AI057160 to H.W.V. We thank B. Cervasi and K. Gill for help with sorting and D. Levesque, D. Bonenberger, and colleagues for animal husbandry. The data presented in this manuscript are tabulated in the main paper and the supplementary materials.

Supplementary Materials

www.sciencemag.org/content/343/6168/313/suppl/DC1
Materials and Methods
Figs. S1 to S27
Table S1
References

4 October 2013; accepted 20 November 2013
Published online 5 December 2013;
10.1126/science.1246829



cell sciences
cytokine center



www.cellsciences.com

Buy one, get one free

Stock up now on select cytokines, growth factors and chemokines.

Order any two vials from this list for just \$235

Enter promo code CYT241 when you place your order on-line or mention the promo code to get your discount when calling our toll-free number 888-769-1246.

These recombinant proteins are low endotoxin, carrier-free, highly pure, biologically active and suitable for cell culture and animal studies. Get two of the same item or pick any two different items from the list.* See our web site for complete product specifications.

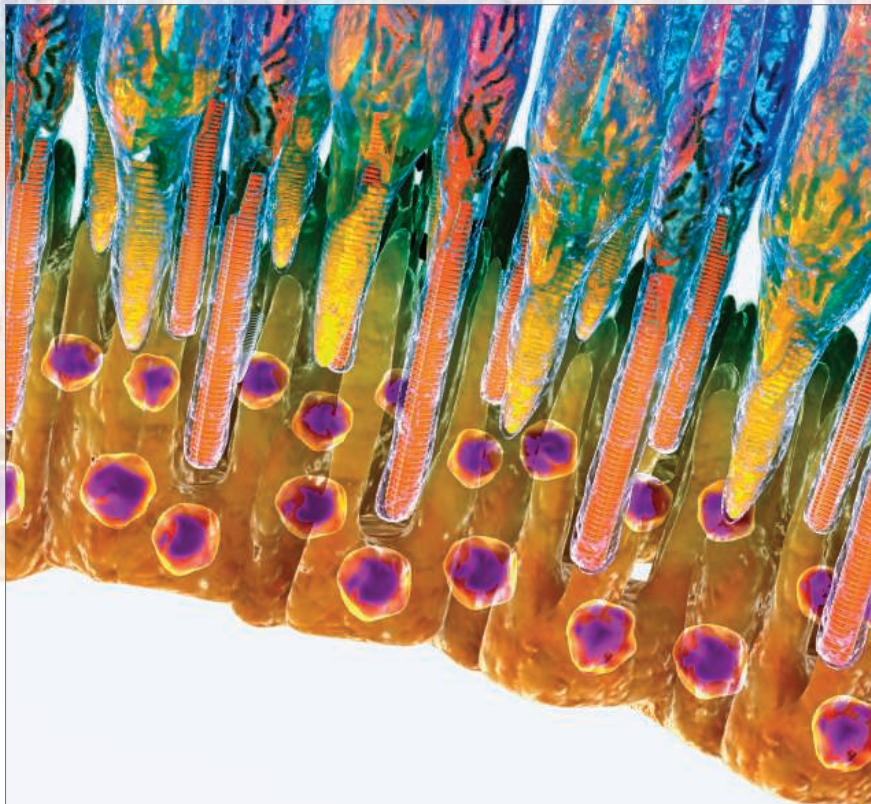
Browse our web site of recombinant proteins, including hundreds more cytokines, growth factors, chemokines and neurotrophins. Bulk quantities of these proteins are available at competitive pricing. Call or visit our web site for details. Cell Sciences also carries corresponding antibodies and ELISA kits.

Catalog No:	Item:	Size:
CRB100B	Recombinant Human BMP-2	10 µg
CRC400B	Recombinant Human CNTF	20 µg
CRF000B	Recombinant Human FGF-acidic/FGF1	50 µg
CRF001B	Recombinant Human FGF-basic/FGF2	50 µg
CRK300B	Recombinant Human FGF-7/KGF	10 µg
CRG300B	Recombinant Human G-CSF/CSF3	10 µg
CRG100B	Recombinant Human GM-CSF/CSF2	20 µg
CRG101B	Recombinant Mouse GM-CSF/CSF2	20 µg
CRG500B	Recombinant Human GRO-alpha/CXCL1	25 µg
CRG502B	Recombinant Rat GRO-alpha/KC/CXCL1	25 µg
CRI004B	Recombinant Human IFN-alpha 2b	100 µg
CRI000B	Recombinant Human IFN-gamma	100 µg
CRI001B	Recombinant Mouse IFN-gamma	100 µg
CRI002B	Recombinant Rat IFN-gamma	100 µg
CRI500B	Recombinant Human IGF-1	100 µg
CRI100B	Recombinant Human IL-2	50 µg
CRI153B	Recombinant Human IL-10	10 µg
CRI137B	Recombinant Human IL-15	10 µg
CRI162B	Recombinant Human IL-17	25 µg
CRI172B	Recombinant Human IL-21	10 µg
CRI225B	Recombinant Human IL-33	10 µg
CRM151B	Recombinant Human M-CSF/CSF1	10 µg
CRR000B	Recombinant Human RANTES/CCL5	20 µg
CRS000B	Recombinant Human SDF-1 alpha	10 µg
CRS002B	Recombinant Human SDF-1 beta	10 µg
CRT100B	Recombinant Human TNF-alpha	50 µg
CRT192B	Recombinant Mouse TNF-alpha	20 µg
CRV000B	Recombinant Human VEGF 165	10 µg
CRV014B	Recombinant Mouse VEGF 165	10 µg

* Good on orders in US and Canada only. This offer may not be combined with other offers or discounts. All products for research use only.

CELL SCIENCES INC • 480 NEPONSET STREET, BUILDING 12A, CANTON, MA 02021 • INFO@CELLSCIENCES.COM

TOLL FREE: (888) 769-1246 • TEL: (781) 828-0610 • FAX: (781) 828-0542 • WEB WWW.CELLSCIENCES.COM



The Scientific World Journal

Hindawi Publishing Corporation
<http://www.hindawi.com>

Volume 2014



Hindawi

- ▶ Impact Factor **1.730**
- ▶ **28 Days** Fast Track Peer Review
- ▶ All Subject Areas of Science
- ▶ Submit at <http://www.tswj.com>

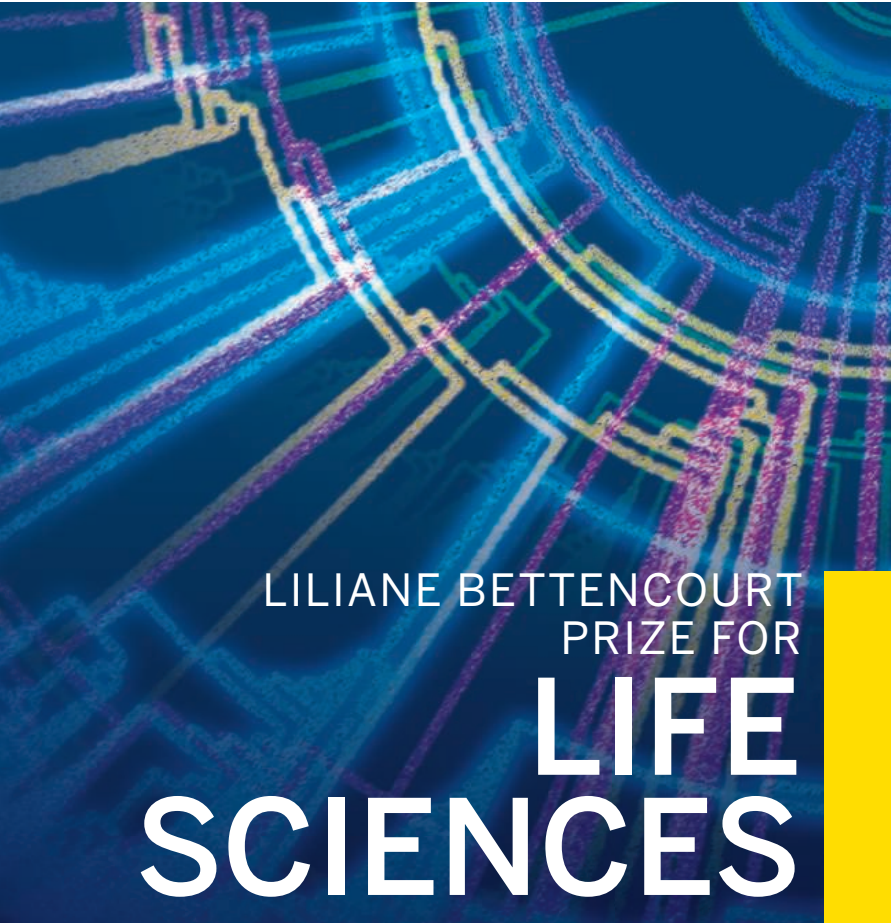
Clone with Confidence.

Whether you are performing your first cloning experiment, or constructing multi-fragment gene assemblies, NEB[®] has the solution for you. Our high quality reagents are available for every workflow, and include specialized enzymes, competent cells, and novel solutions – such as Gibson Assembly[®]. When you are looking to clone with confidence, think of NEB.

Explore the wise choice at
CloneWithNEB.com.

Visit **CloneWithNEB.com** to view online tutorials describing various cloning workflows.





LILIANE BETTENCOURT PRIZE FOR LIFE SCIENCES



2013 PRIZE WINNER MONSEF BENKIRANE

Monsef Benkirane is Research Director at the CNRS Institute of Human Genetics in Montpellier. He is head of the Molecular Bases of Human Diseases Department and leader of the Molecular Virology team. Having obtained a doctorate in Immunology at the University of Aix-Marseille in 1994, Monsef Benkirane worked for four years at the National Institute of Health in Bethesda (USA). Upon his return to France in 1998, he set up a research group in Montpellier dedicated to molecular virology and HIV. In the course of his research, Monsef Benkirane's team made a major breakthrough in our understanding of HIV/host interaction, particularly in understanding viral persistence and cell resistance to HIV. His team identified SAMHD1 gene as the HIV-1 restriction factor in myeloid and quiescent CD4+ T-Cells. This protein prevents dendritic cells, which are responsible for triggering a defensive immune response, from being infected by HIV, thus preventing the virus from being detected as pathogenic.

Monsef Benkirane's current projects aim at understanding the role of SAMHD1 in viral pathogenesis and deciphering the molecular mechanisms of HIV persistence *in vivo* which is important for the development of HIV cure strategies.

The 17th Liliane Bettencourt Prize for Life Sciences was awarded to **Monsef Benkirane**, Director of Research at the CNRS Institute of Human Genetics in Montpellier, Head of the Molecular Bases of Human Diseases Department and leader of the Molecular Virology team.

The Liliane Bettencourt Prize for Life Sciences, worth € 250,000, has been awarded every year since 1997 to a European researcher under the age of 45, who is recognised within the scientific community for the quality of his international publications. In addition to his status as an author and leader in his own scientific field, the candidate must be leading a particularly promising research project and have the personal qualities for mobilising an entire team.

Recognised in 1987 as a public interest foundation, the Bettencourt Schueller Foundation was set up by Liliane, André Bettencourt and their daughter Françoise Bettencourt Meyers, in memory of Eugène Schueller, a renowned researcher and chemist. Its goal is to constantly expand the boundaries of knowledge in the life sciences in order to improve public health; to reveal talent and pass on expertise within the field of artistic creativity; and to relieve suffering, combat exclusion and respond to social welfare emergencies.

Fondation Bettencourt Schueller

27-29 rue des Poissonniers • 92200 Neuilly-sur-Seine • France
www.fondationbs.org • Contact: sciences@fondationbs.org



FONDATION
BETTENCOURT
SCHUELLER

Brave New RNA World

The discovery of RNAi revealed an entire layer of previously unknown gene regulation; new tools are helping more scientists analyze and manipulate this system to probe the secret lives of cells.

See full story on page 328.

Upcoming Features

Proteomics—February 21

Toxicology—March 14

Genomics—April 11



AAAS Travels

KAMCHATKA & Lake Baikal



**Including the
Trans-Siberian Express
July 18–August 2, 2014**

Explore the two finest natural areas in Russia, the Kamchatka Peninsula and Lake Baikal, and take the Trans-Siberian Express from the Russian Far East across the vast taiga of Russia to Irkutsk and Lake Baikal. Baikal is the richest single location in Russia for endemism, a fabulous reservoir of unique flora and fauna. It is the oldest and deepest lake in the world, and stores nearly 20% of the fresh-water on earth. \$5,995 + air.

**For a detailed brochure,
please call (800) 252-4910**

All prices are per person twin share + air



BETCHART EXPEDITIONS Inc.
17050 Montebello Rd, Cupertino, CA 95014
Email: AAASInfo@betchartexpeditions.com
www.betchartexpeditions.com

For your career in science, there's only one

Science

Introducing myIDP: A career plan customized for you, by you.

- The first and only online app that helps scientists prepare their very own individual development plan.
- Recommended by leading professional societies and the NIH.
- Developed by scientists at FASEB, UCSF, and the Medical College of Wisconsin in collaboration with AAAS and *Science* Careers, with support from the Burroughs Wellcome Fund.



Visit the website and
start planning today!
myIDP.sciencecareers.org





Join Us in Chicago

Learn about the science and technology that is addressing current and future global challenges.

- Seminars on innovation, entrepreneurship, and the economy; big data; communicating science; and food security and sustainability.
- 150+ symposia in 16 disciplinary tracks covering the latest research advances.
- Connect with colleagues in all fields of science, technology, and engineering and attend career development workshops.

Browse full program and register:
www.aaas.org/meetings

Connect with us



@AAASmeetings #AAASmtg



www.facebook.com/AAAS.Science

Reporters: The EurekAlert! website hosts the AAAS Annual Meeting Newsroom. Reporters can obtain details and register at www.eurekalert.org/newsroom



ADVANCING SCIENCE, SERVING SOCIETY

AAAS presents the

2014 AAAS ANNUAL MEETING

MEETING GLOBAL CHALLENGES: DISCOVERY AND INNOVATION



Dear Colleagues,

On behalf of the AAAS Board of Directors, it is my honor to invite you to join us in Chicago for the 2014 AAAS Annual Meeting, 13–17 February. This annual event is one of the most widely recognized global science gatherings, with hundreds of diverse scientific sessions and communication opportunities with broad U.S. and international media coverage.

This year's theme—*Meeting Global Challenges: Discovery and Innovation*—will focus on finding sustainable solutions through inclusive, international, and interdisciplinary efforts that are most useful to society and enhance economic growth.

Scientific discovery and innovation are driving solutions to current and future global challenges, including sufficient food, quality healthcare, renewable fuels, and a sustainable environment. Addressing these challenges depends upon international dialogue and discoveries emerging from the convergence of physical, life, engineering, and social sciences in innovative ways that are most useful to society. The scientific program will highlight the increasing interdependence of economic progress and advances in science and technology.

Everyone is welcome at the AAAS Annual Meeting. Those who attend will have the opportunity to choose among a broad range of activities, including plenary and topical lectures by some of the world's leading scientists and engineers, multidisciplinary symposia, cutting-edge seminars, career development workshops, and an international exhibition. You and your family can also enjoy Family Science Days, a free event open to the public.

The Annual Meeting reflects tremendous efforts from the AAAS sections, divisions, and committees. I also acknowledge the members of the Scientific Program Committee who selected and assembled the many excellent ideas and proposals into this outstanding meeting.

We look forward to seeing you in Chicago.

Phillip A. Sharp
AAAS President and Program Chair
Institute Professor, Koch Institute for Integrative Cancer Research
Massachusetts Institute of Technology



President's Address

Thursday, 13 February



Phillip A. Sharp

Institute Professor, Koch Institute for Integrative Cancer Research, Massachusetts Institute of Technology

Dr. Sharp, a noted molecular biologist with a focus on the genetic causes of cancer, shared the 1993 Nobel Prize in Physiology or Medicine for his discovery of “split genes”—the finding that genes could be composed of several separate segments within DNA. His lab now focuses on the therapeutic potential of RNA interference, small RNA molecules that can switch genes on and off. He has co-founded two companies: Biogen (now Biogen Idec) and Alnylam Pharmaceuticals. He received a Ph.D. in chemistry from the University of Illinois at Urbana-Champaign and is an elected member of the National Academy of Sciences, the Institute of Medicine, AAAS, the American Academy of Arts and Sciences, the American Philosophical Society, and a foreign fellow of the Royal Society (U.K.).

Plenary Speakers

Friday, 14 February



Steven Chu

Professor of Physics and Molecular and Cellular Physiology, Stanford University

How Discovery and Innovation Can Meet Our Energy Challenge

Dr. Chu served as the 12th U.S. Secretary of Energy between January 2009 and April 2013. Prior to his post in President Obama's Cabinet, he was the director of

Lawrence Berkeley National Laboratory and a professor at University of California, Berkeley. He had previously worked at Stanford University and Bell Laboratories. Chu is the co-recipient of the Nobel Prize for Physics (1997) for his contributions to the laser cooling and trapping of atoms. His other areas of research include tests of fundamental theories in physics, atom interferometry, study of polymers and biological systems at the single molecule level, and biomedical research. The holder of 10 patents, Chu has published 250 scientific and technical papers. Chu is a member of the National Academy of Sciences, the American Philosophical Society, the Royal Academy of Engineering, the Academia Sinica, and the Korean Academy of Sciences and Technology, an honorary member of the Institute of Physics and the Chinese Academy of Sciences, and a Lifetime Member of the Optical Society of America. He received a bachelor's degree in physics from the University of Rochester and a Ph.D. in physics from the University of California, Berkeley.

Saturday, 15 February



Alan Alda

Visiting Professor of Journalism, Stony Brook University

Getting Beyond a Blind Date with Science

Alan Alda is an actor, writer, director, and visiting professor at the Alan Alda Center for Communicating Science at Stony Brook University, where he helps current and future scientists learn to communicate more clearly and vividly with the public. In collaboration with theater arts faculty at Stony Brook, he is pioneering the use of improvisational theater exercises to help scientists connect more directly with

people outside their field. Alda is best known for his award-winning work in movies, theater, and television, but he also has a distinguished record in the public communication of science. For 13 years he hosted the PBS series *Scientific American Frontiers*, which he has called “the best thing I ever did in front of a camera.” After interviewing hundreds of scientists around the world, he became convinced that many researchers have wonderful stories but need to learn how to tell them better. That realization inspired the creation of Stony Brook's multidisciplinary Alan Alda Center for Communicating Science in 2009.

Sunday, 16 February



Susan Lindquist

Professor of Biology, Massachusetts Institute of Technology

From Yeast Cells to Patient Neurons: A Powerful Discovery Platform for Parkinson's and Alzheimer's Diseases

Dr. Lindquist is a pioneer in understanding protein folding, showing that these changes can have profound and unexpected influences in human disease, evolution, and nanotechnology. She is a member of the Whitehead Institute, where she served as director from 2001 to 2004, and a Howard Hughes Medical Institute investigator. Previously she was a professor of medical sciences and molecular biology at University of Chicago. Lindquist is an elected fellow of the American Academy of Arts and Sciences, the National Academy of Sciences, the Institute of Medicine, and the American Philosophical Society. She is a recipient of the Novartis/Drew Award for Biomedical Research, the Dickson Prize in Medicine, the Sigma Xi William Procter Prize for Academic Achievement, the Nevada Silver Medal for Scientific

CONTINUED >



Achievement, the Genetics Society of America Medal, and the Centennial Medal of the Harvard University Graduate School of Arts and Sciences. In 2010, she received the Mendel Medal from the Genetics Society (U.K.), the Delbruck Medal from Bayer Schering, and the National Medal of Science. She is a member of the scientific advisory board of the Institute for Molecular Biotechnology in Austria. Lindquist is a co-founder of FoldRx Pharmaceuticals, Inc., a subsidiary of Pfizer, Inc.

Monday, 17 February



John A. Rogers

Swanlund Chair and Professor of Materials Science and Engineering, University of Illinois, Urbana-Champaign

Stretchy Electronics That Dissolve in Your Body

Dr. Rogers' research includes fundamental and applied aspects of nano- and molecular scale fabrication. He also studies materials and patterning techniques for unusual electronic and photonic devices, with an emphasis on bio-integrated and bio-inspired systems. He received a Ph.D. in physical chemistry from Massachusetts Institute of Technology in 2005. He has published more than 350 papers and is an inventor on over 80 patents and patent applications, many of which are licensed or in active use by large companies and startups that he co-founded. He previously worked for Bell Laboratories as director of its research program in condensed matter physics. He has received recognition including a MacArthur Fellowship from the John D. and Catherine T. MacArthur Foundation, the Lemelson-MIT Prize, the National Security Science and Engineering Faculty Fellowship from the U.S. Department of Defense, the George Smith Award from IEEE, the Robert Henry Thurston Award from American Society of Mechanical Engineers, the Mid-Career Researcher Award from Materials Research Society, the Leo Hendrick Baekeland Award from the American Chemical Society, and the Daniel Drucker Eminent Faculty Award from the University of Illinois.

Topical Lectures



Cori Bargmann

Torsten N. Wiesel Professor, Rockefeller University
Using Fixed Circuits to Drive Variable Behaviors



Eli Finkel

Professor of Psychology and Management and Organizations, Northwestern University
The Suffocation of Marriage



Heinrich Jaeger

William J. Friedman and Alicia Townsend Professor of Physics, University of Chicago
Granular Matter: From Basic Questions to New Concepts and Applications



Trevor Mundel

President, Global Health Program, Bill and Melinda Gates Foundation
The Surprising Complexity of Simple Health Solutions and the Importance of Measurement in Global Health



Edward Roberts

David Sarnoff Professor of Management of Technology, Massachusetts Institute of Technology
Entrepreneurial Impact of Science and Technology-Based Universities



Amy Smithson

Senior Fellow, James Martin Center for Nonproliferation Studies
Scientists and (the Ultimate) Responsibility



Diana Wall

University Distinguished Professor of Biology, Colorado State University
Lessons from an Antarctic Desert: Documenting Climate Change and Measuring Impact on Soil Life

GEORGE SARTON MEMORIAL LECTURE IN THE HISTORY AND PHILOSOPHY OF SCIENCE



Susan Lederer

Robert Turell Professor of Medical History and Bioethics, University of Wisconsin, Madison
The Living and the Dead: Biomedical Science, American Society, and the Human Body

JOHN P. MCGOVERN AWARD LECTURE IN THE BEHAVIORAL SCIENCES



Susan T. Fiske

Eugene Higgins Professor of Psychology and Public Affairs, Princeton University
Humans are Intent Detectors: Implications for Society

Special Sessions

International Public Science Events Conference

Wednesday, 12 February–Thursday, 13 February
 Pre-registration required

Responsible Professional Practices in a Changing Research Environment Workshop

Thursday, 13 February
 Pre-registration required



Seminars

Thursday, 13 February

Communicating Science

Scientific and technological issues increasingly trigger societal conflicts whenever they intersect with personal or political views. Today's scientists and engineers are challenged to communicate and engage with the public and journalists, particularly amid pressures on research and development budgets and related concerns about transparency and accountability. This seminar will share science communication expertise in working with different types of content, across a range of formats, for various audiences.

Engaging with Journalists

Collaborator: Kavli Foundation and AAAS Kavli Science Journalism Awards
Moderator: Cornelia Dean, *The New York Times* and Brown University, New York City

SPEAKERS

Robert Lee Hotz, *The Wall Street Journal*, New York City
Carl Zimmer, Independent Science Journalist, Guilford, CT
Paula Apsell, NOVA, Boston, MA
David Baron, Public Radio International, Boulder, CO

Engaging with Social Media

Moderator: Dominique Brossard, University of Wisconsin, Madison

SPEAKERS

Kim Cobb, University of Georgia, Atlanta
Navigating the Science-Social Media Space: Pitfalls and Opportunities
Danielle N. Lee, Cornell University, New York City
Raising STEM Awareness Among Under-Served and Under-Represented Audiences
Maggie Koerth-Baker, BoingBoing.net, Minneapolis, MN
What's the Point of Social Media?

Engaging with Public Events

Collaborator: Science Festival Alliance and the International Public Science Events Conference
Moderator: Ben Lillie, The Story Collider, New York City

SPEAKERS

Rabiah Mayas, Museum of Science and Industry, Chicago, IL

Never Too Young: Museum-Based Approaches to Connecting Youth with Scientists

Kishore Hari, Bay Area Science Festival, San Francisco, CA
The Science Education Melting Pot

Amy Rowat, University of California, Los Angeles
Engaging General Audiences in Science Through Interactive Events

Friday, 14 February

Innovation, Entrepreneurship, and the Economy

This seminar will consider opportunities for innovation and entrepreneurship to benefit the economy. Dynamic examples of innovation and challenges in advanced manufacturing and biomedical research will be considered, and strategies to encourage entrepreneurship activity will be explored.

New Business Models for Accelerating Biomedical Innovation

Organized by: Andrew W. Lo, Massachusetts Institute of Technology, Cambridge

SPEAKERS

John McKew, National Center for Advancing Translational Science (NCATS), Rockville, MD
NCATS: Catalyzing Innovation
Pablo Legorreta, Royalty Pharma, New York City
Drug Royalty Investment Companies as Catalysts for Innovation
Bruce Lehmann, University of California, San Diego
Some Simple Economics for Early Stage Drug Development

Science-Driven Entrepreneurship: Determined Pursuit of Innovative Success

Organized by: Anice Anderson, Private Engineering Consulting, Carmel, IN

SPEAKERS

John M. Newsam, Tioga Research Inc., San Diego, CA
Launching a Science-Based Enterprise with an Organic Growth Model
Irwin Jacobs, Qualcomm, San Diego, CA
Qualcomm: From Startup to Leadership in Technology and the Social Impact of 6.6 Billion Wireless Connections
Han Cao, BioNano Genomics Inc., San Diego, CA
Commercializing Innovation: Applying Nanotechnology to Genomics

Organizing the Innovation System for Advanced Manufacturing

Organized by: Stephanie Shipp, Virginia Tech, Arlington; William B. Bonvillian, Massachusetts Institute of Technology, Cambridge

SPEAKERS

Hod Lipson, Cornell University, Ithaca, NY
The Future of 3D Printing: Promise and Peril of a Machine that Can Make (Almost) Anything
Rodney Brooks, Rethink Robotics, Boston, MA
Robotics as a Transformative Manufacturing Technology: Status and Future
Jonas Nahm, Massachusetts Institute of Technology, Cambridge
The Manufacturing Economies in China and Germany: Technology and Process Systems
Suzanne Berger, Massachusetts Institute of Technology, Cambridge
Defining the Innovation Ecosystem for Advanced Manufacturing
Theresa Kotanchek, Evolved Analytics Inc., Midland, MI
Implementing the Advanced Manufacturing Partnership: Progress and Remaining Gaps
Jason Miller, White House National Economic Council, Washington, DC
National Manufacturing Institutes: What Are the Innovation Design Lessons?

Saturday, 15 February

Big Data: Applications and Implications

Innovations in big data are providing challenging new ways to understand large datasets with a wide range of potential applications from biology and medicine to research on urban environments. Realizing the benefits of big data will require an understanding of scientific, legal, policy, and societal implications.

How Big Data Supports Biomedical Discovery

Organized by: Robert L. Grossman, University of Chicago, IL

SPEAKERS

Brian D. Athey, University of Michigan, Ann Arbor
The transSMART Open Data Sharing and Analytics Cloud Platform
Lincoln Stein, Ontario Institute for Cancer Research, Toronto, Canada
The Cancer Genome Collaboratory

Robert L. Grossman, University of Chicago, IL
*Supporting a Biomedical Commons with the
Bionimbus Protected Data Cloud*

Data Availability: Making Sure the Gift Keeps Giving

Organized by: Clifford Spiegelman, Texas A&M University, College Station

SPEAKERS

David Reitze, California Institute of Technology, Pasadena

Big Science, Big Data, Big Challenges: Data from Large-Scale Physics Experiments

Matt Ehling, Public Record Media, St. Paul, MN
Access to Government Data: Examining and Overcoming Barriers

Catherine Grosso, Michigan State University, East Lansing
Finding Data: The Politics and Magic of Accessing Capital Punishment Data

A New Era for Urban Research: Open Data and Big Computation

Organized by: Charlie Catlett, Argonne National Laboratory, IL

SPEAKERS

Philip Enquist, Skidmore, Owings and Merrill, Chicago, IL
Cities, Livability, and Responsibility to the Planet

Steven E. Koonin, New York University Center for Urban Science and Progress, Brooklyn
The Promise of Urban Science

Karen Weigert, City of Chicago, IL
Science-Driven Sustainability Policies in Chicago

Andrew Yao, Tsinghua University, Beijing, China
Urban Sensing and Informatics

Robert Sampson, Harvard University, Cambridge, MA
Ecometrics in the Age of Big Data: Measuring Urban Social Processes and Inequality

Mario Small, University of Chicago, IL
Poverty and Organizational Density

Sunday, 16 February

Food Security and Sustainability

Transformative solutions for sustainable food production are needed as global population approaches 9 billion by 2050 and climate change alters environmental landscapes and resources. The importance of undertaking agricultural research that enables governments to meet food demands and reduce shortages while developing environmentally sound and sustainable food production systems will be discussed. Recent advances in

perennial grain crop development, from genomic innovations to real-world results on farms, will be conveyed.

Feeding a Growing Population While Sustaining the Earth

Organized by: Felix Kogan and Alfred M. Powell, National Oceanic and Atmospheric Administration (NOAA), College Park, MD

SPEAKERS

Thomas R. Karl, NOAA, Asheville, NC
Precipitation Changes in a Warmer World for Major Grain Growing Regions

Paul R. Ehrlich, Stanford University, CA
Feeding 9 Billion and Avoiding a Collapse of Civilization: Science's Main Challenge

Jonathan A. Foley, University of Minnesota, St. Paul
Challenges to Global Food Security and Environmental Sustainability

Felix Kogan, NOAA, College Park, MD
Overexploitation of Earth Resources, Climate Constraints and Food Security

Research and Development for Sustainable Agriculture and Food Security

Organized by: Daniel Bush, Colorado State University, Fort Collins

SPEAKERS

Jerry Hatfield, U.S. Department of Agriculture (USDA), Ames, IA
Natural Resources: The Overlooked Component in Food Security and Sustainable Agriculture

Philip Pardey, University of Minnesota, St. Paul
The Changing Global Landscape for Food and Agricultural Research and Development

Wendy Wintersteen, Iowa State University, Ames
Public-Private Partnerships to Achieve Food Security and Sustainable Agriculture

Perennial Grains for Food Security in a Changing World: Gene to Farm Innovations

Organized by: Jerry Glover, U.S. Agency for International Development (USAID), Washington, DC; Sieglinde S. Snapp, Michigan State University, Hickory Corners

SPEAKERS

Wezi Mhango, Lilongwe University of Agriculture and Natural Resources, Malawi
Shrubby Pigeon Peas Transform Malawi Farming: 1st-Generation Perennial Grain Legumes

Sieglinde S. Snapp, Michigan State University, Hickory Corners
Next Steps and Research Needs in Perennial Grain Development

Andrew Paterson, University of Georgia, Athens
Genomic Innovations for Next-Generation Perennial Grain Crops

Symposium Tracks

Agricultural, Plant, and Food Sciences

A Changing Global Landscape: Evolving Roles of BRIC Nations in Agricultural Sciences

Organized by Rodney A. Hill, University of Idaho, Moscow

Biosciences for Farming in Africa

Organized by David J. Bennett, St. Edmund's College, Cambridge, United Kingdom

Innovative and Integrated Approaches To Reducing Malnutrition

Organized by Jennifer Long and Ahmed Kablan, U.S. Agency for International Development (USAID), Washington, DC

Securing Food, Feed, and Fuel via Natural Diversity: Spotlight on the Maize Genome

Organized by Patrick Regan, Ulrich Marsch, and Barbara Wankel, Technical University Munich, Germany

Anthropology, Culture, and Language

Comparative Advantage: Global Perspectives on Human Biology and Health

Organized by Thomas McDade and William Leonard, Northwestern University, Evanston, IL

Neoracism and Scientific Racism in "Post-Racial" Societies

Organized by Nina Jablonski, Pennsylvania State University, University Park; Robert W. Sussman, Washington University, St. Louis, MO

Preserving Our Cultural Heritage: Science in the Service of Art

Organized by Leonor Sierra and Nicholas Bigelow, University of Rochester, NY

Reconstructing and Deconstructing Paintings: Innovations At and Below the Surface

Organized by Francesca Casadio, The Art Institute of Chicago, IL; Katherine Faber, Northwestern University, Evanston, IL

Rethinking Repatriation of Human Remains: Is It Possible to Move Beyond Conflict?

Organized by Norman MacLeod and Margaret Clegg, Natural History Museum, London, United Kingdom

Talking to Kids Really Matters: Early Language Experience Shapes Later Life Chances

Organized by Anne Fernald, Stanford University, CA

The Large Cognitive Implications of Small Languages

Organized by D. H. Whalen, City University of New York

Variability in Speech and Language in Individuals with Autism and Associated Traits

Organized by Alan C. Yu, University of Chicago, IL

Behavioral and Social Sciences

Building Babies: Development, Evolution, and Human Health

Organized by Katie Hinde, Harvard University, Cambridge, MA

Guns and Violence: Psychological, Economic, Political and Public Policy Implications

Organized by Martin S. Banks, University of California, Berkeley; Garen J. Wintemute, University of California, Davis; Richard N. Aslin, University of Rochester, NY

How to Rebuild Informed Trust in Science: Insights from Social Sciences

Organized by Rainer Bromme, University of Muenster, Germany

Learning about People and Society via Analysis of Large-Scale Data on Human Activities

Organized by Eric Horvitz, Microsoft Research, Redmond, WA

Physiological and Cultural Foundations of Human Social Behavior

Organized by Geraldine Barry, European Commission, Joint Research Center, Brussels, Belgium

Project Teams and Public Expenditures of Scientific Research: An International Comparison

Organized by Julia Lane, American Institutes for Research, Washington, DC

Rhythmic Entrainment in Non-Human Animals: An Evolutionary Trail of Time Perception

Organized by Patricia M. Gray, University of North Carolina, Greensboro

The Science of Resilient Aging

Organized by Elizabeth A.L. Stine-Morrow, University of Illinois, Urbana-Champaign

Using Social Science to Change Decisions and Improve Health Outcomes

Organized by Arthur Lupia, University of Michigan, Ann Arbor

Biology and Neuroscience

Addiction: Our Compulsions and Brain Reward Systems

Organized by Wilson Compton, National Institute on Drug Abuse, Bethesda, MD; Aidan Gilligan, SciCom—Making Sense of Science, Brussels, Belgium

Epigenetic Control of Brain and Behavior

Organized by Joseph Coyle, Harvard Medical School, Belmont, MA

Genetic and Epigenetic Determinants of Susceptibility to Toxicants

Organized by Berran Yucsoy, National Institute for Occupational Safety and Health, Morgantown, WV; Victor J. Johnson, Bureson Research Technologies Inc., Morrisville, NC

Intelligent Autonomous Robots: Biologically Inspired Engineering

Organized by John G. Hildebrand, University of Arizona, Tucson

Inventing New Ways To Understand the Human Brain

Organized by Hillary Sanctuary and Richard Walker, Swiss Federal Institute of Technology (EPFL), Lausanne, Switzerland; Megan Williams, Swissnex, San Francisco, CA

Molecular Basis of Age-Related Susceptibility to Chemicals and Environmental Hazards

Organized by Janice S. Lee, U.S. Environmental Protection Agency (EPA), Research Triangle Park, NC

New Insights into Animal Behavior: The Role of the Microbiome

Organized by Vanessa Ezenwa, University of Georgia, Athens; Daniel Rubenstein, Princeton University, NJ; Joy Bergelson, University of Chicago, IL

Non-Coding RNA in Development and Disease

Organized by Gary Felsenfeld, National Institute of Diabetes and Digestive and Kidney Diseases, Bethesda, MD; Jeannie T. Lee, Massachusetts General Hospital, Boston

Solitary Confinement: Legal, Clinical, and Neurobiological Perspectives

Organized by Michael J. Zigmond, University of Pittsburgh, PA

Synthetic Biology Approaches to New Chemistry

Organized by Michelle C. Chang and Jay D. Keasling, University of California, Berkeley

Video Games, Brains, and Society

Organized by Daphne Bavelier and Susan Hagen, University of Rochester, NY

Your Genome: To Share or Not To Share?

Organized by Yaniv Erlich, Whitehead Institute for Biomedical Research, Cambridge, MA

Communication and Public Programs

Improvisation for Scientists: Making a Human Connection

Organized by Valeri Lantz-Gefroh and Elizabeth Bass, Stony Brook University, NY

Innovative Vehicles for Vetted Information in a Wiki World

Organized by Sarah Bates, Society for Neuroscience, Washington, DC

Religious Communities, Science, Scientists, and Perceptions: A Comprehensive Survey

Organized by Paul Arveson and Jennifer Wiseman, AAAS Center for Science, Policy, and Society Programs, Washington, DC

Science Festivals as Regional Collaborations: Extending Resources by Working Together

Organized by Ben Wiehe, MIT Museum, Cambridge, MA

Science, Religion, and Modern Physicists: New Studies

Organized by Paul Arveson and Jennifer Wiseman, AAAS Center for Science, Policy, and Society Programs, Washington, DC

Securing the Future of Science: Using the Higgs to Inspire the Young

Organized by Timothy Meyer, TRIUMF, Vancouver, Canada; Terry O'Connor, Science and Technology Facilities Council, Swindon, United Kingdom

Stakeholder Engagement in Science: Strategies, Experiences, and Implications

Organized by Samantha J. Jones and Louis J. D'Amico, EPA, Washington, DC

Teen Cafés: Innovative Model for Effective Science Communication with Key Demographic

Organized by Michelle Hall, Science Education Solutions Inc., Los Alamos, NM

What Do People Think about Science and Technology? U.S. and International Public Opinion

Organized by John C. Besley, Michigan State University, East Lansing

Where's My Flying Car? Science, Science Fiction, and a Changing Vision of the Future

Organized by Susan Wolfenbarger and Jonathan Drake, AAAS Center for Science, Policy, and Society Programs, Washington, DC

Computer Science, Mathematics, and Statistics

Advances in Citizen Science: Large-Scale Community Engagement for Sensing and Analysis

Organized by Eric Horvitz, Microsoft Research, Redmond, WA

Elections Through the Lens of Mathematics

Organized by D. Marc Kilgour, Wilfrid Laurier University, Waterloo, Canada

Intelligent Context-Aware Systems for Healthcare, Wellness, and Assisted Living

Organized by Louise Byrne, European Commission, Research Executive Agency, Brussels, Belgium

Outsourcing Science: Will the Cloud Transform Research?

Organized by Ian Foster, Argonne National Laboratory, IL

People and Computing: On Human-Computer Collaborations for Tackling Hard Problems

Organized by Erwin P. Gianchandani, National Science Foundation (NSF), Arlington, VA; Eric Horvitz, Microsoft Research, Redmond, WA

Re-Identification Risk of De-Identified Data Sets in the Era of Big Data

Organized by Xiao Hua Andrew Zhou, University of Washington, Seattle; Leslie Taylor, VA Puget Sound Health Care System, Seattle, WA

Statistical Methods for Large Environmental Datasets

Organized by Charmaine Dean, University of Western Ontario, London, Canada

The Importance of Recreational Mathematics in Solving Practical Problems

Organized by Laura Taalman and Jason Rosenhouse, James Madison University, Harrisonburg, VA

Virtual Humans: Helping Facilitate Breakthroughs in Medicine

Organized by Ram D. Sriram, National Institute of Standards and Technology, Gaithersburg, MD; Ramesh Jain, University of California, Irvine; Donald Henson, George Washington University, Washington, DC

Education and Human Resources

Analogical Processes in STEM Learning

Organized by Dedre Gentner, Northwestern University, Evanston, IL

Beyond the Pipeline: New Strategies to Build a Competitive and Diverse Workforce

Organized by Kenneth Gibbs, NSF, Arlington, VA

Building National Capacity in Science Communication for STEM Graduate Students

Organized by Erica Goldman and Elizabeth Neeley, COMPASS, Seattle, WA

Creating an Ecosystem for Science Learning In and Out of School

Organized by Dennis Schatz, NSF, Arlington, VA; Martin Storksdieck, National Research Council, Washington, DC

Leveling the Playing Field: Why Cultural Relevance Matters in Computer Science

Organized by Legand Burge and Alicia N. Washington, Howard University, Washington, DC

Rebooting Our Approach to Increasing Indigenous STEM Participation: Lessons from Hawai'i

Organized by Timothy F. Slater, University of Wyoming, Laramie

STEM Education Policies and Policymaking: Pushing in the Same Direction

Organized by Catherine Middlecamp, University of Wisconsin, Madison; Judith A. Ramaley, Portland State University, OR

The Central Role of Energy Concepts in K-12 Science Education

Organized by Arthur Eisenkraft, University of Massachusetts, Boston

Thinking Skills for the 21st Century: Teaching for Transfer

Organized by Eleanor V.H. Vandegrift, University of Oregon, Eugene; Amy B. Mulnix, Earlham College, Richmond, IN

Use of Digital Games To Support Youth's Engagement with Science and Technology

Organized by Patricia L. Ward, Museum of Science and Industry, Chicago, IL

Women Poised for Discovery and Innovation: Resolving the Remaining Hurdles

Organized by Lynnette D. Madsen, NSF, Arlington, VA; Catherine Mavriplis, University of Ottawa, Canada

Energy and Renewable Resources

Chemistry and Materials Science of Solar Energy Utilization

Organized by John Rogers, University of Illinois, Urbana-Champaign

Hydraulic Fracturing: Science, Technology, Myths, and Challenges

Organized by Christopher B. Harto and Alfred P. Sattelberger, Argonne National Laboratory, IL

Is It Possible to Reduce 80% of Greenhouse Gas Emissions from Energy by 2050?

Organized by Jane C.S. Long, Lawrence Livermore National Laboratory, Oakland, CA; Steve Hamburg, Environmental Defense Fund, Washington, DC; Armond Cohen, Clean Air Task Force, Boston, MA

Making Power, Taking Power: Renewable Microgrids in National Electricity Strategies

Organized by Michael Isaacson, University of California, Santa Cruz

Nanoelectronics for Renewable Energy: How Nanoscale Innovations Address Global Needs

Organized by William Gilroy, University of Notre Dame, IN; Hillary Sanctuary, EPFL, Lausanne, Switzerland; Patrick Regan, Technical University Munich, Garching, Germany

Next Generation Electrical Energy Storage: Beyond Lithium Ion Batteries

Organized by Jeff Chamberlain and George Crabtree, Argonne National Laboratory, IL

Opportunities and Challenges for Nuclear Small Modular Reactors

Organized by Granger Morgan, Carnegie Mellon University, Pittsburgh, PA; Elisabeth A. Gilmore, University of Maryland, College Park

Engineering, Industry and Technology

Discovery and Innovation in Science and Engineering Security Technologies

Organized by Anice Anderson, Private Engineering Consulting, Carmel, IN; Benn Tannenbaum, Sandia National Laboratories, Washington, DC; Cammy Abernathy, University of Florida, Gainesville

Emergency Response and Community Resilience via Engineering and Computational Advances

Organized by Eva Lee, Georgia Institute of Technology, Atlanta

Innovation in Community Deployment of Water Technologies

Organized by Sushanta Mitra and Thomas Thundat, University of Alberta, Edmonton, Canada

Innovations in Crystallography Meet Demands in Materials Science, Energy, and Health

Organized by Tona Kunz, Argonne National Laboratory, IL

Integrated Cellular Systems: Building Machines with Cells

Organized by Nicholas A. Peppas, University of Texas, Austin; Rashid Bashir, University of Illinois, Urbana-Champaign

Open Science: Reducing Barriers to Scientific Breakthroughs

Organized by Kathryn L. Lovero, University of California, San Francisco; Lina Nilsson and Todd A. Duncombe, University of California, Berkeley

The Future of Cities: Dense or Dispersed?

Organized by Antony Wood, Council on Tall Buildings and Urban Habitat, Chicago, IL; Daniel Safarik and John Ronan, Illinois Institute of Technology, Chicago

U.S. National User Facilities: A Major Force for Discovery and Innovation

Organized by Susan Strasser, Argonne National Laboratory, IL; Ben Brown, U.S. Department of Energy, Washington, DC

Unlocking the Power of Big Data by Integrating Physical, Engineering, and Life Sciences

Organized by Sean E. Hanlon, National Cancer Institute, Bethesda, MD

Environment and Ecology

Agrobiodiversity and Global Change: New Linkages to Sustainability

Organized by Karl Zimmerer, Pennsylvania State University, State College

Canada's Oil Sands: Environmental and Economic Dimensions

Organized by Amir Mokhtari Fard, Southern Alberta Institute of Technology, Calgary, Canada

Changing Earth and Eco Systems in the Antarctic Peninsula

Organized by Eugene W. Domack, University of South Florida, St. Petersburg; Jere H. Lipps, California State University, Fullerton

Discovering Long-Term Climate Vulnerabilities at the Nature-Society Interface

Organized by Christopher I. Roos, Southern Methodist University, Dallas, TX

Earth Observation Data Goes Open Access

Organized by Gilles Ollier, European Commission, Directorate General for Research and Innovation, Brussels, Belgium

Research Challenges in Climate Change: What's New and Where Are We Going?

Organized by Thomas R. Karl, NOAA, Asheville, NC; Jerry Melillo, Marine Biology Laboratory, Woods Hole, MA; Donald J. Wuebbles, University of Illinois, Urbana-Champaign

Santa's Revenge: The Impacts of Arctic Warming on the Mid-Latitudes

Organized by Michael MacCracken, Climate Institute, Washington, DC; Ester Szein, U.S. National Academies, Washington, DC

The Arctic Cocktail: Shaken, Not Stirred

Organized by Franz Immeler, European Commission, Directorate General for Research and Innovation, Brussels, Belgium

The Big Thaw: Impacts on Health of Marine Mammals and Indigenous People in the Arctic

Organized by Andrew Trites, North Pacific Universities Marine Mammal Research Consortium, Vancouver, Canada; Stephen A. Ravery, British Columbia Ministry of Agriculture and Lands, Abbotsford, Canada; Mike E. Grigg, National Institutes of Health, Bethesda, MD

The Evolving Great Lakes: New Techniques, Discoveries, and Management Implications

Organized by Thomas C. Johnson, University of Minnesota, Duluth; Robert E. Hecky, Large Lakes Observatory, Duluth, MN

Global Perspectives and Issues

Accelerating Innovation in the Middle East: Lessons for the Developing World

Organized by Lara Campbell, CUBRC Center for International Science and Technology Advancement, Washington, DC

Building Global Partnerships: Sharing Discovery and Innovation, Safeguarding Difference

Organized by Aidan Gilligan, SciCom-Making Sense of Science, Brussels, Belgium; Daan Du Toit, South African Department of Science and Technology, Brussels, Belgium

Challenges in Conducting Risk Based Technology Assessments Globally

Organized by Umesh Thakkar, U.S. Government Accountability Office, Washington, DC

Competing Universities Collaborate on Standard Metrics for Global Benchmarking

Organized by John Green, Snowball Metrics Steering Committee, Cambridge, United Kingdom

Evaluating the Global Impact of Research Investments

Organized by Shannon L. Griswold and David J. Proctor, NSF, Arlington, VA; Kristina Wagstrom, University of Connecticut, Storrs

Focusing the Gender Lens on Science and Innovation: Improving Lives and Livelihoods

Organized by Sophia Huyer, Organization for Women in Science for the Developing World, Brighton, Canada

Globally Shipped But What's in the Box? Innovation for Better Container Security

Organized by Stephan Lechner, European Commission, Joint Research Center, Ispra, Italy

Grand Challenges: Science and Technology Solutions for International Development

Organized by Ku McMahan, USAID, Washington, DC

Innovation and Collaboration at 17,500 MPH: The International Space Station Experience

Organized by Kirt A. Costello, NASA, Houston, TX

Innovation in Global Health Research: Bridging the Knowledge-to-Action Divide

Organized by Emma Cohen, Canadian Institutes of Health Research (CIHR), Ottawa, Canada

Resolving Our Greatest Public Health Challenges via Science Diplomacy

Organized by Michel Kazatchkine, United Nations, Geneva, Switzerland; Aidan Gilligan, SciCom-Making Sense of Science, Brussels, Belgium

Risk-Based Standards for Cybersecurity: Global Challenges and Solutions

Organized by Elke Anklam, European Commission, Joint Research Center, Geel, Belgium; Igor Linkov, U.S. Army Engineer Research and Development Center, Concord, MA

Web-Based Technologies Change International Research Collaborations

Organized by Stefania Di Mauro-Nava, CRDF Global, Arlington, VA

Innovation and Entrepreneurship

Convergence Science: A Revolution for Health Solutions

Organized by Joseph M. DeSimone, University of North Carolina, Chapel Hill; Amanda J. Arnold and Maggie Lloyd, Massachusetts Institute of Technology, Cambridge

Leveraging Resources, Organization, and Collaboration for Breakthrough Science

Organized by Philip Shapira, University of Manchester, United Kingdom; Jerald Hage, University of Maryland, College Park

Making the Best Use of Academic Knowledge in Innovation Systems

Organized by Koichi Sumikura, Taro Matsubara, and Aska Takeshiro, National Institute of Science and Technology Policy, Tokyo, Japan

New North-South Funding for Fighting Poverty-Related Diseases

Organized by Gianpietro Van De Goor and Line Matthiessen, European Commission, Brussels, Belgium; Charles S. Mgone, European and Developing Countries Clinical Trials Partnership, The Hague, Netherlands

Nurturing Scientific Innovation and Entrepreneurship within the University Ecosystem

Organized by Phil Weilerstein, National Collegiate Inventors and Innovators Alliance, Hadley, MA

U.S. Looks to the Global Science, Technology, and Innovation Horizon

Organized by Elizabeth E. Lyons, U.S. Department of State, Washington, DC

Understanding the Science Needed for Sustainable Urban Development

Organized by Jan Riise, European Science Events Association, Onsala, Sweden

Medical Sciences and Public Health

48 Hours To Save the World: Challenge of the Next Pandemic

Organized by Gianpietro Van De Goor and Line Matthiessen, European Commission, Brussels, Belgium

Air Pollution as a Risk Factor for Central Nervous System Diseases and Disorders

Organized by Deborah A. Cory-Slechta, University of Rochester, NY; Michelle L. Block, Virginia Commonwealth University, Richmond

Approaches for Ensuring Children's Environmental Health Protection

Organized by Sally P. Darney, EPA, Research Triangle Park, NC

Artificial Tissues Engineered To Improve Patient Well-being

Organized by Louise Byrne, European Commission, Research Executive Agency, Brussels, Belgium

Bio-Surveillance: The Interface of Biological, Physical, and Information Sciences

Organized by Basil I. Swanson, Los Alamos National Laboratory, NM

Global Public Health Security: It Takes a Village

Organized by David Blazes, Johns Hopkins University, Baltimore, MD

Harnessing the Immune System: From Bench to Bedside and Back Again

Organized by Angela C. Colmone, AAAS/*Science Translational Medicine*, Washington, DC

How Does Oral Health Fit in the Emerging Health Care Environment?

Organized by Paul H. Krebsbach and Peter J. Polverini, University of Michigan, Ann Arbor

Inside Out: The Impact of Gut Flora on Diabetes and Obesity

Organized by Isabelle Kling, European Molecular Biology Laboratory, Heidelberg, Germany

Nexus of Cell Signaling and Drug Therapy: Oxygen, Phosphorus, Sulfur, and Nitrogen

Organized by Kenneth D. Tew, Medical University of South Carolina, Charleston

Physics and Astronomy

Dark Matter Discoveries: Challenges and Innovation

Organized by Maria Spiropulu, California Institute of Technology, Pasadena

Exploring the Foundations of Magnetism with New Nanoscale Probes

Organized by Michael E. Flatté, University of Iowa, Iowa City

Extremities of the Cosmos: New Experimental Results in Particle Astrophysics

Organized by Craig Hogan, Fermilab and University of Chicago, IL

From Dust and Gas to Disks and Planets

Organized by Mark T. Adams, National Radio Astronomy Observatory, Charlottesville, VA

New Millimeter-Wavelength Insights into Galaxy Evolution in the Early Universe

Organized by Mark T. Adams, National Radio Astronomy Observatory, Charlottesville, VA

Optics and Photonics: An International Perspective

Organized by Erik B. Svedberg, U.S. National Academies, Washington, DC; Alan Eli Willner, University of Southern California, Los Angeles; Paul McManamon, Exciting Technology LLC, Dayton, OH

Quantum Information Technologies

Organized by Martin Laforest, University of Waterloo, Canada

Stars in the Laboratory: Fundamental Nuclear Physics at the National Ignition Facility

Organized by Ani Aprahamian, University of Notre Dame, IN; Elizabeth R. Cantwell and Christopher J. Keane, Lawrence Livermore National Laboratory, CA

Targeting Tumors: Ion Beam Accelerators Take Aim at Cancer

Organized by Karen McNulty Walsh and Stephen Peggs, Brookhaven National Laboratory, Upton, NY; James Siegrist, U.S. Department of Energy, Washington, DC

Technological Innovations and Their Impact on Astronomical Discovery

Organized by Margaret Meixner, Space Telescope Science Institute, Baltimore, MD; Donald Campbell, Cornell University, Ithaca, NY

The Physics of Information

Organized by Michel Devoret and Norman Chonacky, Yale University, New Haven, CT

Public Policy

Air Quality and Climate Change: Science and Policy Challenges

Organized by Julia Schmale and Erika von Schneidemesser, Institute for Advanced Sustainability Studies, Potsdam, Germany

Decision-Making in the Public Domain: Boundary Processes as Catalysts for Innovation

Organized by Steven Courtney, RESOLVE, Washington, DC

Discovery and Innovation: What's the Connection and Why Does It Matter?

Organized by Jason S. Robert, Arizona State University, Tempe

Global Excellence: New Drivers and Innovative Solutions

Organized by Klaus Bock and David Budtz Pedersen, ESO 2014 Danish Ministry of Science, Technology and Innovation, Copenhagen

Responsible Innovation in a Global Context

Organized by David H. Guston, Arizona State University, Tempe

Scholarly Publishing Innovations and Evolution: Views of the Stakeholders

Organized by H. Frederick Dylla, American Institute of Physics, College Park, MD

Science Policy-Making that Meets Social Challenges and Motivates Scientists

Organized by Tateo Arimoto, National Graduate School for Policy Studies, Tokyo, Japan; Chikako Maeda, Japan Science and Technology Agency, Tokyo

Streamlining U.S. Visa and Immigration Policies

Organized by Albert H. Teich, George Washington University, Washington, DC; Amy Flatten, American Physical Society, College Park, MD

The Golden Goose Award: Highlighting the Value of Federal Support for Basic Research

Organized by Tobin L. Smith, Julia Smith, and Jennifer Poulakidas, Association of Public and Land-grant Universities, Washington, DC

Transplant Organ Shortage: Informing National Policies Using Management Sciences

Organized by Michael Abecassis and Sanjay Mehrotra, Northwestern University, Evanston, IL

Will the Workplace of Tomorrow Have Any Workers? Computing, Productivity, and Jobs

Organized by David H. Autor, Massachusetts Institute of Technology, Cambridge

Sustainability and Resource Management

Challenges and Opportunities in Transitioning Small-Scale Fisheries to Sustainability

Organized by Elena M. Finkbeiner and Larry Crowder, Stanford University, CA

Deep-Ocean Industrialization: A New Stewardship Frontier

Organized by Lisa Levin, Scripps Institution of Oceanography, La Jolla, CA; Kristina Gjerde, International Union for Conservation of Nature, Konstancin-Chylce, Poland

Hazards: What Do We Build For?

Organized by Julia R. Wilson, Sense About Science, London, United Kingdom

Making Products Sustainable as Materials Become Scarce

Organized by Erno Vandeweert and Aud Helen Alming, European Commission, Brussels, Belgium

New Modeling Approaches to Inform Climate Change Understanding and Decision-Making

Organized by Thomas Dietz, Michigan State University, East Lansing

New Scenarios for Assessing Future Climate Change

Organized by Peter Backlund and Brian C. O'Neill, National Center for Atmospheric Research (NCAR), Boulder, CO

Securing Fisheries Through Novel Approaches: Opportunities of Genetics and Genomics

Organized by Geraldine Barry, European Commission, Joint Research Center, Brussels, Belgium

The Ocean Tracking Network: Global Innovation in Technology, Science, and Management

Organized by Frederick G. Whoriskey and Sara J. Iverson, Dalhousie University, Halifax, Canada

The Soils of Africa: A Forgotten Resource

Organized by Luca Montanarella, European Commission, Joint Research Center, Ispra, Italy; Geraldine Barry, European Commission, Joint Research Center, Brussels, Belgium

AAAS, publisher of *Science*, thanks the sponsors and supporters of the 2014 Annual Meeting



the **Lemelson** foundation
improving lives through invention



AAAS thanks

THE  KAVLI FOUNDATION

for its generous support of the Science Journalism Awards

 **AAAS | 2014**
ANNUAL MEETING
13-17 FEBRUARY • CHICAGO

Register Today at Discounted Rates

REGISTRATION

Discounted advance registration rates are available until **22 January 2014**.
For more information, visit www.aaas.org/meetings

	Member	New Member	Non-Member
Professional	\$295	\$380	\$399
Postdoc	\$235	\$320	\$335
K-12 Teacher	\$235	\$320	\$335
Emeritus	\$235	\$320	\$335
Student	\$60	\$70	\$90

HOTELS

Special room rates and travel benefits are available to Annual Meeting registrants.

Hyatt Regency Chicago
Rate: \$199 single/double

Fairmont Chicago
Rate: \$168 single/double

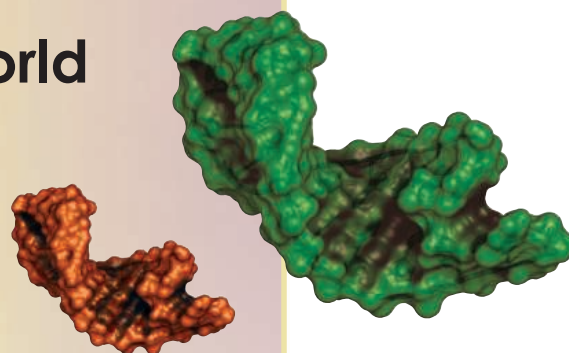
Rooms are available on a first-come, first-served basis until **22 January 2014**.



Brave New RNA World

The discovery of RNAi revealed an entire layer of previously unknown gene regulation; new tools are helping more scientists analyze and manipulate this system to probe the secret lives of cells.

By Alan Dove



In the beginning there was RNA, at least according to some theorists. While life may have originated with self-replicating RNA molecules, molecular biologists have long focused on DNA. There were good reasons for that bias though. Besides being widely perceived as carrying the definitive copy of life's instructions, DNA was also much easier to work with in the laboratory.

Now, though, both of those rationalizations are crumbling. The discovery of an entire layer of gene regulation based on non-protein-coding pieces of RNA, and the simultaneous development of new tools and techniques for working with those molecules, have spurred intense interest in understanding and exploiting the RNA world. In the past few years, the field's innovations have ranged from solving simple problems, such as preserving RNA preparations for future analysis, to opening entirely new frontiers with methods to sequence all of the RNA transcripts in a single cell. The latter method has become so straightforward that some researchers are even using it to replace transcript-profiling chips. Meanwhile, established techniques such as silencing genes with short interfering RNA (siRNA) have been overhauled for improved reliability.

Decoded Messages

A fundamental advance in studying RNA came in 2008, when researchers described a technique for sequencing all of the transcripts in a population of cells. The method, RNA-Seq, entails reverse-transcribing purified messenger RNA, then using next generation sequencing tools to sequence all of the resulting cDNA. The result is a complete sequence of the cells' transcriptomes.

Sequencing entire transcriptomes is powerful, but the original versions of RNA-Seq had some limitations. "In 2009, our first RNA-Seq kit required at least a microgram of RNA, and it was preferably very high

quality [RNA], otherwise you wouldn't get good results," says Gary Schroth, distinguished scientist at **Illumina** in San Diego, California.

Illumina has since refined the procedure, and now offers kits for performing RNA-Seq on as little as 100 ng of RNA, allowing researchers to sequence transcriptomes of small tissue samples. The company also offers reagents for removing ribosomal RNA, one of the major contaminants that complicated first-generation RNA-Seq.

In an evolution of the technique called Smart-Seq, researchers have even managed to sequence the transcriptomes of individual cells. "The notion of being able to do single-cell [RNA sequencing] is something that a few years ago I would've said 'no way,' but it turns out that it's actually not that difficult to go down to those levels ... when you have an isolated, free-floating cell," says Schroth. Smart-Seq doesn't work on crude tissue preparations, though, so RNA-Seq remains the preferred method for studying those samples.

As transcriptome sequencing continues developing and sequencing costs continue falling, many biologists are now using RNA-Seq for routine transcriptome profiling, a job previously reserved for RNA profiling chips. The chips work by hybridizing RNA to an array of short oligonucleotides to determine which transcripts are present. While that approach has been a workhorse of transcriptome analysis for years, it can only identify the RNA sequences the chipmaker predicted a cell would produce. Because RNA-Seq is unbiased, it often reveals alternatively spliced RNA forms and novel transcripts that don't show up on chips, and allows investigators to dig more deeply into the data. Schroth, whose company makes equipment for both types of analysis, argues that the chips may still have an advantage for some researchers processing large numbers of samples.

Regardless of the transcript profiling strategies they use, biologists are now keenly aware that transcription does not guarantee that a gene product is expressed. In particular, the RNA interference (RNAi) system produces numerous short RNA pieces that bind expressed transcripts and target them for destruction. Researchers initially sought to study this system by sequencing the cell's population of short RNAs and quantifying the relative abundance of different sequences. That proved to be tricky.

"What we found doing some in vitro experiments is that some cell populations of small RNAs just aren't represented as well in sequencing libraries as others," says Brett Robb, senior scientist at **New England Biolabs** (NEB) in Ipswich, Massachusetts. In particular, many animal and plant cells modify the 3' ends of their small RNAs, and standard sequencing

Upcoming Features

Proteomics—February 21

Toxicology—March 14

Genomics—April 11

methods underrepresent these modified molecules. To solve that, Robb and his colleagues optimized a ligation-based technique that sticks a specially modified DNA adapter onto the small RNAs before sequencing.

As scientists continue looking more deeply at posttranscriptional gene regulation, they're discovering additional species of RNA. "A lot of the things we've learned as we've been studying small RNAs will be pretty useful for some of the newer things like these long noncoding RNAs (lncRNAs) that have been pretty hot recently," says Robb.

The lncRNAs are pieces of RNA over 200 nucleotides long that don't encode proteins but instead appear to regulate transcription and translation in multiple ways. In large-scale sequencing projects, scientists have estimated that the human genome encodes at least tens of thousands of lncRNAs, suggesting that these molecules represent another major layer of gene regulation.

The lncRNAs are double stranded and can be encoded by either strand of the genomic DNA. That posed a major problem for early lncRNA researchers, who often had difficulty figuring out which DNA strand a particular lncRNA came from. In response, NEB has now developed a kit called NEBNext Ultra to produce strand-specific sequencing libraries.

A Moment of Silence

In addition to sequencing and studying noncoding RNAs, researchers have also been using them as tools to probe gene functions. Knocking down a target protein's expression transiently with synthetic siRNA oligonucleotides has become a standard laboratory technique, and drug developers continue to explore ways to use the RNAi machinery to treat diseases.

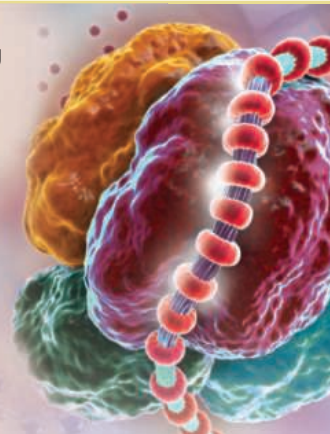
Indeed, RNAi-based therapies have followed the same cycle as many other technologies adopted by the biopharmaceutical industry. "When RNAi was discovered of course there was a lot of excitement, and then it's [been] the rise and the fall and then the rise of RNAi," says Nitin Puri, senior product manager for RNAi technologies at **Life Technologies** in Carlsbad, California.

The initial promise of being able to transiently shut down expression of any gene soon gave way to reality, as researchers discovered that their synthetic siRNAs often targeted multiple transcripts, and often lacked the potency of more traditional drugs. Since that initial letdown, the field has gradually recovered and investigators have begun to address some of those problems. "We see a lot more interest [in siRNA] now with researchers in the last two to three years, because there's this realization of how this technology is helping researchers really understand and get more insights into their high throughput screening," says Puri.

Using improved oligonucleotide design algorithms and chemical modifications, for example, Life Technologies can now synthesize potent and specific siRNAs against individual or multiple genes. By performing high throughput screens with these new siRNAs, scientists can quickly narrow the list of gene products that might be responsible for a particular phenotype.

Even a good high throughput screen still generates a lot of artifacts, though, often highlighting numerous genes that aren't directly related to the phenotype the investigator wants to study. New strategies for

RNA-Seq entails reverse-transcribing purified messenger RNA, then using next generation sequencing tools to sequence all of the resulting cDNA. The result is a complete sequence of the cells' transcriptomes.



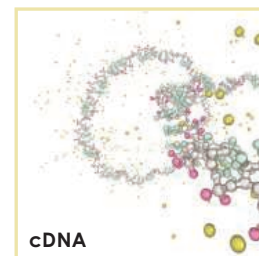
searching through the data may help. "We are working with researchers who are developing new approaches, especially bioinformatic approaches, to weed out some of the nonessential genes," says Puri.

Researchers have also learned to keep their expectations for siRNA realistic. "Those who've been in the field for awhile and using RNAi, they've come to understand and be much more accepting of its natural limitations," says Louise Baskin, senior product manager at **Thermo Fisher** in Waltham, Massachusetts, adding that "it's a promiscuous mechanism by nature—we do what we can to make it very specific, but there's always a chance that something's happening that's unanticipated."

Even highly specific siRNAs against important gene products can fail to produce a phenotype, for reasons biologists know all too well. "One of the frustrations with doing gene-by-gene knockdown is that our cells are very smart, they have secondary pathways and redundant mechanisms to save themselves," says Baskin. To maximize a siRNA screen's chances of success, she suggests using panels of siRNAs against multiple gene targets in a pathway instead of just one. Thermo Fisher supports that strategy with premade libraries of siRNAs to target any known gene in humans, rats, or mice, and the company recently added libraries of siRNAs against long noncoding RNAs as well.

For researchers who want to work with primary cells or intact tissues, just getting siRNAs to their targets can also be a problem, as these cells often **continued**

The field's innovations have ranged from solving simple problems, such as preserving RNA preparations for future analysis, to opening entirely new frontiers with methods to sequence all of the RNA transcripts in a single cell.



cDNA

Featured Participants

Broad Institute
www.broadinstitute.com

Illumina
www.illumina.com

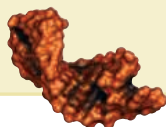
Life Technologies
www.lifetechnologies.com

New England Biolabs
www.neb.com

Sigma-Aldrich
www.sigmaaldrich.com

Thermo Fisher
www.thermoscientificbio.com

TransOMIC
www.transomic.com



As the technologies

for studying

noncoding RNA

continue to develop,

experts in the field

see a promising future

for the RNA world.

in the nucleus, where it is processed through the natural RNAi machinery to form siRNA against a specific transcript. The vector persists in the cell, permanently silencing the target gene product.

By pooling a set of shRNA vectors targeting different transcripts, investigators can produce a population of cells in which each cell has a different gene silenced. Isolating the cells that display a desired phenotype, then sequencing the vectors they're carrying, provides a quick map of the genes that are likely involved in that phenotype. This pooled approach has drastically reduced the cost and complexity of high throughput shRNA screening. "Instead of taking one shRNA into one well of cells and looking at the results, you put many shRNAs, even thousands, into one plate of cells at a time, and if you plan and carry out your experiment carefully ... you can rapidly screen lots of genes at a much lower cost and much faster," says Shawn Shafer, functional genomics market segment manager at **Sigma Life Sciences** in St. Louis, Missouri.

To aid those analyses, scientists in the **Broad Institute's** RNAi Consortium have produced libraries of shRNAs targeting 15,000 human and 15,000 mouse genes. The shRNAs are packaged in lentiviral vectors that can transfect a wide range of cells. Both Sigma and Thermo Fisher now offer these libraries to researchers. The consortium is now trying to create at least two highly potent, validated RNAi-based inhibitors for

resist conventional transformation techniques. To address that, Thermo Fisher has developed a line of self-delivering siRNAs, which carry a chemical modification that allows them to enter cells directly.

A Quick Knockout

While synthetic siRNAs provide a convenient way to knock down gene expression transiently, researchers looking for a more lasting effect usually turn to DNA vectors encoding short hairpin RNAs (shRNA). Cells transformed or transfected with one of these vectors transcribe the shRNA

each human and mouse gene, as well as inhibitors for long noncoding RNAs. Those reagents should make high throughput genetic screens even easier.

As the tools improve, researchers are uncovering new complications. Recent data on the mechanism of RNAi suggest that a small "seed sequence" of only seven nucleotides may determine the specificity of small RNAs. That could help explain the promiscuous effects of many siRNA and shRNA inhibitors; a seven-base sequence can potentially bind many more transcripts than a 22-base sequence. "What they're doing now with pooled screens is requiring two or three shRNAs against the same transcript to pop up as hits, to sort of serve as revalidation of that initial hit," says Shafer.

Sigma also offers kits to apply the same approach to siRNA experiments. In the company's EasyRNA protocol, an experimenter can amplify a segment of a transcript and turn it into a pool of siRNAs covering the entire segment. Targeting the transcript with multiple, custom-made siRNAs may help maximize silencing while minimizing off-target effects.

Designing highly potent shRNAs for long-term gene silencing has been a tougher problem. Originally, biologists simply borrowed the algorithms they'd used to design synthetic siRNAs and applied them to shRNA vectors. That didn't work very well. "If you take a [siRNA] sequence and you put it in and try to express it in a vector, you get a lot of variability in function," says Andy Crouse, senior product manager at **TransOMIC** in Huntsville, Alabama.

The difference in performance between a siRNA and a shRNA with the same sequence probably stems from their very different pathways through the cell. Crouse explains that while shRNAs are transcribed and processed by the same cellular machinery that runs the natural RNAi system, synthetic siRNAs bypass much of that process and bind directly to their target transcripts.

For awhile, scientists worked around the problem by simply using multiple shRNA vectors against each transcript they wanted to silence, in the hope that one or a combination of them would work well enough. The ability to do pooled shRNA screens eventually allowed researchers to isolate the most effective shRNAs from a large set. Analyzing the pool of successful shRNAs led to a new algorithm that can accurately predict the best shRNA sequence for silencing a given target. TransOMIC now uses that algorithm to design custom sets of shRNAs, and also prebuilt shRNA libraries that target particular families of genes.

As the technologies for studying noncoding RNA continue to develop, experts in the field see a promising future for the RNA world. "Human complexity cannot be accounted for by our proportionally small number of protein-coding genes ... the complexity that we have is in the percentage of our genome that is transcribed into RNA but never actually makes a protein," says Thermo's Baskin. She adds that "it's really infinite possibilities in terms of how to study and what those might really mean to our understanding of biological systems."

Alan Dove is a science writer and editor based in Massachusetts.

DOI: 10.1126/science.opms.p1400081

DNA/RNA CLEAN-UP KIT

PowerClean Pro DNA and RNA Clean-Up Kits feature a fast, seven minute protocol for removal of amplification inhibitors including humic substances, polysaccharides, polyphenolics, heme, and lipids from purified DNA or RNA. The PowerClean Pro DNA and RNA Clean-Up Kits are the latest products in MO BIO's Power line of kits which contain patented Inhibitor Removal Technology (IRT). IRT eliminates inhibitory substances often contained in soil, water, stool, plants, seeds, biofilm, and other sample types, resulting in pure nucleic acids that are ready to use in polymerase chain reaction (PCR), qPCR, and next generation sequencing. Features of the PowerClean Pro DNA and RNA Clean-Up Kits include: efficient secondary purification, removal of challenging impurities, and successful amplification.

MO BIO Laboratories

For info: 800-606-6246 | www.mobio.com/powerclean-pro



MICRORNA PROFILING ASSAY

The SmartRNAplex miRNA detection assay is based on proprietary Firefly hydrogel technology. As microRNA-based research evolves from discovery to validation, robust, multiplex methods that can be performed easily at the bench are necessary to continue advancements in the field. The SmartRNAplex assay is an important new tool for customers who are elucidating the role of microRNAs in a broad range of human diseases and need to explore multiple targets across many samples. The innovation lies in the unique properties of the Firefly particles which maximizes signal and widens the assay's dynamic range, while decreasing background noise. MicroRNA detection with SmartRNAplex requires just three steps: hybridize, label, and report. The hybridize step binds the microRNA targets to the target-specific probes attached to Firefly hydrogel particles. The label step ligates a universal biotinylated adapter to the captured targets. A fluorescent reporter binds to the universal adapter during the report step.

EMD Millipore

For info: 978-715-4321 | www.millipore.com/smartnaplex

RNA LIBRARY PREPARATION KIT

The SureSelect Strand-Specific RNA Library Preparation Kit is designed for whole transcriptome and targeted RNA sequencing. The new kit enables researchers to prepare high-quality, strand-specific libraries for next generation sequencing. The ability to gain valuable strand-specific information from RNA-sequencing experiments allows researchers to more easily discern overlapping transcripts and investigate antisense expression for greater understanding of gene regulation. The kit has been optimized to provide outstanding sequencing performance and uniform coverage of the entire transcript. This is achieved through greater library complexity and less 5'/3' bias, even with small amounts of starting material (as low as 50 ng). The kit has also been designed to be as complete as possible, including master-mixed reagents and a streamlined workflow for less hands-on time and faster results. Strand-specific RNA-sequencing library preparation is the latest addition to Agilent's next generation sequencing/gene-regulation portfolio, which offers the most complete integrated solutions from sample to analysis.

Agilent Technologies

For info: 877-424-4536 | www.agilent.com

RNA SEQUENCING KIT

The SMARTer Universal Low Input RNA Kit extends Clontech's next generation sequencing (NGS) solutions to include low input samples of compromised RNA. It combines the patented SMART (Switching Mechanism at 5' End of RNA Template) technology for double-stranded cDNA synthesis with random priming, which facilitates transcriptome sequencing (RNA-Seq) from degraded total RNA samples. Samples acquired via common sample preparation techniques, such as formaldehyde-fixed, paraffin-embedded tissue (FFPE) and laser capture microscopy (LCM), often result in a loss of overall sample quality and/or yield. This kit expands the applications of SMART technology to include cDNA synthesis from samples that contain degraded RNA (e.g., FFPE or LCM samples) or nonpolyadenylated RNA. RNA-Seq has revolutionized gene expression profiling, enabling researchers to characterize a cell's entire transcriptional activity at the nucleotide level. The SMART protocol greatly reduces handling of the RNA sample, thereby minimizing the risk of sample loss and preserving the original message.

Clontech Laboratories

For info: 800-662-2566 | www.clontech.com

RNA METHYLATION KIT

The new EZ RNA Methylation Kit is specifically designed and optimized for bisulfite conversion of RNA for 5-methylcytosine detection. Zymo Research now makes it easy for scientists to investigate RNA methylation, in addition to many other epigenetic modifications, with the comprehensive suite of products and services for epigenetic analysis, including genome-wide platforms for profiling DNA methylation and hydroxymethylation, and other services such as ChIP-Seq and RNA-Seq. The EZ RNA Methylation Kit opens the door for scientists also to look more closely at the modifications of RNA. Because RNA molecules perform many different functions in cells, ranging from protein translation to gene silencing and enzymatic activity, the potential for biologically relevant changes to RNA is significant. RNA methylation is only one more piece in the complex puzzle of epigenetics and the intricate events that comprise and control gene regulation.

Zymo Research

For info: 888-882-9682 | www.zymoresearch.com/epigenetics

Electronically submit your new product description or product literature information! Go to www.sciencemag.org/products/newproducts.dtl for more information. Newly offered instrumentation, apparatus, and laboratory materials of interest to researchers in all disciplines in academic, industrial, and governmental organizations are featured in this space. Emphasis is given to purpose, chief characteristics, and availability of products and materials. Endorsement by *Science* or AAAS of any products or materials mentioned is not implied. Additional information may be obtained from the manufacturer or supplier.

Science Signaling

The Leading Journal for Cell Signaling

Publishing key findings of broad
relevance in the multidisciplinary
field of cell signaling

Submit your research

ScienceSignaling.org

Recommend to your library

ScienceOnline.org/recommend

Join the ranks of high-profile papers
published in *Science Signaling*:

CANCER BIOLOGY

Vemurafenib Potently Induces Endoplasmic
Reticulum Stress–Mediated Apoptosis in
BRAFV600E Melanoma Cells

D. Beck *et al.* (F. Meier), *Sci. Signal.* **6**, ra7 (2013)

NEUROSCIENCE

Requirement for Nuclear Calcium Signaling in
Drosophila Long-Term Memory

J.-M. Weislogel *et al.* (H. Bading), *Sci. Signal.* **6**, ra33 (2013)

CELL AND MOLECULAR BIOLOGY

A Nontranscriptional Role for HIF-1 α as a Direct
Inhibitor of DNA Replication

M. E. Hubbi *et al.* (G. L. Semenza), *Sci. Signal.* **6**, ra10 (2013)

IMMUNOLOGY

Monovalent and Multivalent Ligation of the
B Cell Receptor Exhibit Differential Dependence
upon Syk and Src Family Kinases

S. Mukherjee *et al.* (A. Weiss), *Sci. Signal.* **6**, ra1 (2013)

COMPUTATIONAL AND SYSTEMS BIOLOGY

Cross-Species Protein Interactome Mapping
Reveals Species-Specific Wiring of Stress
Response Pathways

J. Das *et al.* (H. Yu), *Sci. Signal.* **6**, ra38 (2013)

Chief Scientific Editor

Michael B. Yaffe, M.D., Ph.D.

Massachusetts Institute of Technology

Editor

Nancy R. Gough, Ph.D.

AAAS, Washington, DC

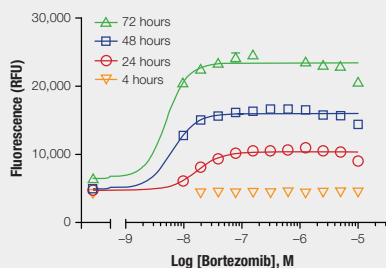


sciencesignalingeditors@aaas.org

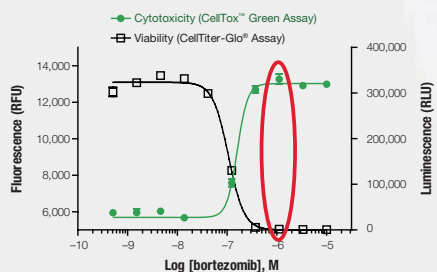
CellTox™ Green

More Biology, Less Work

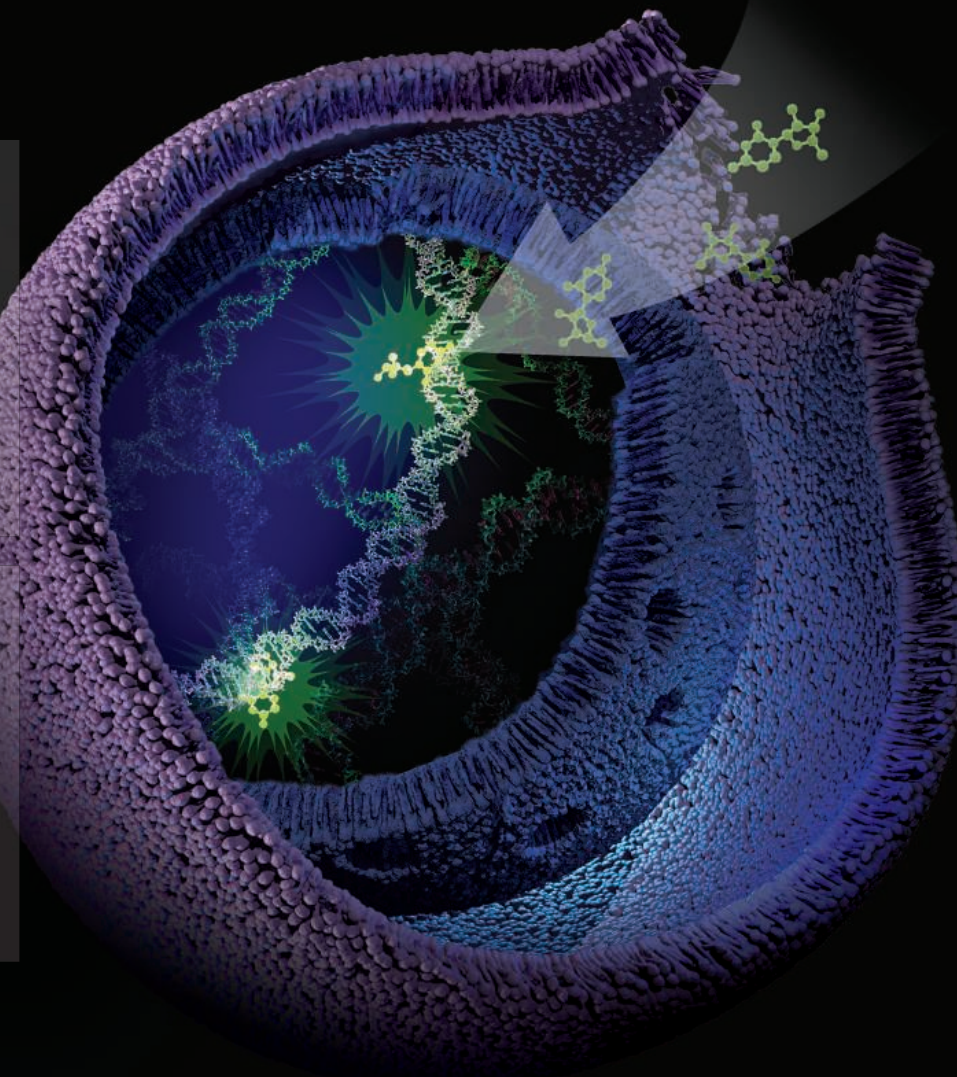
CellTox™ Green enables real-time mechanistic toxicity monitoring with a simple Add & Read protocol. Multiplexing with CellTiter-Glo® allows investigators to monitor temporal changes of membrane-modulated cytotoxicity in parallel with the key cell viability biomarker, ATP.



Easily monitor temporal changes in a key cytotoxicity biomarker for IC₅₀ determinations.



Get more informative data from same-well multiplexing of cytotoxicity and viability assays.



To see how easy better biology can be, request a free sample at:
www.promega.com/newcelltox



There's only one Science

Science Careers Advertising

For full advertising details, go to
ScienceCareers.org and click
For Employers, or call one of
our representatives.

Tracy Holmes

Worldwide Associate Director
Science Careers
Phone: +44 (0) 1223 326525

THE AMERICAS

E-mail: advertise@sciencecareers.org
Fax: 202-289-6742

Tina Burks

Phone: 202-326-6577

Marci Gallun

Phone: 202-326-6582

Online Job Posting Questions

Phone: 202-312-6375

EUROPE / INDIA / AUSTRALIA / NEW ZEALAND / REST OF WORLD

E-mail: ads@science-int.co.uk
Fax: +44 (0) 1223 326532

Axel Gesatzki

Phone: +44 (0)1223 326529

Sarah Lelarge

Phone: +44 (0) 1223 326527

Kelly Grace

Phone: +44 (0) 1223 326528

JAPAN

Yuri Kobayashi

Phone: +81-(0)90-9110-1719
E-mail: ykobayas@aaas.org

CHINA / KOREA / SINGAPORE / TAIWAN / THAILAND

Ruolei Wu

Phone: +86-1367-1015-294
E-mail: rwu@aaaas.org

All ads submitted for publication must comply with applicable U.S. and non-U.S. laws. *Science* reserves the right to refuse any advertisement at its sole discretion for any reason, including without limitation for offensive language or inappropriate content, and all advertising is subject to publisher approval. *Science* encourages our readers to alert us to any ads that they feel may be discriminatory or offensive.

Science Careers

From the journal *Science*



ScienceCareers.org

DIRECTOR Arkansas Children's Nutrition Center

We are seeking to recruit a new Director of the Arkansas Children's Nutrition Center (ACNC) in Little Rock, AR. The Director will be a Professor (Tenure Track) in the Department of Pediatrics and Chief of the Division of Developmental Nutrition at the University of Arkansas for Medical Sciences (UAMS) College of Medicine.



Requirements include a PhD or MD degree and a national reputation in nutrition-related research. He/she should have demonstrated excellence in research as evidenced by accomplishments, such as a long-standing record of nationally competitive funding at the R01 level through NIH; an excellent record of publications in high quality peer-reviewed scientific journals; NIH Study Section Membership; and National Awards. The successful candidate must also have proven and effective management and interpersonal skills necessary to direct a large, interdisciplinary national human nutrition research program.

The ACNC is one of six Human Nutrition Research Centers funded by the USDA/ARS and is housed in a private research building on the campus of Arkansas Children's Hospital, which is one of the nation's largest state-of-the-art children's hospitals and the primary pediatric research and teaching site of UAMS. The position carries a competitive salary and benefits package and will remain open until February 15, 2014.

Interested parties should submit their curriculum vitae and full contact information via email to RFJ@uams.edu or mail to: **Richard Jacobs, MD, FAAP, Search Committee Chair, 13 Children's Way Slot 842, Little Rock, Arkansas 72202-3591.**

UAMS is an inclusive Equal Opportunity and Affirmative Action Employer and is committed to excellence.



Texas State University-San Marcos is a member of the Texas State University System.

Endowed Chair of Water Conservation

The Department of Biology (www.bio.txstate.edu) and the Meadows Center for Water and the Environment (www.meadowscenter.txstate.edu) at Texas State University invite applications for an Endowed Chair of Water Conservation. The successful candidate will be expected to develop an externally funded research program within the general field of aquatic resources, which incorporates the management and conservation of freshwater resources in the context of ecosystem and human needs. The Chair is one of several supported by the Meadows Center to enable a nexus for continued successful collaboration across other academic units such as Geography, Environmental Engineering, and Social Sciences.

Applicants must have a Ph.D., an established externally-funded research program focused on some aspect of aquatic resources, be qualified to serve at the rank of Professor in the Department of Biology, and be an internationally-recognized expert in water conservation. Preference will be given to individuals with some experience working with state and federal agencies, a record of interdisciplinary collaboration, and experience supervising student research at various levels in research complementing the research strengths of the Department. Salary and start-up package are negotiable.

Texas State University is located between two large metropolitan areas (Austin and San Antonio), at the conjunction of several biotic provinces, and is approximately 100 miles from the Gulf of Mexico. The Chair will be located in the Freeman Aquatic Biology Building (FAB) which contains a wet laboratory and raceways receiving artesian well water and houses fully-equipped analytical laboratories. The FAB itself sits on the banks of the San Marcos River, just downstream of its headwaters. The headwaters and River are habitat for several endangered species and the focus of multiple research and conservation projects.

A vitae, statement of research interests, pdfs of five representative publications, and the names and contact information of five people willing to serve as references should be sent, as a single PDF, to Conservation@txstate.edu. Review of applications will begin **March 1, 2014** and continue until the position is filled. Questions about this position should be addressed to **Dr. Michael Forstner, mf@txstate.edu, Texas State University-San Marcos, 601 University Drive, San Marcos, TX 78666.**

Texas State University is an Affirmative Action/Equal Opportunity Employer.



About NUAA

Nanjing University of Aeronautics and Astronautics (NUAA) is a research-oriented national key university of "211 Project". It also enjoys a well-balanced development of multiple disciplines in engineering, technology, natural sciences, economy, management and social sciences with the characteristics of aeronautics, astronautics and civil aviation. NUAA is qualified to be "Dominant Discipline Innovation Platform of 985 Project" and to independently recruit and receive international students who are granted the Chinese Government Scholarship. Now NUAA consists of 16 colleges with more than 3,000 staff members and approximately 26,000 degree students.

Academia and education at NUAA represent strong capacity among all the universities in China. It has acquired national status through the quality of its excellence research work, especially in the areas of Aerospace Engineering, Mechanics, Electromechanics, Economy and Management, etc.

NUAA gives a warm welcome to excellent experts, scholars and young students from both home and abroad, who are willing to serve the country, dedicate themselves to the development of aerospace science and make contributions to the industrialization, information technology of China. NUAA will provide teachers and researchers with a good academic environment, satisfactory working and living conditions and a stage on which they can put their talents to good use.

Contacts

Ms. Zhao Haiyan, Mr. Cao Yunxing

Personnel Division, NUAA

Address: 29# Yudao St. Nanjing, Jiangsu Province, Postcode: 210016

Tel: +86-25-84892461

Fax: +86-25-84895923

Email: zhaohaiyan@nuaa.edu.cn

Web: <http://www.nuaa.edu.cn/nuaanew> <http://rsc.nuaa.edu.cn>



大连理工大学
DALIAN UNIVERSITY OF TECHNOLOGY

“人工光合作用研究所” 科研人才招聘

Faculty positions in solar cells and solar fuels

Openings of more than 15 tenure-track positions of Assistant Professor, Associate Professor and Full Professor are now available in the recently established Institute of Artificial Photosynthesis (IAP), Dalian University of Technology (DUT), China. The research fields of these open positions cover dye sensitized solar cells, quantum dots sensitized solar cells, organic polymer solar cells, organic-inorganic hybrid solar cells, catalytic water oxidation, catalytic proton reduction, catalytic CO₂ reduction, functional devices for light driven total water splitting, new type batteries, light to heat conversion at molecular level. Qualified candidates for these open positions should have obtained PhD degree, postdoc research experience, and well documented research achievements in related research fields. DUT will provide for the positions in IAP competitive salaries at international levels. Applicants should send their curriculum vitae, a statement of research plans together with publication list by email to Xue Sun (zhaopin@dlut.edu.cn), indicating in the email subject with "IAP+applicant's name". All applications should contain information of related interested positions in certain research fields mentioned above and potential reference persons with corresponding addresses.



Faculty Positions Available in Southwest University, Chongqing, China

Southwest University is a national key university of the "211" project directly under the Ministry of Education. It is located in Chongqing, the youngest municipality of China. The university hosts approximately 50,000 students, covering undergraduate, postgraduate and other programs. For more detailed information, please visit the website: <http://www.swu.edu.cn/#>

Applications for full-time professors, associate professors and distinguished scientists are welcome. Competitive salaries and start-up funds will be provided to successful candidates, in line with the national Recruitment Program of Young Experts.

The Recruitment Program of Young Experts (i.e. the Plan for Recruiting 1,000 Professorship for Young Talents): The candidates are required to be under the age of 40 and have obtained a PhD degree in a world-renowned university with at least 3 years of research experience abroad, or have obtained a PhD degree in Mainland China with at least 5 years of research and teaching experience abroad. Special offers will be granted to those who have excellent research achievements during their doctoral study.

Further information is available at <http://renshi.swu.edu.cn/rcgzbgbs/>. The Talents Recruitment Office, Southwest University, Beibei, Chongqing 400715, P. R. China. 0086-23-68254265.

Please kindly send applications or nominations in the form of an application letter enclosing a current CV to rencai@swu.edu.cn.



Faculty Positions in Microbiology and Immunology

Two tenure track faculty positions at the rank of Assistant Professor or Associate Professor are open for scientists with a Ph.D., M.D. or M.D./Ph.D. and postdoctoral research experience. Responsibilities include teaching graduate and medical students and directing a nationally competitive research program in the areas of microbial pathogenesis and/or host defense mechanisms to infection. Ideal candidates will be those who have extramural funding and whose research integrates molecular aspects of pathogenesis with host defense mechanisms and the immune system. The Department faculty of 16 members directs a training program of 40 doctoral students and postdoctoral fellows and an NIH-funded Center for Molecular and Tumor Virology staffed with 18 interactive principal investigators in several Departments. Both the Department and the Center are well-equipped for molecular research and are augmented by the LSUHSC Research Core Facility that offers BSL-3PLUS laboratories and technologies such as flow cytometry, confocal microscopy, laser capture microdissection, DNA array analysis, proteomics, small animal imaging, and positron emission tomography. Information about the Department is provided at the two websites <http://www.lsuhscomicrobiology.com> and <http://www.lsuhscomicrobiology.com/cmtv-overview.htm>.

Applicants should send a curriculum vitae, statement of research goals and funding, and three letters of reference to: **Dr. Dennis J. O'Callaghan, Boyd Professor & Head, Department of Microbiology and Immunology, LSU Health Sciences Center, 1501 Kings Highway, Shreveport, LA 71130-3932.**

*Louisiana State University is an
Affirmative Action/Equal Opportunity Employer.*



DIRECTOR, CENTER FOR GENOMIC MEDICINE AND DIRECTOR, DARBY CHILDREN'S RESEARCH INSTITUTE

The Medical University of South Carolina College of Medicine invites applications and nominations for the position of **PROFESSOR AND DIRECTOR** of the Center for Genomic Medicine and the Charles P. Darby Children's Research Institute. Applicants must possess an MD and/or PhD and have demonstrated administrative experience, strong leadership skills, an outstanding track record of extramural funding and accomplishment in research, and a commitment to education and academic excellence. The selected individual will have the experience and vision to lead multi-disciplinary genomic programs across the College of Medicine as well as child health-related research.

The Director will promote and support basic, clinical, and translational research and training in genetics and genomics and will coordinate genomic resources across the College. This individual will also lead basic research in the Department of Pediatrics. A \$2M endowed chair, the Charles P. Darby Chair for Pediatric Research, has been established for this position. More information regarding the Center for Genomic Medicine and Charles P. Darby Children's Research Institute can be found at <http://dev.musc.edu/com-old/research/GenomicMedicine.pdf> and <http://www.musckids.org/pediatrics/research>. The selected individual will report directly to the Dean of the College of Medicine and the Chair of the Department of Pediatrics.

The Medical University of South Carolina is in the midst of an exciting period of growth with NCI designation for the Hollings Cancer Center, a CTSA award, two new research buildings, and new clinical outreach facilities. The Charles P. Darby Children's Research Institute remains an integral part of the institution. This is an outstanding opportunity for the right candidate in a city known for its enviable quality of life. Nominations and inquiries may be directed to the search committee in care of **Mary McConnell** at mcconnem@musc.edu. Interested individuals should submit a letter of interest, curriculum vitae, and the names and contact information of three references via the MUSC employment website at <http://www.jobs.musc.edu/postings/22569>.

MUSC is an Equal Opportunity Employer, promoting workplace diversity.

TUFTS UNIVERSITY SCHOOL OF MEDICINE

Chair - Department of Integrative Physiology and Pathobiology

Tufts University School of Medicine invites applications for Professor and Chairperson, Department of Integrative Physiology and Pathobiology. The candidate should have a Ph.D. or M.D. and be an internationally recognized scientist with an outstanding research program and a track record of institutional service and leadership at all levels.

The Department of Integrative Physiology and Pathobiology is a newly formed department of likeminded Tufts investigators. Members of the Department have an outstanding history in research and training, with expertise in tissue damage and repair, inflammation, immunity and regeneration. A core faculty of 20 well-funded researchers currently has \$34 million in total costs for research from the NIH, foundations and industry. The Department is based in the Jaharis building and the Chair will be able to recruit new faculty into this modern research space, which also houses outstanding core facilities. An NIH-funded graduate training program in Immunology is based within the department, and departmental members are affiliated with eight other biomedical graduate programs.

This position provides an exciting opportunity to mold and develop the new department. The successful candidate is expected to embrace its wide-ranging interests and utilize new faculty recruitments to bring strength and focus in these areas. Candidates with the ability to develop a departmental research program in inflammation and chronic disease are of particular interest.

Please submit electronic applications including a CV, a statement of research interests and the names and contact information of at least three references by February 28, 2014 to:

<https://academicjobsonline.org/ajol/jobs/3773>.

Inquiries, but not application materials, may be directed to:
IPPChairRecruitment@tufts.edu.

*Tufts University is an
Affirmative Action/Equal
Opportunity employer,
committed to increasing
the diversity of our faculty.*



Seventh International Conference SUMO, Ubiquitin, UBL Proteins: Implications for Human Diseases



Organized by
Edward T.H. Yeh and Guo-Qiang Chen

**May 10-13, 2014
Shanghai, China**



THE UNIVERSITY OF TEXAS
**MD Anderson
Cancer Center**
Making Cancer History®

www.sentrin.com

HHMI Investigator Competition

The Howard Hughes Medical Institute invites applications to its Investigator Program from scientists who have demonstrated originality and substantial accomplishments in biomedical research and who show exceptional promise for future achievement and leadership in research. The Institute seeks to appoint 20 to 25 outstanding scientists as HHMI investigators.

Eligibility

- PhD and/or MD (or the equivalent)
- Tenured or tenure-track position as an assistant professor or higher academic rank (or the equivalent) at an eligible US institution
- More than 5 but no more than 15 years of post-training, professional experience
- Principal investigator on one or more active national peer-reviewed research grants with a duration of at least 3 years

This competition is open to basic researchers and physician scientists who study significant biological problems in all biomedical disciplines, including plant biology, as well as in adjacent fields such as evolutionary biology, biophysics, chemical biology, biomedical engineering, and computational biology.

Additional information www.hhmi.org/inv2015/sci

Deadline to establish eligibility **May 1, 2014, 3 PM ET**

Deadline to submit application **June 3, 2014, 3 PM ET**

HHMI

HOWARD HUGHES MEDICAL INSTITUTE

The Howard Hughes Medical Institute is an equal opportunity employer.



Department Head

Position in Microbiology and Immunology

The newly merged Department of Microbiology and Immunology seeks a distinguished and visionary academic leader with a broad background in microbiology to be Department Head. This individual will play a key role in maintaining and growing an internationally recognized faculty with expertise in General Microbiology, Environmental Microbiology, and Medical Microbiology. The position offers the exciting opportunity for leadership for advancing established areas of excellence and in developing new strategic initiatives. There are opportunities for substantial departmental faculty growth with 3-4 tenure track lines available and unique programmatic grant opportunities due to Montana classification as an IDEa eligible state. The Department Head will be responsible for directing the Department's undergraduate degree programs in General Microbiology, Biomedical Microbiology, Environmental Microbiology, Biotechnology, Pre-Veterinary program, and Medical Laboratory Science program, as well as the department's M.S. and Ph.D. programs. The Department's graduate program is interdisciplinary and coordinates with faculty across departments, colleges, and research centers (e.g., Sciences, Agriculture, Engineering, the Center for Biofilm Engineering, and the Thermal Biology Institute) for graduate-level research. A competitive institutional salary, a generous start-up package, and a renovated state-of-the-art research facility support this position.

Full details about the position and application procedure are available at <http://www.montana.edu/jobs/faculty/14-173>. Potential candidates are encouraged to contact the Search Committee Chairpersons, **Drs. Josh Obar** or **Sandra Halonen**, (joshua.obar@montana.edu; shalonen@montana.edu) for more details. Screening will begin **February 1st, 2014** and will continue until a suitable applicant is hired.

ADA/EO/AA/Veterans Preference.

IOWA STATE UNIVERSITY

OF SCIENCE AND TECHNOLOGY

Assistant Professor: Systems Biology of Plant-Microbe Interactions

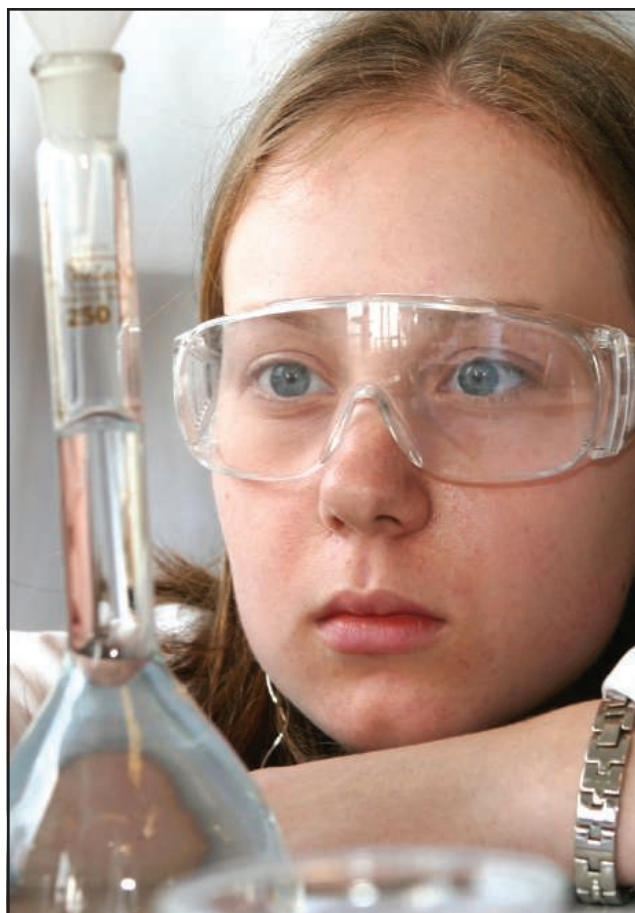
The Plant Pathology & Microbiology Department invites applications for an Assistant Professor in the area of Systems Biology of Plant-Microbe Interactions. This is one in a cluster of twelve Presidential High Impact Hires in the field of Big Data at Iowa State University.

We seek a creative individual who utilizes multidimensional datasets to investigate novel questions in pathogenic or symbiotic interactions between any type of microbe and its plant or plant-associated host(s). The incumbent will test hypotheses at multiple levels, integrating biochemical, synthetic, computational, and omics approaches. The successful candidate will establish an internationally recognized, externally-funded research program, teach in her or his area of expertise, and foster a culture of inclusion. Applications from women and members of underrepresented groups are encouraged.

This position is in an outstanding department on a highly collaborative campus. Iowa State University is located in Ames, Iowa, ranked as one of the most livable small cities in the nation.

To submit an application, see faculty vacancy number **131417** at www.iastatejobs.com. Consideration of applications will begin **February 21, 2014**, and position will start in the Fall of 2014. Send inquiries about this position to plpsysb@iastate.edu.

Iowa State University values diversity, supports work-life balance through an array of flexible policies, and is an AA/EEO Employer.



AAAS is here – promoting universal science literacy.

In 1985, AAAS founded Project 2061 with the goal of helping all Americans become literate in science, mathematics, and technology. With its landmark publications *Science for All Americans* and *Benchmarks for Science Literacy*, Project 2061 set out recommendations for what all students should know and be able to do in science, mathematics, and technology by the time they graduate from high school. Today, many of the state standards in the United States have drawn their content from Project 2061.

As a AAAS member, your dues help support Project 2061 as it works to improve science education. If you are not yet a member, join us. Together we can make a difference.

To learn more, visit
aaas.org/plusyou/project2061



Faculty Position in Translational Tumor Immunology



The Wistar Institute, an NCI-designated Cancer Center and independent research institute in Philadelphia, is seeking outstanding candidates for faculty positions in the newly created program in Translational Tumor Immunology. We are seeking candidates at different ranks to develop or expand their extramurally-funded research programs in different areas of tumor immunology and tumor microenvironment.

Specific areas of interest include (but are not limited to): molecular and cellular mechanisms regulating immune responses in cancer; novel approaches to therapeutic manipulation of the immune system in cancer; the role of metabolic changes in the function of the immune system in cancer; the impact of conventional and targeted cancer therapeutics on the immune system; interaction between cells of the immune system and epithelium/endothelium/stroma. Interest in translational research is desirable.

The Wistar Institute, an NCI-designated Cancer Center, offers highly competitive start-up support including salary and fringe benefits in addition to a superb and interactive research environment, including a newly constructed state-of-the-art research tower and animal facility, along with outstanding core facilities in proteomics, genomics, microscopy, high-throughput molecular screening, bioinformatics, and flow cytometry.

Investigators have access to wide range of clinical materials through a partnership with the Helen F. Graham Cancer Center, Newark, DE. The Institute's location, adjacent to the University of Pennsylvania campus, provides for academic and clinical collaborations and opportunities for training graduate students from universities in the Philadelphia area.

Applications will be reviewed as received and will be accepted until the positions are filled. The application should include: a curriculum vitae, a brief summary of past and future research interests, a history of research funding support (if applicable), and the names of three referees (submitted as a single PDF). Applications should be sent by e-mail to: Dmitry Gabrilovich, Search Committee Chair, c/o Maria Colelli (coelli@wistar.org), The Wistar Institute, 3601 Spruce Street, Philadelphia, PA 19104.



For more information about us, visit our Web site at
www.wistar.org



University of Florida Initiative in Neuroscience and Brain Research

The University of Florida (UF) is recruiting preeminent faculty in a wide variety of brain and neuroscience research areas. This multidisciplinary search is in conjunction with UF's Top 10 Initiative, with the goal of strategic faculty hires to further elevate our national academic and research standing to one of the top 10 public universities in the United States.

We seek 10-12 tenured and tenure-track colleagues (to be recruited at the associate and full professor ranks) to join faculty in the Colleges of Engineering, Liberal Arts & Sciences, Medicine, and Public Health & Health Professions, who have expertise in one of our targeted areas:

- 1) **neuroimaging, cognitive, functional, and molecular mapping** of the central nervous system
- 2) **therapeutic and biomarker discovery** in neurodegenerative and neuromuscular diseases
- 3) **neuromuscular plasticity, neurorehabilitation, and neurotechnology**
- 4) **the "adaptive brain"**, including evolutionary, genetic, and epigenetic influences on brain structure and behavior

The brain and neuroscience research environment at UF is excellent and supported in part by the following programs:

- McKnight Brain Institute
- Center for Translational Research in Neurodegenerative Disease
- Center for NeuroGenetics
- VA Brain Research & Rehabilitation Center
- Center for Movement Disorders & Neurorestoration
- Institute on Aging
- Center for Addiction Research & Education
- Brain and Spinal Cord Injury Program
- Nanoscience Institute for Medical and Engineering Technology
- National High Magnetic Field Laboratory

Individuals may submit a letter of interest, detailed curriculum vitae, a statement of research, teaching goals and synergy with potential UF collaborators, and the names and email addresses of three or more references to **NBR Search Committee c/o Ms. Lorie Martin, Phone: 352/273-6198; Email: lomarti@php.ufl.edu**. Applications will be reviewed and considered on an ongoing basis until the positions are filled. The University of Florida is an Equal Opportunity Employer. The selection process will be conducted in accordance with Florida's "Government in the Sunshine" and Public Records Laws.



Wake Forest[™] School of Medicine

The Department of Neurobiology and Anatomy
at Wake Forest Medical School announces open positions for

Postdoctoral Training in Multisensory Processes

We seek strong candidates for postdoctoral training funded by an NIH T32 Training Grant. The training program provides a rich collaborative research environment that fosters interdisciplinary approaches to understanding how the brain integrates information from multiple senses to produce perception and adaptive behavior. Candidates with direct experience as well as those in related fields are encouraged to apply. Trainees will have access to any of 9 laboratories using human subjects and/or a variety of animal models (rodents-primates) with approaches spanning molecular/cellular to perceptual/behavioral. Fellowships are awarded on a competitive basis.

Applications including a current curriculum vitae or nominations should be sent to the **Training Grant Director: Dr. Barry E. Stein** (bestein@wakehealth.edu), or to its **Co-Directors: Dr. Terrence R. Stanford** (stanford@wakehealth.edu) and **Dr. Dwayne Godwin** (dgodwin@wakehealth.edu). Please also submit your application and CV to job opening **5432** at www.wakehealth.edu/jobsearch/.

A description of the faculty and the program can be accessed via the website: http://graduate.wfu.edu/admissions/t32/training_tpm.html

Wake Forest School of Medicine is an Affirmative Action/Equal Opportunity Employer and especially encourages applications from women and minority candidates.



DIRECTOR UNIVERSITY OF NEBRASKA STATE MUSEUM

The University of Nebraska State Museum (UNSM), the natural history museum located at the University of Nebraska-Lincoln, seeks a Director to provide dynamic leadership for the UNSM.

We invite nominations and applications for Director of the University of Nebraska State Museum, a large comprehensive museum of natural history with a faculty and staff of 40 and research collections in paleontology, parasitology, entomology, zoology, botany and anthropology of more than 15 million specimens.

UNSM has an active, federally-funded education and outreach programs and close collaborations with university programs and school districts. It is accredited by the American Alliance of Museums and is a Smithsonian Affiliate.

The Director provides leadership and is responsible for developing external funding and partnerships, and enhancing facilities and collections. The Director will also develop and implement a new strategic plan to grow the Museum's research, collections, and education programs. The successful applicant will have an earned doctorate in science with a strong research and funding record meriting a tenured faculty position. It is expected that the Director will be tenured in an appropriate department. The Director will have museum experience, effective management and organizational skills, the ability to work well on collaborative teams and excellent interpersonal and fundraising skills.

We are accepting nominations and applications for this position. To nominate someone please email UNLresearch@unl.edu. To apply, go to <http://employment.unl.edu>, search for requisition number **F_130241**. Click on **"Apply to this job."** Complete the application and attach a letter of interest, an up-to-date vitae, and names/addresses of five references. Please contact Peg Filliez at pfilliez1@unl.edu for further information. Applications will be reviewed beginning **February 17, 2014** and will remain open until filled. For more information about this position and UNSM, please visit <http://research.unl.edu/museumdirector>.

The University of Nebraska has an active National Science Foundation ADVANCE gender equity program, and is committed to a pluralistic campus community through affirmative action, equal opportunity, work-life balance, and dual careers.



Stony Brook Medicine

FACULTY POSITION MOOD DISORDERS CLINICIAN RESEARCHER

Stony Brook University is launching an interdisciplinary faculty hiring initiative in **affective neuroscience of anxiety and depression**: <http://www.stonybrook.edu/commcms/clusterhires/clusters/canad.html> Three tenure-track/tenured faculty positions are sought across Psychology, Neurobiology and Behavior, and Psychiatry departments. This hiring initiative focuses on understanding anxiety and depression in terms of fundamental disruptions in core neural systems related to emotion, especially threat and reward. The cluster of hires combined with existing strengths in each of the three lead departments will culminate in a world class multi-disciplinary group of scholars at Stony Brook University dedicated to research in the etiology, pathophysiology and treatment of depressive and anxiety disorders.

We are seeking an MD/PhD clinician researcher who would welcome the challenge of designing and implementing a program of research in mood disorders.

Stony Brook has a very large affected population with unmet clinical and research needs. Particular strengths of the institution are in epidemiology, services and outcomes research, all areas of animal high-resolution imaging and optical recording techniques and human imaging, such as MRI and PET.

The additional two proposed tenure-track hires are described below. For all positions, we are particularly interested in applicants who study core neural systems relevant to anxiety and depression.

- (1) *Developmental cognitive neuroscience of emotion*, to study the development of core emotion systems. We are particularly interested in applicants who study core neural systems from a developmental perspective using neuroimaging methods, but we will also consider strong candidates with other relevant interests and methods. <http://www.stonybrook.edu/commcms/clusterhires/searches/canad.html#t>
- (2) *Systems neurobiologist*. We are looking for a systems neuroscientist who utilizes the latest technologies (e.g., optogenetics, optoelectrophysiology, deep brain imaging) to study emotion in awake behaving animals.

Stony Brook University has excellent and rapidly expanding neuroimaging facilities for animal and human studies including a simultaneous PET/MRI and a research-dedicated 3T MRI. In addition, construction has begun on a cyclotron and radiochemistry facility that will incorporate a PET camera to be used solely for research purposes. This facility will be housed in a new 465,000-sq.-ft. building dedicated to translational medicine and research. Information about the Psychology, Psychiatry, and Neurobiology and Behavior departments can be found at <http://www.psychology.sunysb.edu>, <http://medicine.stonybrookmedicine.edu/neurobiology>, and <http://medicine.stonybrookmedicine.edu/psychiatry>, respectively.

Stony Brook is located in beautiful Suffolk County, on the North Shore of Long Island approximately 40 miles east of New York City. Stony Brook is a wonderful place to live and raise children, with abundant opportunities for recreation as well as ready access to Manhattan.

Required: MD with two years research experience and license to practice in the United States of America. Board Eligible/Board Certified in Psychiatry. Full Time availability.

Preferred: MD and PhD with three years of research experience and NIH funding. Licensed to practice in New York State and specialized in mood disorders.

To qualify for tenure and/or a senior faculty appointment, the candidate must meet the criteria established by the School of Medicine (School of Medicine's Criteria for Appointment, Promotion and Tenure).

Applicants may submit a State employment application, cover letter, curriculum vitae to: **Ramin V. Parsey, M.D., Ph.D., Chairman, Department of Psychiatry and Behavioral Science, Health Sciences Center, Level 10, Room# 020, Stony Brook University, Stony Brook, NY 11794-8101, Fax# 631-444-1560**. For further information visit www.stonybrook.edu/jobs (Ref#: F-8118-13-09).

Stony Brook University/SUNY is an equal opportunity, affirmative action employer.



AAAS is here – helping scientists achieve career success.

Every month, over 400,000 students and scientists visit ScienceCareers.org in search of the information, advice, and opportunities they need to take the next step in their careers.

A complete career resource, free to the public, *Science* Careers offers a suite of tools and services developed specifically for scientists. With hundreds of career development articles, webinars and downloadable booklets filled with practical advice, a community forum providing answers to career questions, and thousands of job listings in academia, government, and industry, *Science* Careers has helped countless individuals prepare themselves for successful careers.

As a AAAS member, your dues help AAAS make this service freely available to the scientific community. If you're not a member, join us. Together we can make a difference.

To learn more, visit aaas.org/plusyou/sciencecareers



WOMEN IN SCIENCE

forging
new pathways in
green
science



Read inspiring stories
of women working in
“Green Science”
who are blending
a unique combination of
enthusiasm for science
and concern for others
to make the world
a better place.

Download this
free booklet
[ScienceCareers.org/
LOrealWiS](http://ScienceCareers.org/LorealWiS)



This booklet is brought to you by the
AAAS/Science Business Office
in partnership with the
L'Oréal Foundation

School of Engineering & Applied Science

THE GEORGE WASHINGTON UNIVERSITY

FOUNDING CHAIR AND TENURED FULL PROFESSOR, DEPARTMENT OF BIOMEDICAL ENGINEERING, THE GEORGE WASHINGTON UNIVERSITY, WASHINGTON, D.C.

The George Washington University invites applications for a tenured full-professor position as Chair of the Department of Biomedical Engineering, to begin in fall semester 2014. This is an exciting opportunity for an outstanding person to develop and lead a new BME department. The Department will open formally in fall 2014 after moving the longstanding ABET-accredited B.S. program, and the M.S. and Ph.D. BME programs, from the Department of Electrical and Computer Engineering. The University is constructing a new 500,000 square-foot Science and Engineering Hall, adjacent to the University Hospital and the Schools of Medicine and of Public Health, which will house state-of-the-art clean rooms, imaging facilities, and BME research and instructional laboratories. The School of Engineering and Applied Science will move into the building in spring 2015. The George Washington University is located in the nation's capital, with close access to many federal funding agencies and government research laboratories.

Responsibilities: The successful candidate will be expected to demonstrate an intense commitment to excellence in teaching and research and to the success of our students. Equally, the new Chair will vigorously catalyze and develop further the Department's collaborations with the Schools of Medicine and of Public Health, and the GWU Hospital, attract new partners across the University, and advance and extend the existing relationships with nearby government laboratories. The new Chair will be an enthusiastic proponent of creativity, innovation, and outreach, and be an effective advocate and spokesperson for the Department, both within and beyond the University.

Basic Qualifications: Applicants must have an earned doctorate in Biomedical Engineering, Bioengineering, or a related field; outstanding research and academic achievements that make the candidate suitable for appointment as a full professor; a demonstrated capability as a visionary leader, with a strong research portfolio that evidences multi-disciplinary expertise, which can complement and expand existing departmental strengths; and the proven ability to teach effectively at both the graduate and undergraduate levels. Applicants must have evidence of substantial management ability and experience in a multi-faceted academic environment that includes success in mentoring of students and faculty, proposal writing, and grant management.

Application Procedure: To apply, complete the online faculty application at <http://www.gwu.jobs/postings/19290> and upload a cover letter, a detailed CV or resume, a concise statement of teaching and research interests, and full contact information for five professional references. Please also indicate your primary area(s) of expertise and interest, and desired professorial rank. Only complete applications will be considered. Review of applications will begin on **February 17, 2014** and will continue until the position is filled.

EEO/AA Policy: The George Washington University is an Equal Opportunity and Affirmative Action Employer. Applications from women and under-represented minority groups are strongly encouraged.

School of Engineering & Applied Science

THE GEORGE WASHINGTON UNIVERSITY

ASSISTANT PROFESSOR (TENURE TRACK), DEPARTMENT OF BIOMEDICAL ENGINEERING, THE GEORGE WASHINGTON UNIVERSITY, WASHINGTON, D.C.

The George Washington University invites applications for a tenure-track assistant-professor position in the Department of Biomedical Engineering, to begin in fall semester 2014. This is an exciting opportunity for an outstanding person to join and contribute to the development of a new BME department. All areas of BME specialization will be considered. The Department will open formally in fall 2014 after moving the longstanding ABET-accredited B.S. program, and the M.S. and Ph.D. BME programs, from the Department of Electrical and Computer Engineering. The University is constructing a new 500,000 square-foot Science and Engineering Hall, adjacent to the University Hospital and Schools of Medicine and of Public Health, which will house state-of-the-art clean rooms, imaging facilities, and BME research and instructional laboratories. The School of Engineering and Applied Science will move into the building in spring 2015. The George Washington University is located in the nation's capital, with close access to many federal funding agencies and government research laboratories.

Responsibilities: The successful candidate will be expected to be an enthusiastic and effective teacher of undergraduate and graduate courses in Biomedical Engineering and, equally, to establish a strong program of high-quality externally-funded research. BME faculty members actively contribute to an environment that values diversity and nurtures collaboration, creativity, and innovation. The new professor will have opportunities to actively support the Department's efforts to attract new multidisciplinary partners across the University, and to advance and extend existing relationships with nearby government laboratories.

Basic Qualifications: Applicants must have an earned doctorate in Biomedical Engineering, Bioengineering, or a related field, outstanding academic credentials, clear evidence of potential for developing a strong externally-funded research program (as evidenced in part by peer-reviewed publications), and the ability to teach effectively at both the graduate and undergraduate levels. ABD applicants will be considered, but must complete all the requirements for the Ph.D. by expected start date.

Application Procedure: To apply, complete the online faculty application at <http://www.gwu.jobs/postings/19294> and upload a cover letter, a detailed CV or resume, a concise statement of teaching and research interests, and full contact information for five professional references. Please also indicate your primary area(s) of expertise and interest, and desired professorial rank. Only complete applications will be considered. Review of applications will begin on February 17, 2014 and will continue until the position is filled.

EEO/AA Policy: The George Washington University is an Equal Opportunity and Affirmative Action Employer. Applications from women and under-represented minority groups are strongly encouraged.

There's only one GALILEO GALILEI

Born in 1564, Galileo Galilei once contemplated a career in the priesthood. It's perhaps fortunate for science that upon the urging of his father, he instead decided to enroll at the University of Pisa. His career in science began with medicine and from there he subsequently went on to become a philosopher, physicist, mathematician, and astronomer, for which he is perhaps best known. His astronomical observations and subsequent improvements to telescopes built his reputation as a leading scientist of his time, but also led him to probe subject matter counter to prevailing dogma. His expressed views on the Earth's movement around the sun caused him to be declared suspect of heresy, which for some time led to a ban on the reprinting of his works.

Galileo's career changed science for all of us and he was without doubt a leading light in the scientific revolution, which is perhaps why Albert Einstein called him the father of modern science.

Want to challenge the status quo and make the Earth move? At *Science* we are here to help you in your own scientific career with expert career advice, forums, job postings, and more — all for free. For your career in science, there's only one *Science*. Visit ScienceCareers.org today.



For your career in science, there's only one **Science**

ScienceCareers.org

Human Genome Meeting 2014

27 – 30 April

CICG – Geneva – Switzerland

“Genome Variation and Human Health”



Confirmed Speakers

As of November 2013

Fowzan ALKURAYA (SA)
Karen B. AVRAHAM (IR)
Jacques S BECKMANN (CH)
Peer BORK (DE)
Carlos BUSTAMANTE (USA)
Ruth CHADWICK (UK)
Aravinda CHAKRAVARTI (USA)
Emmanouil T. DERMITZAKIS (CH)
Jacques FELLAY (CH)
Ada HAMOSH (USA)

Nicholas KATSANIS (USA)
Mary-Claire KING (USA)
Bartha KNOPPERS (CA)
Dominic KWIATKOWSKI (UK)
Partha MAJUMDER (IN)
John MULVIHILL (USA)
Debbie NICKERSON (USA)
Carmencita PADILLA (PH)
Alexandre REYMOND (CH)
Helen ROBINSON (AU)

Charles ROTIMI (USA)
Rickard SANDBERG (SE)
Dirk SCHÜBELER (CH)
Henk STUNNENBERG (NL)
Shamil SUNYAEV (USA)
Sarah TISHKOFF (USA)
Martin VINGRON (DE)
Ellen WRIGHT-CLAYTON (USA)

Abstract Submission Until: 29 January 2014

Early Registration Fee Until: 30 January 2014

www.hgm2014-geneva.org

Science Careers is the forum
that answers questions.



Science Careers is dedicated to opening new doors and answering questions on career topics that matter to you. With timely feedback and a community atmosphere, our careers forum allows you to connect with colleagues and experts to get the advice and guidance you seek as you pursue your career goals.

Science Careers Forum:

- » Relevant Career Topics
- » Timely Advice and Answers
- » Community, Connections, and More!

Visit the forum and join the conversation today!



Your Future Awaits.

Science Careers

From the journal *Science*



ScienceCareers.org



A **POSTDOCTORAL POSITION** is available at the University of Maryland School of Medicine, to investigate serotonin-mediated plasticity at corticostriatal synapses in a mouse model of dyskinesia/Parkinson's disease. Research in the laboratory utilizes modern neuroscience techniques including whole-cell patch-clamp recordings/optogenetics, cyclic voltammetry, and behavior/optogenetic approaches. We are seeking a highly motivated candidate with practical experience in slice electrophysiology and/or mouse behavior. Experience with stereotaxic surgeries is desired, but not required. Interested candidates should send a cover letter, curriculum vitae, and contact information for three references to **Brian N. Mathur, Ph.D.**, e-mail: bmathur@som.umaryland.edu.

University of California, Merced School of Engineering: Materials Science and Engineering tenure-track faculty position at the **ASSISTANT PROFESSOR** rank. Unique opportunity for one individual to join the faculty in the School of Engineering at the new University of California campus. Research focus for this position is Biological/Bio-Materials, broadly defined. Applicants with Ph.D. in Materials Science and Engineering or closely related discipline preferred. To apply, or for more information, please visit our website: <http://jobs.ucmerced.edu/n/academic/position.jsf?positionId=5090>. Evaluation of applications will begin February 15, 2014. *Affirmative Action/Equal Opportunity Employer.*

Your career is our cause.

Get help from the experts.

www.sciencecareers.org

- Job Postings
- Job Alerts
- Resume/CV Database
- Career Advice
- Career Forum

Science Careers

From the journal *Science*

Download your free copy today.

ScienceCareers.org/booklets



From technology specialists to patent attorneys to policy advisers, learn more about the types of careers that scientists can pursue and the skills needed in order to succeed in nonresearch careers.

Science Careers

From the journal *Science*